UNIVERSITY OF
LINCOLN

Towards a Dynamic Vision System – Computational Modelling of Insect Motion Sensitive Neural Systems

Qinbing Fu

Doctor of Philosophy

2018

School of Computer Science

University of Lincoln

Towards a Dynamic Vision System – Computational Modelling of Insect Motion Sensitive Neural Systems

Qinbing Fu

School of Computer Science

University of Lincoln

A thesis submitted in partial fulfilment of the requirements of the University of Lincoln for the degree of Doctor of Philosophy in Computing

Supervisor
Professor Shigang Yue

June 2018

Abstract

For motion perception, vision plays an irreplaceable role, which can extract more abundant useful movement features from an unpredictable dynamic environment compared to other sensing modalities. Nowadays, building a dynamic vision system for motion perception in a both reliable and efficient manner is still an open challenge. Millions of years of evolutionary development has provided, in nature, animals that possess robust vision systems capable of motion perception to deal with a variety of aspects of life. Insects, in particular, have a relatively smaller number of visual neurons compared to vertebrates and humans, but can still navigate smartly through visually cluttered and dynamic environments. Understanding the insects' visual processing pathways and methods thus are not only attractive to neural system modellers but also critical in providing effective solutions for future intelligent machines.

Originated from biological researches in insect visual systems, this thesis investigates computational modelling of motion sensitive neural systems and potential applications to robotics. This proposes novel modelling of the locust and fly visual systems for sensing looming and translating stimuli. Specifically, the proposed models comprise collision selective neural networks of two lobula giant movement detectors (LGMD1 and LGMD2) in locusts, and translating sensitive neural networks of direction selective neurons (DSNs) in flies, as well as hybrid visual neural systems of their combinations. In all these proposed models, the functionality of ON and OFF pathways is highlighted, which separate visual processing into parallel computation. This works effectively to realise neural characteristics of both the LGMD1 and the LGMD2 in locusts and plays crucial roles in separating the different looming selectivity between the two visual neurons. Such a biologically plausible structure can also implement the fly DSNs for translational movements perception and guide fast motion tracking with

a behavioural response to visual fixation.

The effectiveness and flexibility of the proposed motion sensitive neural systems have been validated by systematic and comparative experiments ranging from off-line synthetic and real-world tests to on-line bio-robotic tests. The underlying characteristics and functionality of the locust LGMDs and the fly DSNs have been achieved by the proposed models. All the proposed visual models have been successfully realised on the embedded system in a vision-based ground mobile robot. The robot tests have verified the computational simplicity and efficiency of proposed bio-inspired methodologies, which hit at great potential of building neuromorphic sensors in autonomous machines for motion perception in a fast, reliable and low-energy manner.

Declaration

I, Qinbing Fu, declare that this thesis describes an original research carried out on my own. It has not been previously submitted to any university for the award of any degree. Where I have quoted from the work of others, the source is always given.

Acknowledgements

First and foremost, I would like to thank my Ph.D. research advisor, Professor Shigang Yue, for his tolerance and patience in guiding me to start a new research topic and explore a field full of interest. I would like to express my sincere gratitude and great respect to him. Professor Shigang Yue gave me continuous support and let me learn how to be a mature and independent researcher in academia. He introduced me into the Computational Intelligence Lab (CIL) and Lincoln Centre for Autonomous Systems (L-CAS). He encouraged me to conquer difficulties throughout tough research and taught me to think deeply and creatively. He also taught me how to effectively communicate my research in papers and presentations. I trust I have got the proper ways including methods, and more importantly, thinking style to do research via the Ph.D. training with Professor Shigang Yue. He set an excellent example for me to guide my future potential students. I enjoyed and cherished every moment of work with Professor Shigang Yue, and colleagues in the CIL and the L-CAS in school of computer science.

I would also like to sincerely thank my second supervisor, Dr Nicola Bellotto for his patience and help on my research papers. He provided me with helpful feedbacks to improve my writing skills and organisation of articles. Dr Grzegorz Cielniak and Dr Patrick Dickinson were my previous M.Sc. advisers. Though they did not directly conduct my Ph.D. research, they always encouraged me to publish every progress during the Ph.D. research.

Research life is tough and sometimes boring. I thank colleagues in the CIL and the L-CAS who kindly discuss interesting topics with me to broaden my sights. I would thank the CIL members, Dr Jiawei Xu, Dr Cheng Hu, Dr Biao Zhao, Dr Feng Zhao, Dr Farshad Arvin, Dr Daqi Liu, Dr Xuqiang Zheng, Mr Hongxin Wang, Mr

Jingmin Huang, Mr Tian Liu, Mr Ziteng Wang and et al., for their kindly help and constructive suggestions to my Ph.D. research. I particularly thank Dr Cheng Hu, who had outstanding works on design of both hardware and software of the *Colias* micro-robots for enrich the testing of my models. We worked together productively creating many papers.

Within my four-year Ph.D. career, I was seconded to our projects partner Xi'an Jiaotong University (XJTU) as the research assistant for a long period of around 24 months. I would like to thank Professor Jigen Peng for his enlightening of my research. I also thank the colleagues in XJTU for the help on mathematics. During the last year of my Ph.D. period, I briefly visited two project partners, Newcastle University and Tsinghua University. I thank our partners Dr F. Claire Rind and Dr Peter J. Simmons for their great efforts in locust visual systems research for decades, which have been forming my solid research background.

I would like to take this chance to express my great gratitude to my family – my dear parents for their selfless love and constant support to my Ph.D. career. I am also grateful to my relatives, girl friend and friends who consistently support me. I want to say sorry to them for the absence of some important events during my study abroad.

Last but not least, I would like to thank the assistance and funding from a few projects to my Ph.D. research, that is, EU FP7-IRSES Projects EYE2E (269118), LIV-CODE (295151), and EU FP7-PEOPLE Project HAZCEPT (318907), and EU Horizon 2020 Project: STEP2DYNA (691154).

List of Publications

1. **Q. Fu** and S. Yue, "Modelling lgmd2 visual neuron system," in *Proc. IEEE International Workshop on Machine Learning for Signal Processing* (***MLSP***), Sep. 2015.

2. **Q. Fu**, S. Yue and C. Hu, "Bio-inspired collision detector with enhanced selectivity for ground robotic vision system," in *British Machine Vision Conference* (***BMVC***), Sep. 2016.

3. **Q. Fu** and S. Yue, "Modeling direction selective visual neural network with on and off pathways for extracting motion cues from cluttered background," in *International Joint Conference on Neural Networks* (***IJCNN***), May. 2017.

4. **Q. Fu**, C. Hu, T. Liu and S. Yue, "Collision selective lgmds neuron models research benefits from a vision-based autonomous micro robot," in *IEEE International Conference on Intelligent Robots and Systems* (***IROS***), Sep. 2017.

5. **Q. Fu** and S. Yue, "Mimicking fly motion tracking and fixation behaviors with a hybrid visual neural network," in *IEEE Int. Conf. on Robotics and Biomimetics* (***ROBIO***), Dec. 2017.

6. **Q. Fu**, C. Hu and S. Yue, "Collision selective visual neural network inspired by lgmd2 neurons in juvenile locusts," in *arXiv:1801.06452*, 2017.

7. **Q. Fu**, C. Hu, P. Liu and S. Yue, "Towards computational models of insect motion detectors for robot vision," in *Towards Autonomous Robotic Systems* (***TAROS***), Jul. 2018.

8. C. Hu, **Q. Fu** and S. Yue, "Colias IV: the affordable micro robot platform with bio-inspired vision," in *Towards Autonomous Robotic Systems* (***TAROS***), Jul. 2018.

9. C. Hu, **Q. Fu**, T. Liu and S. Yue, "A hybrid visual-model based robot control strategy for micro ground robots," in *The 15th International Conference on the Simulation of Adaptive Behavior* (***SAB***), Aug. 2018.

10. **Q. Fu**, C. Hu, J. Peng and S. Yue, "Shaping the collision selectivity in a looming sensitive neuron model with parallel ON and OFF pathways and spike frequency adaptation," *Neural Networks*, vol. 106, pp. 127-143, 2018.

11. **Q. Fu**, N. Bellotto and S. Yue, "A directionally selective neural network with separated on and off pathways for translational motion perception in a visually cluttered environment," in *arXiv:1808.07692*, 2018.

12. **Q. Fu**, N. Bellotto, C. Hu and S. Yue, "Performance of a visual fixation model in an autonomous micro robot inspired by *drosophila* physiology," in *IEEE Int. Conf. on Robotics and Biomimetics* (***ROBIO***), Dec. 2018.

Contents

List of Figures

List of Tables

List of Acronyms and Abbreviations

LGMD	lobula giant movement detector
DCMD	descending contra-lateral motion detector
DSN	direction selective neuron
DSMDN	directionally selective motion-detecting neuron
STMD	small target motion detector
LPTC	lobula plate tangential cell
EMD	elementary motion detector
FDN	figure detection neuron
SFS	small field system
LGN	lobula giant neuron
OF	optic flow
HR(C)	Hassenstein-Reichardt (correlation or correlator)
DS	direction selectivity
HSS	horizontal sensitive system
VSS	vertical sensitive system
PD	preferred direction
ND	null (non-preferred) direction
2-Q	two-quadrant
4-Q	four-quadrant
6-Q	six-quadrant
ESTMD	elementary small target motion detector
DSTMD	directional small target motion detector
FFE	feed forward excitation
FFI	feed forward inhibition
FFM	feed forward mediation
SFA	spike frequency adaptation
P	photoreceptor
HPF	high-pass filter
LPF	low-pass filter
HR	half-wave rectifier
BPF	bandpass filter
LT	Lipetz transformation
E	excitation or excitatory cell
I	inhibition or inhibitory cell
S	summation cell
G	grouping cell
FDSR	fast depolarisation slow re-polarisation
SIZ	spike initiation zone

L	luminance (grey-scale)
M	multiplication
SUM	summation
RE	retina neuropile layer
LA	lamina neuropile layer
LMC	large mono-polar cell
RTC	rectifying transient cell
DoG	Difference of Gaussians
ME	medulla neuropile layer
LO	lobula neuropile layer
LP	lobula plate layer
DSNN	directionally selective neural network
DSS	directionally selective system
DSL	directionally selective layer
MAX	maximisation
MP	membrane potential
SMP	sigmoid membrane potential
PNN	partial neural network
exp	exponentiation
FR	firing rate
TR	turning response
PP	position pathway response
LOCAL	local motion detector
VC	view centre
RP	relative position
UAV	unmanned aerial vehicle
MAV	micro air vehicle
SR	success rate
DTC	distance to collision
fps	frames per second
sd	sampling distance
p/f	pixels per frame
VLSI	very large scale integration
FPGA	field-programmable gate array
ASIC	application specific integrated circuit
DVS	dynamic vision sensor

Chapter 1

Introduction

1.1 Research Background

In nature, animals' sensory systems are essential to survival [57]. Amongst a variety of sensing modalities, vision plays irreplaceable roles of motion perception, since it can extract abundant motion cues from dynamic complex environments. Motion vision serves a wealth of daily tasks for animals and humans [58]. For the vast majority of animals, a critical ability of all visual systems is the detection and analysis of motion. Seeing the motion and direction in which a chased prey, a striking predator or a mating partner is moving is of particular importance for the survival of any animal species [28]. Millions of years of evolutionary development has produced, in nature, animals that possess robust and efficient vision systems capable of motion perception deciding a variety of aspects of life, including foraging, escaping from predators, chasing preys or mates and so forth. Not only mammals but also invertebrates are competent for sensing motion and distinguishing different classes of motion patterns for decent visual course control and navigating through an unpredictable environment [59, 28].

Across the animals kingdom, a large number of species are various kinds of insects [60]. Compared to vertebrates, insects have more compact visual systems in tiny brains. Despite that, much evidence has demonstrated their amazing ability to deal with visual motion in dynamic and cluttered scenes corresponding to flexible reactions like collision avoidance, target tracking and following and etc., even on some aspects, performing better than vertebrates and humans [61, 28, 62, 58]. For example, locusts

Figure 1.1: A swarm of locusts flies over a beach. This figure is adapted from [1].

can fly for hundreds of miles in dense swarms free of collision (Fig. 1.1); preying mantises can fixate small moving targets within visual clutter.

Insects possess complicated visual systems. The underlying circuits and mechanisms remain largely unknown until today [59, 58]. Understanding the fundamental characteristics and functionality of motion detection circuits thus is not only attractive to biologists and neural system modellers but also critical in providing effective solutions to future artificial machines. While the biological substrates are elusive, the computational modelling is of particular usefulness to help understand the mysterious biological visual processing methodologies.

From biology to computational intelligence, the revealed neurons and mechanisms in the insects' visual brains have provided us with a lot of inspirations for constructing dynamic vision systems, e.g. [37, 59, 63]. In order for mobile agents to initiate proper behaviours in complicated and dynamic environments, especially interacting with human hosts, a practical and robust motion-detecting system should possess the ability to extract meaningful motion cues from busy backgrounds in real time. Such an ability is of great significance for both animals and intelligent machines like unmanned/micro aerial vehicles (UAVs and MAVs), autonomous robots and also future robots and autonomous vehicles, which are now playing crucial roles or may greatly influence our daily life in the near future. However, the performance of current state-of-the-art methodologies for motion perception is far from the acceptable level. In this thesis, we investigate the computational modelling of insect motion sensitive neural systems which may provide possible solutions to this promising research area.

1.2 Traditional Computer Vision Techniques

In case of visual/image processing for motion perception, current state-of-the-art traditional computer vision techniques can handle with the vast majority of tasks including visual tracking, object detection and recognition and etc. More specifically, for motion detection and estimation, there are many methodologies showing good performances. For instance, several 3-D motion segmentation based methods have been proposed in the last two decades [64]. Recently, monocular-vision based models and methods have demonstrated both high accuracy in the estimation of multi-body motion including ego-motion and other independent motions, for example using a motion-segmentation strategy [65], and also good performance in the navigation control of quadcopters [66, 67, 68]. In addition, new event-driven cameras [69], which directly report pixel-wise brightness changes instead of traditional intensity images, have been used for motion detection and tracking with clustering and learning algorithms in robotics [70]. Moreover, specifically for real-time visual collision detection, the vast majority of methods implement object-and-scene segmentation, estimation or classification algorithms [71, 72]. Some vision-based collision-detecting systems have also been applied in ground-vehicles dealing with driving scenarios to improve road safety [71]. In addition, the state-of-the-art visual sensors like RGB-D [73], Kinect [74, 75] and event-driven cameras [69], can provide mobile machines with more visual features compared to traditional cameras which facilitate obstacle recognition, object segmentation and map reconstruction for collision detection.

However, these vision-based techniques, based on segmentation, classification and localisation algorithms, are either computationally costly or heavily restricted by specific visual sensors. In addition, the efficiency of these approaches also depends on the degree of complexity of real physical scenes. As a result, the fast, reliable and low-power methodologies for visual motion detection within complex and dynamic scenarios are still open challenges and required to be developed in the future.

1.3 Biological Inspiration

On the other hand, biological visual systems can be prominent models to study motion perception strategies. As mentioned above in Section 1.1, these biological circuits and mechanisms through millions of years of evolutionary development will be undoubtedly forming solid modules for constructing dynamic vision systems and providing possible solutions to the above mentioned challenges in the domain of vision-based motion perception.

In the real world, the diversity of motion patterns can be categorised into a few types that involve expansion and contraction of objects, translating, rotational motion, small targets movements and etc. Perceiving and recognising these different motion patterns, opportunely, in a visually cluttered and dynamic environment is critically important for the survival of insects. Though our current understanding to biological visual systems is very limited, there have been specialised visual neurons and circuits identified in locusts and flies that are sensing expanding edges of objects, namely, looming, as well as translating. This research takes inspiration from two categories of insects, i.e. the locusts and the flies (*drosophila*), which are competent for fast motion detection and safely visually-guided navigation in complex dynamic environments.

More precisely, in locusts, much progress has been made in understanding the cellular mechanisms underlying looming or collision detection. A group of large interneurons – the lobula giant movement detectors (LGMDs) in the third neuropile layer of lobula in the locust visual systems have been gradually discovered [76, 77, 78, 79]. Two amongst them, named LGMD1 and LGMD2, have been identified to respond most strongly to looming (approaching) objects moving in depth with high-frequency spikes [80, 81, 82, 83]. Moreover, compared with the LGMD1, the LGMD2 matures early in adolescent locusts and is only selectively reacting to darker objects approaching embedded in bright background, representing swooping predators (e.g. birds) from the light sky. Such robust collision detection neurons have attracted computational modellers and engineers to build cheap and fast collision detectors for mobile machines like robots, e.g. [84, 85, 21], which may require only monocular and ordinary cameras. Though the LGMD1 has been simulated by a variety of models and hardware re-

alisations, there is lack of systematic modelling studies on the LGMD2 neurons. This research for the first time investigates the computational modelling of LGMD2 visual neurones and provides empirical studies of corresponding applications to robotics.

Another kind of visual neurons, i.e. direction selective neurons (DSNs), that are sensitive to four cardinal wide-field translating movements, have been found in many animal species; these include insects like locusts [86, 87] and flies [88, 89, 28, 90] and so on, but also in mammals like rabbits [91], cats [92] and mice [58] and etc. Especially in the recent decade, a good number of physiological researches together have clearly drawn a signal tuning map of the fly preliminary visual systems, e.g. [28, 62, 58, 61, 93, 94, 95, 39, 40, 96, 97, 98, 99, 100, 101]. In comparison with the physiological research, only a few computational models have been proposed to implement the cutting-edge biological findings [102, 103, 53], let alone the potential of building low-cost and low-energy translating sensitive sensors for intelligent machines. Taken bio-inspiration from the fly visual systems, this thesis presents systematic modelling studies to mimic fly visual processing ON and OFF pathways and realise corresponding behaviours of fast motion tracking and visual fixation. This also demonstrates the usefulness of proposed bio-inspired methods for motion detection in mobile autonomous robots.

1.4 Original Contributions

In this dissertation, we have explored new methodologies to construct dynamic vision systems with biological inspiration. The original contributions of this dissertation are summarised in the following:

1. In Chapter 2, this dissertation reviews computational models sensitive to multiple motion patterns including looming, translating and small target motion that are originated from several kinds of insects visual systems research. There are a lot of publications in motion perception and modelling of insect visual systems in the past decades, shedding light on significant breakthrough in bio-inspired artificial vision systems for future robotics and autonomous vehicles. These

publications cover computational modelling of different motion patterns, such as looming, translating, small target motion, and rotation and etc., as well as various applications. However, there is no systematic review on this promising research field though some of them have been casually touched upon in different papers. Moreover, this thesis summarises similarities in computational modelling of insect visual systems, as well as generation of direction and size selectivity diversity in insect motion sensitive neural systems.

2. In Chapter 3, this thesis proposes the first computational model of biological LGMD2 neurons with unique looming selectivity to dark objects that approach. This also provides us with systematic studies on the different characteristics between the LGMD1 and the LGMD2. A good number of computational models have been proposed to simulate the LGMD1, some of which are applicable to robotics as well. However, no modelling studies have involved the LGMD2, let alone its great potential in machine vision. In this thesis, a novel modelling of parallel ON and OFF pathways has been demonstrated a crucial role of separating the functionality between the LGMD1 and the LGMD2 based visual neural networks. For the first time, the LGMD2 model works well in responding selectively to only dark looming objects against bright background but not to white/bright objects embedded in dark background or to other translating moving objects, demonstrating the unique characteristics of LGMD2 neurons.

   Although the biological LGMD1 is robust to recognise both bright and dark looming stimuli whilst the LGMD2 can not detect the light looming objects, we found that the proposed LGMD2 model is especially effective for daylight navigation of ground mobile robots. More precisely, the LGMD2 model is not affected by dark receding movements at all, whereas the state-of-the-art LGMD1 models are greatly influenced by such stimuli, sometimes representing spike frequency similarly to the looming situations, which is not acceptable for a practical collision detector.

3. In Chapter 4, the ON and OFF visual pathways have also been shown the efficacy of realising the fly DSNs that are only sensitive to wide-field translational

motion. In respect of cutting-edge biological research in fly preliminary visual systems, this thesis proposes a directionally selective neural network (DSNN) simulating thoroughly fly visual motion sensing pathways and neurons throughout multiple layers, from the first retina neuropile layer to the lobula plate tangential cells (LPTCs). Similarly to the modelling of locust visual systems, we highlight the functionality of ON and OFF pathways that separate visual processing into parallel channels encoding onset (ON) and offset (OFF) responses, separately.

Due to the current-stage challenges of visual motion perception within complex dynamic environments, we have demonstrated the importance of spatiotemporal pre-filtering of visual signals to obtain cleaner motion features via combining two bio-plausible mechanisms, that is, the spatial filtering of polarity Difference of Gaussians (DoGs) algorithm and the temporal filtering of fast-depolarisation-slow-repolarisation (FDSR) mechanism. Both effectively filter out irrelevant motion from the complex background. In addition, compared to related computational models, the ensembles of ON/OFF local motion correlators are modelled in space within the dual-pathways to improve the speed response. Furthermore, the proposed neural system has been extended to behavioural levels of mimicking fly fast motion tracking and fixation behaviours, which has been successfully realised on the embedded system.

4. In Chapter 5, this thesis investigates the preliminary modelling of multiple neural vision systems inspired by locust and fly visual systems that possess complementary direction selectivity covering both looming and translating motion patterns. The proposed hybrid visual systems have been validated by systematic bio-robotic experiments, which demonstrate satisfactory performance in the coordination between visual neurons with different collision and direction selectivity for recognising more motion patterns in real time and within dynamic scenes. As a result, the proposed visual models can conduct quick, simple and proper behaviours of mobile robots in navigation, like reactive collision avoidance, motion tracking, visual fixation and object following.

5. All the proposed computational models of insect visual systems have been successfully realised on the embedded system in a vision-based ground mobile robot, which has very limited computational resources for on-board visual processing. The robot implementation has verified the computational simplicity and flexibility of these bio-inspired motion detectors for real-time visual tasks. More precisely, the frame rate of each embedded vision system can reach no less than 30 frames per second (fps) that meets well the requirements of real-time image processing. The corresponding robotic applications have also demonstrated great potentials of these proposed motion perception models towards building low-cost, low-energy consumption neuromorphic sensors for volume production and widely used in future intelligent machines.

1.5 Organisation of the Thesis

This dissertation is composed of six chapters. Chapter 1 introduces background of this research in Section 1.1, traditional computer vision techniques for motion detection in Section 1.2, biological inspiration of this research in Section 1.3, and the original contributions in Section 1.4.

Chapter 2 reviews the related fields of studies, systematically. This begins with presenting relevant surveys of biological visual systems research, corresponding computational models and applications to robotics in Section 2.1. Then, this surveys on bio-inspired visual motion detectors including the proposed computational models, over decades, depending on the diversity of direction and size selectivity to different motion patterns. These comprise looming sensitive neuronal models for collision detection inspired by locust visual systems in Section 2.2, translating sensitive neural systems inspired by locusts and fruit flies in Section 2.3, small target motion sensitive models inspired by hover flies and dragonflies in Section 2.4. After that, this summarises the commonality in computational modelling of both looming and translating sensitive neural systems, and moreover demonstrates computational generation of the diversity of direction and size selectivity in different neuron models. This also reviews a few researches on multiple neural systems integration for motion perception

in Section 2.7, as well as related hardware realisation of these insect visual motion detectors, and more importantly points out their great potential to build neuromorphic sensors in Section 2.8. A relevant brief review paper is the publication [7] in the list of publications in page *VI*.

Chapter 3 presents the computational modelling of locust looming sensitive neuronal models for collision recognition. Firstly, this discusses about the physiological similarities and differences between the LGMD1 and the LGMD2 and presents the modelling of LGMD2 neuronal model with detailed algorithms and systematic experiments in Section 3.1. This also proposes a general LGMDs model which can implement both the LGMD1 and the LGMD2 via the modelling of ON and OFF pathways in Section 3.2. Importantly, this chapter summarises different methodologies to shape the looming selectivity in the literature so far. Further discussion is given to the lack of computational modelling and studies on looming detectors in flies and invertebrates like crabs which could learn from the modelling of locust looming detectors. This chapter is summarised in Section 3.3. The publications [1], [2], [6], [8] and [10] are fully in support of this chapter.

Chapter 4 presents our systematic modelling studies on translating perception visual neural networks relying upon the cutting-edge biological findings in fly preliminary visual pathways. A summary of physiological research progress in the recent decade is introduced in Section 4.1. After that, the proposed DSNN is presented in Section 4.2, which has been extended to higher behavioural levels of mimicking insect visual motion tracking and fixation behaviours in Section 4.3. Furthermore, a DSNN based motion tracking and fixation model has been smoothly implemented on the embedded system in Section 4.4. Further discussion about the current challenges in translating motion detectors and possible solutions is carried out in Section 4.5. This chapter is summarised in Section 4.6. This chapter is a well-organisation and enriched version of publications [3], [5], [11] and [12].

Chapter 5 presents the design of hybrid neural vision systems for extracting multiple motion features in dynamic scenes. This chapter first introduces a hybrid LGMDs model that is implemented on the embedded system in Section 5.1; this includes a

bilateral control strategy by a pairwise combination of the proposed LGMD1 and LGMD2 neuron models for reactive collision avoidance and investigation of different neural characteristics between these two looming detectors. This then presents a synthetic neural vision system which combines the functionality of two LGMDs and two DSNs with logic and switch functions for motion pattern recognition in dynamic robot scenes in Section 5.2; each spiking neuron can recognise a particular motion pattern corresponding to a proper robot behaviour in an arena mixed with multiple agents. Moreover, we have further discussion about the possibility of integrating bio-inspired visual models with other fields of methods like statistical model for vision-based robot control in swarm robotics research in Section 5.3. At last, we summarise this chapter in Section 5.4. Partial work in this chapter has been published in [4] and [9].

Chapter 6 concludes this dissertation within Section 6.1 and discusses potential future works within Section 6.2.

Chapter 2

Literature Review

Within this chapter, the related fields of research will be reviewed. There are a lot of publications in motion perception and modelling originated from animals' visual systems research in the past decades, shedding light on significant breakthrough in bio-inspired artificial vision systems for future robotics and autonomous vehicles. These publications cover computational modelling of different motion patterns, such as looming, translating, small target motion, and rotation and etc., as well as various applications. However, there is no systematic review on this promising research field though some of them have been casually touched upon in different papers.

To the best of our knowledge, this dissertation for the first time covers computational models sensitive to different motion patterns including looming, translating, small target motion, that are originated from several kinds of insects' visual system research. These insects include locusts, fruit flies (or drosophila), dragonflies, hover flies, and bees (bumblebees and honeybees). The vast majority of biological and computational studies have been focusing on the various kinds of flies and locusts. Although there have been a few reviews on biological and computational models, as well as applications of fly visual systems, e.g. [59, 37, 62]; no survey has been provided to touch upon the looming sensitive neuron models inspired by locust visual systems and the small target motion sensitive neuron models inspired by dragonflies and hover flies and corresponding applications, systematically.

In the real world, the diversity of motion patterns can be categorised into a few types that involve expansion and contraction of objects, translating, rotational motion

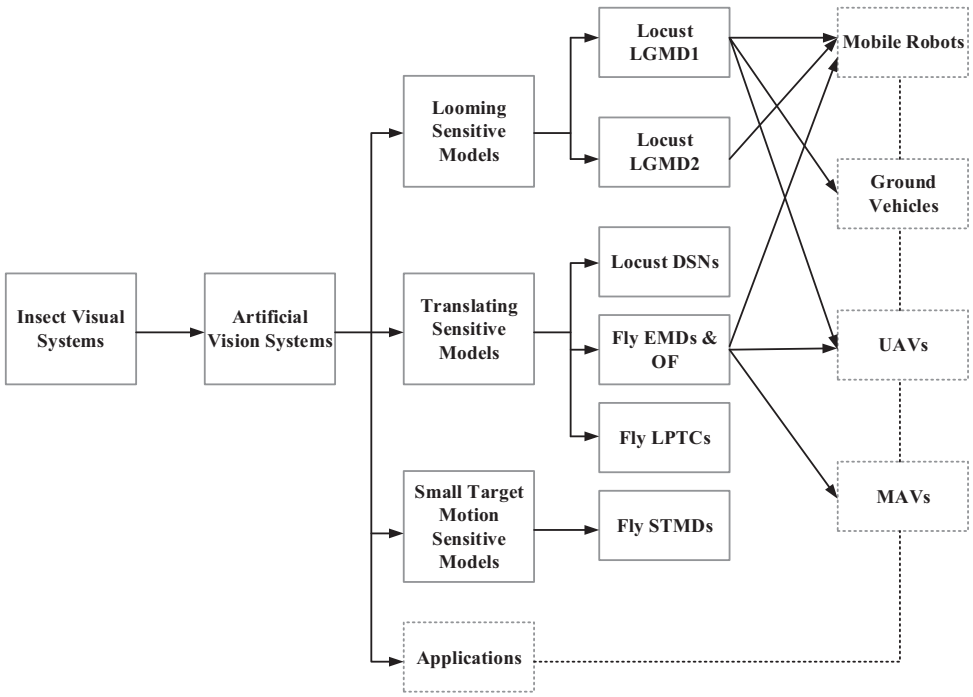

Figure 2.1: The taxonomy proposed in Chapter 2.

and etc. Depending on the distance between moving objects and the observer, it can be also defined the other specific motion pattern of small target movements. Perceiving and recognising these different motion patterns in a visually cluttered and dynamic environment is critically important for the survival of insects. With regard to the diversity of visual neurons that possess specific sensitivity to different motion patterns, this thesis reviews the current bio-inspired motion perception models and applications according to different direction and size selectivity, as illustrated in Fig. 2.1. These include the distinct direction selectivity (DS) to looming and translating stimuli in visual neurons of locusts, fruit flies and bees, as well as the specific size selectivity to small target motion in visual neurons of dragonflies and hover flies.

This chapter is organised as follows: first, related reviews of biological research, bio-inspired models and applications will be introduced in Section 2.1; then, the looming sensitive neuronal models and applications of two LGMDs in locusts will be reviewed in Section 2.2; in Section 2.3, we will introduce translating sensitive neural systems and their wide applications in flying robots including UAVs and MAVs; we also present the cutting-edge research of ON and OFF pathways for translational motion perception and latest relevant modelling studies; in Section 2.4, we will survey a specific group of visual neural networks for sensing small target motion; in addi-

tion, we will summarise similarities in modelling of different visual neural systems in Section 2.5, and computational generation of different direction and size selectivity in these models in Section 2.6; we also have further discussion about multiple systems integration in Section 2.7, as well as potential of these bio-inspired dynamic vision systems for building neuromorphic sensors for volume production in Section 2.8. Finally, this chapter is summarised in Section 2.9.

2.1 Survey of Insect Visual Systems Research

2.1.1 Related Survey of Biological Research

The past several decades have witnessed much progress in our understanding of cellular and sub-cellular mechanisms of mysterious biological visual systems. There have been a few visual neurons or pathways identified in insects like various kinds of flies [34, 104, 105, 32, 106, 107, 108, 109, 110, 111, 112, 113], locusts [114, 5, 82, 115, 2, 116, 117, 19], bees [118, 119, 120], as well as ants [121] and mantises [122, 123] and etc. Two researches have reviewed fundamental mechanisms in insect visual motion detection; these comprise classic models and functions [124, 90]. At early stages, fly visual systems are prominent models to study animals' motion-detecting strategies [125]. Borst et al. have reviewed thoroughly the step-by-step physiological findings on the fly visual systems and summarised the visual course control; these include behaviours, algorithms and circuits [90, 61, 62, 28, 126]. Importantly, they have also pointed out the commonality in design of fly and mammalian motion vision circuits [58]. By contrast to the correlated elementary motion which is velocity-dependent, Aptekar briefly reviewed the higher-order figure detection with non-Fourier or statistical features in flies that correlates with human vision [127]. In addition, Rind et al. devoted to research the underlying structures and mechanisms of locust visual systems to learn looming perception and collision avoidance schemes from locusts [81, 128, 129, 83, 80, 79, 2, 116, 19, 117, 130, 78, 131]. On the behavioural level, a research reviewed escape behaviours in insects caused by visual stimuli, and moreover, demonstrated the complexity of both visual and escape circuits [132].

2.1.2 Related Survey of Bio-inspired Models and Applications

These naturally evolved vision systems have been providing us with a rich source of inspiration for developing artificial visual systems for motion perception. As swift development of hardware, these bio-inspired models have been applicable to robotics. A good number of surveys emerged to demonstrate how machine vision benefits from computational modelling of insects vision. Iida reviewed the models motivated by flying insects and the applications to robotics [133]. Dario et al. proposed an overview of applying bio-inspired control methodology for vision-based wheeled and flying robots [134]. Srinivasan et al. studied rigorously the models and control methods inspired by visual systems in flying insects like honeybees for visually guided flight control and navigation [135, 136, 137]. Huber presented visuomotor control in flies and visually behaviour-based models, control and design for robotics [138]. Franceschini devoted to survey biological research and computational models on the basis of a scheme of fly elementary motion detectors (EMDs) and relevant bio-robotics applications, systematically [37]. Recently, Serres and Ruffier reviewed the applications of fly optic flow-based strategies to UAVs and MAVs for multiple visually guided behaviours, like collision avoidance, terrain following, tunnel crossing and etc [59]. More generically, Desouza and Kak surveyed vision techniques, that varied from traditional computer vision methods to insects optic flow strategies, for mobile robots navigation [72]. On the other hand, Webb reflected with the influence of robot-based research including bio-inspired vision on biological behaviour of animals [139, 140]; importantly, these seminal works revealed that the bio-inspired robotic studies could be good paradigms for studying biological behaviours.

2.2 Looming Sensitive Neuronal Models

This section reviews looming sensitive neuronal models as collision-detecting systems and applications inspired by locust visual systems. These include two neuronal models of the LGMD1 (Section 2.2.1) and the LGMD2 (Section 2.2.2), and different methods to shape the looming selectivity in models to date (Section 2.2.3). This section covers

also corresponding applications of these looming detectors to mobile robots, UAVs and ground vehicles.

The looming stimuli indicate movements in depth of objects that approach, which are very frequent visual challenges to animals. Recognising looming, timely and accurately, is certainly crucial for animals' survival. These looming sensitive neurons have been found in insects like locusts [76] and flies [141], arthropods like crabs [142]. Amongst these animals, the locusts have offered prominent visual models to study looming perception schemes and building effective collision-detecting and avoiding systems [2, 116, 114]. As the result of millions of years of evolutionary development, locusts are experts in collision detection and avoidance, that can fly in very dense swarms for hundreds of miles free of collision; possessing this fascinating ability is demanded for future intelligent machines, like autonomous robots and vehicles.

2.2.1 LGMD1-based Neuronal Models and Applications

Background As early as in the 1970s, biologists had anatomically explored large inter-neurons in the lobula neuropile layer of locusts' visual brain that sense looming objects, called the lobula giant movement detectors (LGMDs) [76, 77]. A group of LGMDs have been found, yet only two of them have been identified on functional level so far, that is, the LGMD1 [80, 76] and the LGMD2 [83]. The LGMDs respond most strongly to looming stimuli over other kinds of visual challenges like receding and translating movements [79, 2, 116]. Such specific looming selectivity of LGMDs allow locusts to well discriminate objects that approach from other motion patterns; this represents the highest spike frequency by looming stimuli.

Biological research The vast majority of researches have been concentrating on the LGMD1 of locusts. This has been demonstrated to play dominant roles in locusts that can fly and especially in the adulthood [5, 2, 128, 19, 117, 79]. In terms of neuromorphology, Fig. 2.2 illustrates an LGMD1 neurone and both its pre-synaptic and post-synaptic structures. Generally speaking, the LGMD1 integrates visual signals from different dendritic areas; these generate two kinds of flows – the excitations and the inhibitions. The neural processing within the circuit is a competition between

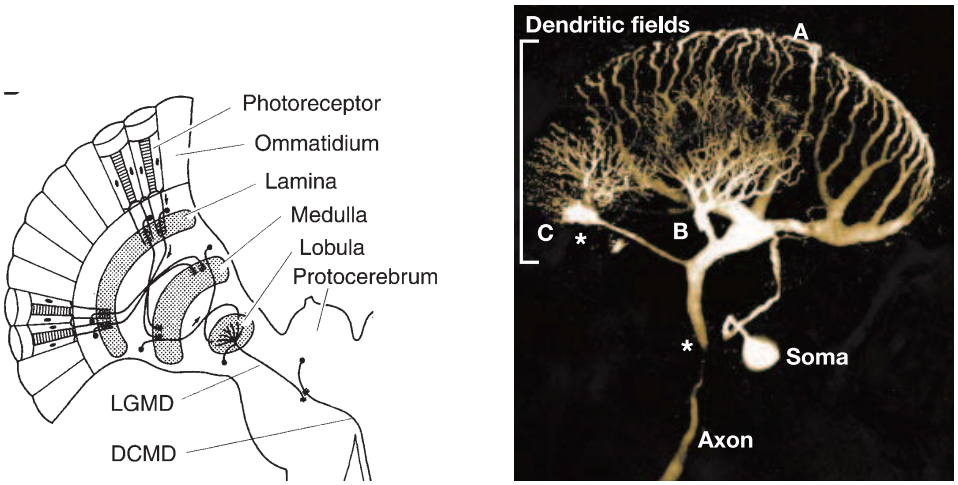

Figure 2.2: LGMD1 morphology: (a) illustration of the pre-synaptic neuropile layers to the LGMD1 neuron and the post-synaptic one-to-one target DCMD neuron, adapted from [2] (Rind and Simmons, 1999), (b) illustration of the LGMD1's large dendritic fan (A) and two additional dendritic fields (B, C) that receive distinct synaptic inputs, adapted from Gabbiani[3] (Gabbiani et al., 2002).

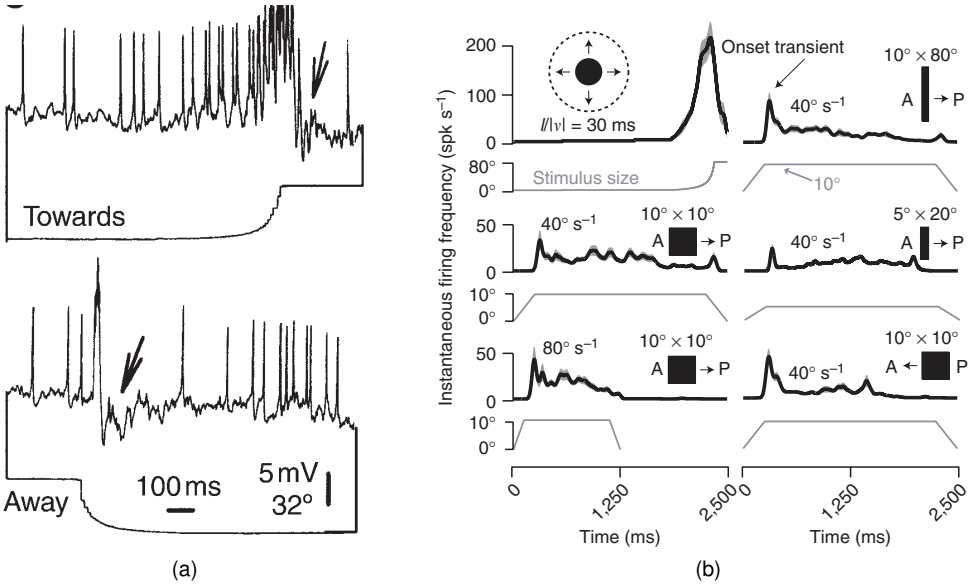

Figure 2.3: LGMD1 neural response to approaching and receding stimuli (a), adapted from [2] (Rind and Simmons, 1999): arrows indicate a hyper-polarisation response of strong inhibition after activation. (b) LGMD1 neural response to approaching and translating stimuli by a variety size and speed of moving objects, adapted from [4] (Peron and Gabbiani, 2009).

these two flows [79, 143]. As a result, the activation of LGMD1 requires the 'winner' to be the excitatory flow. In addition, the descending contralateral movement detector (DCMD) is a one-to-one connection of post-synaptic target neuron to the LGMD1 [78, 130, 131, 144]; this conveys the generated spikes by LGMD1 to further motion

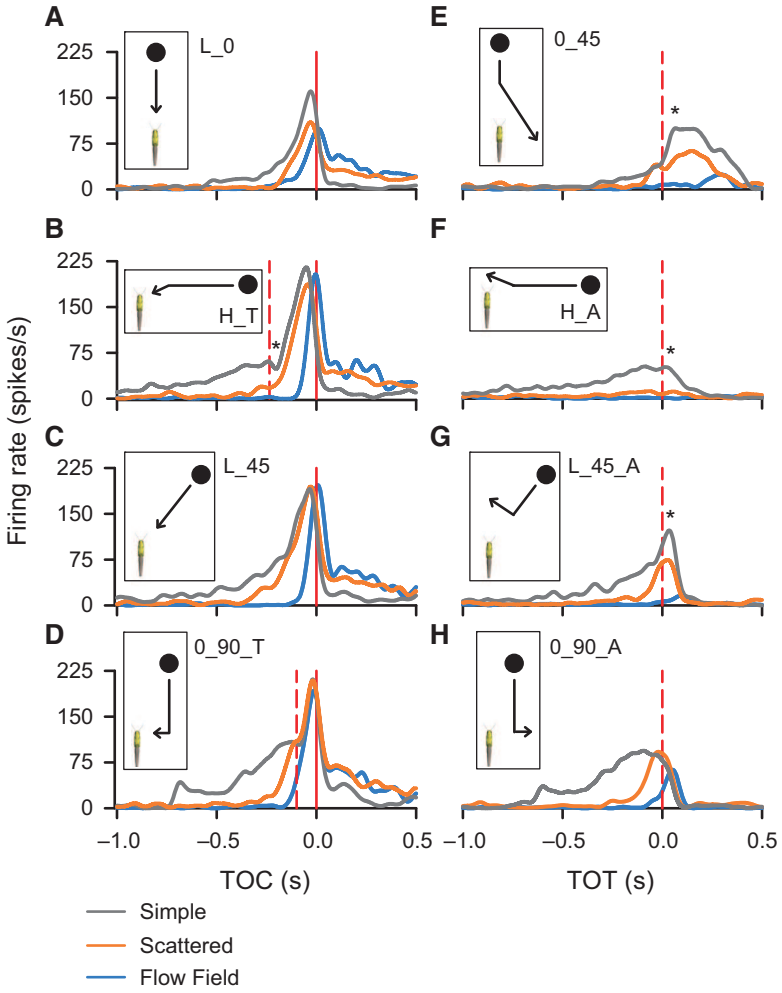

Figure 2.4: The LGMD1/DCMD pathway in locusts responds to a variety of courses of collision and deviations from collision, against a simple background or dynamic clutter, adapted from [5] (Yakubowski et al., 2016). Red solid vertical lines indicate time of collision. Red dashed vertical lines represent time of transition. Asterisks indicate the time of a local valley or peak in response to a transition.

control neural systems.

So, what does the LGMD1's neural response look like? Fig. 2.3 demonstrates the responses to different visual stimuli; these comprise objects approaching and receding (Fig. 2.3a), as well as translating stimuli by varied sizes of dark objects and speeds of translations (Fig. 2.3b). It can be clearly seen from Fig. 2.3 that the LGMD1 neuron responds most strongly to looming objects that approach, representing the highest firing rates. It is only briefly excited by the object moving away. The translating stimuli bring about short-term and weak responses of the LGMD1 regardless of the size, direction and speed of objects. More recently, Yakubowski et al. demonstrated the neural response of LGMD1 in locusts against a visually cluttered or dynamic background and more abundant visual stimuli including objects deviate from a collision course [5]. It

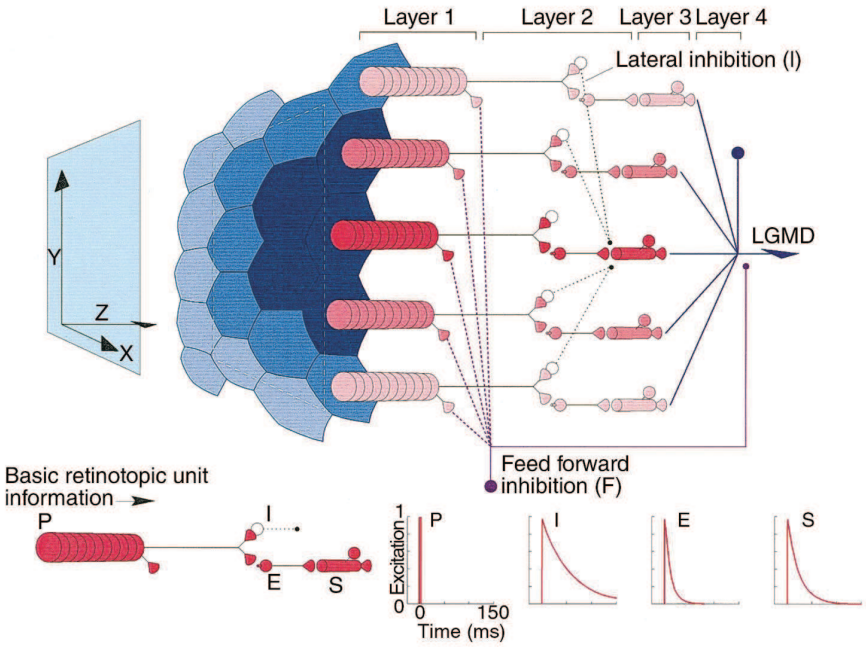

Figure 2.5: Schematic of LGMD1 visual neural network proposed by Rind, adapted from [2] (Rind and Simmons, 1999): this consists of four layers of photoreceptors (P), excitations (E), lateral inhibitions (I) and summation cells (S), as well as two cells of LGMD1 and feed forward inhibition (F).

can be seen from Fig. 2.4 that the LGMD1 responds vigorously to a variety of oncoming threats; it can well discriminate collision from movements that objects transit to recession; this response is also affected by the degree of complexity of background motion like dynamic visual clutter.

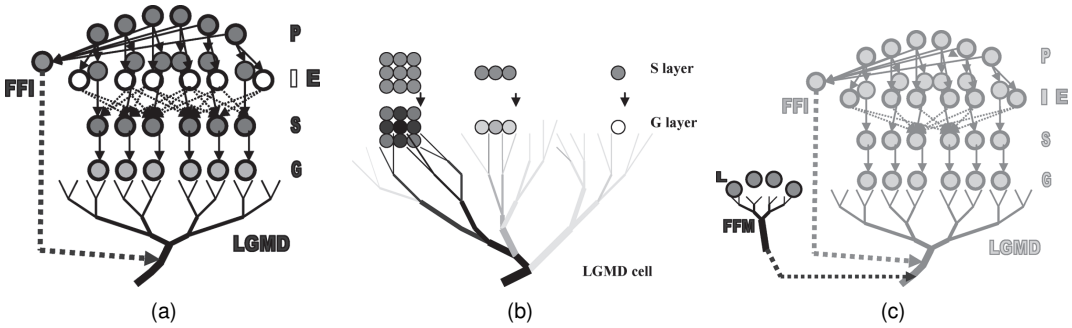

Figure 2.6: Schematic of LGMD1 visual neural network taken only 6 cells as an instance (a), with a G (grouping) layer (b) and a FFM (feed forward mediation) mechanism (c), adapted from [6] (Yue and Rind, 2006).

Computational models Computational modelling of such a fascinating looming sensitive neuron has emerged since 1990s. A seminal work was proposed by Rind and Bramwell to model an LGMD1-based visual neural network [79], as illustrated in Fig. 2.5. In this research, they dissected the pre-synaptic signal processing methodologies

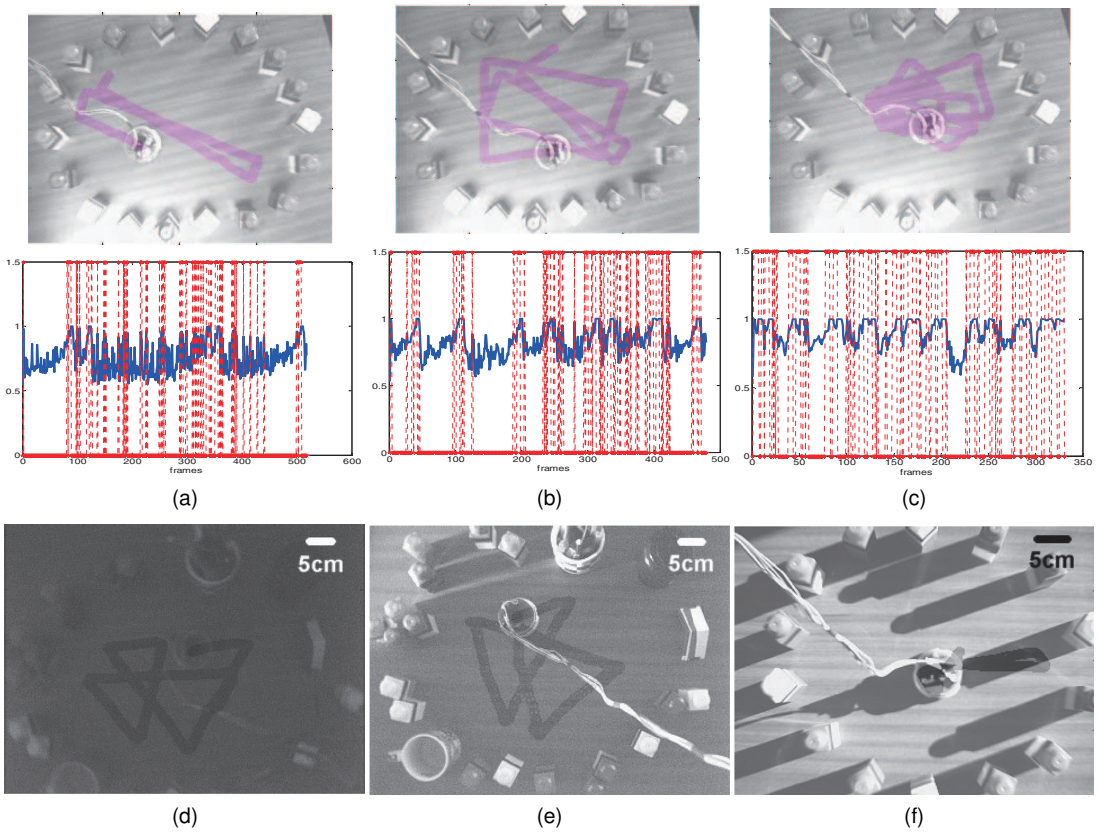

Figure 2.7: The results of robot collision detection with normalised neural responses (blue lines) and burst of spikes (red-dashed lines), tested by different speeds from slow (a) to fast (c) as well as light conditions from dim (d) to extremely bright (f): the overtime trajectory is shown for each result. (a)–(c) are adapted from [7] (Yue and Rind, 2005) and (d)–(f) are adapted from [6] (Yue and Rind, 2006).

in the looming sensitive neural network and analysed how the inhibitions can play crucial roles to cut down the excitations in a both spatial and temporal mode; importantly, this effectively shapes the LGMD1's looming selectivity to respond most powerful to approaching objects. More precisely, this work highlighted that the visual information sensed by the first layer of photoreceptors is divided into two kinds of signals within the pre-synaptic structure – excitations and lateral inhibitions; the lateral inhibitions are temporally delayed relative to the excitations and spread out to neighbouring cells, symmetrically in space and decaying in temporal; such a mechanism determines the specific looming selectivity of LGMD1 to approaching rather than receding and translating stimuli. In addition, a feed forward inhibition can suppress the LGMD1 neuron directly, which can also mediate its looming selectivity at some critical moments like the end of approach and the start of recession.

Based on this LGMD1 modelling theory, a good number of models have been pro-

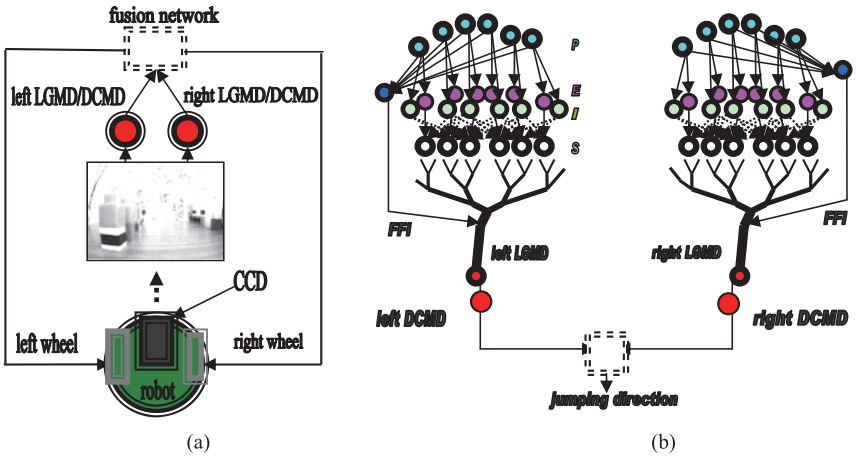

Figure 2.8: A reactive collision avoidance strategy via integrating a bilateral pair of LGMD1 neuronal models to control left and right wheels of the robot, respectively, adapted from [8] (Yue et al., 2010): (a) the control strategy in robot, (b) the bilateral LGMD1/DCMD visual neural networks.

duced during the past two decades; these works have not only been extending and consolidating its original functionality for looming perception, but also investigating the possible applications to mobile machines like robots and UAVs. More specifically, the proposed LGMD1 neuronal model by Rind [79] was for the first time implemented in a ground mobile robot for collision detection in two seminal works [145, 84]. Rind demonstrated further the usefulness of LGMDs for guiding flying robot behaviour and pointed out another group of directional selective neurons that sense ego-motion could be integrated with the LGMDs for better performance [63]. In addition, Yue et al. applied the LGMD1 model as an optimised collision-detecting solution for cars; a novel genetic algorithm was for the first time incorporated in this neuronal model for bettering collision detection performance in driving scenes [146]. After that, Yue and Rind developed new mechanisms in the LGMD1-based visual neural network, to enhance the ability of extracting looming features from complex and dynamic environments and adapting to different illuminations [6], as illustrated in Fig. 2.6. This method was verified by a vision-based mobile robot [7, 6] with better performance in collision detection. Compared with previous bio-robotic studies, the robot can recognise potential collision tested by different speeds and light conditions (Fig. 2.7). With similar ideas, Yue and Rind continued exploring the potential of LGMD1 model in robotic applications like near range path navigation; these include a development of a visually guided control with a bilateral pair of LGMD1/DCMD neurons for reactive collision avoid-

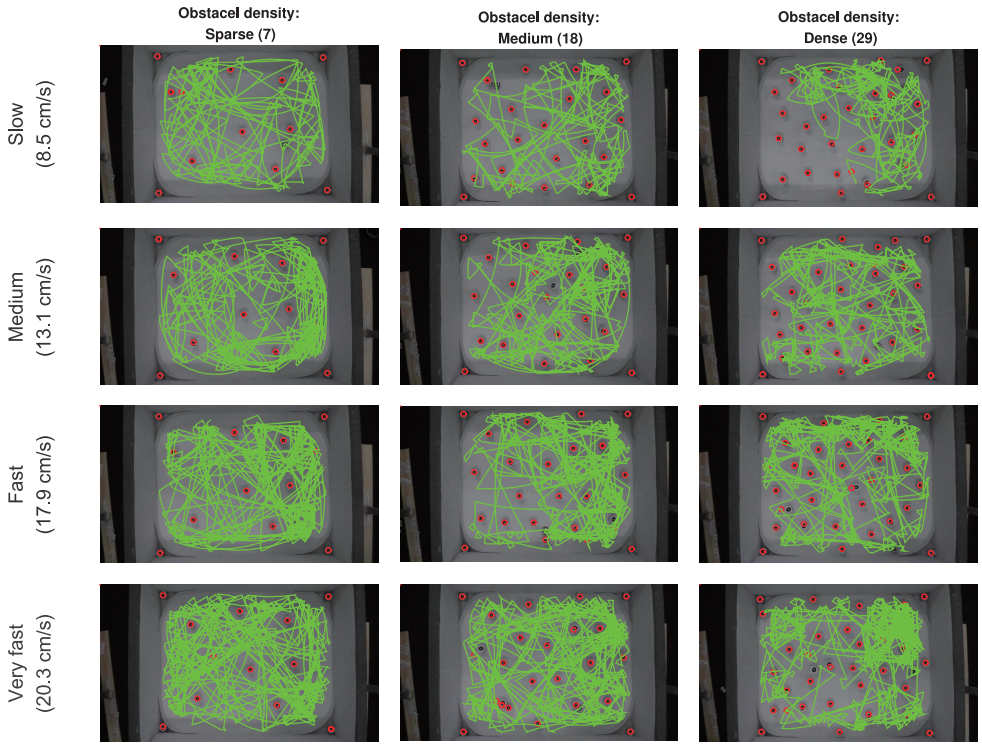

Figure 2.9: Robot arena tests implemented with an LGMD1 model [9] as the only collision-detecting sensor: the micro-robot was tested by different speeds and densities of obstacles in an arena. The green line indicates robot overtime trajectory and the red circles denote the obstacles. The experimental data is adapted from [9] (Hu et al., 2017).

ance [8, 85] (Fig. 2.8). Hu et al. applied a similar LGMD1 visual neural network as an embedded vision system in a vision-based autonomous micro-robot to demonstrate its computational simplicity for in-chip visual processing [147, 9]. To verify its reliability and validity, the robot was tested in an arena mixed with multiple obstacles, as shown in Fig. 2.9; this demonstrated very high success rate of collision detection tested by different speeds of robot and densities of obstacles. Very recently, the similar approach has been implemented in a small quad-copter for short-range navigation, as well [148].

Moreover, there are many derivatives of the proposed LGMD1-based neural network by Rind [79], as illustrated in Fig. 2.10; these consist of new methods to enhance the collision selectivity to approaching objects [13], new layers to reduce environmental noise [15, 16], new mechanisms to enhance the performance in high degree of complexity required scenarios [149] and dim scenes [150], and etc. There are also researches on corresponding applications for cars [151, 17] and mobile robots [152], as well as implementations in hardware like the FPGA [14].

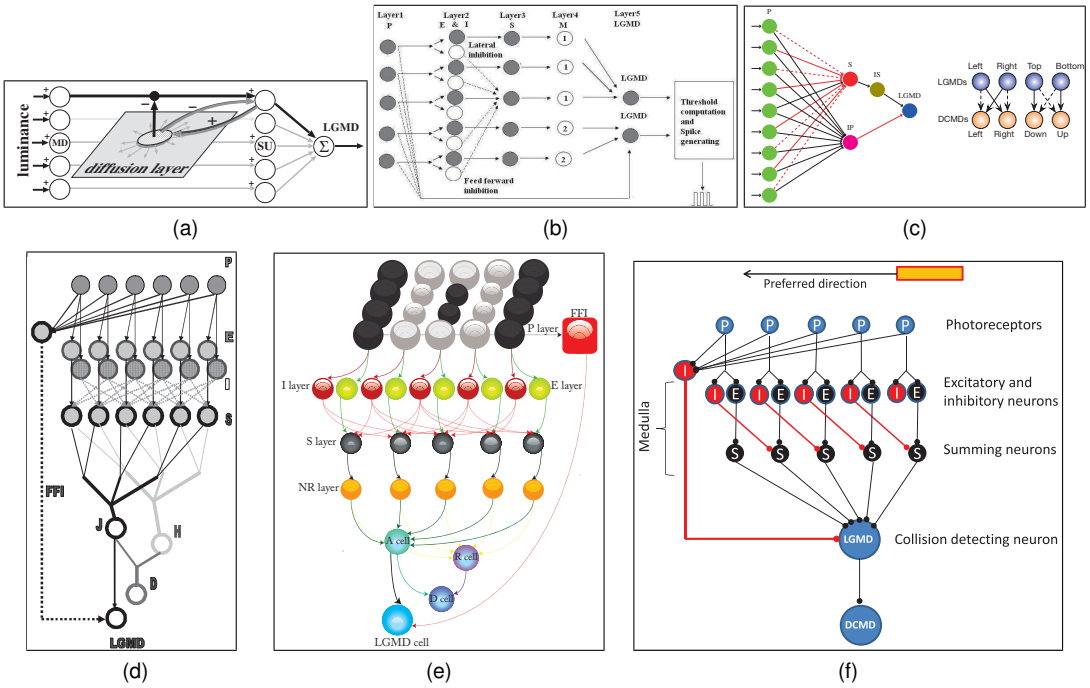

Figure 2.10: Schematics of a variety of LGMD1-based visual neural networks: (a) an LGMD1 model encoding onset and offset responses by luminance increments and decrements, adapted from [10] (Keil et al, 2004), (b) a modified LGMD1 model for multiple looming objects detection, adapted from [11] (Yang et al., 2012), (c) a simplified LGMD1 model for collision avoidance for an UAV, adapted from [12] (Salt et al., 2017), (d) a modified LGMD1 model with enhancement of collision selectivity, adapted from [13, 14] (Meng et al., 2009, 2010), (e) a modified LGMD1 model with a new layer for noise reduction and spiking-threshold mediation, adapted from [15, 16] (Silva and Santos, 2013), (f) an LGMD1 neural network based on the modelling of elementary motion detectors for vehicle collision detection, adapted from [17] (Hartbauer, 2017).

Interestingly, Gabbiani has pointed out that there are many ways to build the looming sensitive neuronal models like the locust LGMDs [153]. Therefore, another important theory highlights the non-linearity in the modelling of looming sensitive neurons, that is, the LGMD1 represents a non-linear processing or competition between inhibitory and excitatory flows, proposed by Gabbiani et al. [154, 155, 3]. They have also demonstrated the correspondence between the calculations of feed forward excitation/inhibition and the angular speed/size of looming objects within the field of view. Here, the feed forward inhibition features a critical role to shape the collision selectivity of the LGMD1 [156]. With respect to the non-linear interactions between the excitations and inhibitions, the LGMD1 neuronal model could possess a biologically plausible invariance to varied shape and contrast of looming objects, as well as the

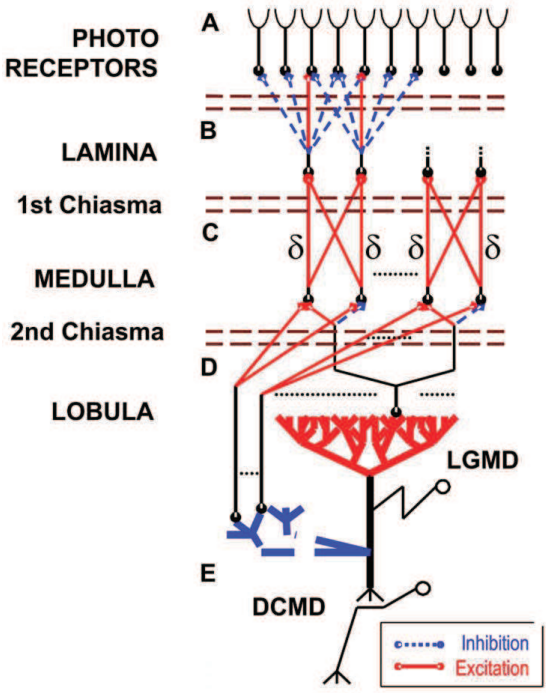

Figure 2.11: Schematic of a locust non-linear LGMD1 model, adapted from [18] (Badia et al., 2010): this visual neural network emphasises the non-linear interactions between the feed-forward excitation and the feed-forward inhibition.

approaching angles [157, 143].

Based on the non-linear theory of modelling the LGMDs, Keil gave an insight into the mathematical explanations for the generating of non-linearity in the LGMD1 neuronal model [158, 159]. Badia et al. incorporated the non-linear (multiplicative) elementary motion detectors (EMDs) to construct the LGMD1 for sensing and avoiding potential collision [160]. Stafford et al. also applied similar strategies to model the LGMD1 for handling looming perception in driving scenarios [161]. In addition, as illustrated in Fig. 2.11, a non-linear LGMD1 visual neural network was proposed by Badia et al. [18]; the functionality of this model fits well the non-linear properties of an LGMD1 neuron given by Gabbiani [3], and it possesses the invariance of collision detection to looming stimuli with varied shapes, textures and approaching angles [143]. Importantly, they demonstrated also the LGMD1 model can encode onset and offset response depending on luminance increments and decrements, like a seminal work with ON/OFF mechanisms proposed in [10]; this brings about different delayed information of excitations and inhibitions. Moreover, this model has been successfully implemented in a ground mobile robot and tested in an arena for collision detection.

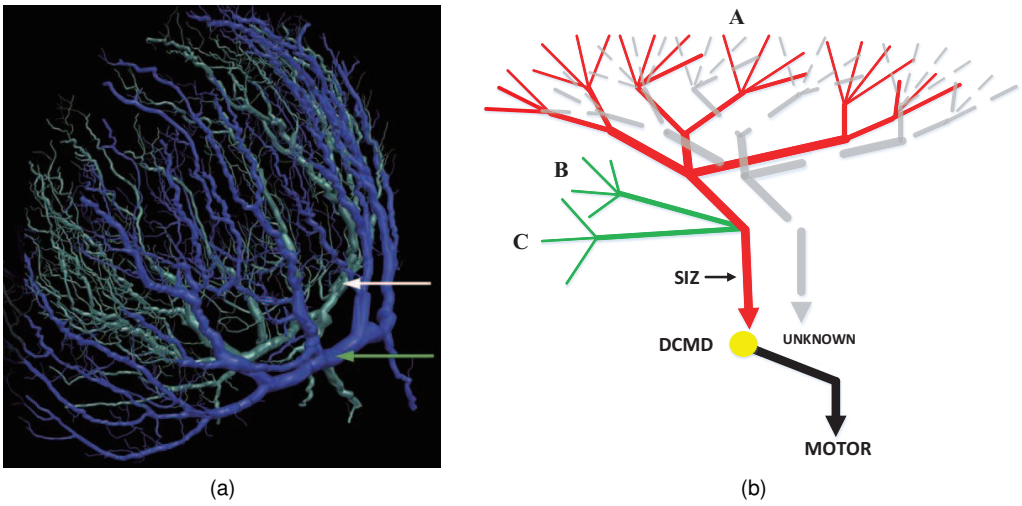

Figure 2.12: Neuromorphology of LGMDs: (a) 3D reconstruction of dendritic trees of LGMD1 and LGMD2 indicated by white and green arrows, respectively, adapted from [19] (Sztarker and Rind, 2014), (b) a schematic diagram of both the pre-synaptic and post-synaptic areas of LGMD1 (red) and LGMD2 (grey).

2.2.2 LGMD2-based Neuronal Models and Applications

Characterisation The LGMD2 neurone is a neighbouring partner to the LGMD1 as a looming detector, as well. It has close relation to the LGMD1 in not only neuromorphology but also neural characteristics and functionality [83, 116, 19, 80, 130, 128, 87]. On the aspect of neuromorphology, as illustrated in Fig. 2.12, the LGMD2 has similar large fan-shaped dendrite trees within its pre-synaptic area; however, comparing to the LGMD1, the lateral fields (B, C in Fig. 2.12b) that convey feed forward inhibitions are not found to the LGMD2, and moreover the post-synaptic target neuron to the LGMD2 has still been elusive. Importantly, a physiological study has demonstrated the development of both neurons in locusts, from adolescence to adulthood; this has pinpointed also that the LGMD2 neuron matures earlier in juvenile locusts that are lack of wings and living mainly on the ground [19]. As a result, LGMD2 neurones play crucial roles in juvenile locusts for looming perception and likely lead to hiding behaviours [19, 22].

More precisely, the specific living environment for young locusts endows the LGMD2 neuron a particular neuronal characteristic – it is only sensitive to darker looming objects with a light-to-dark luminance change tendency whilst not responding to oncoming brighter objects against dark background. Compared with the LGMD2 neuron, the LGMD1 neuron can respond to either dark or light objects that approach [83].

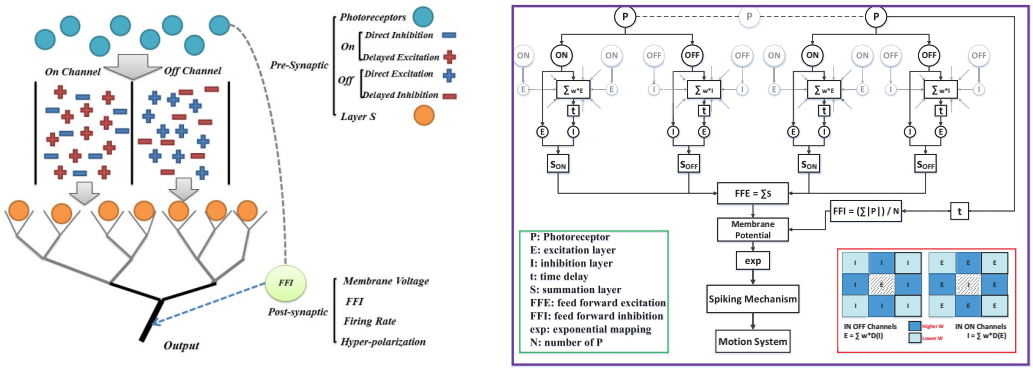

Figure 2.13: Schematics of LGMD2-based visual neural networks with ON and OFF mechanisms that encode brightness increments and decrements, separately: the ON channels are rigorously suppressed to realise the LGMD2's specific looming selectivity to dark objects. Figures (a) and (b) are adapted from [20] (Fu and Yue, 2015) and [21] (Fu et al., 2016).

Rind et al. recently has looked into the pre-synaptic neuropile layer of Medulla in the locust's visual brain; this proposed that the specific looming selectivity in both of the LGMDs has been formed well in the pre-synaptic fields [116]; however, the underlying mechanisms and structures remain largely unknown until today. While the biological substrate has not been fully identified, the computational modelling is of particular usefulness to study and simulate the functionality of visual motion sensitive neurons.

Computational models For computationally modelling the LGMD2, only a handful of studies have been proposed so far. A seminal work appeared in 2015; Fu and Yue proposed an LGMD2-based visual neural network to for the first time realise the particular selectivity of an LGMD2 neuron to light-to-dark luminance change by the modelling of ON and OFF mechanisms [20]; this separates luminance change into parallel channels and encodes both via spatiotemporal computations, as illustrated in Fig 2.13. More concretely, to achieve the specific looming selectivity of LGMD2, the ON channels are rigorously suppressed with a bias; the ON and OFF mechanisms also bring about different temporally delayed information in each separate pathway. The effectiveness of the LGMD2-based visual neural network, as an embedded vision system, has been validated by a vision-based micro-robot in arena tests [21, 22], as illustrated in Fig. 2.14. For the first time, the specific functionality of an LGMD2 neuron revealed by biologists have been demonstrated fully by these computational

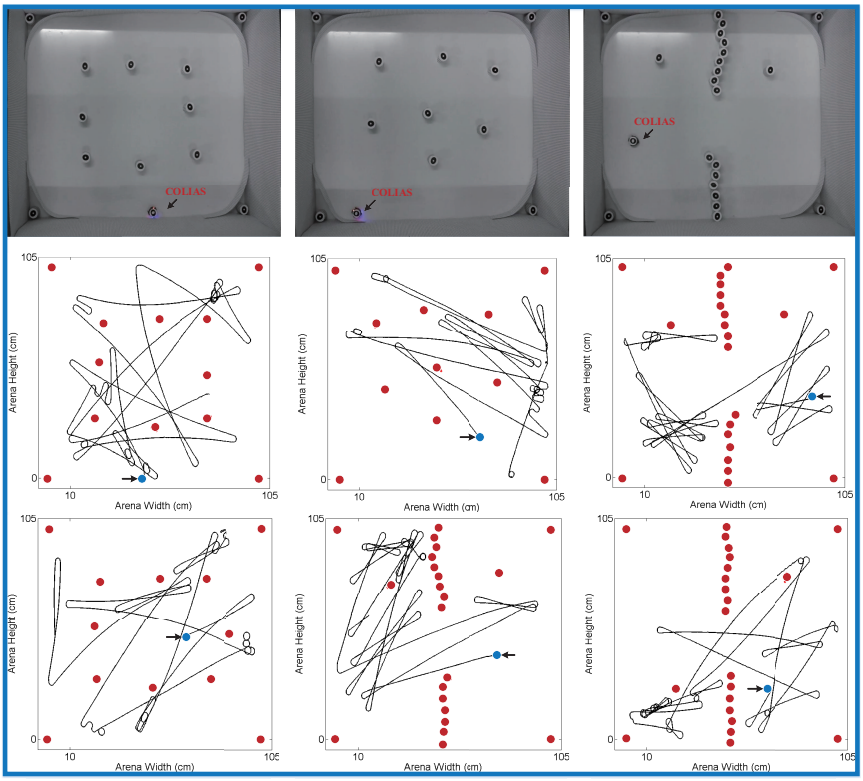

Figure 2.14: Robot arena tests implemented with an LGMD2 neural network: the micro-robot was tested by different layouts and densities of obstacles in an arena. The black line indicates robot overtime trajectory; the red circle denotes the obstacles; the blue circle indicates the start position of robot. The experimental data is adapted from [21] (Fu et al., 2016).

models; compared with the LGMD1, it only responds to the looming of dark objects and briefly to the receding of light objects representing a preference to light-to-dark luminance change, as depicted in Fig. 2.16a.

For further investigating the different looming selectivity between the LGMD1 and the LGMD2, Fu et al. proposed a hybrid visual neural model, as an embedded vision system, that was smoothly implemented in an autonomous micro-robot for collision detection in dynamic robot scenes [55]. In this research, both the LGMDs in a micro-robot were tested in an arena mixed with multiple robots in dark and bright environments, respectively. Each looming sensitive neuron handles a half region of the receptive field for a bilateral control of robot avoidance behaviours [55]. The bio-robotic test results demonstrated clearly the robustness of both LGMDs in collision detection, and more important, verified the realisation of different collision selectivity between the two neurons via the modelling of ON and OFF mechanisms. It is also worth to notice that for ground robotic navigation, the LGMD2-based collision-detecting sys-

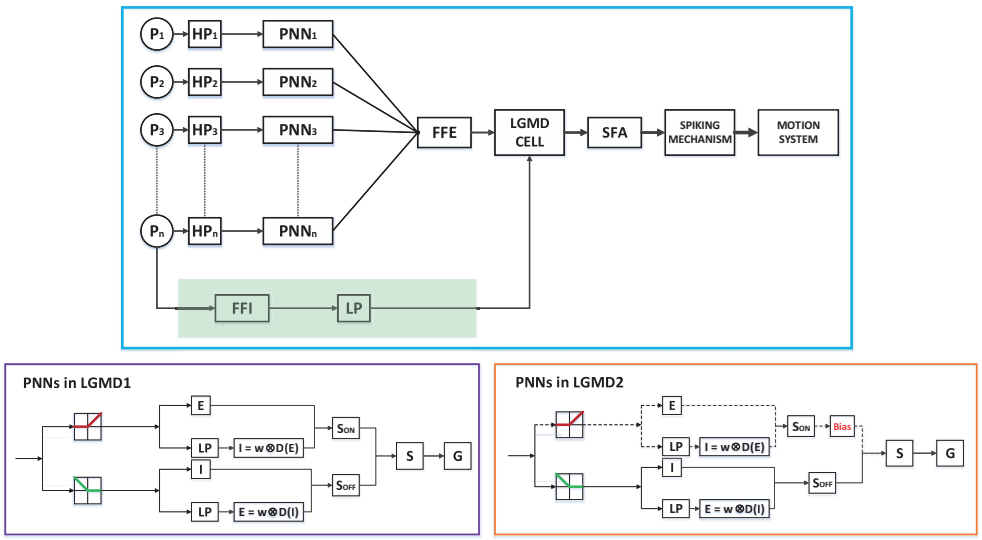

Figure 2.15: Schematic of a general LGMDs model [22] (Fu et al, 2017): in this visual neural network, the functionality of ON and OFF pathways and spike frequency adaptation mechanism are modelled. This universal LGMDs model can realise the characteristics of both the LGMD1 and LGMD2 neurons, each of which has specific partial neural networks.

tems can outperform the LGMD1-based models, since the former has been pinpointed the enhanced looming selectivity to darker approaching objects [20, 21, 22, 55]. With similar ideas of the modelling of ON and OFF mechanisms in the LGMDs neuronal model, Fu et al. recently proposed a general LGMDs model, as illustrated in Fig. 2.15, which can realise the underlying functionality and characteristics of both the LGMD1 and the LGMD2 visual neurones [23].

To briefly summarise, these LGMD2-based visual neural networks have demonstrated both the efficacy and efficiency of the modelling of ON and OFF mechanisms in locust looming detectors. Although there is little physiological evidence of the existence of such polarity pathways in the locust's visual brain [77, 117], these computational modelling works can evidence similar mechanisms in the locust's motion-detecting pathways [23].

2.2.3 Methods to Mediate the Looming Selectivity

The looming selectivity to moving objects that approach over other kinds of visual challenges has been formed very well in locusts through millions of years of evolutionary development. The locust LGMDs neurons are robust to spike most frequently to

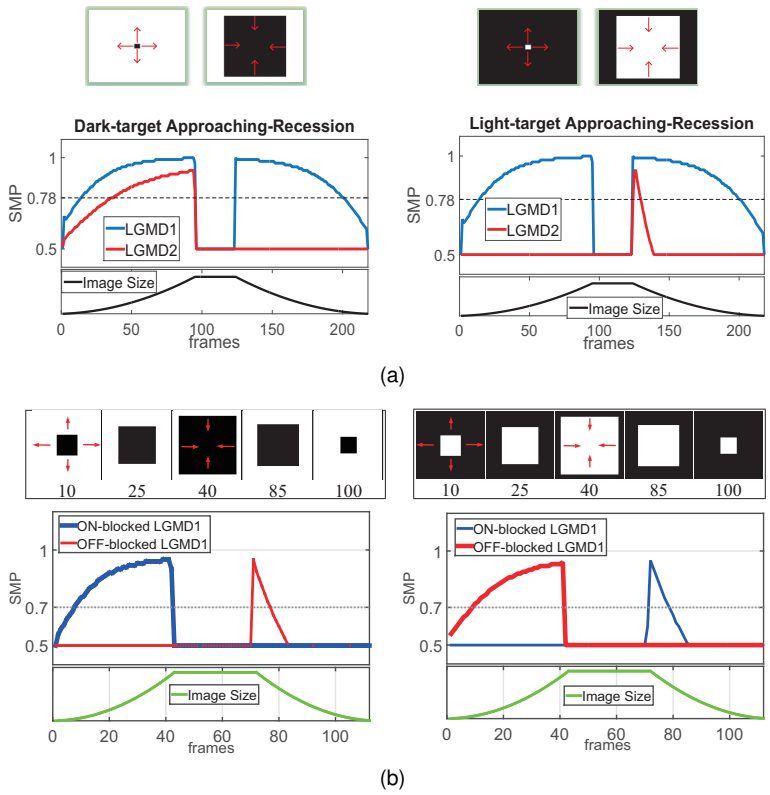

Figure 2.16: Results of shaping the looming selectivity between LGMD1 and LGMD2 neuronal models with the modelling of ON and OFF pathways and spike frequency adaptation: (a) the LGMD2 responses to dark and light looming-receding movements, compared to an LGMD1 model [6], adapted from [22] (Fu et al., 2017), (b) the effects of shaping the looming selectivity in an LGMDs general visual neural network by blocking either ON/OFF pathways, adapted from [23] (Fu et al., 2018).

looming stimuli. However, from the perspective of computational modellers, it is still an open challenge to shape the looming selectivity in looming sensitive neural systems. In the future, artificial machines should possess similar ability to locusts with efficient and robust collision-free systems in navigation. This requires the collision-detecting systems can well discriminate approaching objects from other kinds of visual stimuli.

There have been a few methodologies proposed to mediate the looming selectivity. Rind et al. demonstrated that two kinds of inhibitions – the pre-synaptic lateral inhibitions and the feed forward inhibition can cooperatively mediate the looming selectivity; this effectively cuts down the excitation caused by receding and translating stimuli [79]. Gabbiani et al. showed also the non-linear computations make the neuron liable to differentiate looming from receding stimuli [143]. In addition, they revealed an intrinsic neural property of such looming sensitive neurons, that is, spike frequency adaptation (SFA), which leads the LGMD1 to discriminate objects that approach from

recession and translation, well [4, 51, 162].

However, for computationally modelling these mechanisms, there is a trade-off between the algorithmic efficiency and the effectiveness of the mediation of looming selectivity. Computational modellers have always been trying to balance both, in order to facilitate the applications to intelligent machines like mobile robots and etc. Yue and Rind proposed a hybrid neural system by incorporating a translating sensitive neural network, in order to extract colliding information from complex dynamic scenes [163]; this effectively handled driving scenarios. Meng et al. designed a new post-synaptic organisation of LGMD1 neuronal model to monitor the gradient change of model output – the normalised membrane potential, for discriminating approach from recession [13] (Fig. 2.10d); this was also smoothly implemented in the FPGA [14]. In addition, a neural network of directional motion-detecting neurons in locusts was integrated with the LGMD1 neural network to ensure the recognition of imminent collision [164]; in this research, the field of view was manually divided into different regions processed by specialised neurons, separately. More recently, Fu et al. has demonstrated both the efficacy and efficiency of combining two bio-plausible mechanisms – ON and OFF pathways and spike frequency adaptation to shape the looming selectivity and separate the functionality between the LGMD1 and the LGMD2 neuronal models [55, 23, 22]; these has been validated by bio-robotic tests on embedded system. Some example results are illustrated in Fig. 2.16b to clarify the effects of separating visual processing in parallel pathways to achieve different looming selectivity between LGMD1 and LGMD2, and differentiate darker/brighter objects that approach from moving away.

2.3 Translating Sensitive Neural Systems

This section reviews computational models and applications of translating sensitive visual motion detectors and neural networks inspired by both the locust and the fly visual systems. First, the modelling of directionally selective motion-detecting neurons in locusts, namely locust direction selective neurons (DSNs) will be introduced in Section 2.3.1. Then, we review a classic model of fly elementary motion detectors (EMDs) and corresponding applications to flying robots in Section 2.3.2. After that, the cutting-

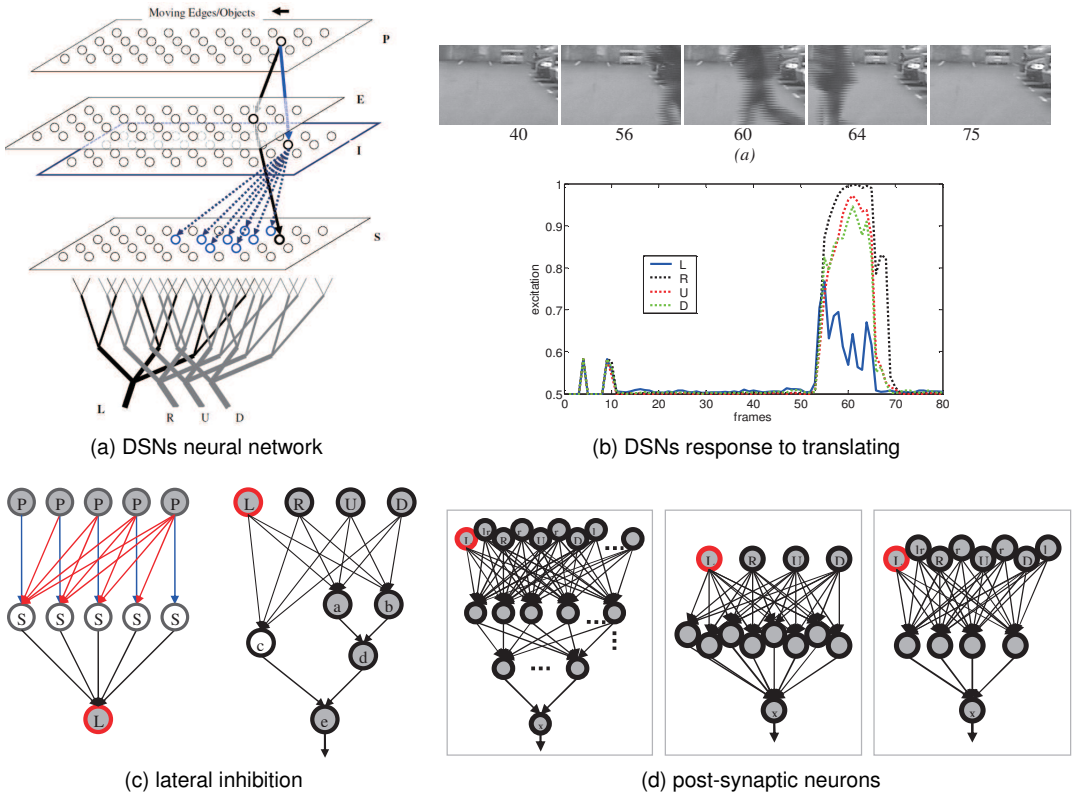

Figure 2.17: Schematics of locust DSNs visual neural networks with both pre-synaptic and post-synaptic structures, adapted from [24, 25] (Yue and Rind, 2007, 2013).

edge biological findings and computational models of fly ON and OFF pathways and lobula plate tangential cells (LPTCs), namely fly DSNs, will be presented in Section 2.3.3.

Compared to the non-directional neurons like the looming sensitive neurons, the research of DSNs in animals has a much longer history; it can be even dated back to two centuries ago. Franceschini pointed out that an initial idea of 'directionally selective motion sensitive cells' was proposed by Exner early in 1894 [27]. The past several decades have witnessed much progress in our understanding of the cellular mechanisms underlying the DS. The DSNs have been found in many animal species; these include invertebrates like flies [90], locusts [87] and etc, as well as vertebrates like rabbits [91], mice [58] and etc. Borst and Helmstaedter have demonstrated the similarities of circuits and algorithms in design of insects' and vertebrates' motion detection systems for translating perception [58]. Here, we focus on presenting the possible methodologies adopted by insects.

2.3.1 Computational Models of Locust DSNs

For locusts, Rind explored the characteristics of DSNs in 1989, physiologically and morphologically [87, 86]. These neurons respond to horizontal directional motion; they are rigorously excited by visual stimuli in preferred direction (PD) and inhibited by movements in null (non-preferred) direction (ND).

On the basis of these biological findings, a few computational models have been proposed by Yue and Rind [24, 25]. Generally speaking, these translating sensitive visual neural networks have been applied for collision recognition, especially in driving scenarios. Interestingly, as illustrated in Fig. 2.17, these locust DSNs models arise from the LGMD1-based visual neural networks, the computational structure of which has similarities to the modelling of LGMD1, yet with different lateral inhibition mechanisms. More concretely, in the LGMD1 neural networks, the inhibitions spread out to the surrounding areas of a corresponding excitatory cell, symmetrically (Fig. 2.6); on the contrary, in the DSNs neural networks, the inhibitions spread out, asymmetrically and directionally, as shown in Fig 2.17a and 2.17c. Therefore, the specific DS can be shaped by such directional lateral inhibitions mechanism that cuts down excitations. For example, with a strong inhibition from the right side with temporal delay, the excitation caused by left moving edges can be eliminated or attenuated (Fig. 2.17b). Likewise, each directionally sensitive cell is inhibited by the same directional motion. With design of post-synaptic networks, this can recognise impending collision caused by objects that approach, angularly. Furthermore, Yue and Rind extended the functionality of DSNs visual neural network to sense four and eight directional motion with similar methods; they also investigated the effects of different postsynaptic organisations on collision detection via evolutionary processes, as depicted in Fig. 2.17d [25].

It appears that the locust DSNs and LGMDs models are both effective solutions to collision detection. A question emerges that which type of visual neurons in locusts could play dominant roles of collision recognition. To address this, Yue and Rind designed a hybrid visual neural network integrating the functionality of both neural networks [26], as illustrated in Fig. 2.18. In this research, two individual neural net-

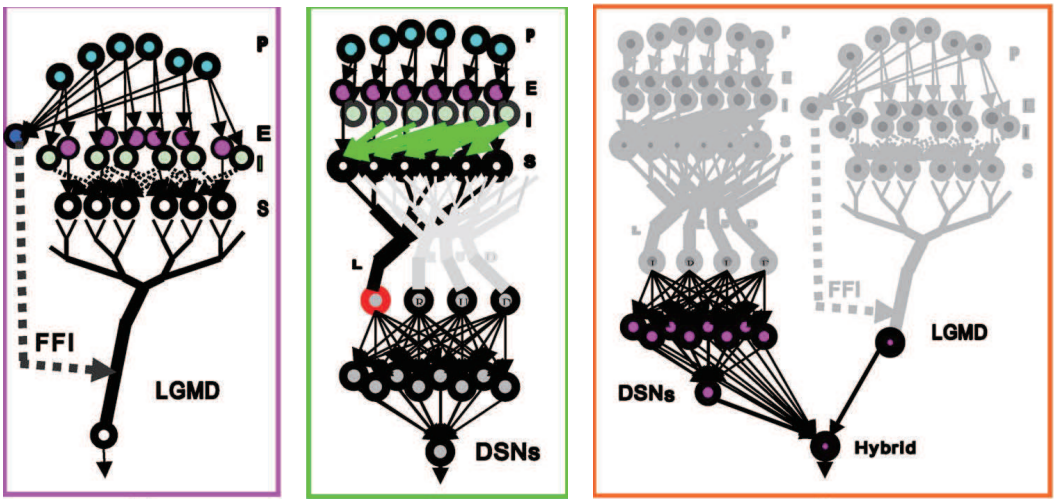

(a) LGMD1 model (b) DSNs model (c) Hybrid model

Figure 2.18: Schematic of a hybrid visual neural network with three sub-models competing for the collision recognition role by genetic algorithms, adapted from [26] (Yue and Rind, 2013).

works competed with the hybrid neural network via a switch gene and evolutionary computation methods. As a result, the LGMD1-based neural network outperforms other forms of computational models for collision recognition as a low-consumptive and reliable approach.

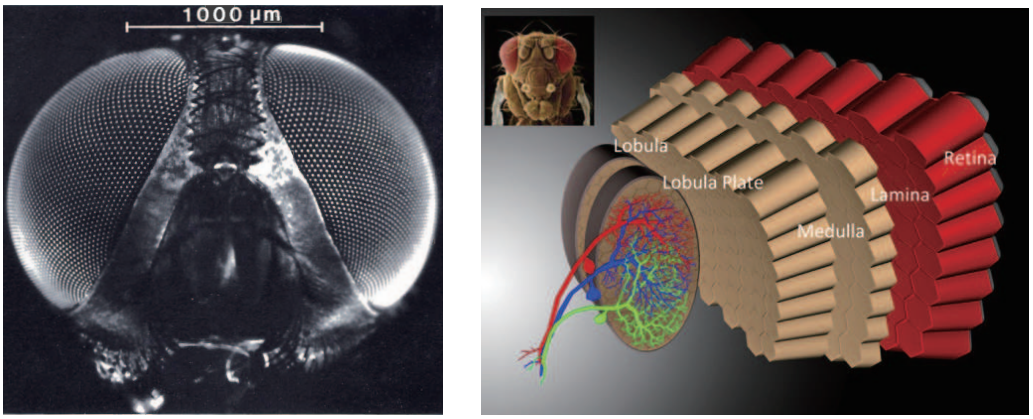

(a) Fly compound eyes (b) Fly visual neuropile layers

Figure 2.19: Illustrations of fly compound eyes (a) and underlying neuropile layers (b) for motion perception, adapted from [27] (Franceschini et al., 1989) and [28] (Borst and Euler, 2011), respectively.

2.3.2 Fly EMDs and Optic Flow Strategy

Background Compared with research in locust DSNs, a much larger number of studies have been concentrated on the fly DSNs since the appearance of seminal work-

s early in 1890s [27]. As introduced in Chapter 1, fly visual systems are prominent models for studying biological motion-detecting methods for constructing artificial dynamic vision systems, from early stages [89, 90, 61, 125, 126]. With development of biological techniques, the fundamental structures of neuropile layers and cellular implementations in the fly preliminary motion vision pathways have been better explored and studied by biologists, with a good number of papers, e.g. [27, 34, 106, 165, 112, 105, 107, 166, 112]. In addition, researchers have attempted the understanding of underlying mechanisms to form the DS to translating stimuli, in order to facilitate the computational modelling of fly DSNs [110, 111, 30, 112, 38]. Fig. 2.19 illustrates fly compound eyes and underlying neuropile layers of preliminary visual pathways for motion perception.

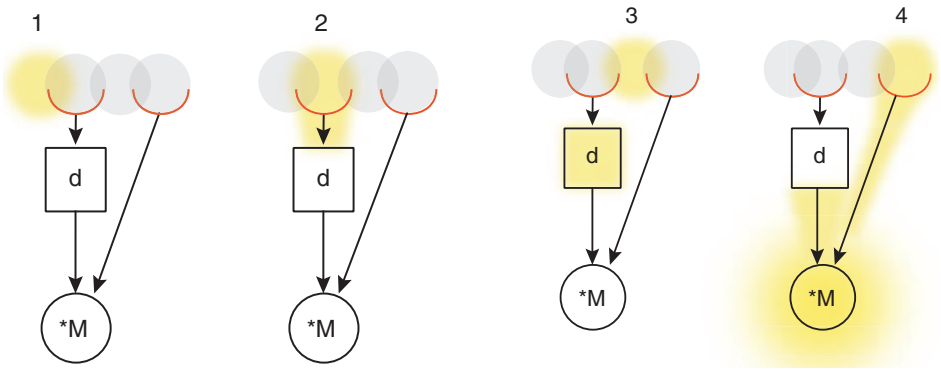

Figure 2.20: Schematic of an EMD process in four steps: d and M indicate a time delay and a multiplication process on correlated signals from two sensitive cells (red). These are adapted from [29] (Frye, 2015).

Fly motion detectors For defining the computational roles of fly motion detection, a few theories have been proposed in the past half-century, as summarised in [30] (Fig. 2.21). A classic and elegant mathematical model was proposed by Hassenstein and Reichardt to account for translational motion perception of animals [89]. It was named as 'HR detector' or 'HRC' (Hassenstein-Reichardt Correlation) model; this has become commonly referred to as Reichardt detectors or simply the EMDs [167, 125, 168, 29]. As illustrated in Fig. 2.20, it is devised to explain motion perception strategy by the activity of adjacent photoreceptors in the field of view. We can summarise that the EMD has the following characteristics for translating detection:

1. The direction of motion can be recognised only by comparing the activity of at

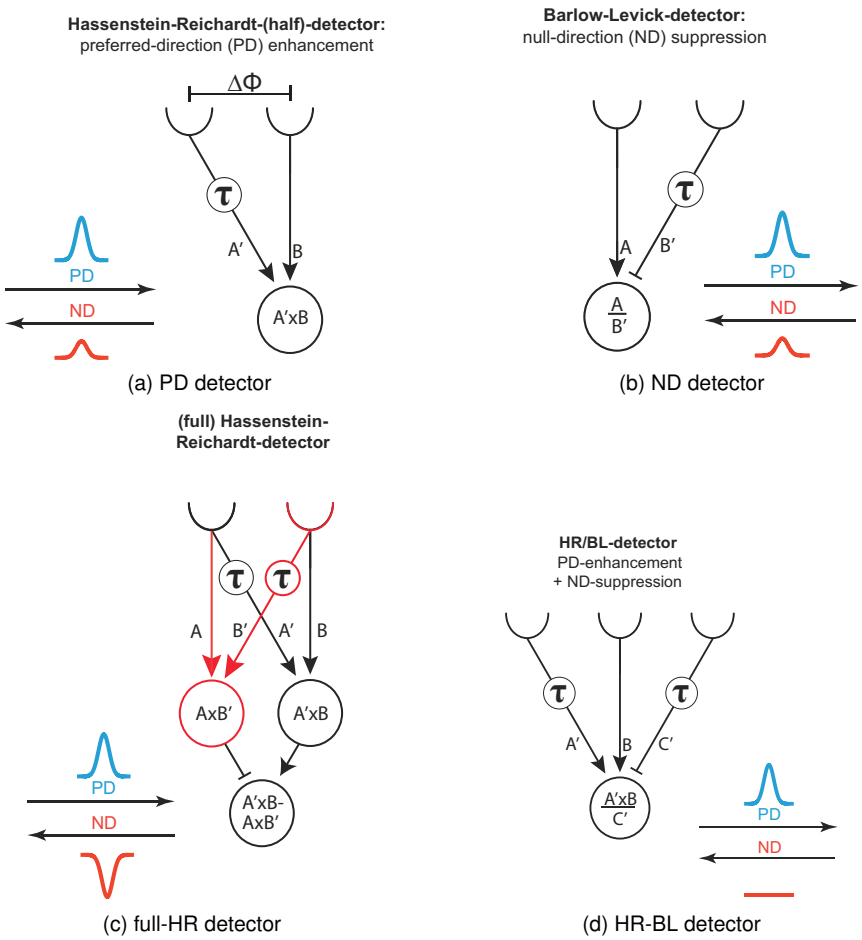

Figure 2.21: Schematics of a variety of classic fly motion detectors adapted from [30] (Arenz et al., 2017).

least two correlated photoreceptors in space.

2. The EMD can not tell the true velocity of a translating pattern; it is sensitive to the spatiotemporal frequencies of stripes that pass over the stationary detectors.

3. It is also affected by the contrast between a moving pattern and its background, that is, the model responds more strongly to higher contrast translating objects with an identical speed.

4. There are two basic parameters in the EMDs – the spacing between a pairwise detectors and the temporal delay in the low-pass filters; both influence significantly the detection of motion direction and intensity.

Recently, two studies in fly motion detectors [30, 38] brought together previous famous algorithmic models of visual motion detection in the literature, like the HR half-detector (Fig. 2.21a) to enhance motion in PD, the Barlow-Levick (BL) detector

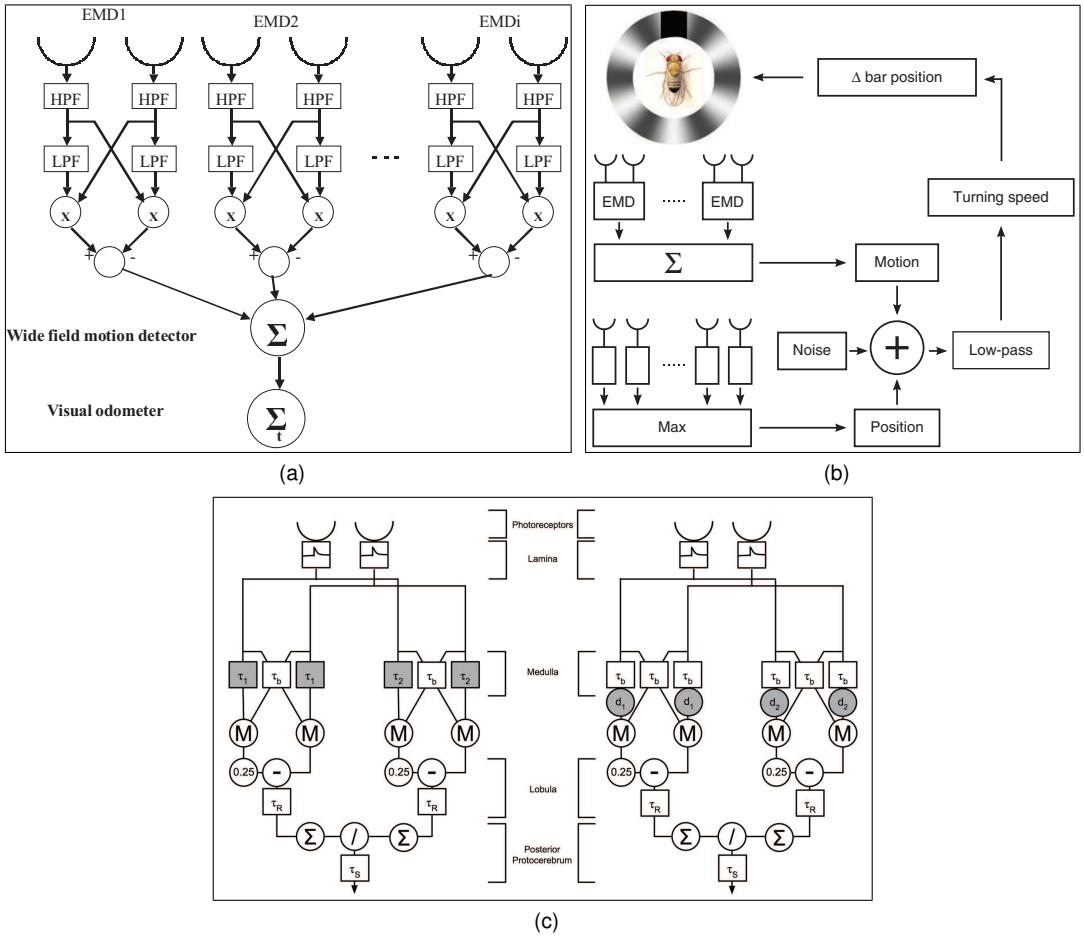

Figure 2.22: A variety of EMDs model: (a) this integrates each pairwise EMDs to compute the visual odometer, adapted from [31] (Iida and Lambrinos, 2000); (b) this model is used to simulate fly fixation behaviour by combining the EMDs with an individual location pathway, adapted from [32] (Bahl et al., 2013); (c) these are two version of models for estimating angular velocity in the bee brain, adapted from [33] (Cope et al., 2016).

(Fig. 2.21b) to suppress motion in ND, and the full HR detectors (Fig. 2.21c) that map PD and ND motion to positive and negative outputs, respectively. More importantly, both proposed that both the HR and BL mechanisms work in different sub-regions of fly receptive field [38]. It also appears that visual motion detection in flies relies upon the processing of three input channels that integrates a HR detector with a BL detector [30], as illustrated in Fig. 2.21d.

EMDs-based models and OF-based strategies There are quite a lot of computational models and applications that arise from the EMDs. A main utility of EMDs is to mimic fly and bee optic flows (OF) in the receptive field, e.g. [169, 170, 171, 172, 173, 34]. As illustrated in Fig. 2.23a, the OF can be defined as a flow vector-field perceived

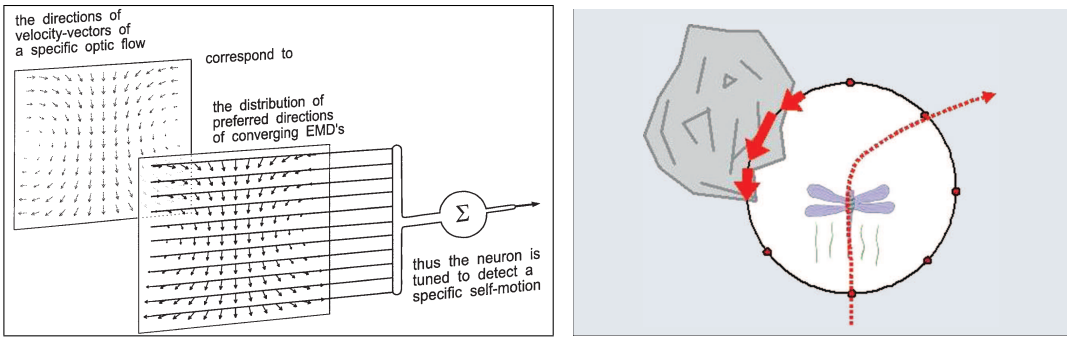

Figure 2.23: Fly optic flow strategies based on the EMDs: (a) an integration of local optic flow for the estimation of self-motion, adapted from [34] (Krapp et al., 1998), (b) a collision avoidance strategy based on optic flow by a dragonfly, adapted from [35] (Green and Oh, 2008).

by the visual modality of either animals or machines [34, 59]; this field is generated by the relative and apparent motion between an observer and the scene. The OF includes two sub-fields of translational flow and rotational flow; both are rigorously dependent on the structure of the environment including the textures and brightness and etc. Most Importantly, such a visual strategy can be used to conduct various forms of insect behaviours, like landing [174, 120], terrain following [59], tunnel crossing [119], corridor-centring response [175, 33], collision avoidance [109, 176] (Fig. 2.23b), target tracking [113] and fixation behaviours [32] and etc.

More specifically, Iida proposed a method to integrate each pairwise local EMDs, spatially and temporally, to compute the visual odometer over time (Fig. 2.22a); this approach was validated by navigation of a flying robot [31, 177]. Snippe and Koenderink demonstrated possible solutions to extract optical velocity by the design of ensembles of HR detectors [178]. Zanker et al. investigated the speed tuning and estimation of EMDs [179, 180]; they also analysed video sequences of outdoor scenes from a panoramic camera and performed optic flows as motion signal maps using two dimensional EMDs [181]. Rajesh et al. modified the traditional HR detector to improve the velocity sensitivity and reduce the dependence on contrast and image structure; this matched the neurobiological findings that an adaptive feedback mechanism is effective to normalise contrast of input signals in order to improve the reliability of velocity estimation [182]. In addition, Bahl et al. incorporated in the EMDs a parallel position pathway to track a translating stripe or object and mimic a behavioural

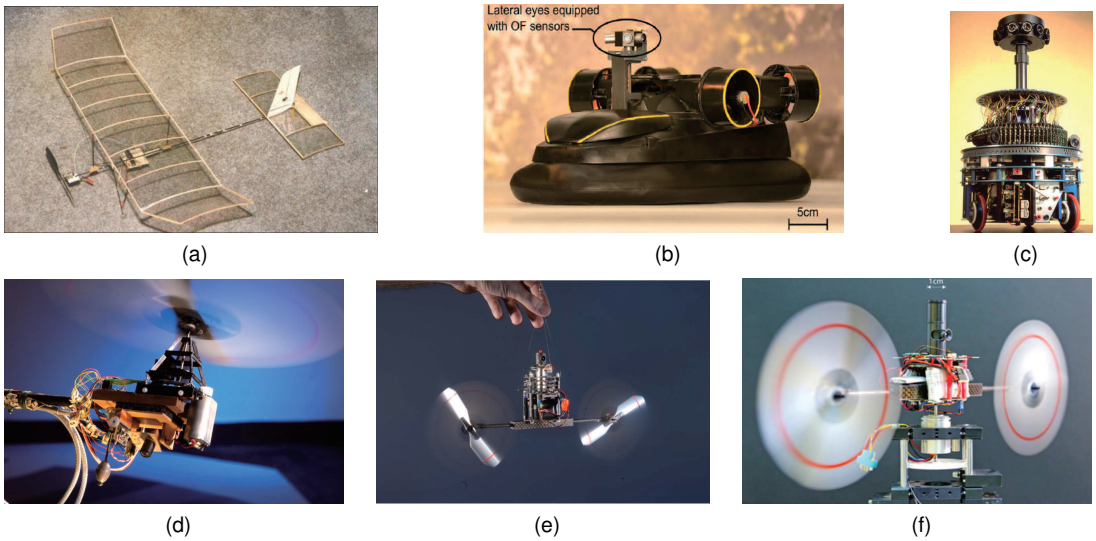

Figure 2.24: Instances of bio-robotic applications of fly EMDs and OF: (a) the prototype of a lightweight wingspan fly (fixed-wing hovering MAV) with two cameras that sense optic flow, adapted from [35] (Green and Oh, 2008), (b) the prototype of an autonomous sighted hovercraft with OF sensors, adapted from [36] (Roubieu et al., 2014), (c) the 'Robot Fly' developed in 1991, equipped with a panoramic compound eye implementing an array of hundred of EMDs, (d) a $100 - g$ micro-helicopter equipped with a single ventral OF sensor, (e) a flying robot named 'OSCAR I' with $0.1 - kg$ mass equipped with a micro-scanning eye, (f) a flying robot named 'OSCAR II', (c) – (f) are adapted from [37] (a review by Franceschini, 2014).

response to fixation, as shown in Fig. 2.22b; this was reconciled with physiological recordings from motion-blind flies very well [32]. As a variation of the EMDs, a few angular velocity detectors models was proposed to account for corridor-centring behaviours of bees [33, 183], as illustrated in Fig. 2.22c; similarly to [31], the integrated response can be used as a visual odometer. Moreover, there also have been studies on the temporal adaptation of EMDs [184, 168], the contrast sensitivity of EMDs [185], and an EMDs-based algorithm for global motion estimation [186], as well as a non-directional HR detectors model for simulating insect speed-dependent behaviour [187] and etc.

Applications to robotics The computational effectiveness and simplicity for translational motion perception have been demonstrated by the considerable number of modelling studies on the fly EMDs and OF strategies. These can be used to design and construct mini-robots in order to control their navigation on the basis of the bio-inspired motion detectors. As some instances of bio-robotic applications shown in Fig. 2.24,

fly EMDs and OF can be applied to guide robots, especially flying robots, the navigation with insect-like behaviours, such as collision avoidance [35, 37, 59] (Fig. 2.24a, 2.24c), tunnel crossing [188, 36, 59] (Fig. 2.24b), terrain following, take-off and landing behaviours [37] (Fig. 2.24d, 2.24e, 2.24f). As introduced in Section 2.1.2, there have been two prominent review papers that introduce relevant bio-robotic approaches of fly EMDs and OF, systematically [37, 59].

2.3.3 Modelling of Fly ON and OFF Pathways and LPTCs

Background Within this subsection, we present the state-of-the-art biological research in fly visual systems, which have attempted to understand the underlying circuits with complex functions in fly visual brains for preliminary motion detection. We have now understood from Section 2.3.2 that visual neurons compute the direction of motion conforming to a HR detector; flies and bees apply the EMDs to sense optic flows, such a strategy of which is effective to deal with a variety of navigating behaviours. However, a question still remains here: where does the optic flow is processed by neurons in the fly visual circuits, and how does it connect to corresponding visuomotor response?

Biological exploration To address these, fly ON and OFF parallel visual pathways and LPTCs have been evidenced the proper places to carry out directionally selective signal processing, as illustrated in Fig. 2.25a [61, 62, 28, 58]. A seminal work by Franceschini et al., early in 1989, proposed a transient ON-OFF nature of EMD response in the housefly; in this research, a splitting of an EMD into an ON-EMD and an OFF-EMD was demonstrated to sense light and dark edge translating, respectively [27]. Though the underlying neural mechanisms and circuits in fly visual systems still remain largely unknown until today, a good number of physiological researches have contributed to explore the flies' visual brains and study the cellular implementations that generate the DS to translating in neuronal levels, particularly in the recent two decades [98, 108, 110, 111, 30, 38, 112, 189, 190, 191, 96, 192, 101, 106]. A nice progress was made by Joesch et al. in 2010; they looked into the downstream processing of photoreceptors and found that the visual signals are split into two parallel

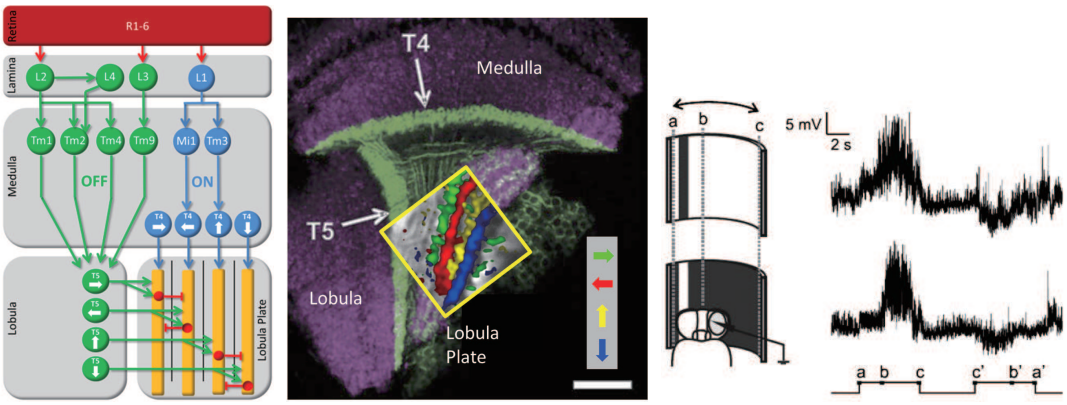

Figure 2.25: Schematic diagrams of fly preliminary motion-detecting neuropile layers: (a) The underlying ON and OFF pathways with interneurons and LPTCs perceive visual motion stimuli and generate the DS. (b) The neuromorphology of fly visual circuits – the LPTCs pool directionally specific motion signal, individually into each sub-layers. (c) The LPTCs respond to directional translating stimuli by movements of dark and light bars, respectively. (a), (b) are adapted from [38] (Haag et al., 2016) and (c) is adapted from [28] (a review by Borst and Euler, 2011).

polarity pathways by L1 (ON) and L2 (OFF) interneurons in the neuropile layer of Lamina [93] (Fig. 2.25a). After that, Maisak et al. revealed the characteristics of T4 and T5 cells in the neuropile layers of Medulla and Lobula [97] (Fig. 2.25a). In addition, a group of LPTCs in the Lobula Plate has been also identified [97, 193, 99, 165] (Fig. 2.25b). Importantly, LPTCs have been demonstrated to process the optic flow field sensed by photoreceptors on a higher level corresponding to the control of visual flight course [59]. Furthermore, as shown in Fig. 2.25c, the LPTCs are rigorously activated by PD motion yet inhibited by ND motion underlying the DS.

On the basis of these biological findings, we can draw a directional tuning map of fly preliminary visual processing through multi-layers to demonstrate the following courses for translational motion perception in fly visual brain, according to Fig. 2.25a:

1. The motion detection starts with splitting visual signals captured by photoreceptors in the first Retina layer into two parallel ON and OFF pathways; this is done by the large mono-polar cells (LMCs) – L1 and L2 in the Lamina layer.

2. L1 interneurons convey onset response by luminance increments to neurons in the Medulla layer; whilst L2 interneurons relay offset response by luminance decrements to neurons in the Lobula layer.

3. The EMDs are equipped to the T4 cells in the Medulla layer in the ON pathway, and the T5 cells in the Lobula layer in the OFF pathway in order to generate directional motion signals. It is worth emphasising that the four cardinal directions are formed in different groups of T4 and T5 cells, separately.

4. Finally, the LPTCs integrate signals from ON and OFF channels in the Lobula Plate; motion information with an unanimous direction congregates at a same sub-layer and jointly flow downstream to circuits like motion-driven neural systems (Fig. 2.25a and 2.25b).

5. There is another pathway, that is, the L3–Tm9–T5 (Fig. 2.25a) that provide locational information of objects to the OFF pathway and is regardless of the direction of motion [189]; this hits at usefulness of conducting fly fixation behaviour [32].

ON and OFF motion detectors Since the cellular implementations of EMDs have been demonstrated to happen in the ON and OFF pathways, there are a few fly motion detectors been proposed, as illustrated in Fig. 2.26; these fundamental computations conform to the full HR detectors. More precisely, a 4-Quadrant (4-Q) detector encodes input combinations of ON-ON, OFF-OFF, ON-OFF and OFF-ON cells, which mathematically corresponds to the traditional EMDs (Fig. 2.26a). Eichner et al. proposed a 2-Quadrant (2-Q) motion detector, as illustrated in Fig. 2.26b; this processes input combinations of only same sign signals, i.e., ON-ON in the ON pathway and OFF-OFF in the OFF pathway [39]. In addition, they revealed also a small fraction of original signals can pass through into the motion-detecting ON and OFF pathways; this demonstrates that not only the transient luminance change but also the permanent brightness can be encoded to generate directional motion. Moreover, Clark et al. demonstrated a 6-Quadrant (6-Q) detector through behavioural experiments on fruit flies, as illustrated in Fig. 2.26c; this model was constructed to match the behavioural observations in L1 and L2 blocked flies [40]. In this computational theory, either polarity pathways convey positive and negative contrast changes with edge selectivity to motion detection circuits. To make a decision between these alternatives to motion detection in flies, a

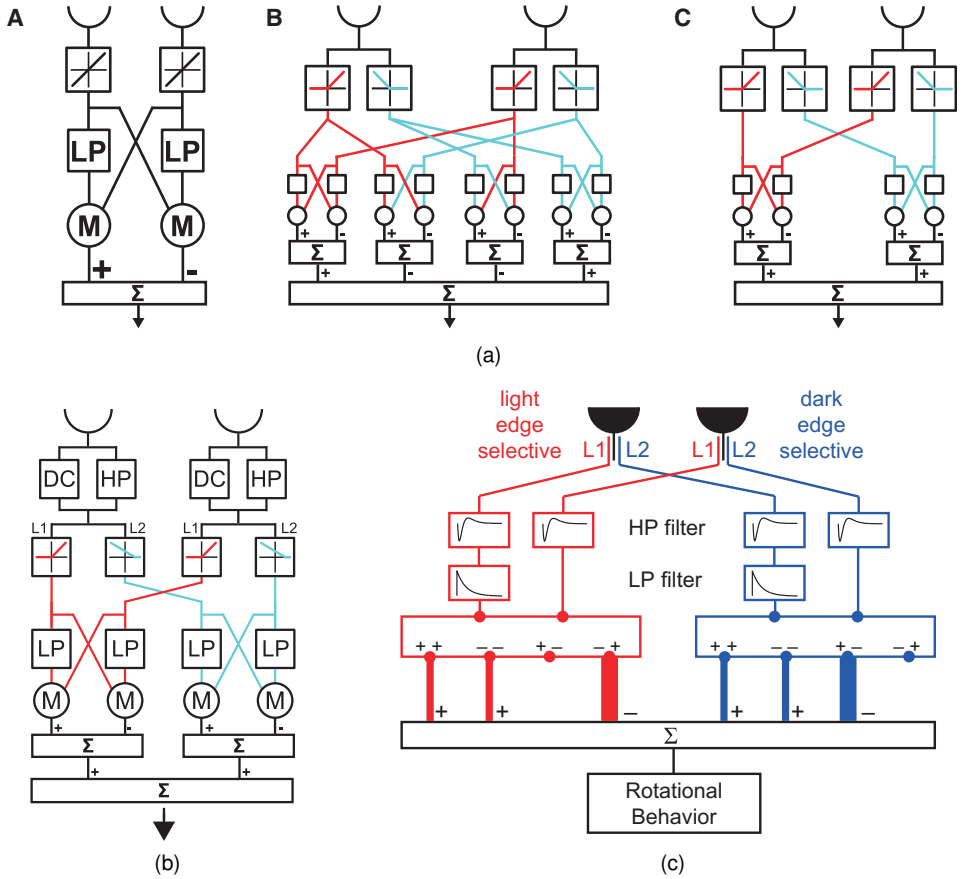

Figure 2.26: Schematics of classic fly motion detectors with different combinations of ON and OFF detectors: (a) three basic types – a pairwise EMDs (A), a 4-Q model (B) and a 2-Q model (C), adapted from [39] (Eichner et al., 2011), (b) the 2-Q detector with input combinations of the same sign polarity detectors, adapted from [39], (c) a 6-Q detector processes ON and OFF edge information in both pathways, adapted from [40] (Clark et al., 2011).

case study evidenced the existence of two over six quadrants detectors, by genetically silencing either ON or OFF pathway, respectively [94].

Computational models These different fly motion detectors significantly benefit our understanding of complex fly visual systems; however, there is vacancy in systematic modelling and testing of fly ON/OFF motion detectors and LPTCs in visually cluttered real world scenes. To fill this gap, recently, Fu and Yue proposed a fly DSNs model with ensembles of 2-Quadrant detectors to extract translational motion cues from a cluttered real physical background [53]; they also extended this visual neural network to a behavioural response to fixation, by incorporating in a newly-modelled position pathway of the L3-Tm9-T5 (Fig. 2.25a) [52], and then successfully implemented it on the embedded system [194]. Likewise, Wang et al. estimated the background motion

by LPTCs responses; in this modelling study, a maximisation operation mechanism was proposed to simulate the functionality of the wide-field Tm9 neurons [102].

2.4 Small Target Motion Sensitive Models

In previous sections, we have reviewed insect motion sensitive systems that possess specific DS to looming and translating visual stimuli. This section reviews computational models of a specific group of visual neurons including small target motion detectors (STMDs) in Section 2.4.1 and figure detection neurons (FDNs) in Section 2.4.2 that have particular size selectivity to small target motion, with relevant biological findings about STMDs and FDNs in the insects' visual systems.

Due to the long sight distance, targets such as mates or preys, always appear as small dim speckles whose size may vary from one pixel to a few pixels in the field of view. Being able to detect such small targets in a distance and early, could endow insects with more competitiveness for survival. However, from the perspective of computational modellers, small target motion detection against naturally cluttered backgrounds has been considered as a challenging problem; this include several aspects: (1) small targets cannot provide sufficient visual features, such as shape, color and texture, for target detection; (2) small targets are often buried in cluttered background and difficult to separate from background noise; (3) ego motion of the insects may bring further difficulties to small target motion detection. These challenges have been solved well by insects after long-term evolutionary development, and their small target motion detection visual systems are efficient and reliable.

2.4.1 Small Target Motion Detectors

Biological research In the insect visual systems, a class of specific neurons, called small target motion detectors (STMDs), is characterized by their exquisite sensitivity for small target motion. STMD neurons have been observed in several insect groups, including hawkmoths [195], hoverflies [196], and dragonflies [197, 198, 199]. In the past two decades, the anatomy and physiology of STMD neurons have been further

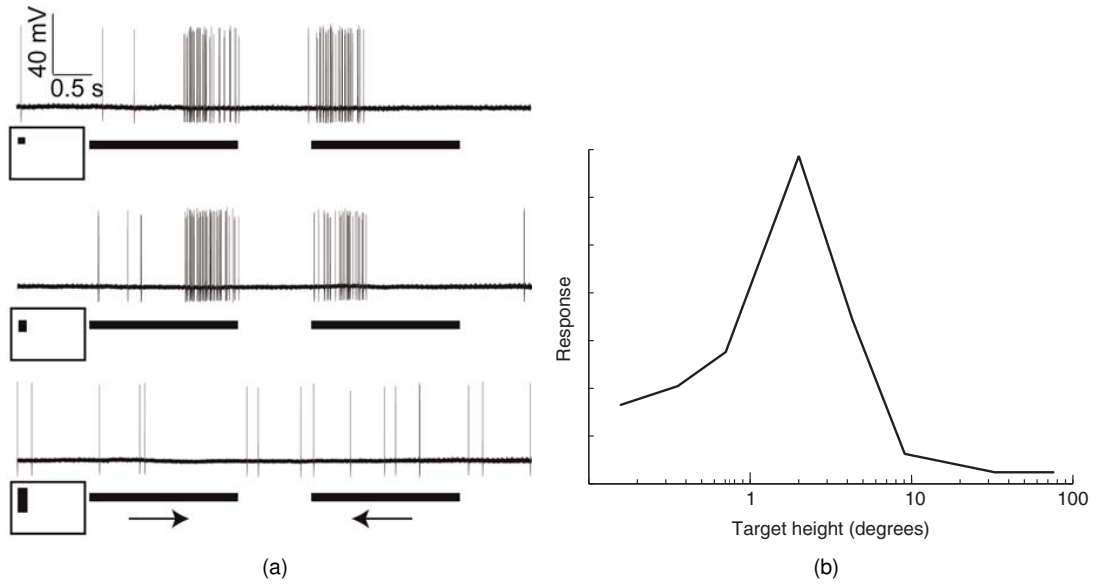

Figure 2.27: STMD neuronal raw responses: (a) neuronal responses to motion of three different-sized targets ($0.8°$, $3°$, or $15°$ high by $0.8°$ wide) drifted against bright backgrounds: the horizontal bars indicate the movement duration and the arrows denote the direction of target motion, adapted from [41] (Nordstrom et al., 2006). (b) the response of an STMD to targets of varying height, adapted from [42] (Nordstrom, 2012).

investigated [200, 41, 201, 45, 42, 202, 203].

The most significant difference between STMDs and other motion-sensitive neurons, like LGMDs and DSNs and etc., is that the STMDs have specific size selectivity. More precisely, STMDs represent peak responses to targets subtending $1 - 3°$ of the field of view, yet have no response to larger bars (typically $> 10°$) or to wide-field grating stimuli [41, 42]. To clearly demonstrate the size selectivity of STMD neurons, the response of the STMD neuron to targets of varying heights is shown in Fig. 2.27. From Fig. 2.27a, we can see that the two smaller targets whose heights are equal to $0.8°$ and $3°$, respectively, can elicit stronger neural response. However, the response to the larger target whose height equals to $15°$, is much weaker and indistinguishable from spontaneous activity. The selectivity of STMDs to target height can be clearly seen in Fig. 2.27b. These demonstrate the STMDs have an optimal size sensitivity corresponding to the strongest neural response. When target height is higher or lower than the optimal one, the neural response will significantly decrease.

Some STMD neurons have also demonstrated DS [200, 41]. These directionally selective STMD neurons respond strongly to small target motion oriented along a PD, but show weaker or no, even fully opponent response to ND motion. Fig. 2.28a il-

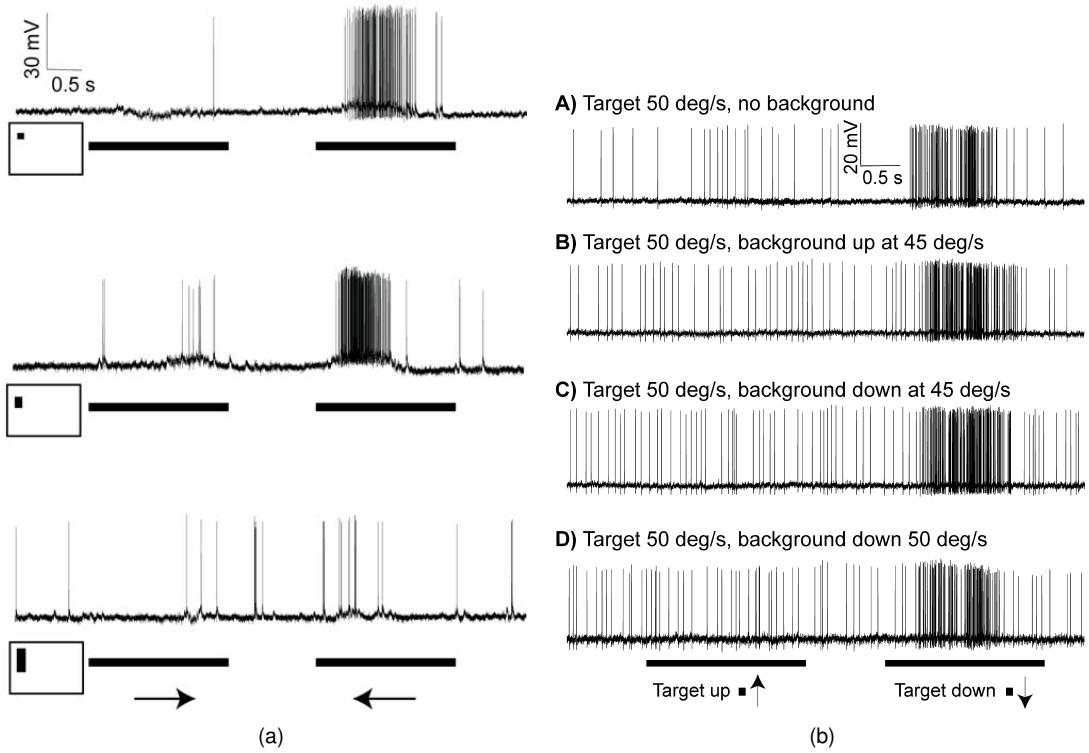

Figure 2.28: (a) Raw responses of the directionally selective STMD neuron which prefers target motion to left, tested by motion of three different-sized targets ($0.8°$, $3°$, or $15°$ high by $0.8°$ wide) drifted against bright backgrounds: the horizontal bars indicate the stimuli duration and the arrows denote the direction of target motion, adapted from [41]. (b) Responses of STMD neurons which prefers target motion downward, to targets drifted against cluttered backgrounds, adapted from [41].

lustrates raw responses of a directionally selective STMD neuron which prefers target motion to left, stimulated by three different-sized targets; this demonstrates that the larger target whose height equals to $15°$, cannot activate the STMD neurone though by PD motion. However, for the smaller targets whose heights are equal to $0.8°$ and $3°$, the STMD neuron responds strongly to PD motion. On the other hand, when the smaller targets move in ND, the response of the STMD neuron is not significantly different from spontaneous activity, that is, it is rigorously inhibited. In the further research [41, 201], biologists assert that both the size and the DS of STMDs is independent on background motion. More concretely, STMDs will rigorously respond to small target motion against visually cluttered backgrounds regardless of background motion direction and velocity. In Fig. 2.28b, we can see that the STMD neuron shows strong response to the small target moving along the PD (downward), but much weaker response to the ND (upward). Besides, the response to the small target motion is quite robust in spite of either the direction or the velocity of background motion. In anoth-

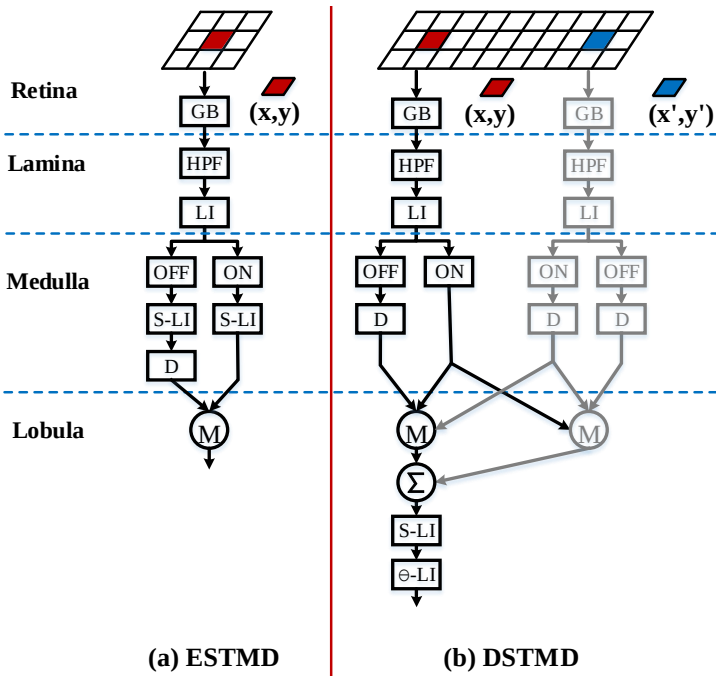

Figure 2.29: Schematics of an ESTMD [43] and a DSTMD [44] computational models for the detection of small target motion: (a) schematic of an ESTMD with visual field centred at (x, y) – In the ESTMD, the luminance signal from position (x, y) is firstly spatially Gaussian blurred in retina layer, then high-pass filtered and laterally inhibited in lamina layer, and finally half-wave rectified into separate ON and OFF signals in medulla layer. A second-order lateral inhibition mechanism [45] is implemented on ON and OFF signals for size selectivity of STMD neurons. After this second-order lateral inhibition mechanism, OFF signal is temporally delayed before multiplying with ON signal. (b) schematic illustration of a DSTMD with visual field centred at (x, y) and a preferred direction θ – The most significant difference between the DSTMD and ESTMD is that the DSTMD integrates signals from two different positions (x, y) and (x', y') where $x' = x + \alpha_1 \cos\theta$, $y' = y + \alpha_1 \sin\theta$, α_1 is a constant. However, the ESTMD integrates signals from a single position (x, y). Therefore, for each position (x, y), the DSTMD has multiple model outputs corresponding to different PDs θ, while the ESTMD just has a single output without DS.

er word, the STMDs can recognise small target motion even without relative motion between the moving objects and the environment.

Computational models On the basis of these biological findings, in the past decade, a few computational models have been put forward to simulate the STMDs. Wiederman et al. [43] proposed a seminal work of an elementary small target motion detector (ESTMD, see Fig. 2.29(a)) to account for the specific size selectivity of the STMDs. However, the ESTMD model has not considered to realise the DS of STMDs, as well. In addition, two hybrid models, i.e., ESTMD-EMD and EMD-ESTMD, were proposed for achieving the DS of STMDs [204]. The ESTMD-EMD denotes that the ESTMD

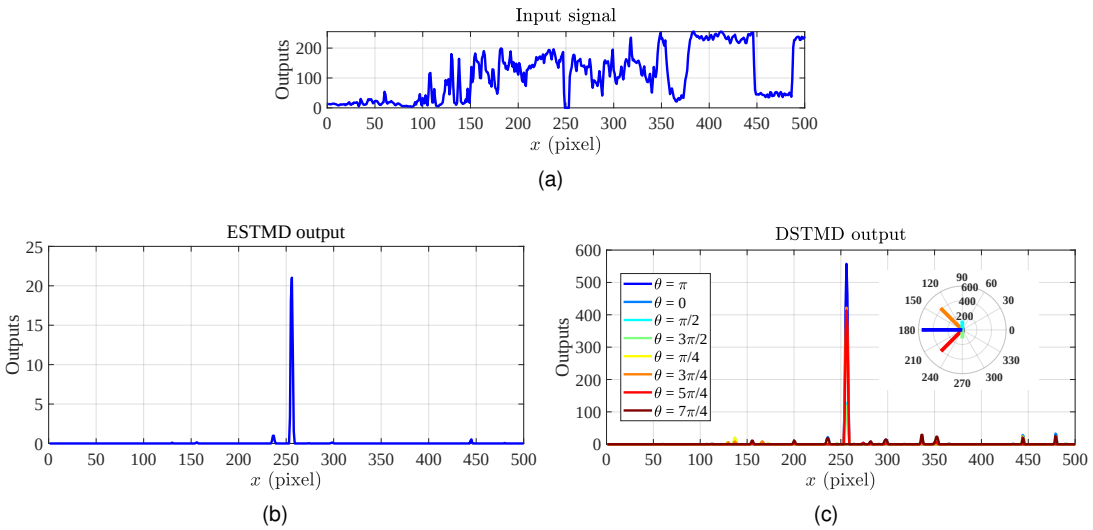

Figure 2.30: The input signal (a) and the model outputs of the ESTMD (b) and the DSTMD (c): in each sub-figure, horizontal axis denotes the position x while vertical axis denotes the model outputs. In (c), the DSTMD has eight outputs corresponding to eight PDs θ, represented by eight colors; these are shown in polar coordinate. Angular coordinate denotes PD motion θ while radial coordinate denotes the strength of neural response along this PD.

cascaded with the EMD while the EMD-ESTMD indicates the EMD cascaded with the ESTMD. These two hybrid models have been used for target tracking against cluttered backgrounds in [205, 206, 207]. Another directionally selective STMDs model, called directionally selective small target motion detector (DSTMD, see Fig. 2.29(b)), was proposed by Wang et al. [44]. Compared to other STMDs models, the DSTMD provides unified and rigorous mathematical descriptions. Besides, the DS of DSTMD has been systematically studied and the motion direction of small targets can be estimated using directionally selective outputs of DSTMD [44]. To compare the DSTMD with the ESTMD, both model outputs and the input signal are shown in Fig. 2.30. We can obtain from Fig. 2.30b and 2.30c that the most significant difference between the DSTMD and the ESTMD is that the former can generate the DS to small target motion. More precisely, in Fig. 2.30c, the DSTMD has eight outputs corresponding to eight PDs θ, $\theta \in \{0, \frac{\pi}{4}, \frac{\pi}{2}, \frac{3\pi}{4}, \pi, \frac{5\pi}{4}, \frac{3\pi}{2}, \frac{7\pi}{4}\}$. On the other hand, in Fig. 2.30b, the ESTMD produces only a single directional response. To clearly show the DS, the DSTMD responses to a small target are shown in polar coordinates as well (see the right part of Fig. 2.30c): the DSTMD exhibits strongest response along the direction $\theta = \pi$ which is consistent with the motion direction of the small target translating. The other seven

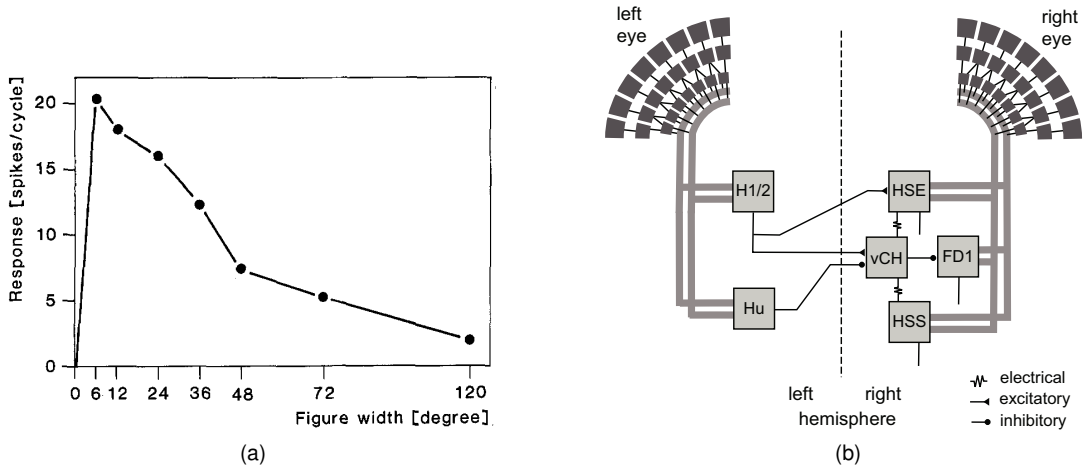

Figure 2.31: (a) The response of an FDN to targets of varying width: horizontal axis denotes target width (degree) while vertical axis denotes neural response (spikes/cycle), adapted from [46] (Egelhaaf, 1985). (b) Wiring sketch of the FD1 cell input circuit, adapted from [47] (Hennig and Egelhaaf, 2012): the FD1 cell is a most thoroughly analysed FDN.

outputs of DSTMD decrease as the corresponding direction θ deviates from the small target motion direction.

2.4.2 Figure Detection Neurons

Biological research Moreover, one class of lobula plate tangential cells, i.e. FDNs, has also been demonstrated preferentially responding to small targets [208, 46, 209, 210, 211]. Although both the FDNs and the STMDs exhibit size selectivity to moving targets, they differ in the preferred size. More specifically, the STMDs show strongest response to targets as small as a size within $1 \sim 3$ degrees [41, 42]. However, the FDNs respond best to targets whose size is in the range of $6 \sim 12$ degrees [46, 49]. Fig. 2.31a presents the response of FDNs to targets with varying widths. In Fig. 2.31(a), we can see that the optimal width of FDNs is 6 degrees which is larger than that of STMD neurons ($1 - 3$ degrees). Another difference between these two types of small target motion sensitive neurons is the underlying mechanisms for size selectivity. To be more precise, the STMDs do not receive inhibition from wide-field neurons [41] and their size selectivity results from a second-order lateral inhibition mechanism [45]. However, the size selectivity of FDNs is assumed to be the result of inhibition from wide-field neurons[212, 49]. Fig. 2.31b demonstrates the wiring sketch of an FDN

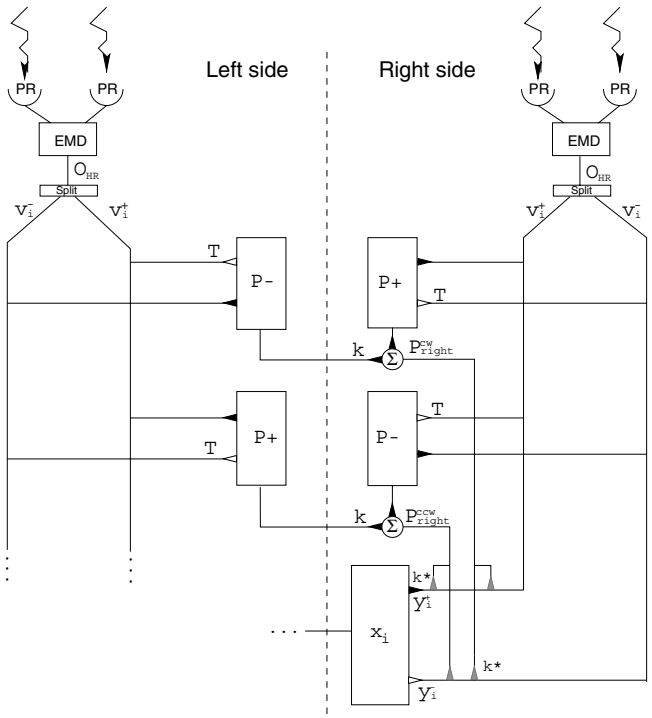

Figure 2.32: Schematic of an SFS based on the FDNs: excitatory and inhibitory synapses are indicated by black and white triangles, respectively. Shunting inhibition is indicated by grey triangles. $\sum$ indicates a sum. Responses from neighbouring photoreceptors (PR) are input to EMDs. The EMD outputs are split into positive and negative components. These components are aggregated into directionally selective monocular pool cells (P^+, P^-) and then into CW and CCW binocular pool cell responses ($P^{CW}_{right}, P^{CCW}_{right}$). These directionally selective binocular pool cells interact via shunting inhibition with the individual motion detector output channels prior to their combination by unit x_i . For simplicity, only the right-side computation is diagrammed. This figure is adapted from [48] (Higgins and Pant, 2004).

input circuit; the FDN is inhibited by the vCH cell [212] which receives excitatory and inhibitory inputs from other motion sensitive LPTCs including HSE, HSS, H1, H2 and Hu cells [213, 214, 215].

Computational models For computationally modelling the FDNs, a few models called small field systems (SFSs) have been proposed to account for the specific size selectivity of FDNs [46, 216, 217]. These SFS are quite similar; an instance is shown schematically in Fig. 2.32. The SFS is composed of an output neuron, the FDN (x_i) which receives retinotopic input (V_i^+, V_i^-), as well as input from inhibitory neurons ($P^{CW}_{right}, P^{CCW}_{right}$). The retinotopic input (V_i^+, V_i^-) denotes motion information which is detected by the EMDs. In [47], these SFS were modified to allow a simulated fly to track a small moving target in a virtual environment. Although the size selectivity of

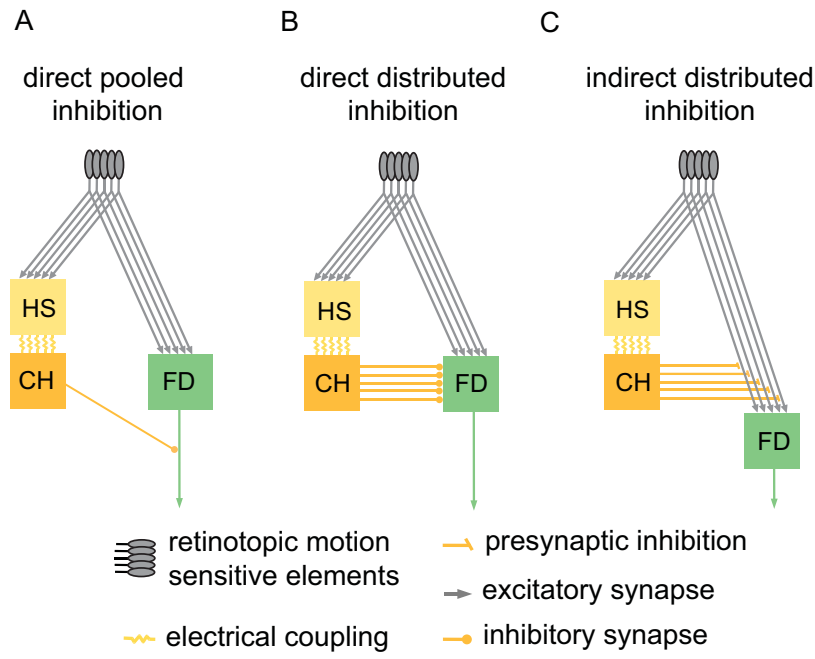

Figure 2.33: Schematics of potential circuits of the input organisation of an FDN: the small-field selective FDN receives excitatory retinotopic input from motion sensitive elements. Inhibitory input of the FDN is mediated by the CH cell via HS cells. For simplicity, only one of the two HS cells that provide input to the CH neuron is shown in this sketch. (A) The CH inhibits the FDN after spatial pooling ('direct pooled inhibition' DPI). (B) The CH inhibits the FDN in a direct distributed way (DDI). (C) The CH inhibits the retinotopic input elements of the FDN in an indirect distributed way (IDI). This figure is adapted from [49] (Hennig et al., 2008).

FDNs is the result of inhibition from wide-filed neurons, the wiring scheme between the wide-field neurons and the FDNs is unclear. In [49], Hennig et al. analysed three kinds of wiring schemes between the wide-field neurons and the FDNs, based on new anatomical and electrophysiological findings [218, 219], as illustrated in Fig. 2.33. The authors indicated that the latter two wiring schemes, i.e., direct distributed inhibition and indirect distributed inhibition in Fig. 2.33, can account well for the size selectivity of FDNs and the dependence of FDNs on the relative velocity between the small target and the background. In [47], Hennig et al. further improved the existing SFS by modelling the pre-synaptic neurons to the FDNs, including H1, Hu, HSE and HSS [220] (see Fig. 2.31b). They integrated the responses of pre-synaptic neurons in the proposed FDN circuit; this effectively matches the corresponding biological structure. Besides, comparing to the existing studies on modelling FDNs that all use simple synthetic stimuli, the authors applied naturalistic stimuli to test the proposed FDN circuit and demonstrated its characteristics.

2.5 Similarities in Modelling Insect Motion Detectors

Through above surveys on computational visual motion perception models that possess different direction and size selectivity originated from insect visual systems research, we have demonstrated their underlying functionality and characteristics of sensing different motion patterns including looming, translating and small target motion. We have also demonstrated their applications to mobile machines like robots, MAVs, UAVs and ground vehicles. This section will further discuss about the similarities in modelling of different insect motion detectors.

Though these motion detectors indicate different direction or size selectivity, there are similarities that can be summarised through the computational studies. Taken the fly and locust inspired visual neural networks as examples, a great majority of these models have been focusing on structural modelling of internal circuits or pathways of insect visual brains. These models thus can share similar visual processing ways:

1. The first layer of Retina consists of photoreceptors that capture grey-scaled images and retrieve motion information by calculating transient luminance change, as the LGMDs models illustrated in Fig. 2.6, 2.11, 2.5, 2.10, 2.13, and the fly DSNs models in Fig. 2.25, 2.26, and the STMDs models in Fig. 2.29.

2. Since the biological findings of ON and OFF pathways in many animals including the various kinds of flies, the second Lamina layer consists of LMCs separating visual signals into parallel pathways. Although this structure has not been found in locusts, recent computational studies on LGMD2 neurons can evidence similar ON and OFF mechanisms in locust visual systems [23, 22, 20, 21, 55].

3. Within the computational layers of Medulla and Lobula, both the direction and size selectivity is generated and shaped to specific motion patterns.

4. The modelled LGMDs and DSNs are all wide-field motion sensitive visual neurons that pool the pre-synaptic local directional motion information and then generate spikes to further sensory neural systems including motion systems.

5. The ON and OFF visual pathways can be modelled in insect motion detectors in-

cluding LGMDs, DSNs and STMDs and etc., in order to encode polarity motion signals, separately. The other relevant modelling of biological visual systems like the LGNs in crabs [142] may learn from the existing models.

2.6 Realisation of Direction and Size Selectivity

This section continues to summarise the computational generation of both the direction and the size selectivity diversity to proposed different motion patterns. Through above reviews of looming and translating sensitive neural systems, we summarise 1) the different direction selectivity of various neuronal models is shaped pre-synaptic to the wide-field motion detectors of DSNs and LGMDs, that is, in the Medulla and Lobula neuropile layers, as illustrated in Fig. 2.2 and 2.19; 2) spatiotemporal computation including the lateral inhibition mechanisms and the non-linear methods mediates the specific direction selectivity to either looming or translating visual stimuli.

For locusts, as reviewed in Section 2.2 and Section 2.3.1, there are two types of motion sensitive visual neurons, i.e. the locust LGMDs and the locust DSNs. Though they are all utilised as collision-detecting systems, the different direction selectivity exist between the LGMDs and the DSNs, as the schematics shown in Fig. 2.6, 2.13 and 2.17. First, to fulfil the specific direction selectivity of the LGMDs to looming stimuli, movements in depth, these computational neuron models or neural networks have demonstrated a lateral inhibition mechanism of spatiotemporal and non-directional convolution processes; the inhibitions in the computational Medulla layer convolve surrounding temporally delayed excitations, which can be expressed by [6, 79, 26, 146]:

$$I(x,y,t) = \iiint E(u,v,s)\, W(x-u, y-v, t-s)\, dudvds, \tag{2.1}$$

where W is a local convolution kernel. I and E denote the inhibition and excitation. After that, there is a competition between the excitatory and inhibitory signals in each local cell – the inhibition will cut down the excitation. In addition, with regard to the modelling of ON and OFF mechanisms in the LGMD2 model, the excitations can also

convolve the surrounding inhibitions, in a same manner [21, 23, 22]. Therefore, such a method makes the LGMDs respond most strongly to the expanding of object edges over other kinds of movements.

Unlike the LGMDs, each directionally specific neuron of the locust DSNs responds to motion along a particular PD. However, with similar ideas to the modelling of LGMDs, the direction selectivity can be realised by a directional convolution process on asymmetrically spreading out information [24, 25, 26]:

$$I(x, y, t) = \iint E(u, y, s)\, W(x - u, y, t - s)\, duds, \tag{2.2}$$

in horizontal directions and,

$$I(x, y, t) = \iint E(x, v, s)\, W(x, y - v, t - s)\, dvds, \tag{2.3}$$

in vertical directions.

With regard to fly EMDs and LPTCs models that sense translating stimuli, reviewed in Section 2.3.2 and Section 2.3.3, the direction selectivity to four cardinal orientations of translations is accomplished by non-linearly spatiotemporal computations according to the classic HR detector [125]:

$$R(t) = X_1(t - \epsilon) \cdot X_2(t) - X_1(t) \cdot X_2(t - \epsilon), \tag{2.4}$$

where R is the output of each pairwise motion detectors. X_1 and X_2 are two adjacent motion sensitive cells. ϵ is the time delay. Such a fundamental computational role has been widely used in a variety of EMDs models, e.g. [31, 33, 181] and ON/OFF polarity motion detectors, e.g. [39, 40, 94, 99], and LPTCs models [53, 52, 102, 194], and STMDs models, e.g. [103, 43, 44, 221], as well as fly optical flow strategies, e.g. [59, 37], for the purpose of generating direction selectivity to translating movements.

Regarding to the generation of size selectivity, as reviewed in Section 2.4, the STMDs and FDNs are small-field motion sensitive neurons which have the specific size selectivity to small target motion that is different from these wide-field motion detectors like the LGMDs and the DSNs. There are two basic categories of STMDs

visual neural networks, i.e. the ESTMD and the DSTMD. The latter possesses the direction selectivity to small target motion that can be achieved by similar methods of the EMDs. Wiederman et al. have proposed that the lateral inhibition mechanism plays a crucial role to shape the size selectivity, in a both temporal and spatial manner [43, 95]. Based on this, Wang et al. mathematically analysed the way of generating the size selectivity in motion sensitive visual pathways of insects; in this research, they applied a second-order lateral inhibition mechanism in the computational layer of Lobula, which can be represented by an algorithm of 'Difference of Gaussians' (DoGs) [44].

2.7 Multiple Neural Systems Integration

These insect visual neurons are functionally specialised in different motion patterns recognition. In animals, much evidence has shown the complex visuomotor response is guided by various visual neurons or circuits, rather than a single unit. From a computational modeller's perspective, the computational models and applications can undoubtedly benefit from the cooperation of different visual neurons to handle complicated visual tasks mixed with multiple motion patterns and background visual clutter by integrating multiple motion perception neural systems.

A few computational studies have already demonstrated the usefulness of building a hybrid neural system for motion perception. Specifically, the locust DSNs visual neural network itself is an instance of multiple neural systems integration [24, 25] (Fig. 2.17). In this study, each directionally selective neural network is specialised in the detection of a specific PD motion, and the post-synaptic organisation of multiple DSNs can match well the requirements of collision recognition in dynamic scenes. In addition, combining the translating sensitive neuronal models with the LGMD1 model can effectively enhance the collision selectivity, especially in complex driving scenarios [163, 164]. Moreover, a computational model that senses rotational motion patterns integrated the mechanisms of locust DSNs and fly EMDs for computation in the pre-synaptic and post-synaptic neural networks, respectively [222]; this neural system can recognise both clockwise and anticlockwise rotations.

To briefly summarise, a visual system that possesses multiple functional neurons

can extract more abundant motion features from a dynamic and visually cluttered environment; this is very necessary in vision-based mobile machines like UAVs and robots and future autonomous machines like self-driving cars.

2.8 Hardware Realisation of Insect Motion Detectors

To achieve higher processing speed, larger scale or real-time solutions, the implementation of neuromorphic visual models on hardware could be extremely advantageous.

From an engineering perspective, the neuromorphic visual sensors are realised towards two different trends. One is single-chip solution featured by the compact size and specialised functions. Another trend is featured by high performance circuits such as the FPGA.

The single-chip solutions [223, 224, 225, 226] are usually implemented by CMOS VLSI process with mixed-signal[227]. The photoreceptors are also integrated inside. Taking advantage from the compact design and low power-consumption, these silicon implementations could be widely deployed as individual sensors for distributed systems, or as components on size-sensitive platforms such as micro robots or UAVs[12]. This kind of integrated chip can also be utilized as an optic sensor for further applications. For instance, the dynamic vision sensor (DVS) [228, 229] technology is featured by its low-latency and low-data volume.

On the other hand, the high-performance solutions [230, 14, 231] aim to capture images from commercial cameras with high resolution and high frame rate, and to established the signal processing within FPGA or even ASICs. Due to the feature that data array can be dealt in parallel, the total frame rate can reach even up to 350 fps at the resolution of 256×256 [230], or 5 kHz with 12 photo-diodes [232]. These high-performance approaches could significantly enhance the visual model's spacial sensitivity and temporal response for further researches with critical requirements. As presented above, these bio-inspired motion perception models could be ideal choices for design of neuromorphic vision sensors as a possible trend of hardware realisation of visual processing.

2.9 Chapter Summary

In this chapter, we have provided an overview of computational motion perception models originated from insect visual systems research, as well as corresponding applications to navigation of mobile machines for visual motion detection and behaviours control like collision avoidance, landing, tunnel crossing, motion tracking and etc. We have reviewed these bio-inspired models according to their specific direction and size selectivity to different motion patterns including looming, translating and small target motion. To a large extent, the underlying cellular and sub-cellular mechanisms of visual processing in insects' brains are elusive until today. However, the revealed diversity in direction and size selectivity in different types of visual neurons can be realised by spatiotemporal computation within the neural networks, on the basis of different methodologies including lateral inhibition mechanisms and non-linear computation and etc. In addition, both biological and modelling studies over decades have demonstrated the similarities in different motion sensitive neural systems. The effectiveness and efficiency of these bio-inspired models have been validated by a variety of applications to bio-robotics and other vision-based platforms for motion perception in a both low-power and reliable mode. Through the existing modelling studies, we point out the great potential of these dynamic vision systems in building neuromorphic sensors for volume production and utility in future intelligent machines.

A question remains here that how researchers evaluate these bio-inspired neural systems. Normally, the models are in comparison to real biological experiments data. If a model does all as its biological counterpart does, this would be perfect. However, a vast majority bio-inspired models could only achieve the key features of simulated neurons or neural circuits.

In the following chapters, this dissertation will introduce the computational modelling of two categories visual motion sensitive neural systems – the looming and the translating perception models inspired by locusts and flies including model description and experimental validation in Chapter 3 and Chapter 4. In addition, this thesis presents our initial investigation on the integration of different visual models in Chapter 5.

Chapter 3

Modelling of Locust Looming Perception Visual Neural Networks

Within this chapter, this dissertation presents the modelling and applications of locust looming perception visual neural networks. Section 3.1 presents the modelling of LGMD2 visual neuronal model and robot applications. Section 3.2 proposes a general LGMDs model that is applicable to realise both the LGMD1 and the LGMD2 neuron models. Finally, this chapter is summarised with further discussion on future work in Section 3.3.

3.1 Modelling LGMD2 Visual Neuron System

Collision detection is of critical importance for artificial mobile machines, like ground vehicles, autonomous vehicles including self-driving cars, UAVs or MAVs, and also robots. The ability to quickly and accurately detect collisions is vital for both animals and robots to initiate proper behaviours, navigate through unpredictable dynamic environments, and also interact with humans. There are many physical sensors used for collision detection, such as infra-red, radar, laser, ultrasound, vision and various combinations of these [22]. However, those solutions are restricted heavily from wider application due to their size, price, efficiency, reliability and/or energy consumption [6]. Therefore, it is still a big challenge for developing a robust collision detector which can work without human intervention, especially in complex and dynamic environments.

For visual modalities, the degree of background complexity heavily restricts the motion perception performance with more abundant information extracted. In addition, the traditional segmentation or registration based computer vision techniques can not fulfil the requirements of real-time collision detection tasks. As the result of millions of years evolutionary development, biological visual systems are robust for collision detection. To be more specific, the locust visual systems have demonstrated amazing ability interacting with the dynamic world with only a small number of neurons compared to vertebrates and humans. For example, locusts can fly over hundreds of miles free of collision. The collision (looming) detection systems in locusts thus can be ideal models to design collision free artificial vision systems.

Research progress has been gradually made by physiologists toward understanding the underlying characteristics and mechanisms of the LGMDs in locusts, e.g. [76, 77, 233, 80, 83, 79, 2, 117, 19, 162]. More precisely, in the lobula area of locusts' visual brain, the LGMD1 neuron was first identified as a movement detector [76, 77] and gradually recognised as a looming objects detector, e.g. [80, 79, 2]. In the same place, the LGMD2 neuron was also identified but with unique characteristics that are different to the LGMD1 [83, 131, 19]. Next, we introduce the similarities and differences between the two looming sensitive neurons.

3.1.1 Characterisation of LGMDs

Firstly in neuromorphology, both the LGMDs have a characteristic, extensive fan-shaped arbour, as shown in Fig. 3.1. The lobula arbour of LGMD1 is beneath that of LGMD2; there are also two dendritic sub-fields (B and C in Fig.3.1) located more ventrally in the lobula area of LGMD1, which are lacking from the LGMD2. The descending contra-lateral motion detector (DCMD) is a one-to-one post-synaptic target neuron to the LGMD1, which is directly excited through a chemical synapse between them and conveys information to further motion control neural system [233, 78, 130, 131, 144, 234]. However, the post-synaptic partner to the LGMD2 is still remaining elusive [83].

Compared with the LGMD1, recent research revealed that the LGMD2 matures

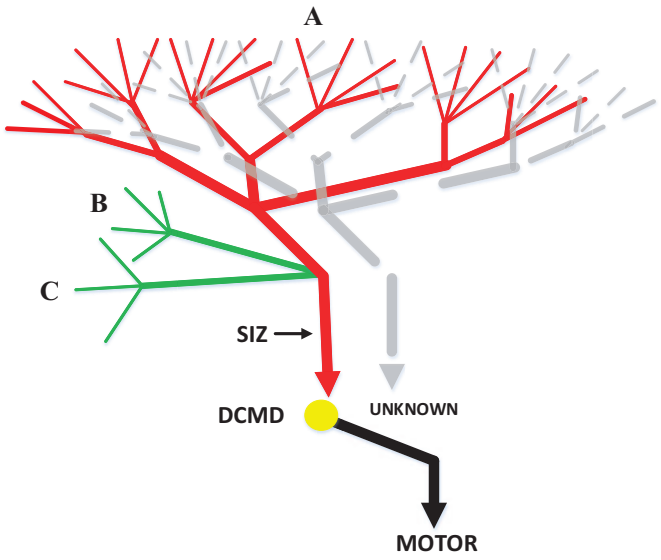

Figure 3.1: Schematic of LGMD1 and LGMD2 neural circuitry: **A** The red area indicates the LGMD1's dendritic tree whilst the gray-dashed one denotes the LGMD2's. DCMD (yellow neuron) as a one-to-one connected post-synaptic partner to LGMD1 passes signals further to the motion motor; the target to post-synaptic area of LGMD2 remains unknown. SIZ indicates the spike initiation zone. The LGMD1's dendritic tree consists of additional two ventral subfields **B** and **C**, that are absent from the LGMD2.

early in juvenile locusts. More interestingly, even the newly hatched locusts respond to looming stimuli [19]. The adolescent locusts are lack of wings so that living mainly on the ground, whereas they are already capable of reacting to objects that impinge on compound eyes, e.g. swooping predators from the light sky. Recent investigation suggests that the LGMD2 neuron could be a dominant collision-detector for juveniles to evoke hiding behaviours against looming stimuli [19].

In terms of neural response to visual motion, both the LGMDs respond most strongly to objects that rapidly approach. Both represent increasing firing rates peaked before the objects reach a particular angular size in the retina [83, 79, 115, 19]. Against translating stimuli, both are activated shortly and then inhibited during remaining translating movements [83]. Both are also inhibited during either the whole-field luminance change or grating movements [79, 83, 131]. However, when challenged by accelerating movements like approaching and speeding up translating objects, both neurones will be rigorously activated. Therefore, we can also summarise that the LGMDs are more sensitive to visual stimuli of increasing rather than constant intensity.

More specifically, the LGMD2 neurons mature very early in adolescent locusts [19], and one of its unique features is that it only responds to the light-to-dark lu-

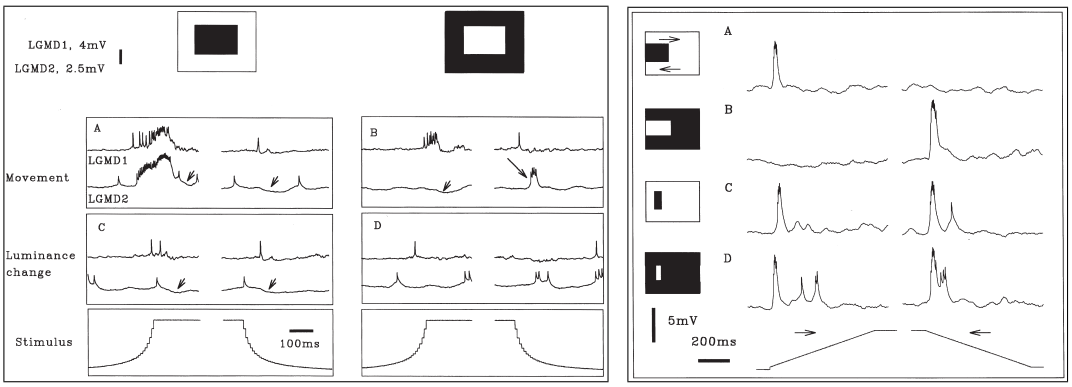

(a) LGMD1 and LGMD2 responses to looming stimuli (b) LGMD2 responses to translating stimuli

Figure 3.2: Biological data of LGMD2 neuron responses to (a) dark and light objects looming and (b) translating, adapted from [83].

minance change, the situation of which corresponds to predators from the light sky. The special selectivity, i.e, it is able to detect moving dark objects embedded in the bright background in depth selectively while not responding to light objects approaching against the dark background, makes it outside of normal expectation and an unique neuron to model. Though briefly excited by the recession of brighter objects, like the LGMD1, it will be inhibited very soon during objects move away [83]. On the other aspect, early researches have demonstrated that the LGMD1 respond to both darker and brighter objects that approach [79, 2, 131]. For easy understanding, the Fig. 3.2 represents the neural responses of both LGMDs against looming and translating.

As reviewed in the last Section 2.2, in order to realise the neural characteristics of LGMDs, a good number of computational models have been proposed for LGMD1, for instance [6, 85, 15, 16, 18], and successfully utilised as cheap and quick collision detectors in vision-based platforms such as ground vehicles [161, 151, 146] and ground robots [84, 7, 85, 8] and also UAVs [148, 12]. Nevertheless, little modelling works have been conducted for the LGMD2. This dissertation proposes a visual neural network to fulfil the specific looming selectivity of biological LGMD2 neurones and investigates the applicative potential in robot vision.

3.1.2 Framework of the Proposed LGMD2 Neuronal Model

In this subsection, we present the proposed LGMD2 neuronal model (or visual neural network) in detail. The key components of the proposed LGMD2 model is an archi-

tecture of biased-ON and OFF pathways splitting visual signals into parallel channels, each of which involves multiple layers for spatiotemporal computations. Brightness increments flow into ON channels whilst decrements flow into OFF channels. Signals in separated pathways are spatially and temporally filtered, then pooled to form the membrane potential which is later mapped to sigmoid potential for spike coding. Finally, a few continuous spikes elicited in a short time window, that is, the high firing rate corresponds to a potential collision recognition.

Schematic of the proposed LGMD2 neuron model is shown in Fig. 3.3. It is worth emphasising that the internal partial neural networks can mediate the specific looming selectivity of LGMD2. More specifically, the ON channels corresponding to each local photoreceptor are rigorously sieved with a bias to achieve the LGMD2's unique collision selectivity to proximity of darker objects embedded in light background. It is also necessary to note that compared to other vision-based collision detectors, the proposed framework only involves low-level image processing methods [235], detects potential collision by reacting to the expanding edges of an object. Those computationally expensive methodologies, such as target classification, scene analysis are not applied in this study at all. Therefore, the proposed bio-inspired algorithms can be ideal model systems to design low-cost and low-energy modules or sensors for collision detection.

3.1.2.1 Photoreceptor Layer

The first retinal layer of the proposed neuronal model consists of photoreceptors arranged in a two-dimensional matrix form with the total amount corresponding to the number of pixels in the field of view. The photoreceptors capture input imagery of grey-scale format. A first-order high-pass filtering process retrieves the luminance change between every two successive frames. That is,

$$P(x,y,t) = L(x,y,t) - L(x,y,t-1) + \sum_{i}^{n_p} a_i \cdot P(x,y,t-i), \tag{3.1}$$

where $P(x,y,t)$ is the photoreceptor value corresponds to each local pixel (x,y) at frame t. $L(t)$ and $L(t-1)$ are the original brightness of two successive frames. The persistence of luminance change could last for a while of n_p frames. The decay coef-

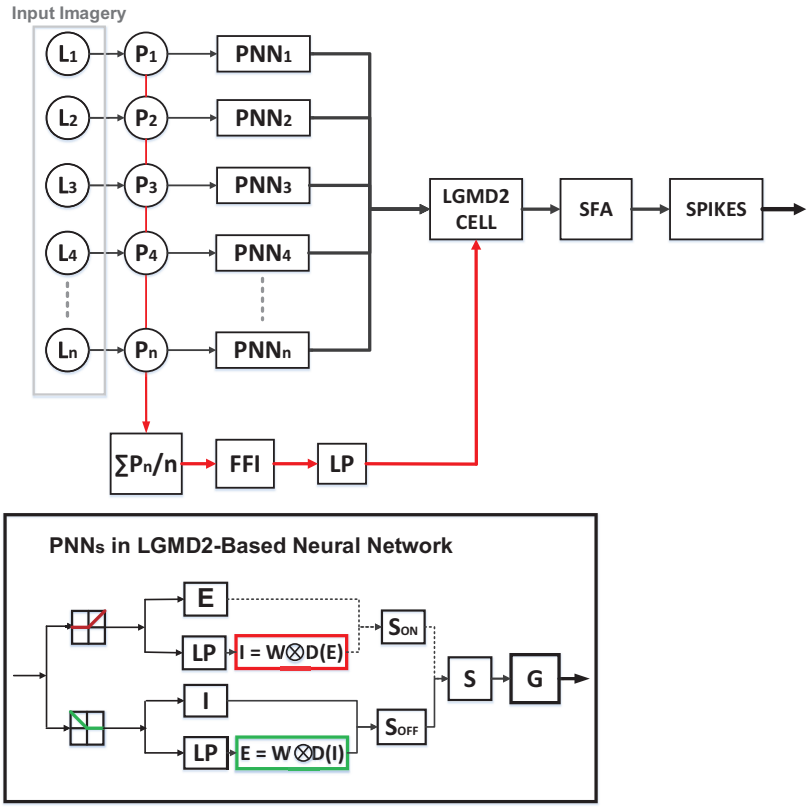

Figure 3.3: Schematic illustration of the LGMD2-based neural network for collision detection. The input is grey-scale imagery. Pixel-wise luminance (L) is captured by photoreceptors (P) to retrieve motion information which is relayed into ON and OFF pathways with multi-layers within partial neural networks (PNN). ON and OFF cells implement the functions of half-wave rectifiers. E, I, S and G are short for excitation, inhibition, summation and grouping cells. LP indicates the low-pass filtering. Notably, in ON channels, the inhibition is convolved by the surrounding delayed excitations; while in OFF channels, the excitation is convolved by the periphery delayed inhibitions. Dashed lines in the PNN indicate strongly suppressed pathway by the local lateral-inhibition mechanism. The LGMD2 cell pools intact pre-synaptic local excitations which is then sieved by the SFA mechanism and mapped to spikes as the model output. FFI denotes the feed-forward inhibition conveyed separately to the LGMD2.

ficient a_i is calculated by

$$a_i = (1 + e^{u \cdot i})^{-1}, \tag{3.2}$$

where $u \in (-\infty, \infty)$ and $u = 1$ in this modelling study. If there is no difference between continuous frames, the photoreceptors will not be activated.

3.1.2.2 ON and OFF Mechanisms

Unlike previous LGMD1-based neural networks, the photoreceptors pass motion information into separated ON and OFF pathways depending on luminance increments or decrements. As illustrated in Fig. 3.3, the functionality of ON and OFF transien-

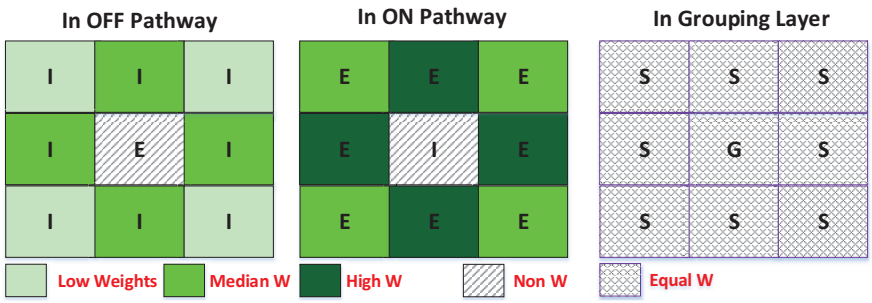

Figure 3.4: Illustrations of spatiotemporal convolution process kernels within the pre-synaptic visual processing structure, for forming excitations, inhibitions and grouped signals in the OFF, the ON and the grouping layer, respectively.

t cells in the partial neural network (PNN) is implemented by half-wave rectifying. More precisely, at each local cell, the luminance increment flows into ON channels by onset response, whilst the brightness decrement flows into OFF channels by offset response. That is,

$$\begin{aligned} P_{on}(x,y,t) &= [P(x,y,t)]^{+} + \sigma_p \cdot P_{on}(x,y,t-1), \\ P_{off}(x,y,t) &= -[P(x,y,t)]^{-} + \sigma_p \cdot P_{off}(x,y,t-1). \end{aligned} \tag{3.3}$$

Here, $[x]^{+}$ and $[x]^{-}$ denote $max(0,x)$ and $min(x,0)$, respectively. Despite building collision sensitive neurons, the ON and OFF rectifying transient cells have also been proposed the potential to encode small target movement detectors [43, 44], as well as direction selective neurons [53]. In addition, a small fraction (σ_p) of onset and offset responses at previous frame are allowed to pass through.

3.1.2.3 The Partial Neural Network

Within such looming-sensitive sensory neurons like the LGMDs, there are two main kinds of signal flows – excitation and inhibition, interacting and competing with each other. If the former one wins, the neuron will immediately spike; otherwise, it remains quiet. Such neural signal competition plays crucial roles of not only realising the collision perception ability of the LGMDs, but also shaping their selectivity.

In previous LGMD1-based models, after the photoreceptor layer, visual motion information is processed in a single pathway, e.g. [6, 9]. The output from photoreceptors forms the input to two separate cell types in the next layers. One type is the excitatory

cell, through the excitation is passed directly to the excitation layer. Another type is the one-frame-delayed lateral inhibitory cell, relaying inhibition to the inhibition layer. This plays roles to cut down the motion-dependent excitations when an object growing on the retina [79, 6, 23].

Moreover, in the state-of-the-art LGMD1 models, the lateral inhibition is always delayed relative to the excitation. However, the excitation has also been supposed to be postponed [153, 18]. With respect to the ON and OFF mechanisms, this research proposes that the polarity cells lead effects on different delayed neural signals. More precisely, in terms of the onset response by ON cells activated, the excitation is time advanced relative to the inhibition in the ON pathway; otherwise, the excitation is delayed relative to the inhibition in the OFF pathway by offset response. In case of the proposed LGMD2 model, this works effectively to rigorously suppress the ON rather than OFF channels in order to achieve its specific selectivity to dark looming objects. Therefore, in the proposed neural network, signals are split downstream into two parallel pathways, each of which comprises a cascade of layers.

Spatiotemporal Computation in the ON Channels Firstly, in the ON channels, the onset response leads the excitatory flow to pass directly to the excitation (E) layer. That is,

$$E_{on}(x, y, t) = P_{on}(x, y, t). \tag{3.4}$$

Meanwhile, it is fed into a first-order low-pass filtering which gives feedback on delayed information. That is,

$$\frac{dD_{on}(x, y, t)}{dt} = \frac{1}{\tau_1}(P_{on}(x, y, t) - D_{on}(x, y, t)), \tag{3.5}$$

where τ_1 is a time constant corresponding to the temporal delay in the I layer. The inhibition (I) in the ON pathway is thus convolved by surrounding delayed excitations. That is,

$$I_{on}(x, y, t) = \sum_{i=-r}^{r} \sum_{j=-r}^{r} D_{on}(x + i, y + j, t) \cdot W_{on}(i + r, j + r), \tag{3.6}$$

where W_{on} denotes a convolution kernel with the radius r set at 1 in our case, as shown in Fig. 3.4. More precisely, the delayed information spreads out to neighbouring cells with higher weightings at four nearest than diagonal ones. The W_{on} meets the following matrix:

$$W_{on} = \begin{pmatrix} 1/4 & 1/2 & 1/4 \\ 1/2 & 0 & 1/2 \\ 1/4 & 1/2 & 1/4 \end{pmatrix}. \tag{3.7}$$

It is important to state that compared to the kernel in the OFF pathway, the weightings are higher in the ON pathway indicating stronger lateral inhibitions to suppress the onset response in order to implement a LGMD2 neuron. In addition, the r can be increased which nevertheless will require much more computational power as the convolution algorithm goes through each local cell within either ON or OFF pathways.

Spatiotemporal Computation in the OFF channels Secondly, in the OFF pathway, similarly to the ON pathway, visual signals conveyed by OFF cells form the input downstream to two flows in the E and the I layers, whereas the excitation is temporal delayed relative to the inhibition by offset response. The inhibition is directly fed into the I Layer,

$$I_{off}(x, y, t) = P_{off}(x, y, t). \tag{3.8}$$

Meanwhile this also undergoes the first-order low-pass filtering. That is,

$$\frac{dD_{off}(x, y, t)}{dt} = \frac{1}{\tau_2}(P_{off}(x, y, t) - D_{off}(x, y, t)), \tag{3.9}$$

where τ_2 is the temporal delay for excitations in the E layer. Contrary to the ON pathway, the excitation is convolved in the E layer by surrounding delayed inhibitions. That is,

$$E_{off}(x, y, t) = \sum_{i=-r}^{r} \sum_{j=-r}^{r} D_{off}(x + i, y + j, t) \cdot W_{off}(i + r, j + r), \tag{3.10}$$

where W_{off} denotes the convolution kernel (Fig. 3.4), with a same radius of $r = 1$ and fits the following matrix:

$$W_{off} = \begin{pmatrix} 1/8 & 1/4 & 1/8 \\ 1/4 & 0 & 1/4 \\ 1/8 & 1/4 & 1/8 \end{pmatrix}. \tag{3.11}$$

Local Summation Following the spatiotemporal interactions between excitations and inhibitions in the ON and OFF pathways, there are local summation cells for each polarity channel, which depict linear calculations. That is,

$$\begin{aligned} S_{on}(x,y,t) =& E_{on}(x,y,t) - w_i \cdot I_{on}(x,y,t), \\ S_{off}(x,y,t) =& E_{off}(x,y,t) \cdot w_e - I_{off}(x,y,t), \end{aligned} \tag{3.12}$$

where w_i and w_e are local biases to the inhibition and the excitation in the ON and OFF pathways, respectively. Notably, only the non-negative value of either the ON or OFF local summation cell can reach to the forthcoming computation.

Summation and Grouping Layers As exhibited in the PNNs in Fig. 3.3, there are interactions between ON and OFF channels at every local cells of the summation (S) and grouping (G) layers. This research conforms to a supra-linear computation between ON and OFF channels of biological motion detection system [95], wherein ON and OFF excitations interact in both a linear and multiplicative manner. That is,

$$S(x,y,t) = \theta_1 \cdot S_{on}(x,y,t) + \theta_2 \cdot S_{off}(x,y,t) + \theta_3 \cdot S_{on}(x,y,t) \cdot S_{off}(x,y,t), \tag{3.13}$$

where $\{\theta_1, \theta_2, \theta_3\}$ denote the combination of term coefficients that allows us to represent different 'balances' between excitations from ON and OFF pathways. This can realise either pure-linear neural computation by setting θ_3 at zero, or multiplicative relationship between polarity channels by setting θ_1 and θ_2 at zero. More importantly, the calculation plays a role of achieving the specific looming selectivity of LGMD2 neurons, which can rigorously suppress excitations from the ON channels by expanding of light objects or contracting of dark objects, both with dark-to-light luminance

change. The supra-linear computation has also been demonstrated effectiveness of implementing the small target movement detection neurons [95] and the LGMD1 neurons [23].

In this LGMD2-based neural network, for the purpose of reducing noise and improving the collision detection ability within complex backgrounds, the expanded edges represented by clustered excitations are enhanced to extract looming features from complex backgrounds. This is implemented with a passing coefficient matrix Ce, which is defined by a convolution process with an equal-weighted kernel for each local cell in the S layer (Fig. 3.4). That is,

$$Ce(x,y,t) = \sum_{i=-r}^{r} \sum_{j=-r}^{r} S(x+i, y+j, t) \cdot W_g(i+r, j+r), \tag{3.14}$$

where the W_g denotes

$$W_g = \frac{1}{9} \times \begin{bmatrix} 1 & 1 & 1 \\ 1 & 1 & 1 \\ 1 & 1 & 1 \end{bmatrix}. \tag{3.15}$$

Therefore, in the G layer, the excitations thus become

$$G(x,y,t) = S(x,y,t) \cdot Ce(x,y,t) \cdot \omega^{-1}, \tag{3.16}$$

where ω is a scale parameter computed at every frame by

$$\omega = max([Ce](t)) \cdot C_w^{-1} + \Delta_C, \tag{3.17}$$

where C_w is a constant and Δ_C denotes a small real number. The isolated excitations in the S layer are consequently sieved by the G layer. From the S layer to the G layer, a local threshold is set to filter decayed excitations. That is,

$$\bar{G}(x,y,t) = \begin{cases} G(x,y,t), & \text{if } G(x,y,t)C_{de} \geq T_{de} \\ 0, & \text{if } G(x,y,t)C_{de} < T_{de} \end{cases}, \tag{3.18}$$

where C_{de} is the decay efficient and $C_{de} \in (0,1)$, T_{de} is the decay threshold. Through

the G layer processing, the edges of looming features are enhanced and the background detail caused excitations are largely reduced.

3.1.2.4 LGMD2 Cell

After pre-synaptic visual processing, the modelled LGMD2 cell integrates local excitations from the G layer, in a purely linear manner, to form the neural membrane potential

$$k(t) = \sum_{x}^{R} \sum_{y}^{C} \bar{G}(x, y, t), \tag{3.19}$$

where R and C are the rows and columns of the G layer. The membrane potential is then exponentially transformed by

$$K(t) = (1 + e^{-k(t)\cdot(n_{cell}\cdot C_{sig})^{-1}})^{-1}, \tag{3.20}$$

where n_{cell} indicates the total amount of local cells in the G layer and the coefficient C_{sig} shapes the output of sigmoid function within $[0.5, 1)$.

3.1.2.5 Spike Frequency Adaptation Mechanism

We also apply an SFA mechanism in the spiking initiation zone for further sharpening up the LGMD2's specific selectivity to looming over translating objects. The computational role is defined as a conditional first-order high-pass filtering. That is,

$$\bar{K}(t) = \begin{cases} \sigma_1 \cdot K(t), \text{ if } \dfrac{d^2K(t)}{dt^2} \geq 0 \\ \sigma_2 \cdot K(t), \text{ if } \dfrac{d^2K(t)}{dt^2} < 0 \;\&\; \dfrac{dK(t)}{dt} \geq 0 \\ \sigma_2 \cdot (\bar{K}(t-1) + K(t) - K(t-1)), \text{ if } \dfrac{dK(t)}{dt} < 0 \end{cases}, \tag{3.21}$$

where σ_1 and σ_2 are two adaptation coefficients indicating slow and fast adaptations to visual stimuli, respectively. These can be computed by the following time parameters:

$$\sigma_1 = \frac{\tau_3}{\tau_3 + \tau_{in}}, \quad \sigma_2 = \frac{\tau_4}{\tau_4 + \tau_{in}}, \tag{3.22}$$

where τ_3, τ_4 are two time constants and $\tau_3 \geq \tau_4$; τ_{in} is the time interval between every two successive frames and corresponding to sampling frequency. It is worth emphasising that as the digital signals do not have continuous derivatives, we compute the gradient by comparing signals at successively discrete frames. It is also necessary to notice that the delays (τ_3 and τ_4) could vary within a wide range from hundreds to thousands of milliseconds in order to mediate different adaptation rates for the LGMD2's response.

Generally speaking, such a mechanism only allows the neural response with a positive derivative profile to overcome the adaptation. Specifically for the LGMD2, in case of dark objects approaching, the derivative of neural response could reach to or above the second order, whereby the LGMD2 is able to overwhelm the SFA blocking.

3.1.2.6 Spiking Mechanism

Compared to the previous LGMD1-based models, e.g. [7, 6, 14, 9], the proposed LGMD2 model could produce more than one spikes at each time step. The neural membrane potential is exponentially mapped to spikes indicating spiking frequency by an integer-valued function. That is,

$$S^{spike}(t) = [e^{(C_{sp}\cdot(\bar{K}(t)-T_{sp}))}], \tag{3.23}$$

where T_{sp} indicates the spiking threshold and C_{sp} is a scale parameter. Accordingly, a potential collision detection (Col) at the current frame is recognised by

$$Col(t) = \begin{cases} \text{True, if } \sum_{i=t-N_{ts}}^{t} S^{spike}(i) \geq N_{sp} \\ \text{False, otherwise} \end{cases}, \tag{3.24}$$

where N_{sp} and N_{ts} denote the number of successive spikes and frames, respectively. N_{sp} is set to be greater than N_{ts} in the LGMD2 neuronal model, so as to match well the exponential mapping from membrane potential to firing rate.

3.1.2.7 FFI Mechanism

Two kinds of inhibitions cooperate to mediate the selectivity in looming sensitive neurons like the LGMDs. The first is the lateral inhibition introduced above. Another is the FFI mentioned in Section 3.1.1 and illustrated in Fig. 3.1. More concretely, there are two ventrally dendrites connecting the LGMD1 neuron, which receive object-size dependent inhibition, i.e. the FFI. This can directly inhibit the neuron. Although such a structure has not yet been found for the LGMD2 neurons, the vigorous inhibition from the physiological experiments, at the critical moments of either the end of dark object approach or the start of light object recession demonstrating a similar mechanism on the LGMD2 [83]. Therefore, similarly to previous LGMD1 models, the proposed LGMD2 model has the FFI mechanism to handle with transient luminance change over a large area within the retina. This is calculated by the absolute value of average luminance change in the photoreceptor layer. That is,

$$F(t) = \sum_{x}^{R} \sum_{y}^{C} |P(x, y, t)| \cdot n_{cell}^{-1}. \tag{3.25}$$

And it is temporally delayed by also a first-order low-pass filtering:

$$\frac{d\bar{F}(t)}{dt} = \frac{1}{\tau_5}(F(t) - \bar{F}(t)), \tag{3.26}$$

where τ_5 is a time constant. Once the FFI value exceeds its threshold T_{ffi}, spikes in the LGMD2 neuron are shut down immediately:

$$S^{spike}(t) = 0, \text{ if } \bar{F}(t) \geq T_{ffi}. \tag{3.27}$$

3.1.2.8 Model Parameters Setting

We have presented the formulation of the proposed LGMD2 neuronal model. Within this subsection, the parameters setting is introduced and given in Table 3.1. The proposed LGMD2-based neural network processes visual signals in a feed-forward structure without any feedback pathways or learning methods. All the parameters are decid-

Table 3.1: Parameters Setting of the Proposed LGMD2 Neuron System

Parameter	**Description**	**Value**
n_p	frames of luminance change persistence	2
σ_p	a fraction in [3.3]	0.1
W_{on}	convolution kernel in the ON pathway	$0 \sim 0.5$
τ_1	delay time in the ON channels (ms)	$15 \sim 45$
W_{off}	convolution kernel in the OFF pathway	$0 \sim 0.25$
τ_2	delay time in the OFF channels (ms)	$60 \sim 180$
r	radius of convolution kernels	1
w_i	local inhibition bias	0.8
w_e	local excitation bias	0.3
$\{\theta_1, \theta_2, \theta_3\}$	term coefficients in [3.13]	$\{0.5, 1, 1\}$
W_g	convolution kernel in the G layer	$1/9$
C_w	a constant to calculate ω in [3.16]	4
Δ_C	a small real number in [3.17]	0.01
C_{de}	decay coefficient in the G layer	0.5
T_{de}	decay threshold in the G layer	15
R, C	rows and columns of the G layer	adaptable
n_{cell}	total number of cells in the retina	$R \times C$
C_{sig}	a scale parameter in sigmoid function	$0.5 \sim 1$
τ_3	slow-adaptation time constant (ms)	$700 \sim 1000$
τ_4	fast-adaptation time constant (ms)	$300 \sim 500$
τ_{in}	sampling frequency of video clips	adaptable
C_{sp}	a scale parameter in spiking mechanism	4
T_{sp}	spiking threshold	$0.65 \sim 0.78$
N_{ts}	number of successive frames	4
N_{sp}	number of successive spikes	6
τ_5	delay time in the FFI pathway (ms)	10
T_{ffi}	FFI threshold	10

ed empirically with considerations and optimisations of the functionality of proposed bio-plausible pathways and mechanisms to implement a biological LGMD2 neuron, and moreover as an embedded vision system in a ground miniaturised robot. All the adaptable parameters rely upon the physical properties of input video clips, i.e. the resolution ($C \times R$) and the sampling frequency (Hz) or frames per second (fps).

Crucially, in comparison with previous LGMD1 models, e.g. [6, 23], the proposed neuronal model process visual information in separate pathways with strong bias in the ON channels. This is realised by two aspects of 1) the stronger lateral inhibition in the ON channels, 2) and the interaction between ON and OFF channels in the S layer. The functionality of such polarity pathways to realise the LGMD2's unique characteristics will be exhibited in the systematic experiments.

Table 3.2: The *Colias* Robot Main Configuration

Dimensions	ϕ 40 x h 32 mm
SRAM	256 Kbyte
Embedded Camera	99 x 72 YUV422 at 30 fps
Battery	320 mAh, 3.7 V
Max Linear-Speed	25 $\sim$ 30 cm/s
Autonomy	1 $\sim$ 2 hours

3.1.3 Robot Configuration

As introduced in Chapters 1 and 2, the proposed visual neural model with low computational consumption has been successfully realised on embedded system in a vision-based ground miniature robot for on-board visual processing. As illustrated in Fig. 3.5, the mobile robot platform used in robot experiments is named '*Colias*'. It is an open-hardware modular micro-robot which is developed to be used in swarm robotic applications [236, 237]. There have been two generations of *Colias* robots that possess visual sensing modality. As exhibited in Fig. 3.5, they have nearly a same size. In the modelling study of LGMD2, we applied the *Colias* autonomous micro robot in all designed bio-robotic experiments.

On the whole, the *Colias* robot consists of two main components. One is the motion actuator with diameter of 4cm, which is deployed on the bottom to provide power and motion controls. It applies an AVR micro-controller with 8 MHz clock source. Two micro DC motors and two diameter 2.2cm wheels are employed to actuate Colias [238]. Another one is the extension vision module which is placed on the top of *Colias*. Three LEDs are embedded in this module to be the indicators of different real-time status. With the help of a full-duplex serial port used as the debugging interface, *Colias* can send image samples and model data to the host in real-time, when the debugging mode is allowed. Meanwhile, it can receive varied configuration commands including system, camera, model and motion units from the host.

To be more specific, a miniature camera is assembled to the upper board representing as an eye of the robot, which is essential in the vision-based control of robotic applications. A low voltage CMOS image sensor OV7670 module is utilised. The low-cost camera is capable of operating up to 30 frames per second (fps) in VGA with

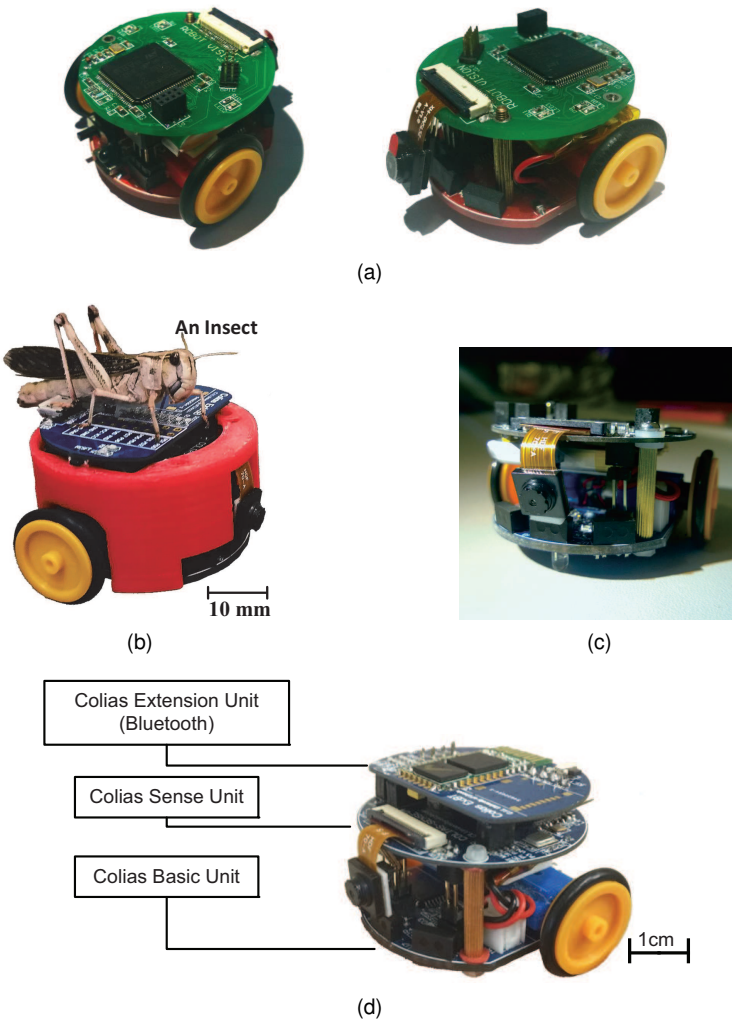

Figure 3.5: Two generations of the micro-robot *Colias* prototype: (a) *Colias*-III robot prototype applied in this LGMD2 modelling study: the upper board processes visual models; the bottom board is the motion actuator; a mini camera module is assembled to the upper board; two wheels and a battery are assembled to the bottom board. (b) – (d) *Colias*-IV prototype with a same size to *Colias*-III: (b) a locust is used to compare the size. (c) a frontal view of the vision-based mini-robot, (d) *Colias* units including three boards, adapted from [50].

output support for RGB422, RGB565, and YUV422. The angle of view could reach approximately 70 degrees. All these features make the camera suitable for using in such micro robots [147, 9]. We chose a resolution of 72×99 pixels at 30 fps with the output format of 8-bit YUV422. Second, the micro-controller is an ARM Cortex-M4F core, which is deployed as the main processor for monitoring all the modules and serving the image processing task. The 32 bit MCU STM32F427 clocked at 180 MHz provides the necessary computational power to have a real-time image stream processing. Its 256 Kbyte internal SRAM supports the image buffering and computing. In both the LGMD1 [9] and the proposed LGMD2 cases, though very limited SRAM,

the time cost for on-board visual processing plus motion decision making is always no more than 30 milliseconds. There is a digital camera interface (DCMI) which is an embedded one for transmitting of captured images by *Colias*. The DCMI can sustain a data transfer rate up to 54 MHz. In my case, through such an interface, we can collect the images within different computational neuro-layers. We can also retrieve various types of model outputs including membrane potential and elicited spikes from the mini-robot to the host. The main robot configuration applied in this thesis is given in Table 3.2.

3.1.4 Experimental Evaluation

In this subsection, this dissertation carries out systematic experiments to demonstrate the unique characteristic of the LGMD2 neural network. All the experiments can be categorised into two types of tests: the off-line tests and the on-line tests. In the off-line tests, the input stimuli consist of synthetic and recorded video streams. For comparison, both the performance of an LGMD1 [7] and the proposed LGMD2 neuron models are presented against all the synthetic stimuli. In the on-line tests, the proposed LGMD2 neural network was implemented as an embedded system in a miniature robot for real-time experiments.

3.1.4.1 Experimental Set-up

The proposed framework was set up in Visual Studio 2015 (Microsoft Corporation) and Keil (uVision4) for handling off-line simulations and on-line robotic experiments, respectively. Data analysis and visualisation were realised in Matlab $2015b$ (The MathWorks, Inc. Natick, USA). The computer used was a laptop (DELL INSPIRON) with two 2.30 GHz CPUs and Windows 7 operating system. The parameters of proposed LGMD2 model were adopted from Table 3.1; the comparative LGMD1 model in off-line tests with parameters setting-up was suggested in [7]. The input image frames were all converted to the grey-scale with intensity valued within $[0, 255]$. The resolutions of simulated and real physical recorded stimuli were 320×240 and 432×240, respectively. The spiking threshold T_{sp} was separately set at 0.78 for off-line tests and

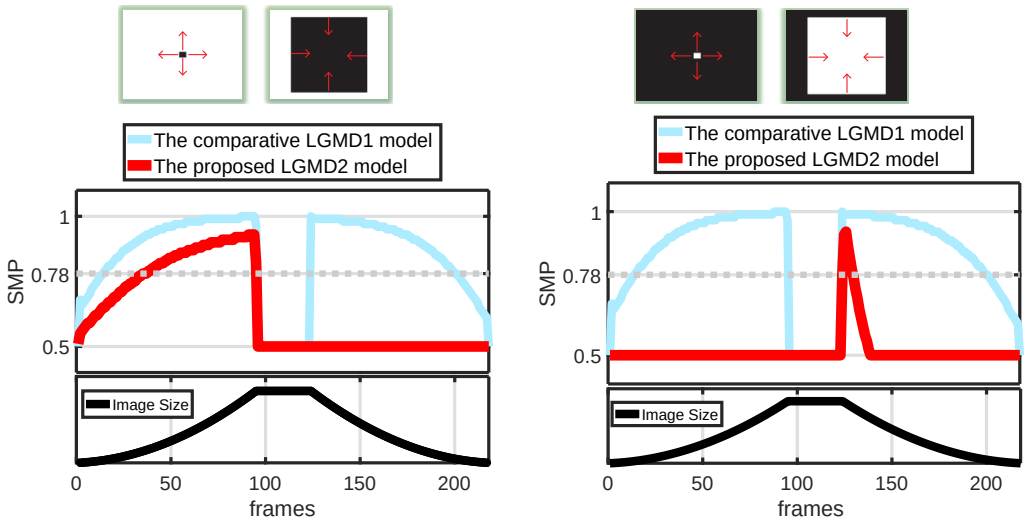

Figure 3.6: Neural response of the proposed LGMD2 and the comparative LGMD1 models by dark and light looming stimuli: the image size is depicted at each bottom. The horizontal dashed line indicates the firing threshold.

0.65 for robot tests.

3.1.4.2 Off-line Tests

Challenged by Synthetic Stimuli The experiments were started from testing the proposed LGMD2 neuronal model using computer-simulated stimuli and comparing it with the previous biological data [83] as shown in Fig. 3.2, and also results from the comparative LGMD1 model [7]. All the synthetic movements can be categorised into a few types including approach, recession, translation, elongation, shortening, whole-field luminance change and sinusoidal grating movements.

Firstly, we examined if the proposed model possesses similar unique selectivity as biological LGMD2 neurons. As shown in Fig. 3.6, when challenged against a dark approaching object, the neural responses of both models rapidly increase as the image size projected in the retina grows. However for a dark receding object, the proposed model shows no response; while the comparative model is activated. For a light (or white) approaching-receding object, the LGMD1 model responds to it in a way similarly to the dark object moving in depth. As expected, the LGMD2 model dose not respond to the white approaching object and is shortly activated during the start of recession. A fast adaptation happens to the receding light object. This fulfils the revealed unique selectivity of biological LGMD2 neurons with preference to only

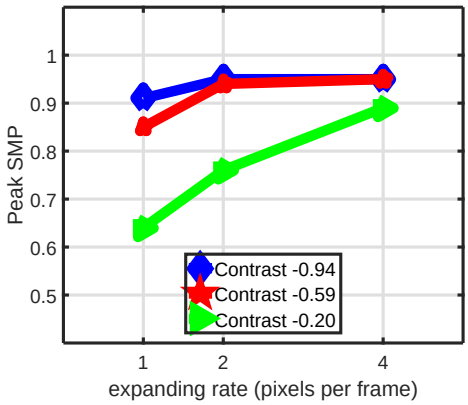

Figure 3.7: The peak neural response tested by looming objects at three contrasts and approaching speeds or edge expanding rate.

the light-to-dark luminance change, as demonstrated in Fig. 3.2a.

Moreover, we investigated the effects of contrast and approaching speed on the proposed model, which was tested by looming objects with different contrasts and edge expanding rates. In this case, the contrast is denoted by

$$Contrast = (L_{obj} - L_{back})/L_{back}, \tag{3.28}$$

where L_{obj} and L_{back} are the average luminance of the moving objects and the background. As shown in Fig. 3.7, the contrast can influence the peak neural response of the proposed model, especially when the approaching speed is low. Interestingly, as the speed increases, the influence of contrast declines. With a same contrast, the proposed model also shows speed response. This suggests the LGMD2 neuron may be more effective at a critical moment when predators become very close to locusts.

For the X-Y planes stimuli (i.e. translating, elongating-and-shortening movements), as illustrated in Fig. 3.8, with either dark or light translations on two directions at constant speed, the LGMD2 neuron model only shows briefly weak response at the beginning of each course, which well conforms to the biological research [83] and data in Fig. 3.2b. On the other hand, the comparative LGMD1 model exhibits much higher-level outputs sustaining to the end of each course. As a special case of translating stimuli, the elongation and shortening movements represent the situations that translating objects moving very close to the field of view. More precisely, the single translating edge leads to the light-to-dark luminance change during dark-elongating and light-

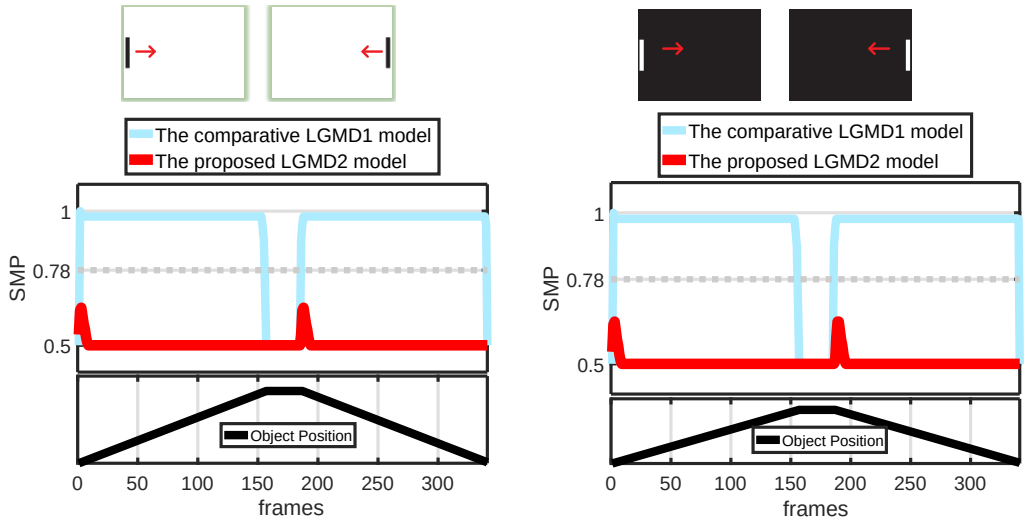

Figure 3.8: Neural response of two models against dark and light translating stimuli: the bar position is depicted at each bottom.

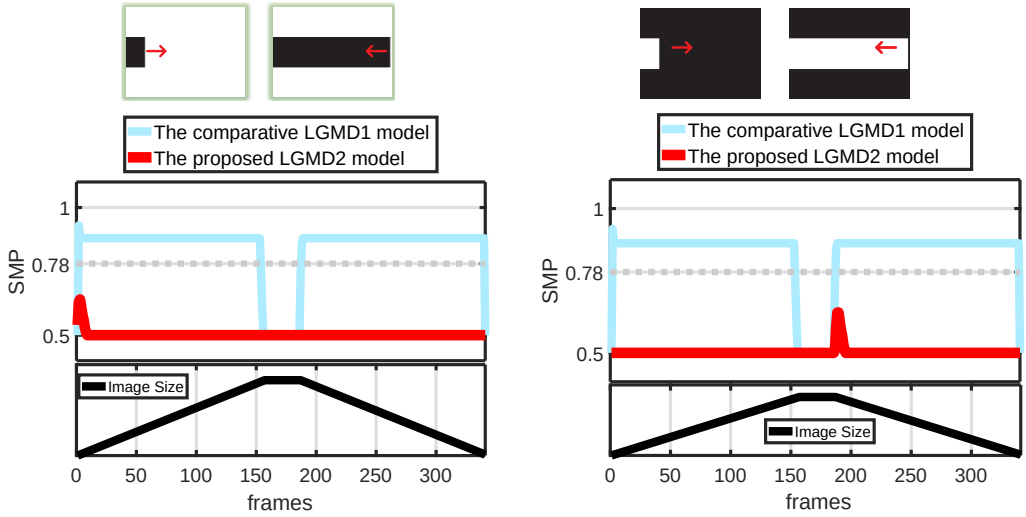

Figure 3.9: Neural response of two models against dark and light elongating-and-shortening movements: the image size change is depicted at each bottom.

shortening; otherwise it gives rise to the dark-to-light luminance change. Similarly to the data in Fig. 3.2b, the proposed model only responds briefly to dark-elongating and light-shortening movements (Fig. 3.9).

With the similar stimuli in Fig. 3.2a, we also simulate the whole sub-field luminance change. As illustrated in Fig. 3.10, within either darkening or lightening course, both models are rigorously inhibited which reconcile with the neural response of biological LGMD1 and LGMD2 neurons [83]. And for the systematic grating movement tests, Fig. 3.11 demonstrates the proposed LGMD2 model is not responding to the tested gratings with a wide range of spatiotemporal frequencies representing the antago-

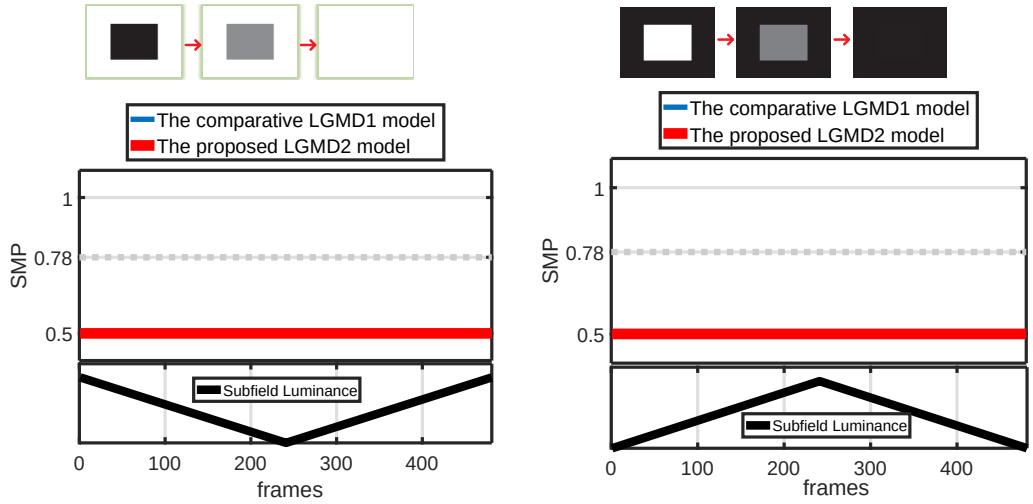

Figure 3.10: Neural response of two models against wide-field luminance change with intensity depicted at each bottom.

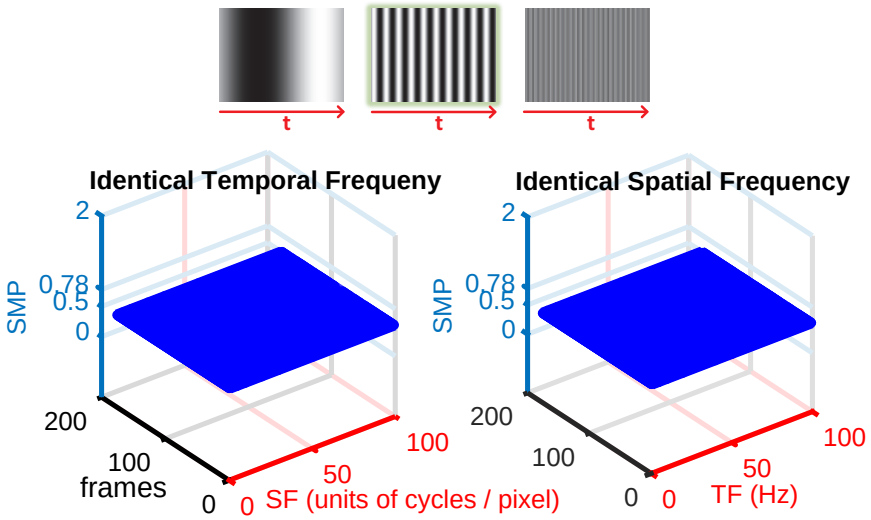

Figure 3.11: A wide range of spatiotemporal grating tests: the spiking threshold is set at 0.78. The proposed LGMD2 model remains quiet to gratings at all tested spatial and temporal frequencies (SF and TF).

nism to a variety of visual cluttered backgrounds in the real world. This is achieved by the inhibition mechanisms in the proposed model. The biological collision-detecting visual systems can perform robustly against visual clutter, which is a critical criteria for an artificial vision system for collision detection.

To sum up the synthetic stimuli tests, compared to the comparative LGMD1 model, the proposed model demonstrates similar neural response to a LGMD2 neuron which responds most strongly to dark looming objects. Such specific selectivity is realised by the modelling of parallel biased-ON and OFF pathways and the SFA mechanism. Our results match well the biological data depicted in Fig. 3.2.

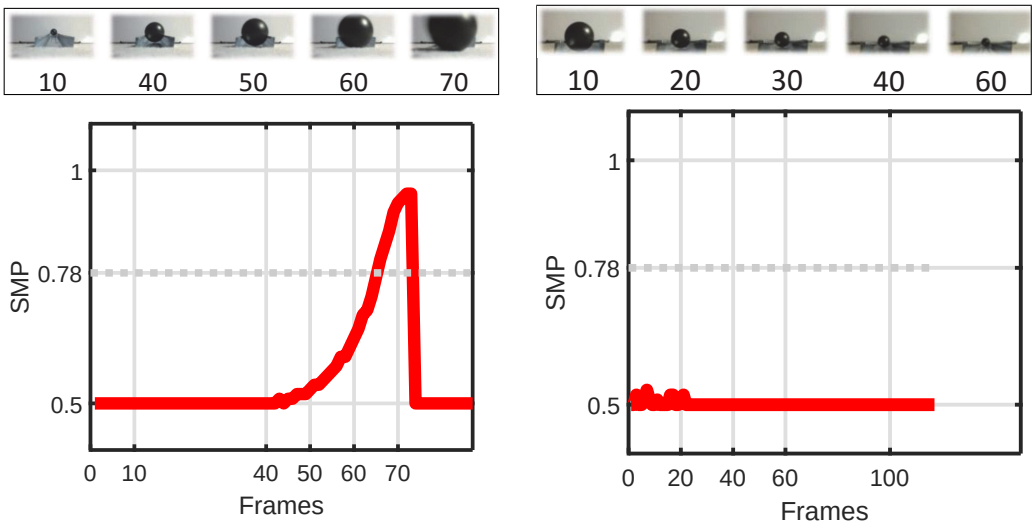

Figure 3.12: Neural response of the proposed LGMD2 neuronal model tested by approaching and receding dark objects embedded in light background.

Challenged by Real Physical Stimuli After that, the proposed LGMD2 neuronal model was tested using real-world visual stimuli. Compare to the simulated scenarios, there is background noise in real physical scenes such as light flash and shadows and etc. In addition, unlike the simulated movements, the object's moving speeds could not be controlled to, or maintained at, a constant level. Therefore, the visual challenges presented to the proposed collision-detecting system are 'real'.

Firstly, the LGMD2 model was tested by a dark object moving in depth within bright background. As depicted in Fig. 3.12, it is no surprise that the proposed model detects the direct collision. Importantly, like a biological LGMD2 neuron, the proposed model keeps quiet during the whole recession course.

We also looked into the model performance challenged by angular approaches. Fig. 3.13a demonstrates the experimental setting. More precisely, a frontal collision corresponds to a 0-degree approach and others represent the 'near-miss' scenes. Fig. 3.13b illustrates that as the angle increases, the LGMD2 peaks later, and the peak responses of both the neural response and the FFI shrink. More intuitively, the statistical results from repeated tests demonstrate the proposed model is more sensitive to frontal looming objects. As introduced in the previous sections, locusts can detect imminent collision corresponding to timely avoidance behaviours especially at some critical moments that objects approach rapidly and frontally. This reveals the LGMDs respond

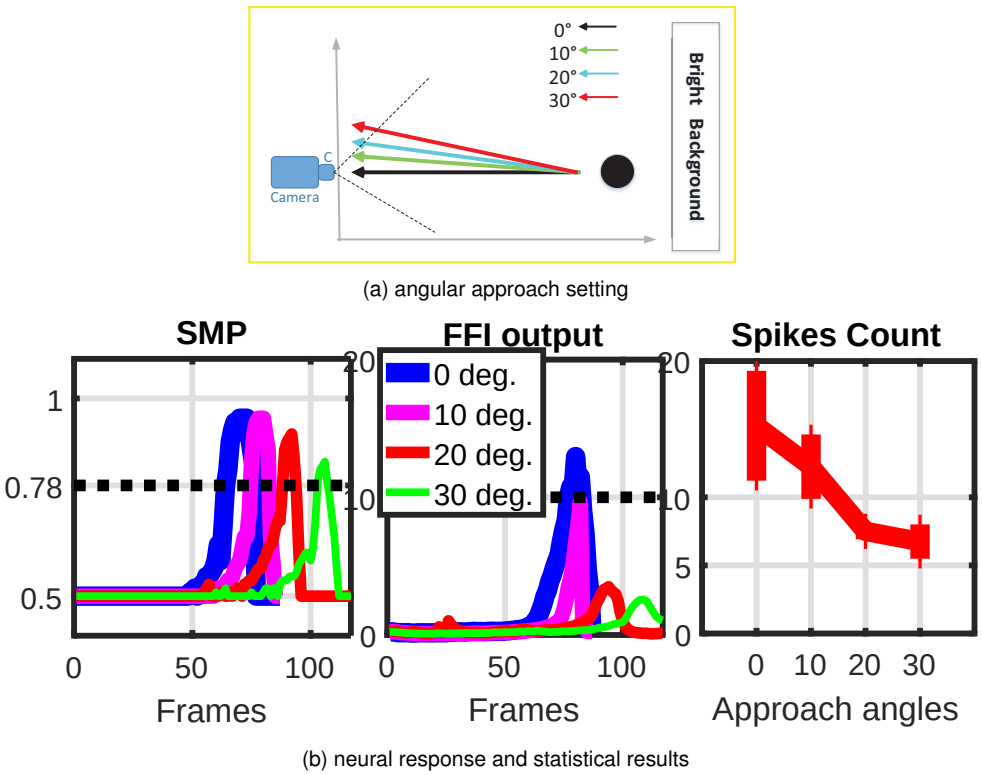

Figure 3.13: Angular approach tests: the horizontal dashed lines are the specified thresholds. The proposed model is tested by looming from four angles. Each angular approach was repeated ten times. The modelled LGMD2 neuron spikes at the highest rate by direct approaching stimuli.

most strongly to oncoming objects, whereat our results match well.

In the second type of real physical stimuli tests, the proposed model was challenged by a few sets of translations against a visually cluttered background, as shown in Fig. 3.14a. The statistical results in Fig. 3.14b demonstrate that 1) the proposed model exhibits lower-level peak response compared to looming tests, and more importantly all below the firing threshold; 2) the proposed model shows speed response to translating stimuli, that is, faster translational motion leads to stronger neural response.

In the last type of real physical stimuli tests, the proposed model was challenged by a turning cluttered scene. As illustrated in Fig. 3.15, the proposed model remains quiet within the intact turning course, since the FFI climbs significantly to overstep its threshold and remains at very high level till the end of movement. This demonstrates that with a similar FFI-pathway like the LGMD1 model, the LGMD2 neuron model can also deal with the situation appropriately even a large amount of photoreceptors are highly activated, simultaneously.

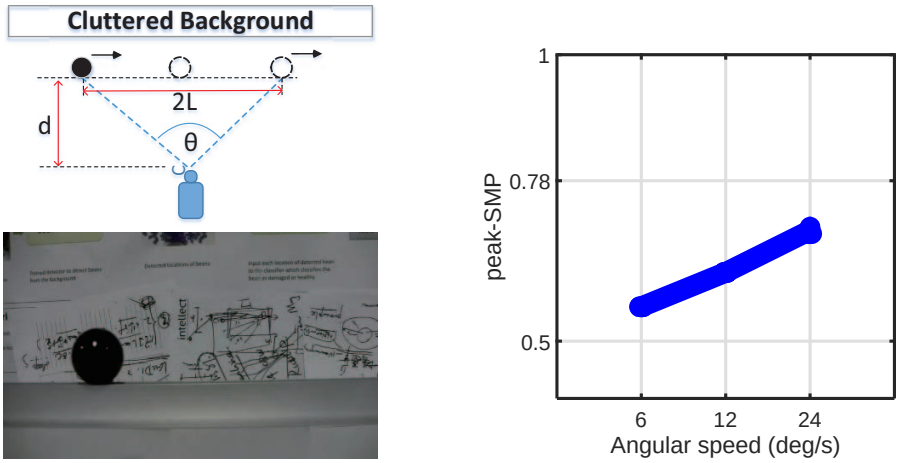

(a) experimental setting (b) statistical results

Figure 3.14: Systematic translation tests with (a) the experimental setting and an example snapshot from video clips: the distance d is fixed, and the angular size thus can be calculated by $\theta = 2tan^{-1}(L/2d)$, in order to estimate the angular speed. (b) The statistics of peak neural response of the proposed model tested by three angular speeds, each throughout ten repeated courses.

3.1.4.3 On-line Robot Tests

Within this subsection, the on-line robot tests will be presented. The proposed LGMD2 neuronal model was implemented as an embedded vision system in a *Colias* robot. The experiments can be categorised into two types of tests: 1) open-loop tests: the robot was stimulated by overhead looming, and translating movements, in order to investigate the LGMD2's model features; 2) closed-loop tests: the robot was tested in an arena for collision avoidance in near range navigation mixed with many obstacles, at varied linear speeds.

Investigation of Model Characteristics For deepening our understanding of LGMD2's unique characteristics and verifying robustness of the proposed model as an embedded vision system for collision recognition in the ground miniaturised robot, a few types of real-time experiments were carried out. In this kind of tests, the motion unit of the tested robot was closed. We collected the model outputs from the Bluetooth. Firstly, we simulated the scenarios that a locust on the ground stimulated by overhead looming stimuli representing predators from the sky. The experimental setting is illustrated in Fig. 3.16. The *Colias* robot was firstly tested by the darkest object approaching from four different heights (H in Fig. 3.16). The results in Fig. 3.17 demonstrate that the

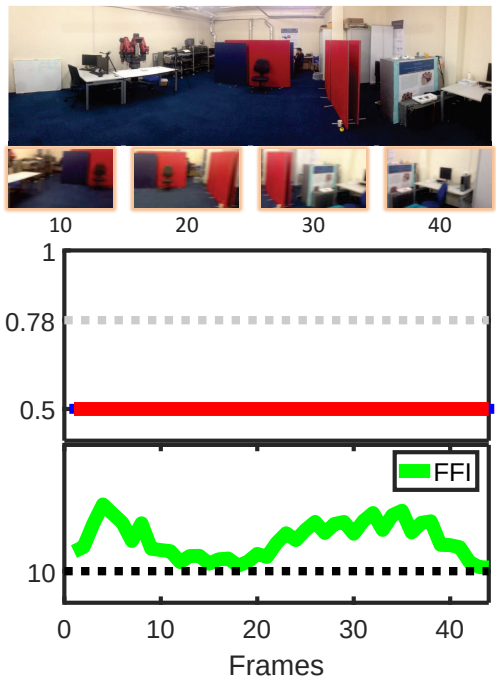

Figure 3.15: The results of processing a rapid turning scene with visual clutter.

LGMD2-based embedded vision system is able to recognise all imminent collisions. More precisely, the neural response increases within each looming stimuli and then brings about high-rate spikes corresponding to the collision recognition.

For further verifying the unique features of the proposed LGMD2 neuronal model against darker and lighter looming objects, as shown in Fig. 3.16, varied grey-scale objects, from white to dark, were applied to trial the looming selectivity. Each RGB-colour object possesses a certain grey level. Notably, with regard to the biological tests on LGMD2 neurons (Fig. 3.2), we set up a dark and a bright environments, respectively, as presented in the experimental setting in the Fig. 3.16. In the first case, only the global illumination (source A in Fig. 3.16) is applied to make up a purely bright background. As a result, all objects including the white one are darker than the background (Fig. 3.18a). The results in Fig. 3.18c clearly show that the neural response of proposed LGMD2 model steeply increases by impending collisions caused by rapid looming objects. The embedded system can recognise collisions by most of the grey-scale approaching objects, yet the white looming object gives rise to a relatively weaker response which could not activate the modelled LGMD2 neuron for high-frequency spikes. Intuitively, the statistical results from repeated tests reveal that the proposed model performs robustly in detecting dark looming objects. In addition,

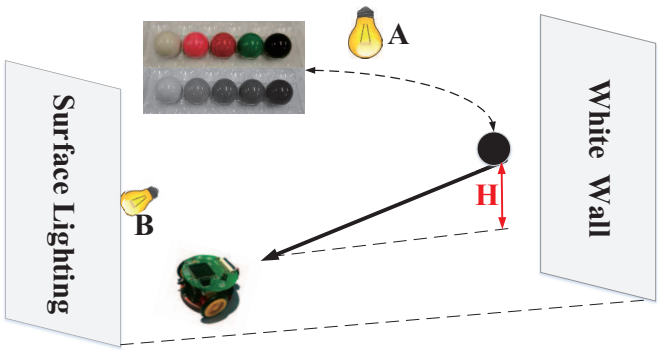

Figure 3.16: Robot looming tests setting: five grey-scale objects approach the *Colias* robot along a slot with a slope to the ground, respectively. There are two light sources capable of forming a light or a dark environment, separately. The lighting point A alone is a global top-down illumination to form a bright environment. And the lighting source B on its own supports a local surface illumination behind the robot to form a dark scenario.

it appears that the darker objects bring about stronger neural responses, which means the model is sensitive to the contrast. This matches well the synthetic tests results as depicted in Fig. 3.7.

In the second round of looming tests, we changed the illumination by replacing the global with the local surface lighting (B in Fig. 3.16). In this case, as shown in the sampled views from the tested *Colias* robot in Fig. 3.18b, all targets including the black ball are lighter than the background. As a result, each looming course brings about the dark-to-light luminance change. The results in Fig. 3.18d demonstrate the embedded system otherwise is not sensitive to this type of collisions by lighter approaching objects. This is exactly consistent with the revealed neural properties of biological LGMD2 neurons in locusts which are only sensitive to the light-to-dark luminance change. Amongst other grey-levels, although the white looming object leads to strongest responses, the peaks are all far below the defined threshold (Fig. 3.18d).

With similar experimental setting in Fig. 3.16, the embedded LGMD2 model was tested by translating movements, i.e. the non-colliding scenarios. We investigated the effects of different translating distances and speeds on the model performance. The darkest ball was used to be the stimulus translating across the tested *Colias*'s field of view at different distances and speeds, respectively. The following conclusions can be drawn from the statistical results in Fig. 3.19: 1) At a same translating speed, further distance leads to weaker neural response (Fig. 3.19a). If the distance is far enough to

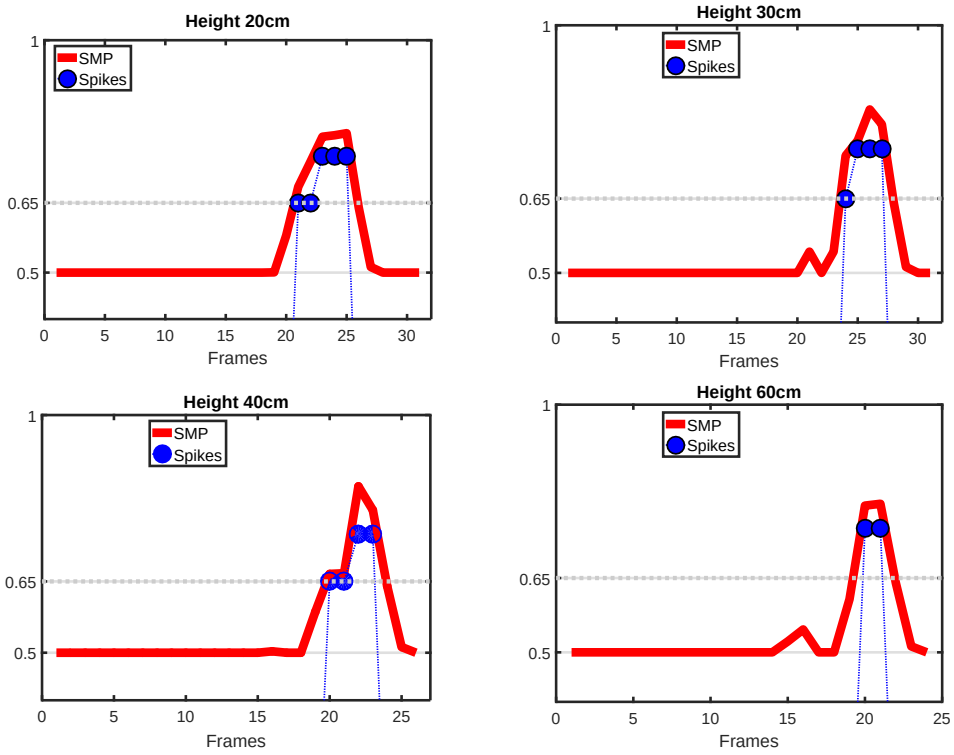

Figure 3.17: Neural response of the embedded LGMD2 model challenged by overhead looming from four heights: the membrane potential and elicited spikes are shown. The spiking threshold is depicted in grey dashed line.

the tested robot agent (50cm in our case), the LGMD2 model remains quiet. On the other hand, if the distance is very close to the field of view, the LGMD2 neuron could be highly activated. It is conceivable that such an situation could be also treated as a potential threat or collision. 2) When the translating distance is fixed (Fig. 3.19b), the LGMD2 model responds more strongly to translation at faster speed, which demonstrates the speed response and matches well the results in the real physical tests (Fig. 3.14).

To sum up, the open-loop robot experiments have verified that our proposed computational model fulfils the unique characteristics of LGMD2 in the locust's visual pathway, that is, it responds most strongly to dark looming objects within bright background over other visual challenges. This could benefit building robust collision detectors with enhanced selectivity for ground mobile robots.

Arena Tests In the second type of robot tests, we examined effectiveness and robustness of the proposed LGMD2 model as a quick collision detector for ground robot near range navigation. We built an arena with approximately $95 \times 115cm^2$ in area. A *Col-*

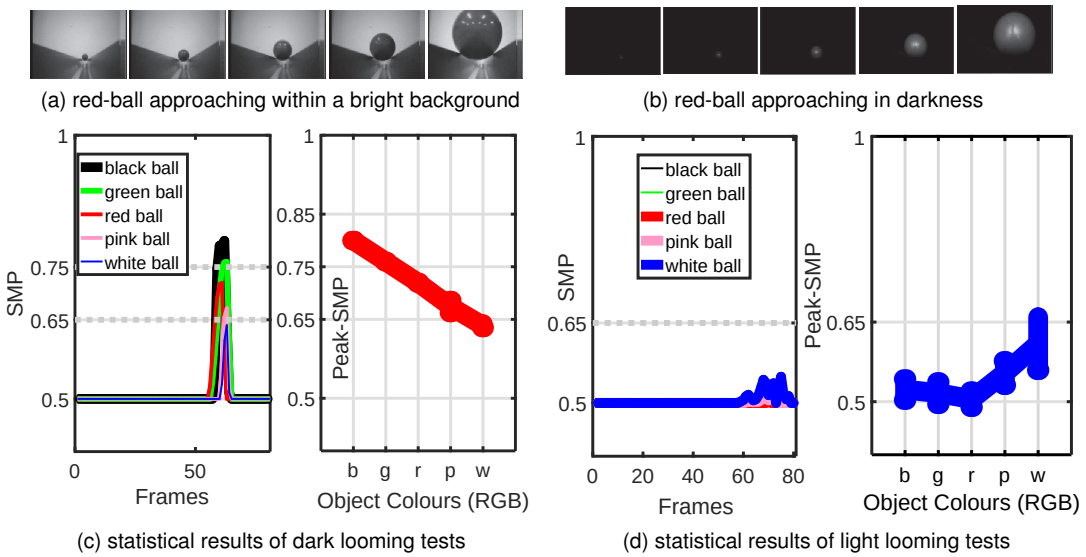

Figure 3.18: The systematic overhead looming tests to investigate the specific characteristics of proposed model: the example views from the tested *Colias* robot are shown in (a), (b). Each grey-scale looming course was repeated ten times, respectively, in bright and dark environments.

ias robot agent with the embedded vision system as the only collision sensing modality was tested in the arena mixed with a number of $(10 \sim 20)$ stationary obstacles for different layouts and under the same illumination. The white internal walls of the arena and the white surface of obstacles are marked with densely distributed dark patterns. A CCD-camera is fixed above the arena to form a top-down view to record performances of the *Colias* robot. There are also specific patterns on top of the micro-robot and the poles for a localisation system [56]. Therefore, we can get the very precise trajectories of the tested robot throughout each test. In the arena tests, the goalless *Colias* agent was initialised to go forward autonomously until a potential collision detected. The robot linear speed was set at approximately 10cm/s. The avoidance behaviour was simply set to turn right or left randomly with a large angle, as the mobile robots can only run on the 2D surface. After each avoidance, it resumes to go forward, and so on.

Fig. 3.20 illustrates eight arena tests results. The tested agent performed well for collision avoidance in the arena interacting with obstacles. The results have verified the proposed LGMD2 neuronal model on embedded system can be an ideal collision detector for ground mobile robots.

We also tested the proposed embedded vision system in the *Colias* robot at different linear speeds from extremely slow to very fast, each of which lasted for approximately

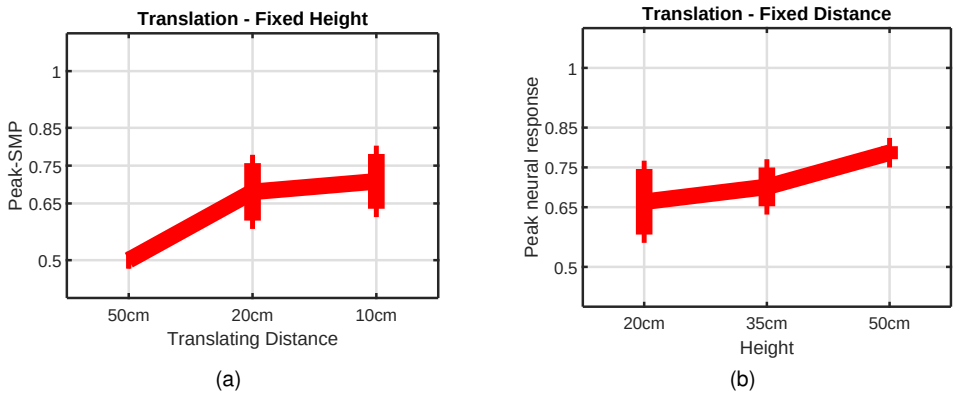

Figure 3.19: Statistical results of translating tests on the proposed embedded LGMD2 model: the translating distances varied in 10, 20 and 50cm; and the height of slot varied in 20, 35 and 50cm indicating translating speeds from slow to fast. Each test was repeated ten times.

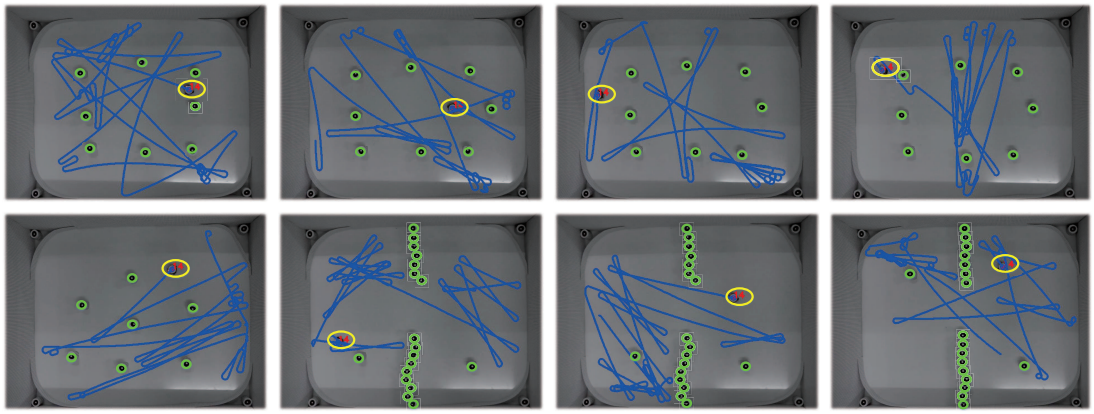

Figure 3.20: The top-down views of arena tests for collision detection in robot near range navigation with stationary obstacles: each test lasted for one-minute. The over-time trajectories are depicted in blue line. The final position of robot with identified ID is within yellow circle. The poles are marked by green circle.

one-hour. The success rate (SR) thus can be denoted by

$$SR = EV_a/(EV_a + EV_m), \tag{3.29}$$

where EV_a and EV_m indicate the specified events of avoidance and missed-detection. We can conclude from the statistical results shown in Table 3.3 that 1) In general, the proposed LGMD2-based embedded system performs well for collision recognition in near range navigation, event at the extremely slow (3cm/s) and fast (20cm/s) linear speeds. 2) The proposed model performs better at faster moving speeds. More precisely, the SR peaks at the tested velocity of 15cm/s. This demonstrates that for the ground mobile robots, the LGMD2 model could be better sensing dark objects that approach

Table 3.3: Success Rates of Collision Detection in Arena Tests

Linear speed(cm/s)	Success rate(%)
3	85.8%
6	92.4%
10	93.3%
15	**96.0%**
20	91.5%

rapidly, which reconciles with the situation juvenile locusts on the ground perceiving predators swooping from the sky.

3.1.5 Further Discussion

Through the above systematic experiments, we have shown that the proposed neuronal model, with parallel biased-ON and OFF pathways, demonstrates the similar characteristics to biological LGMD2 neurons in the locust's visual systems. In locusts, both the LGMD1 and the LGMD2 respond to rapid expanding object representing an imminent collision or a strike from predator. Nevertheless, the biological functions of LGMD2 differ from the LGMD1 in a number of ways. First, the LGMD2 is not sensitive to a light or white looming object whereas the LGMD1 is. Second, the LGMD2 does not respond to dark objects that recede at all, while the LGMD1 is often excited though very briefly. The proposed computational model has fully exhibited the above two critical features, as shown in the results in Fig. 3.6, 3.12, 3.17 and 3.18. These also satisfy the biological data on the LGMD2 in locusts in the Fig. 3.2a.

The LGMD2 matures earlier than the LGMD1 and plays crucial roles of collision detection for juvenile locusts living on the ground. As the locusts grow up, the visual environments become more complex due to innate flying behaviours. The LGMD1 gradually take place of the LGMD2 which could deal with more plentiful colliding scenarios. A possible reason is that the LGMD1 can recognise also light looming objects. However, the LGMD2 still exists in the visual systems of adult locusts. How both neurons cooperate in the locust's looming perception pathways still remains unknown. From a modeller's perspective, if we could build multiple visual pathways combining features of both the LGMD1 and the LGMD2, the collision selectivity could be further

enhanced.

A biophysical mechanism, the spike frequency adaptation, has been modelled in this neuronal model. This contributes to largely reduce the LGMD2's neural response to translating stimuli, especially with constant intensity. Our results in the Fig. 3.8, 3.14, 3.19 demonstrate that the proposed model has achieved this and matches well the biological data shown in the Fig. 3.2b. However, such a mechanism has little influence on visual stimulus with increasing intensity, for example, the approach and the accelerating translation.

There is valuable data on different protocols for shaping the collision selectivity in such looming sensitive neurons like the proposed LGMD2. For example, Badia et al. proposed the non-linearity between the feed-forward excitatory and inhibitory responses can shape the selectivity to approaching objects [18]. The FFI mechanism modelled in this study also contributes effectively (Fig. 3.15), which cannot be disregarded. In addition, a recent biological research also demonstrates a self-inhibition mechanism which could coordinate with the lateral-inhibition to shape the LGMDs' selectivity to looming versus translating stimuli [116]. In the near future, we will investigate the roles of these different mechanisms in shaping the selectivity in such looming sensitive neuron models.

The arena tests have verified the robustness of proposed neuronal model for collision detection. In the literature so far, there have been a handful of candidates inspired by biological visual systems for collision detection, like the fly optic flow based methods [176, 59], the locust DSNs [24, 25] and the LGMD1-based detectors [7, 6, 9]. This research has provided an alternative solution to the repository of bio-inspired collision detection methodologies. However, there is lack of comparative study on the different models. Furthermore, these naturally inspired methods also need to be tested in more complicated real-world scenarios and with more kinds of mobile platforms.

3.1.6 Summary

In this section, we have proposed a collision selective visual neural network based on an unique neuron LGMD2 in the locust's visual pathway. The LGMD2 neuron is sensi-

tive to looming objects but only responds selectively to dark objects that approach within bright background underlying a preference to the light-to-dark luminance change. Through the modelling of biased-ON and OFF pathways encoding onset and offset responses separately in a computational structure, such unique selectivity of LGMD2 has been fully demonstrated in this modelling study. In addition, a biophysical mechanism of spike frequency adaptation is modelled to sharpen up the LGMD2's selectivity to dark objects approaching versus translating. The proposed LGMD2 neuronal model has been validated with systematic experiments challenged by stimuli ranging from synthetic to real world. The robot arena tests have verified its robust collision sensing performance in a ground mobile robot. The computational simplicity of the proposed model has been also demonstrated by the miniaturised robot implementation. Similarly to other neuromorphic computation structures, the proposed LGMD2 model can be easily realised in VLSI chip for volume production.

3.2 An LGMD1 Model with ON and OFF Pathways

In the above section, we have shown the computational modelling of an LGMD2 visual neuron in locusts and the satisfactory realisation on the embedded system. With former useful modelling experience, we found that the ON and OFF visual pathways have great potential in not only building the LGMD2 neurons that possess unique looming selectivity, but also realising the functionality and characteristics of the LGMD1 neurons. More importantly, while such polarity cells have not been fully identified in the locust visual systems with only a few assumptions like [77, 117, 116, 18, 160], the computational modelling and testing under similar conditions to the physiological and ethological experiments could provide biologists with useful implications.

In this section, this thesis continues to demonstrate biologically plausible methods to construct an LGMD1 neuron model, and shape the collision selectivity. Importantly, this can be a general LGMDs neuronal model that meets the biological functions of both the LGMD1 and the LGMD2. In this research, we highlight also the functionality of ON and OFF visual pathways. We will demonstrate the important role of such a computational structure to separate the different looming selectivity between the two

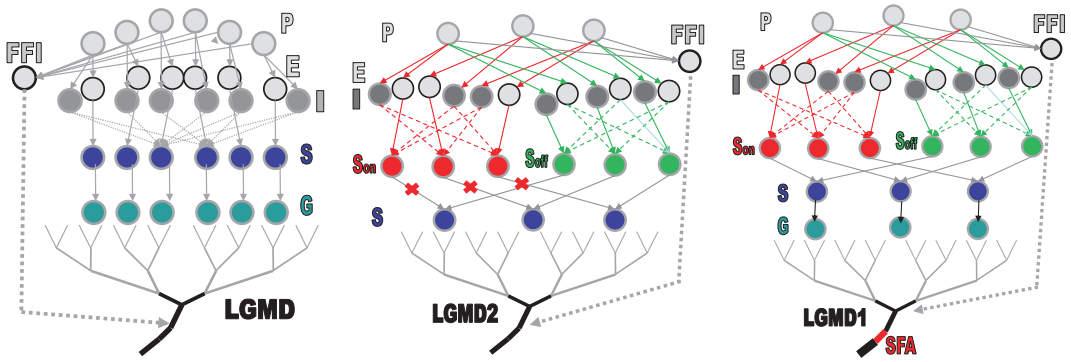

(a) comparative LGMD1 (b) previous LGMD2 (c) proposed LGMDs

Figure 3.21: Schematics of former LGMDs models adapted from [6, 9, 21, 20] and the proposed general LGMDs model: (a) The previous LGMD1 model [6] (taken 6 pixels from the visual field) processes visual information in a single pathway, that is composed of five layers (P, E, I, S, G) and two cells (FFI, LGMD). (b) The LGMD2 model from my partial research [20, 21] (taken 3 pixels) processes signals in separated ON (red-arrows) and OFF (green-arrows) pathways each with three layers (E, I, S), whilst the ON channels are rigorously blocked. (c) The proposed LGMDs universal model processes signals in the ON and OFF pathways without bias, and a new SFA mechanism is modelled. In all models, the dashed lines indicate transmissions of delayed neural signals.

LGMDs through systematic experiments.

More concretely, in the vast majority of LGMD1 neuronal models, visual information is processed in a single pathway, as a case study shown in Fig. 3.21a. Compared with the seminal work on modelling ON and OFF mechanisms in an LGMD-based computational model by Keil et al. [10], we model the ON and OFF pathways each with multiple layers for spatiotemporal computations and investigate its functionality of achieving different collision selectivity. In addition, the non-linear modelling study proposed in [18] also demonstrated the effectiveness of an ON and OFF mechanism of encoding for onset and offset responses separately to implement a biological LGMD1 neuron. More specifically, luminance increments/decrements give rise to onset and offset responses, respectively. In the general model, with a similar idea, we demonstrate that the onset and offset responses bring about delayed inhibitory and excitatory information in the ON and OFF pathways respectively, as can be seen in the schematic diagram shown in Fig. 3.21c. While in previous LGMD1 models like 3.21a, the inhibitory flows are always delayed relative to the excitatory flows. Moreover, as shown in Fig. 3.21b, we have shown initial methods with ON and OFF pathways to realise the characteristics of a LGMD2 neuron [20, 21]. We have shown initial methods to realise

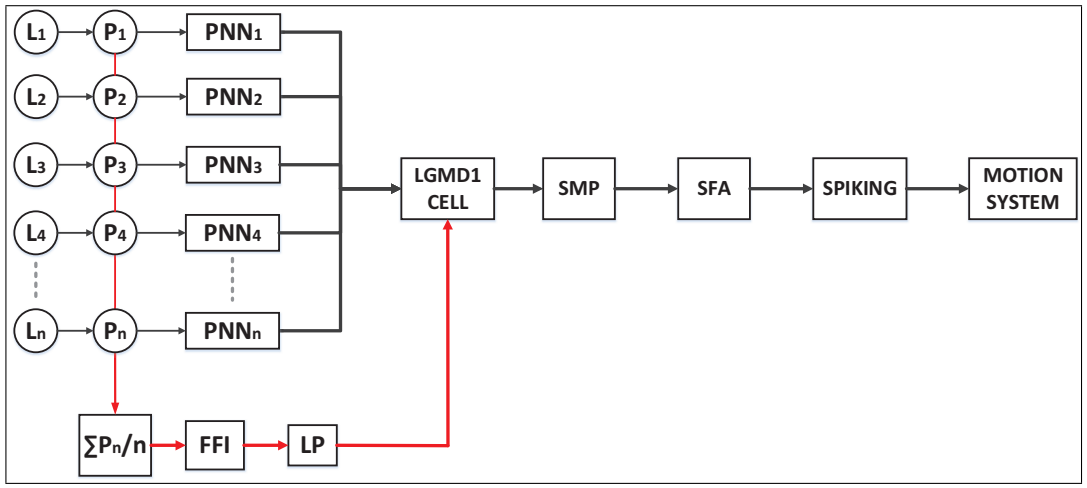

(a) LGMD1 visual neural network

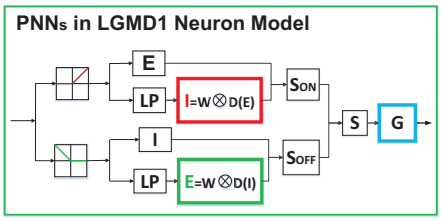

(b) partial neural network

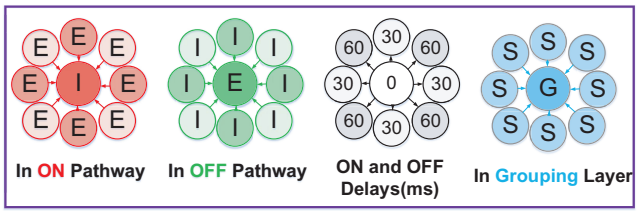

(c) spatiotemporal convolutions

Figure 3.22: Schematic of the proposed LGMDs general model to realise an LGMD1 neuron: **(a)** a schema of signal processing to implement an LGMD1 neuron model: the pixel-wise luminance (L) is captured by photoreceptors (P), which convey motion information to the partial neural networks (PNN); the LGMD1 cell integrates the local excitations from intact pre-synaptic PNNs forming the sigmoid membrane potential (SMP) towards the spike frequency adaptation (SFA) and spiking mechanisms; the generated spikes are transmitted to motion neural systems. **(b)** a schema of PNN depicts the ON and OFF mechanisms: in ON channels, the inhibition (I) is computed via convolving surrounding delayed excitations (D(E)); in OFF channels, the excitation (E) is computed via convolving surrounding delayed inhibitions (D(I)); excitations and inhibitions compete with each other in local summation (S) cells; the grouping (G) layer convolves excitations from S cells. **(c)** spatiotemporal convolutions in PNNs.

the characteristics of a LGMD2 neuron. In this section, a more systematic study will be presented to model a biological LGMD1.

3.2.1 Framework of the Proposed LGMD1 Neuronal Model

Within this subsection, we present the modelling of LGMD1 neuron model with ON and OFF pathways (Fig. 3.22), and moreover prove that the proposed neural network can be a general LGMDs model to meet biological functions of both the LGMD1 and LGMD2. In the pre-synaptic field, compared with similar LGMD1 models, e.g. [6, 9], we highlight the functions of separate ON and OFF pathways with spatial convolution

and dynamically temporal filtering. A new mechanism of spike frequency adaptation is modelled in the spike initiation zone. Generally speaking, the neural network includes (1) a photoreceptors layer to retrieve initial motion information, (2) two separated visual pathways to encode ON and OFF depth features – each of which has three local layers of excitation, inhibition and summation cells, (3) a summation-grouping layer to combine relayed excitations from both pathways, (4) an LGMD1 cell to exponentially map feed-forward excitation to membrane potential, (5) an individual feed-forward pathway for an 'all-or-none' law to control the activation of LGMD1, (6) SFA and spiking mechanisms to transform neural response to spikes. Like the proposed LGMD2 model in Section 3.1, the proposed LGMD1 model also perceives collisions by reacting to the expanding edges of objects.

Notably, compared with the proposed LGMD2 model introduced in the above Section 3.1, there are two main differences in this modelling study:

- The core structure of the proposed model is the ON and OFF polarity pathways. In Section 3.1, we have demonstrated that such a bio-plausible structure can fulfil the functions of an LGMD2 neuron that is only sensitive to dark looming objects. In this section, we will continue to demonstrate its efficacy in implementing an LGMD1 neuron. More precisely, it can bee seen from Fig. 3.3 and 3.22 that the ON channels are rigorously blocked in the LGMD2 but the LGMD1 model.

- The proposed LGMD1 model applies dynamic temporal filtering in a computational structure, as the convolution kernels shown in Fig. 3.22c; whilst the previous LGMD2 model uses same temporal delay for postponed neural signals. This better matches the biological modelling theories in [79]. In the experiments, we will investigate the effects of proposed new mechanisms on collision detection.

Fig. 3.22 depicts a schema of the proposed framework with the partial neural network structure and spatiotemporal convolutions. To illustrate the algorithms, we underline the different parts to the proposed LGMD2 model in the Section 3.1, so that the repetitive ones are omitted here.

3.2.1.1 Photoreceptors

The first layer consists of photoreceptors arranged as a 2D matrix. The total number of photoreceptors correspond to the number of local pixels in the field of view. Photoreceptors capture grey-scaled brightness and compute the change of luminance between every two successive frames. The computation corresponds to the Eq. 3.1.

3.2.1.2 ON and OFF Rectifying Transient Cells

Next, the relayed visual signals from photoreceptors are split into parallel ON and OFF visual pathways via the mechanisms of ON and OFF rectifying transient cells (RTCs), encoding luminance increments (onset response) and decrements (offset response), respectively. Technically speaking, as shown in the PNN of an LGMD1 model (Fig. 3.22b), the functionality of these polarity cells is reconciled with a 'half-wave' rectifier, which filters out negative/positive inputs for ON and OFF pathways, and inverts negative inputs to positive in the OFF pathway. Each photoreceptor corresponds to a pairwise ON and OFF RTCs. The calculation is consistent with the Eq. 3.3.

3.2.1.3 Spatiotemporal Visual Processing in ON and OFF Channels

After the 'half-wave' rectifying, the ON cells convey brightness increments to the ON pathway including the excitation (E), the inhibition (I) and the local ON-summation (S_{on}) cells. ON cells elicit onset responses, i.e., excitations are time-advance relatively to inhibitions and transmitted directly to the excitation cells in the ON pathway:

$$E_{on}(x, y, t) = ON(x, y, t). \tag{3.30}$$

Meanwhile, it is delayed by tens to hundreds of milliseconds, the mechanism of which is reconciled with a first-order low-pass filtering:

$$\frac{dD_{on}(x, y, t)}{dt} = \frac{1}{\tau_s}(ON(x, y, t) - D_{on}(x, y, t)), \tag{3.31}$$

where τ_s is a dynamic time parameter, which can vary between tens to hundreds of milliseconds in the low-pass filter. Inhibitions in the ON pathway are formed by con-

volving surrounding delayed excitations, as shown in Fig. 3.22c. Compared with previous LGMD1 models, wherein the inhibition was computed by convolving surrounding one-frame-delayed excitations, we propose a dynamic spatiotemporal convolution: the nearest four neighbouring cells share relatively higher weightings and shorter delays than the four diagonal cells. The temporal dynamics are illustrated in Fig. 3.22c, and the weightings of convolution kernel ($[W_i]$) fits the matrix in the Eq. 3.11. It is worth noticing that the delayed information only spreads out to their neighboring cells rather than to its direct counterpart. In this modeling study, the radius (r) of convolution kernel is set to 1, for the purpose of saving computational power, as the convolution process goes through each local cell in both ON and OFF pathways. Therefore, the inhibition in each interneuron of the ON pathway is calculated by the following equation:

$$I_{on}(x,y,t) = \sum_{i=-r}^{r} \sum_{j=-r}^{r} D_{on}(x+i, y+j, t) \cdot W_i(i+r, j+r). \tag{3.32}$$

The OFF pathway processes visual information similarly to the ON pathway. However, since OFF cells elicit offset responses by brightness decrements, inhibitions are directly conveyed to the inhibition cells, whilst the excitation is formed by convolving surrounding delayed inhibitions, as illustrated in Fig. 3.22b and Fig. 3.22c. In this LGMD1 based modelling study, we set the excitatory convolution kernel ($[W_e]$) equal to the $[W_i]$. The dynamic temporal parameter τ_s is used to filter inhibitions in the OFF pathway as well:

$$\frac{dD_{off}(x,y,t)}{dt} = \frac{1}{\tau_s}(OFF(x,y,t) - D_{off}(x,y,t)). \tag{3.33}$$

Accordingly, the excitation and inhibition are calculated as follows:

$$\begin{aligned} I_{off}(x,y,t) &= OFF(x,y,t), \\ E_{off}(x,y,t) &= \sum_{i=-r}^{r} \sum_{j=-r}^{r} D_{off}(x+i, y+j, t) \cdot W_e(i+r, j+r). \end{aligned} \tag{3.34}$$

After that, each polarity summation cell linearly integrates excitation and inhibition

with the biases w_1 and w_2, in order to suppress each inhibitory flow:

$$\begin{aligned} S_{on}(x,y,t) &= E_{on}(x,y,t) - w_1 \cdot I_{on}(x,y,t), \\ S_{off}(x,y,t) &= E_{off}(x,y,t) - w_2 \cdot I_{off}(x,y,t). \end{aligned} \tag{3.35}$$

3.2.1.4 Summation and Grouping Layers

With similar ideas in a few biological and computational modelling studies on a fly's visual system, [95, 43, 53], the relayed local excitations from ON and OFF channels interact with each other in a supra-linear (both multiplicative and linear) way at each summation cell in the PNN (S in Fig. 3.22b). The computation conforms to the Eq. 3.13. As introduced in Section 3.1, such a neural computation plays a crucial role to separate the looming selectivity between the LGMD1 and the LGMD2 neuron models, and moreover it can achieve the non-linear properties of visual motion detectors.

Similarly to the LGMD2 model in Section 3.1.2, we implement the selectivity to expanded edges by clustering excitations of looming objects in this general model, through a simplified grouping layer (G in Fig. 3.22b) relative to the similar LGMD1 models [6, 9] in Fig. 3.21a. It is basically a convolution course:

$$G(x,y,t) = \sum_{i=-r}^{r} \sum_{j=-r}^{r} S(x+i, y+j, t) \cdot W_g(i+r, j+r), \tag{3.36}$$

where W_g is an equal-weighted kernel as shown in Fig. 3.22c and agrees with the matrix in the Eq. 3.15, and the radius of convolving area is also set to 1. For the grouped cells, the clustered and stronger excitations will pass through to the LGMDs cell, whilst the smaller isolated (or decayed) excitations are eliminated by a local threshold:

$$\hat{G}(x,y,t) = \begin{cases} G(x,y,t), & \text{if } G(x,y,t) \geq T_g \\ 0, & \text{otherwise} \end{cases}. \tag{3.37}$$

3.2.1.5 LGMD1 Cell

At the LGMD1 cell, the neural processing is a competition between the feed-forward excitation and the feed-forward inhibition: if the excitation wins, the neuron is activat-

ed to generate spikes, otherwise, it is rigorously inhibited. The feed-forward excitation is formed by linearly pooling all local excitations from the grouping layer which can be represented by the membrane potential in the terminology of biology. The calculation is consistent with the Eq. 3.19. The membrane potential is then exponentially transformed which mimics the activation of artificial neurons. The computation is in line with the Eq. 3.20.

On the other hand, the FFI is formed and then delayed in a parallel pathway relatively to the whole pre-synaptic area, similarly to the proposed LGMD2 model in Section 3.1. Like the former LGMD1 models, e.g. [79, 6, 13, 9], the FFI mechanism obeys an 'all-or-none' law, meaning it can directly suppress the LGMDs cells if a large area of luminance change occurs rapidly within the field of view. The mathematical expression corresponds to the Eq. 3.25 and the Eq. 3.26. Once the postponed FFI output exceeds a predefined threshold level, the generated membrane potential is cut off directly; otherwise, the FFI has no effects on the LGMD1 cell.

3.2.1.6 Spike Frequency Adaptation

As presented in Section 3.1.2, in order to further enhance the visual looming selectivity, we computationally model the biophysical SFA mechanism. Its computational role allows a neural response with a positive derivative profile to overcome adaptation selectively, otherwise, the neural response is heavily blocked causing a quick decline. The computation equals the Eq. 3.21. It is worth emphasising that as the digital signals do not have continuous derivatives, we compute the gradient by comparing signals at successively discrete frames. It is also necessary to notice that the latencies in the SFA mechanism could vary within a wide range from hundreds to thousands of milliseconds in order to partition adaptation rates for different profiles of the LGMDs neural response.

3.2.1.7 Spiking Mechanism

After the SFA mechanism, a different number of spikes could be generated at each time point by an exponential mapping from the neural membrane potential to the firing

rate. The calculation conforms to the Eq. 3.23. As a result, compared with previous works on LGMD1 modelling, such as [6, 9], there could be more than one spike at each frame being generated. Finally, a potential collision recognition is given by the Eq. 3.24. In case of the proposed LGMD1 neuron model, the generated spikes are conveyed to its post-synaptic target-neuron, the DCMD, and towards further motion neural systems for collision avoidance behaviours.

3.2.1.8 Parameters Setting for LGMD1 Model

All the parameters of the proposed LGMD1 based visual neural network are decided empirically with considerations and optimisations of the underlined functionality of ON and OFF pathways and the SFA mechanism to implement the underlying characteristics of a biological LGMD1 visual neurone as an embedded vision system in our proposed *Colias* robot, as illustrated in Fig. 3.5. Compared to the proposed LGMD2 model in Section 3.1, a few key parameters are different in this LGMD1 visual neural network. More precisely, the time latency is dynamic and can vary from tens to hundreds milliseconds. In our case, the $\tau_s \in [15, 120]$. In addition, the combination of term coefficients in the ON and OFF pathways vary from those in the proposed LGMD2 model, which is critically important to separate the different selectivity between the LGMD1 and the LGMD2. In the LGMD1 model, the local excitations from both polarity pathways are balanced. As same as the proposed LGMD2 model, there are adaptable parameters that correspond to the physical properties of the input visual streams, i.e., the resolution of images and the sampling frequency of video clips from synthetic or real-world visual stimuli and a visual modality of a micro-robot. It is worth emphasising that the parameters learning and training methods are not applied to this LGMD1 neuron model. The full parameters setting can be referenced in [23]. Compared to the previous LGMD1 modelling studies, e.g. [6, 7, 9], as well as the former LGMD2 study in Section 3.1, we will investigate and demonstrate the effects of several neuron model parameters on collision detection, including the spiking threshold as well as temporal parameters for the ON and OFF pathways and SFA mechanism in the next subsection of experiments.

3.2.2 Experiments and Results

This subsection presents systematic and comparative experiments to demonstrate the proposed methods including ON and OFF pathways and spike frequency adaptation to model a general LGMDs model and shape the required looming selectivity. All of the experiments can be categorised into two types, off-line and on-line. For off-line, we tested the proposed framework using synthetic stimuli and physical stimuli. For comparison, we compared its performance with a previous LGMD1 computational model [6, 9]. We also compared the proposed model with the biological data and a biological LGMD1 model [4, 51]. For the on-line tests, the proposed framework was embedded into a visual module of a ground micro-robot for both arena tests and other investigations. The main objectives are as follows: firstly, to examine the effectiveness and robustness of the proposed LGMD1 neuron model in collision detection and, secondly, to provide insights into the underlined mechanisms of ON and OFF pathways and SFA in shaping the collision selectivity.

3.2.2.1 Experimental Set-up

Software set-up The off-line tests, proposed framework and comparative LGMD1 model [6, 9] were all set up in Visual Studio 2015 (Microsoft Corporation). Data analysis and visualisations were generated in Matlab 2015b (The MathWorks, Inc. Natick, USA). The resolution of input synthetic stimuli of looming-receding, translating and sinusoidal-grating movements are 300×300, 400×200 and 320×240, respectively, and were all at 30 fps. The resolution of real-world stimuli is 352×288 at 23 fps. Model parameters of the proposed framework to realise the LGMD1 corresponded to [23], whilst parameters of the comparative LGMD1 model were obtained from previous research [6, 9].

Hardware set-up In the on-line tests, we applied a versioned *Colias* robot, as illustrated in Fig. 3.5c, that is, the *Colias*-IV [50] that has the same size to the previous module and uses the monocular camera as the only sensor in this research.

In order to test the essential collision-detecting abilities of the proposed framework,

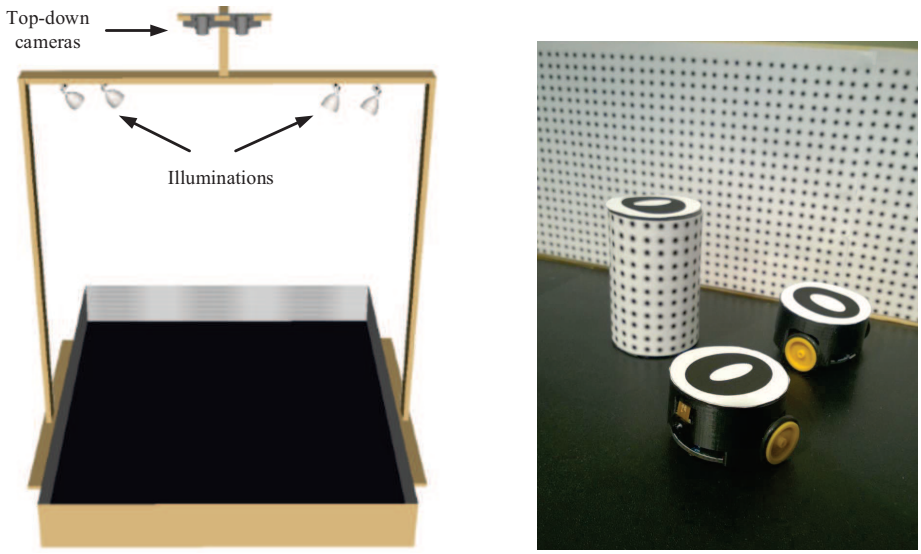

(a) arena profile (b) robot and obstacle

Figure 3.23: Illustrations of the big arena and *Colias* the robot used in the on-line tests: (a) the arena profile, (b) a subregion view of the arena with *Colias* robots and obstacles.

we built a bigger arena with an area of $170 \times 160\ cm^2$, compared to the previous arena used to test the proposed LGMD2 neuronal model in Section 3.1. The bounds of the arena consisted of $15\ cm$ in height walls, as illustrated in Fig. 3.23a. In order to ensure an even illumination, the arena was lit from the top down covering the whole field. Cameras were also mounted from a top-down perspective for the purpose of tracking and recording overall performance of the *Colias* robots. Obstacles and the arena walls were all decorated with a distinct dark pattern texture on a white background, as depicted in Fig. 3.23b. In addition, there were also ID-specific patterns on the top of the *Colias* robot and all stationary obstacles that were tracked by a practical localisation system [56, 240, 241], to get the robots overall trajectories and calculate the success rates of collision detection.

3.2.2.2 Off-line Tests

Challenged by synthetic stimuli First of all, the experiments started by testing the proposed LGMD1 model using synthetic stimuli and comparing its looming selectivity with a previous LGMD1 model [6, 9]. All the synthetic visual stimuli can be categorised into the following types: approaching-receding (Fig. 3.25), translating (Fig. 3.26) and sinusoidal gratings (Fig. 3.29). There is no environmental noise in the synthetic scenes. We also compared the results with the neural response of biological

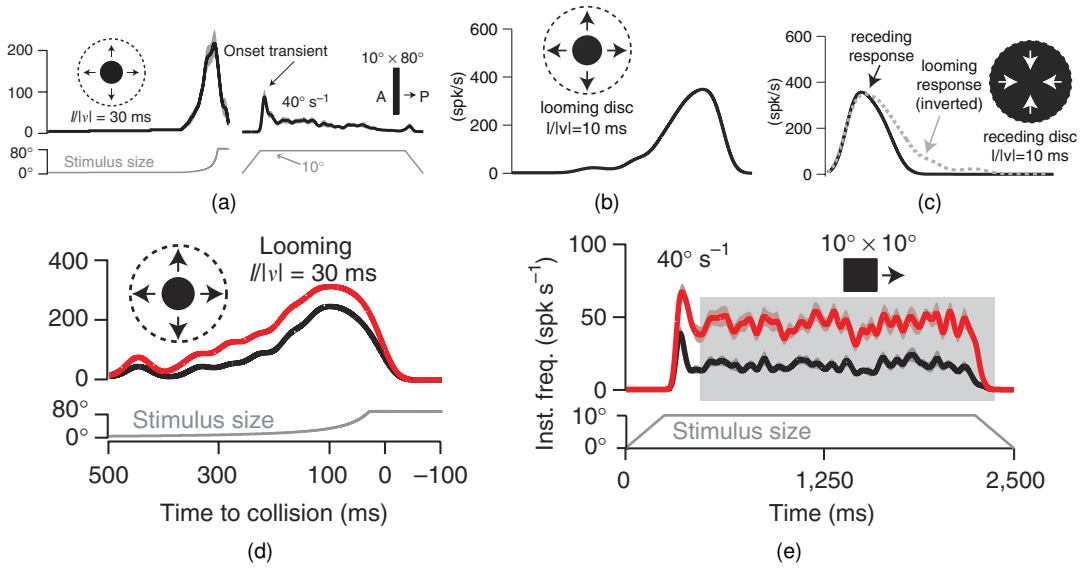

Figure 3.24: Neural response of a biological LGMD1 neuron or model adapted from [4, 51]: (a) biological LGMD1 neuronal response to looming and translation, (b) biological LGMD1 model response to looming. (c) biological LGMD1 model response to recession, The LGMD1 model shows asymmetric responses that the response is quickly decayed by receding stimuli. (d) Biological model response to looming stimuli without (red-curve) and with (black-curve) the SFA mechanism, (e) biological model response to translation stimuli.

LGMD1 neuron and model [4, 51] (Fig. 3.24), by using the similar visual stimuli. In the grating tests, we examined its performance challenged by grating movements with a broad range of spatial and temporal frequencies, which were reconciled with visual clutter in the real world.

In the first part of synthetic tests, we examined if the proposed LGMD1 model possesses similar characteristics to a biological LGMD1 neuron. Fig. 3.24 illustrates the biological LGMD1 neuron and model response by looming, receding, and translating stimuli, which reveals three important points: (1) the LGMD1 neuron can overcome adaptation in looming; (2) the LGMD1 represents asymmetric response at the end of looming and the start of recession, i.e., the neural response decays quickly by receding; (3) the response of LGMD1 decays quickly by translation at a constant speed. The results in Fig. 3.25 and Fig. 3.26 show that the proposed LGMD1 neuron model has demonstrated all of these characteristics. On the other hand, when challenged by looming and receding stimuli, the comparative LGMD1 model demonstrates symmetrical responses. It also appears that the comparative LGMD1 model is affected by translations more significantly with continuously high-level neural responses. There-

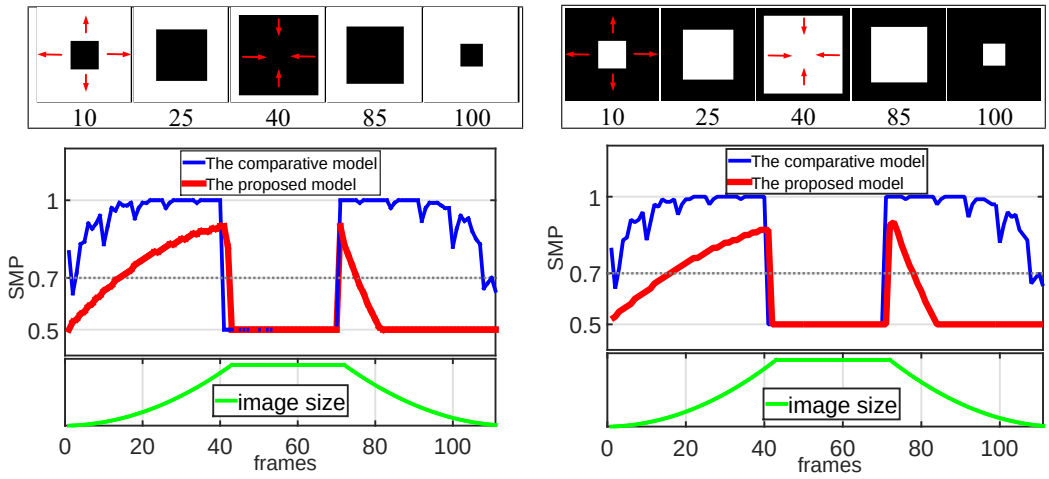

Figure 3.25: Neural responses of the proposed LGMD1 model and the comparative model by synthetic looming and receding movements of a dark and a light objects embedded on light and dark backgrounds, respectively: the image size is depicted at the bottom. The snapshots are shown at top. Y-axis indicates the SMP. X-axis denotes the time window in frames. The horizontal dashed-lines designate the spiking threshold.

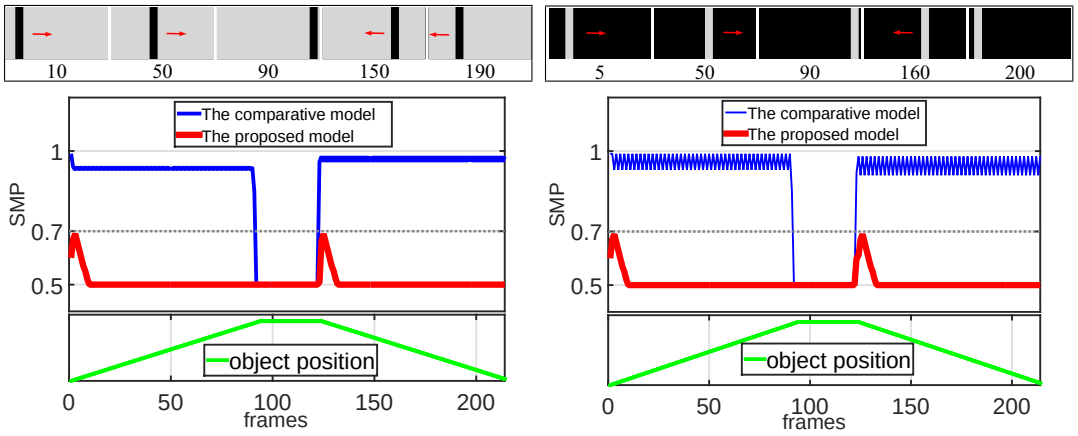

Figure 3.26: Neural response of the proposed LGMD1 model and the comparative model by synthetic dark/light translating movements: the object-position is indicated at the bottom of the result.

fore, compared with the previous LGMD1 neuron model [6], the collision selectivity is effectively enhanced for looming rather than receding and translating stimuli. The neural response of the proposed model is consistent and match the results in Fig. 3.24.

In the second part of synthetic tests, we investigated the functionality of the ON and OFF visual pathways in the proposed LGMD1 model. As illustrated in Fig. 3.27, we blocked either the ON or OFF pathways in looming and receding tests. Interestingly, the results demonstrate that blocking the ON pathway rigorously abolishes the underlying functionality of ON polarity cells for the onset response by luminance in-

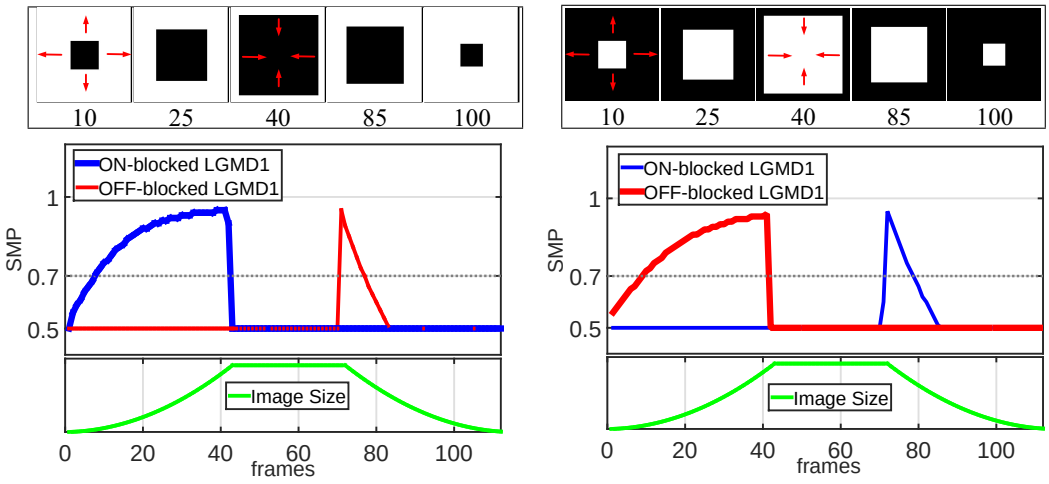

Figure 3.27: Neural response of the proposed LGMD1 model challenged by the similar looming and receding stimuli to Fig. 3.25, yet with ON and OFF pathways alternately being blocked.

crements, i.e., the LGMD1 model only responds to the dark object looming and the light object receding. While after blocking the OFF pathway, the model is sensitive to only dark object receding and light object looming. My previous research (Fig. 3.21b) has demonstrated that such a bio-plausible structure has great potential to realise the underlying functionality of a biological LGMD2 neuron, which is only sensitive to the light-to-dark luminance change, and consistent with the proposed ON-blocked LGMD1 model in Fig. 3.27.

Furthermore, we systematically investigated the effects of two basic properties of visual stimuli on neuronal responses of the proposed LGMD1, the speed and the contrast, and comparative model for the movement of dark objects approaching and translating. In this case, we define the contrast between the moving objects and the background to be calculated by the Eq. 3.28: The results in Fig. 3.28 allows the following conclusions to be drawn: both LGMD1 models represent comparable speed response. The neural responses all steadily peak at higher levels when the approach and translation movements speed up (Fig. 3.28b and 3.28d). By fixing the edge expanding rate of looming objects (Fig. 3.28a), the peak responses of both models reach a valley with the smallest contrast. And compared with the former LGMD1 model, the proposed model demonstrates more significant reduction of peak response. The proposed LGMD1 model could fail to perceive looming stimuli once the contrast decreases below $|-0.51|$ (Fig. 3.28a), which validates that the proposed LGMD1 model is more sensitive to the

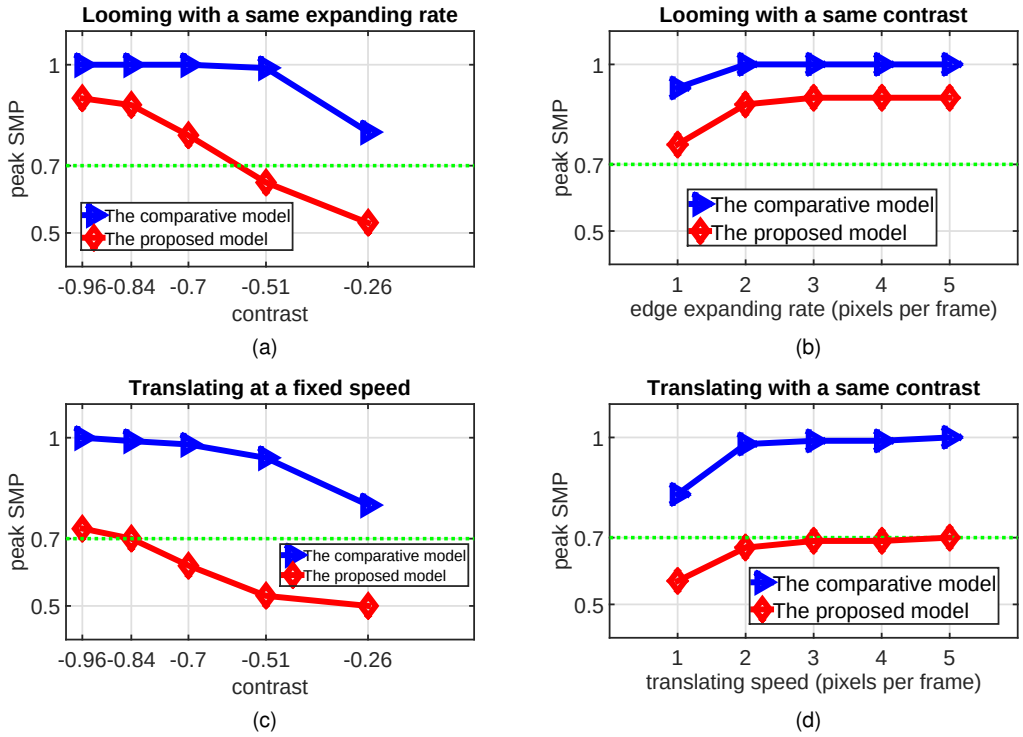

Figure 3.28: Peak neural responses of the proposed (red) and comparative (blue) LGMD1 models by synthetic looming and translation movements of dark objects in a bright background: the stimuli of dark objects are with different contrasts to the background and moving at different speeds. The green dashed lines indicate the spiking threshold. The proposed LGMD1 model demonstrates contrast sensitivity and speed response to looming and translating stimuli, better than the comparative LGMD1 model. The proposed model is not significantly activated by translations at constant speeds.

contrast between moving objects and the background.

Challenged by translations, the results in Fig. 3.28c, by movements at fixed speeds, reveal the proposed framework could also treat the translations, with larger contrasts or at faster speeds, as potential collisions. Intuitively, when challenged against translation movements, the proposed LGMD1 model is not easily activated like the previous LGMD1 model, as the neural response is largely weakened. To briefly summarise, compared with the comparative LGMD1 model, the proposed bio-plausible mechanisms and spatiotemporal computations play roles in shaping the LGMD1's collision selectivity to looming rather than translation.

In the last part of the synthetic tests, we examined the performance of the proposed neuron model against gratings with a wide range of spatial and temporal frequencies. In previous biological research [79, 83, 116], these locust looming detectors have proposed robust performance against gratings corresponding to visual clutter in the real

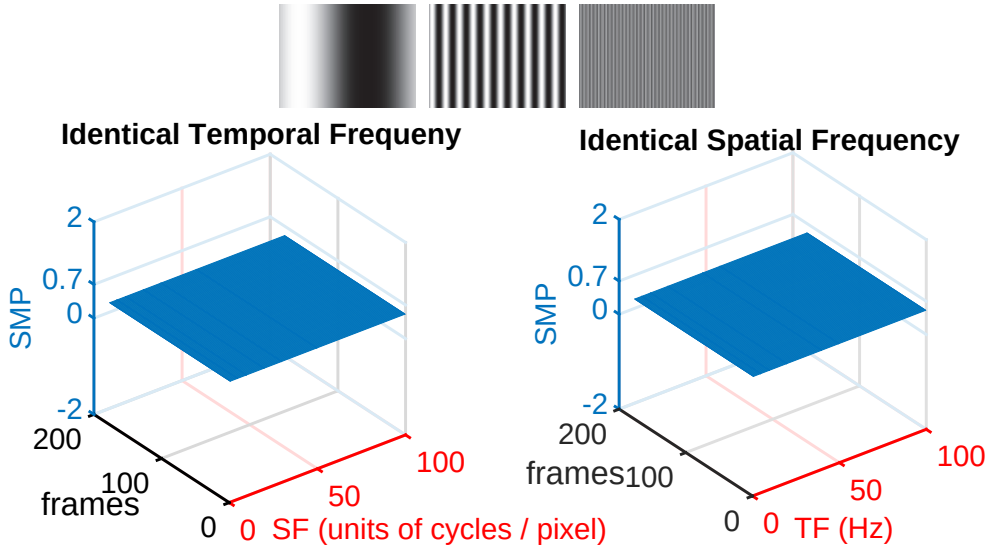

Figure 3.29: Neural responses of the proposed LGMD1 model are challenged by sinusoidal grating stimuli with a wide range of spatial and temporal frequencies (SF/TF), respectively. The example grating patterns, as input, are shown at the top. The spiking threshold is set at 0.7.

world. The locust LGMD1 neuron is rigorously inhibited by gratings. Fig. 3.29 illustrates that we have achieved similar results to previous biological findings, which is a critically important ability for a practical collision detector. In the proposed neuron model, we realise such an ability by low-level spatiotemporal visual processing, instead of the registration or classification based methodologies.

Challenged by driving scenarios In the second set of off-line tests, we also gave an initial insight into the efficacy of proposed collision perception vision systems in ground vehicle applications. We used on-road recordings from dashboard cameras as the visual stimuli to test the LGMD1 model. As illustrated in Fig. 3.30 and Fig. 3.31, the input from off-line stimuli involved both colliding and non-colliding driving scenarios in complex and dynamic scenes, which are frequent visual challenges to drivers.

In the first case, as shown in Fig. 3.30, the results demonstrate that the proposed LGMD1 model successfully recognises these impending vehicle-collisions: the LGMD1 neuron is highly activated by these fast approaching stimuli. Interestingly, the FFI can also indicate a potential collision, which increases dramatically before colliding. A defect of the current model is that the predefined FFI threshold influences the collision-detecting ability since the FFI can directly suppress the LGMD1 neuron

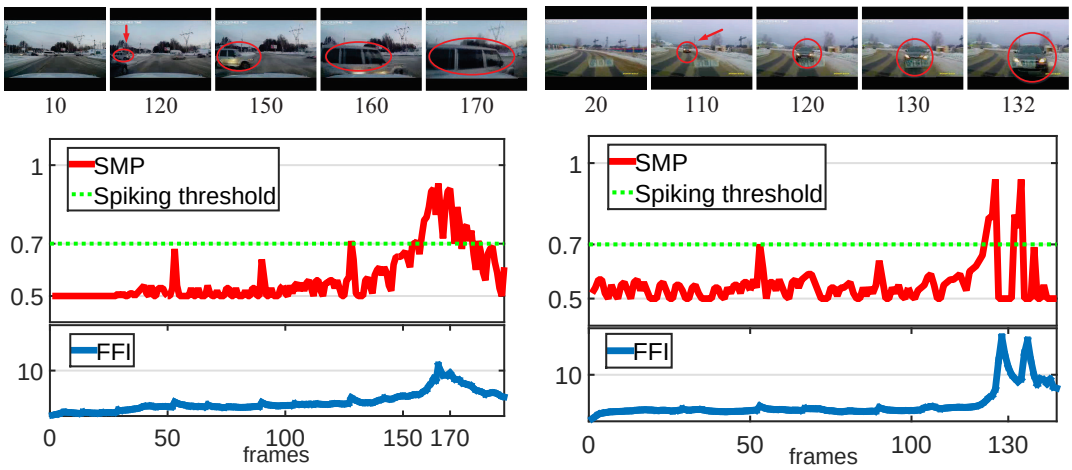

Figure 3.30: Neural responses of the proposed LGMD1 model challenged by 'colliding scenarios' of real-world stimuli from recordings of ground-vehicle dashboard cameras. The snapshots are shown at each top.

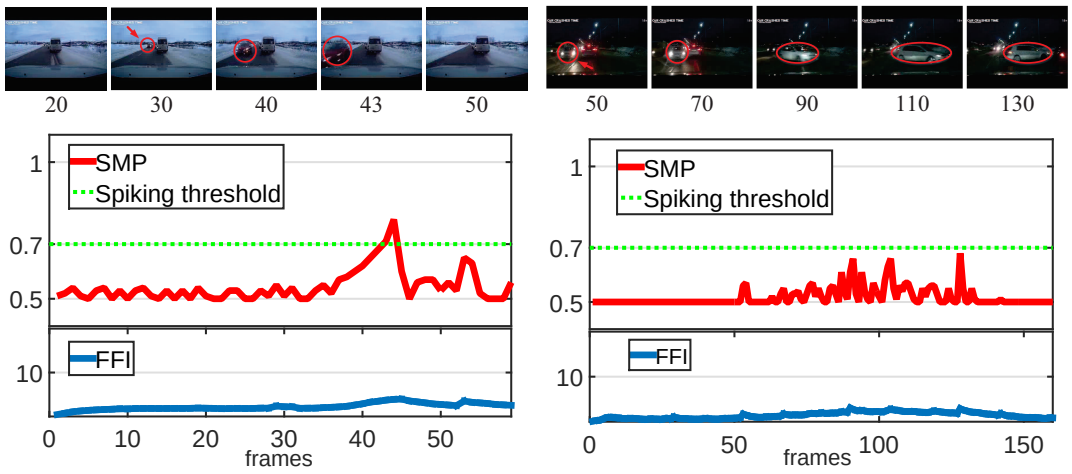

Figure 3.31: A neural response of the proposed LGMD1 model challenged by 'non-colliding scenarios' of real-world stimuli including 'near-miss' and translation scenes.

in the critical moments before the end of the rapidly approaching stimuli in this neuron model. Therefore, an automated adjusting of the FFI threshold is demanded in the future research.

In the second case, to make the comparison, we also tested the proposed LGMD1 model with two non-colliding scenarios – a near-miss and a translation scene. My results in Fig. 3.31 demonstrate that the proposed LGMD1 neuron model successfully recognises these movements as non-collision events. The initial tests with driving scenarios can provide important implications for the future research on applying the locust looming sensitive vision systems to build neuromorphic sensors in the applications of ground vehicles for improving driving safety.

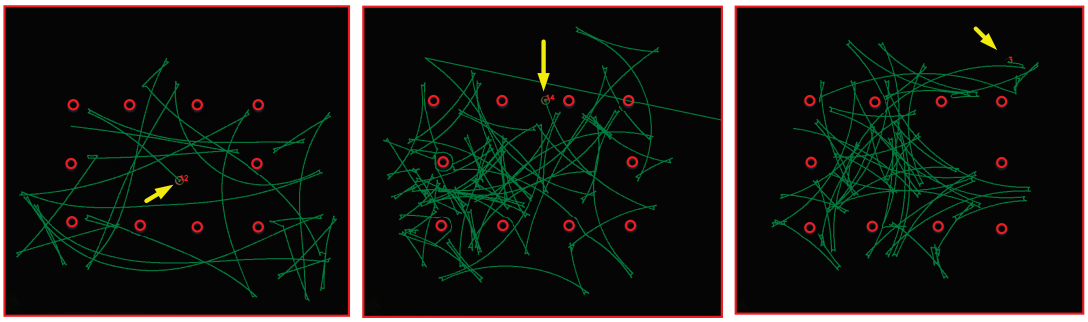

Linear speed: 5 cm/s | Linear speed: 10 cm/s | Linear speed: 15 cm/s

Figure 3.32: Example results of arena tests with overtime trajectories of a *Colias* robot implementing the proposed LGMD1 neuron model: the yellow arrow indicates the end-position of the robot with the specific ID in each arena test; the obstacles are indicated by red circles for the same layout. The *Colias* robot was tested at different linear speeds.

Table 3.4: Success Rates of Collision Avoidance

Success Rate(SR), Correct Avoidance(CA), Miss Avoidance(MA) $SR = CA/(CA + MA) \cdot 100\%$					
linear speed(cm/s)	3	5	10	15	20
CA	61	115	306	322	460
MA	18	19	34	14	20
SR	77.2%	85.8%	90.0%	95.8%	95.8%

3.2.2.3 Robot Tests

In this subsection, we continue to present the on-line bio-robotics experiments. The proposed LGMD1 neuron model was implemented in the monocular vision based *Colias* robot. We applied the camera sensor as the only utilised modality for collision detection. To examine its performance in robotic applications and deepen the understandings of the underlined bio-plausible mechanisms in shaping LGMD1's collision selectivity, we designed two kinds of on-line tests: the arena tests and the other systematic tests.

Arena tests In the first type of on-line tests, we inspected the basic collision-detecting ability of the proposed method in an arena with many obstacles. In the arena tests, we investigated the effects of linear-speed of the *Colias* robot on the success rate of collision detection and avoidance. The linear speeds thus varied from the slowest speed of 3 cm/s to the fastest speed of 20 cm/s as shown in Table 3.4. It is necessary to point out that the maximum speed whereby the robot can reach is about 25 cm/s [50], as given in

Table 3.5: Comparative Success Rates of Collision Avoidance

LGMD1 neuron models	3 (cm/s)	5	10	15	20
Proposed LGMD1	77.2%	**85.8%**	**90.0%**	**95.8%**	**95.8%**
Comparative LGMD1	**81.3%**	83.6%	85.0%	88.8%	87.4%
Proposed (ON-blocked)	79.0%	85.0%	86.5%	92.7%	89.0%
Proposed (OFF-blocked)	60.0%	70.5%	73.9%	78.0%	73.2%

Table 3.2. Moreover, for comparison, we also did arena tests for the comparative model on embedded system [9, 6], as well as the proposed neuron model with ON or OFF pathway blocked, respectively. The arena experimental setting was identical for each kind of LGMD1 neuron model. More specifically, in the arena tests, the *Colias* robot with each tested neuron model was initialised to go forward until a potential collision was detected. The collision-avoidance behaviour was simply set to turn right or left randomly with equal probability. After each avoidance, it resumed going forward. For all tested neuron models, the time window was set to 7 minutes for each test, whilst each speed test was repeated four times.

Firstly, Fig. 3.32 illustrates the trajectories of collision avoidance for the *Colias* robot with the proposed LGMD1 neuron model from my repeated tests. Moreover, Table 3.4 shows the statistical success rates of collision avoidance. We defined the 'miss avoidance' as any human interventions in the arena tests after the *Colias* robot got stuck at the edges of the arena or collided with an obstacle. The statistical results in Table 3.4 demonstrate that the *Colias* robot at the slowest linear speed (3 cm/s) has the lowest success rate of collision avoidance in the arena tests. Increasing the linear speed gives rise to a rising of the success rate, which seems to peak around 15 cm/s for the tested *Colias* robot. As a result, faster moving speeds make the visual neuron more sensitive to the looming stimuli by approaching the obstacles. However, we observed the larger distances to collisions (DTC) of the *Colias* robot at faster linear speeds.

For comparison, under the same arena test settings, we investigated the performance of the collision avoidance with the comparative LGMD1 neuron model, as well as the effects of blocking either ON or OFF pathways for the proposed model with the collision avoidance. Table 3.5 demonstrates that my proposed LGMD1 model outperforms the comparative model in the arena tests, despite it being at the slowest speed of

3 cm/s. Interestingly, after blocking the ON pathway, the performance of the collision avoidance for the proposed model is only slightly affected; while the collision avoidance performance deteriorates sharply after blocking the OFF pathway in arena tests. The results demonstrate that the ON and OFF pathways play a role in the proposed neuron model for collision detection. Importantly, for the ground robotic navigation tests, the OFF pathway has a more significant influence on looming perception than the ON pathway, as most objects are darker than the background in the arena.

Open-loop tests For systematically studying the unique characteristics of the proposed neuron model in robotic applications, we designed a few types of open-loop tests. The first kind of open-loop test was to test the proposed embedded LGMD1 model with movements in depth (Fig. 3.33). The second kind of open-loop test was to investigate the DTC response (Fig. 3.34 and 3.35). After that, we also studied the effects of angular approach (Fig. 3.37) and translation (Fig. 3.38) stimuli on the neural response of the proposed model. The experimental settings for the angular approach and translation tests are illustrated in Fig. 3.36. In the two former test types, the motion controls unit was used for the *Colias* robot for approaching or receding from the targets; while in the angular approach and translation tests, the *Colias* robot was a motionless observer stimulated by another moving robot. In all the open-loop tests, we collected the neural response of the proposed model including the SMP and spikes through a Bluetooth device attached to the visual module of the tested *Colias* robot.

Firstly, Fig. 3.33 demonstrates that when challenged by direct looming stimuli caused by ego-motion of the *Colias* robot, the proposed LGMD1 model overcomes adaptation representing continuously increasing neural response as the size of the projected object grows in the field of view. It is fully activated by the end of approaching. The neural response is consistent and matches Fig. 3.24a, 3.24b, 3.24d. On the other hand, when receding from the object, the proposed embedded LGMD1 model is only activated for a short period of time. The adapted neural response decreases dramatically, which matches Fig. 3.24c.

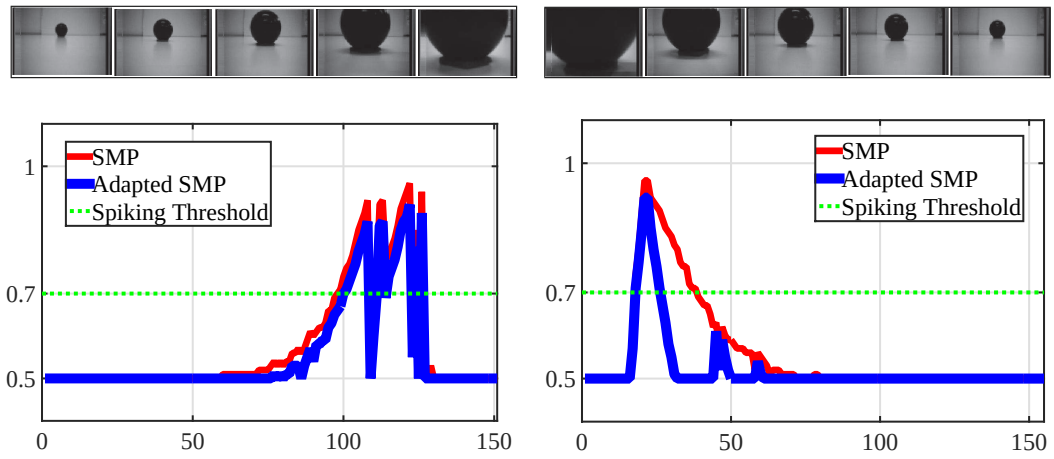

Figure 3.33: Neural responses of the embedded LGMD1 model in the stimulated *Colias* robot challenged by the looming and recession of a dark object: the first example views are shown at the top of each result. X and Y axes indicate the time window in frames and SMP from the tested robot. Both the neural responses before and after the proposed SFA mechanism are shown.

DTC tests As mentioned in the arena tests, for deepening the understanding of the underlined correlations between the DTC and the looming speed, we also designed experiments to test the proposed framework with various combinations of model parameters, including the spiking threshold, the temporal parameters in the low-pass filtering of the ON and OFF pathways and the high-pass filtering of the SFA mechanism. More specifically, the spiking threshold plays a crucial role in mediating the spike frequency of the proposed model. Compared with the comparative LGMD1 model, we apply a strategy of exponentially mapping the membrane potential to the firing rate. Moreover, instead of the 'one-frame-delay' strategy in the comparative model, we compute the delayed signals by linear and temporal filtering the original signals with these investigated time parameters.

In the first round of DTC experiments, the *Colias* robot with the proposed model was used to approach an identical dark object at three constant linear-speeds. As illustrated in Fig. 3.34, the statistical results demonstrate the parameters all influence the DTC's response when tested at all speeds. The faster approaching speed gives rise to higher DTC response with each combination of parameters, underlying the speed response of the proposed looming detector. More concretely, as shown in Fig. 3.34a, reducing the spiking threshold gives rise to larger DTC at all tested speeds. At each tested speed, the DTC increases by the shrinking of the spiking threshold. The re-

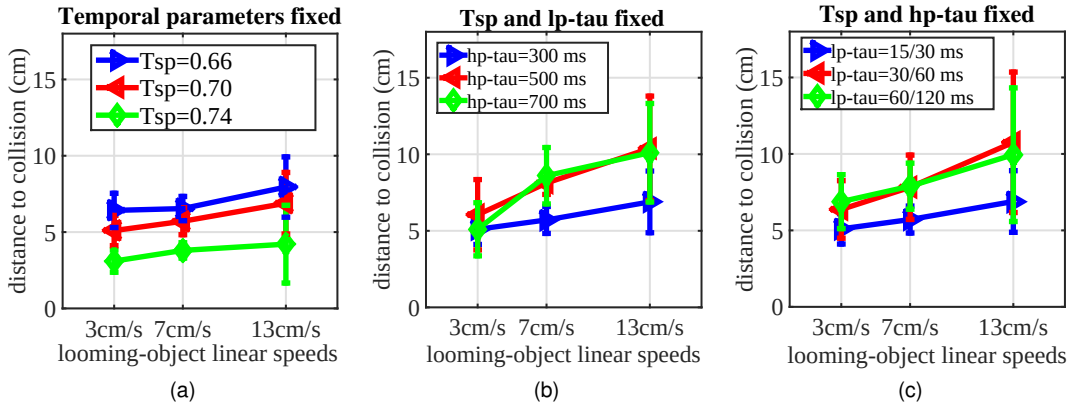

Figure 3.34: Statistical results (error bars) of DTC tests on different combinations of investigated parameters: the *Colias* robot approached an identical dark object at three linear-speeds. Each combination of parameters was repeated ten times at each speed. (a) The spiking threshold varies. (b) The temporal parameter in the SFA mechanism varies. (c) The temporal parameters in the ON and OFF pathways vary.

sults are in accordance with the computational rule of Eq. 3.23, that is, lower spiking threshold corresponds to higher firing rate with other parameters fixed.

On the aspect of temporal parameters in the proposed framework, Fig. 3.34b and 3.34c illustrate that these time parameters all have an influence on the speed response of the proposed neuron model. It appears that the DTC response at each tested speed peaks by a combination of temporal parameters of 500 ms for the high-pass filtering and $30/60$ ms for the low-pass filtering. The results are also consistent with the spatiotemporal computations in the proposed framework: for temporal filtering in the polarity pathways, the delayed information decays more slowly by raising the time parameters (Eq. 3.31, 3.33), corresponding to stronger feedforward excitation and higher firing rate with other parameters fixed. Similarly, increasing the time parameter in the SFA mechanism also leads to higher firing rate (Eq. 3.21, 3.22) with other parameters fixed. In the future research, we aim to explore a method for optimising the selection of model parameters adapting to different visual environments.

In the second round of DTC experiments, we let the robot approach different objects, each with a certain grey-scale (Fig. 3.35a), in order to examine whether the contrast influences the DTC response. The statistical results in Fig. 3.35, demonstrate that the proposed neuron model is also sensitive to the contrast between looming objects and background in robot vision, which are consistent and also match the synthetic

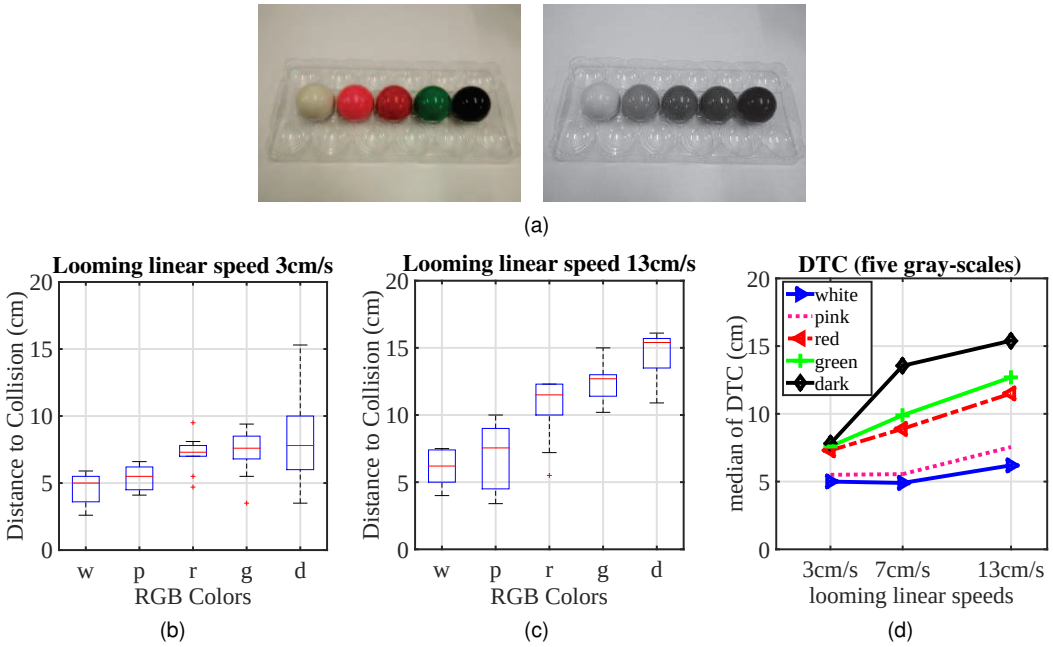

Figure 3.35: Statistical results of DTC tests on different grey-scaled looming stimuli: the *Colias* robot approached five grey-scaled obstacles (a) under the same parameters set at three linear speeds, respectively. Each test repeated ten times. (b) – (c) the box plots of DTC results at a slow and a fast linear speed, respectively, (d) The medians of DTC results.

tests in Fig. 3.28. The LGMD1 model is more sensitive to darker looming objects even at the lowest linear speed of 3 cm/s, representing relatively larger DTC response (Fig. 3.35b). When the approach speed rises up, the DTC response by approaching each grey-scaled object also climbs up (Fig. 3.35c) – the looming stimulus with larger contrast leads to sharper rising of DTC response. The statistical results in Fig. 3.35d demonstrate more intuitively the speed response and the contrast sensitivity of the proposed LGMD1 neuron model. As the robot accelerates when approaching, the darkest looming object corresponds to the most significant increase of DTC response. The green and red looming objects with the medium contrast levels give rise to an increase in the DTC response in a linear manner. The pink and white looming objects with the smallest contrasts nevertheless have little influence on DTC response.

Angular approach tests In the angular approach tests, we investigated the effects of direct looming as well as 'near-miss' scenes by the approaching stimulus from other angles. As illustrated in Fig. 3.36a, the motionless *Colias* robot was stimulated by an identical dark looming object from four distinct angles against a cluttered

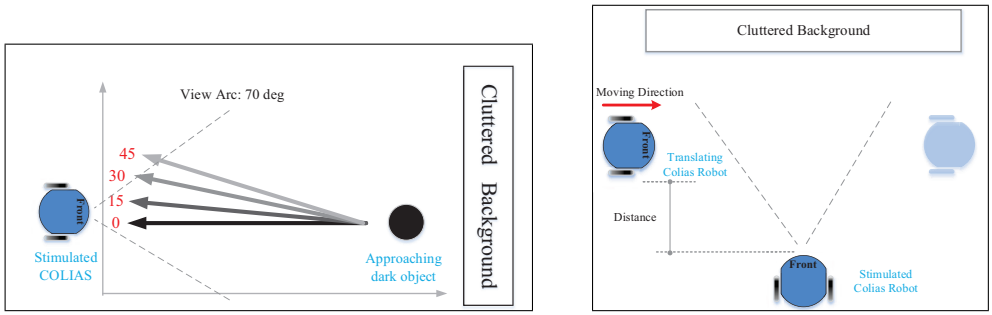

(a) Angular approaches (b) Translations

Figure 3.36: Experimental settings of the angular approach and translation tests. In the angular approach tests, the stimulated *Colias* robot was motionless and challenged by a same dark object approaching from different angles against a cluttered background. In the translation tests, the stimulated *Colias* robot was challenged by translations of a moving robot.

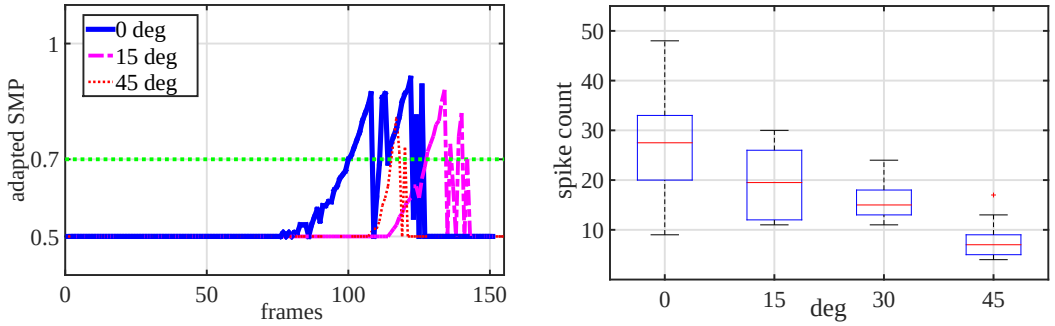

(a) (b)

Figure 3.37: Angular approach tests results: (a) neural response of the embedded L-GMD1 neuron model tested by three different angular approaches, (b) statistical results of the spike count (firing frequency) with each angle of looming tested by ten times.

background: a 'direct looming' corresponds to the 0-degree angular approach, whilst looming from other angles simulate the 'near-miss' scenes, which are also frequent challenges for visual collision detectors. We accumulated the elicited spikes from the proposed LGMD1 model during each angular approach with a course of approximately the same length of time throughout repeated tests. The results in Fig. 3.37 clearly demonstrate that the spike frequency (firing rate) of LGMD1 peaks when directly approaching. The spike rate declines gradually along with the increase of approaching angles. When stimulated by looming from 45 degrees, the largest angle tested, the LGMD1 model represented the lowest spike frequency. My results verify that the proposed neuron model possesses similar characteristics to a biological LGMD1 neuron in locusts, which responds most strongly to directly approaching objects that represent the most powerful strikes from predators.

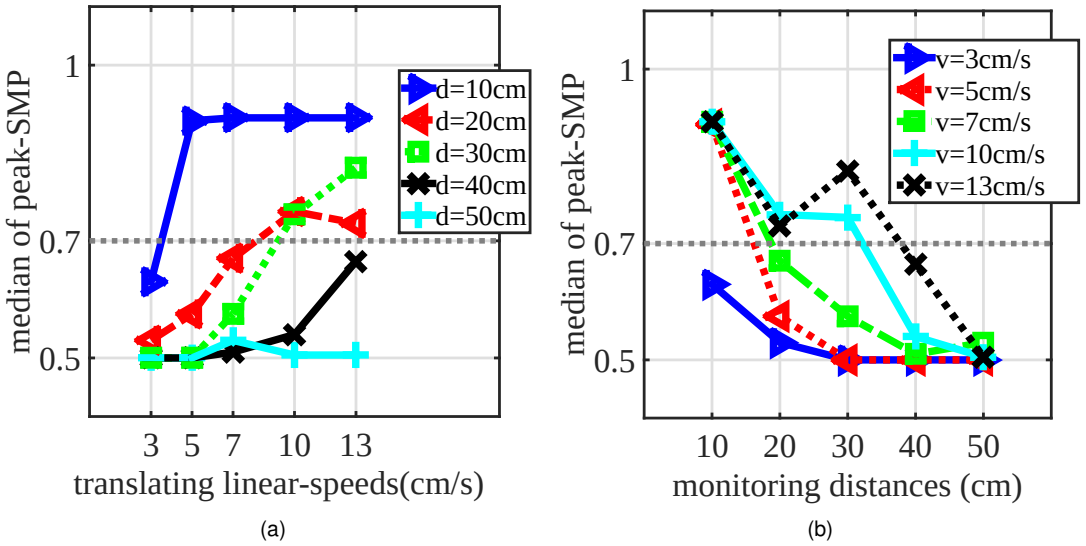

Figure 3.38: Statistical results of systematic translation experiments: each speed or distance was tested for ten times, respectively. The horizontal dashed-lines indicate the spiking threshold.

Translation tests In the last part of the open-loop robot experiments, the *Colias* robot was challenged by translations against a cluttered background, as illustrated in Fig. 3.36b. We investigated effects of the translation speed of visual stimulus and the distance from the stimulated robot. More specifically, the linear speed of the translating robot (stimulus) was set at approximately 3, 5, 7, 10 and 13 cm/s, whilst the distance varied from 10 to 50 cm.

As illustrated in Fig. 3.38, the statistical results demonstrate that both the translating speed and the distance to the stimuli affect the peak neural response of the proposed LGMD1 neuron model. Concretely, the embedded LGMD1 neuron model represents the response speed to translation movements despite translations from the tested distance of 50 cm. These results are consistent with the synthetic tests in Fig. 3.28. The faster translating speed gives rise to the stronger neural response of the proposed model. In addition, the nearby translations from a distance of 10 cm or closer also highly activate the proposed LGMD1 neuron model. It is conceivable that the locusts also treat the nearby fast translating objects as potential collision or dangers. In addition, if the translating distance is very far from the field of view ($40 \sim 50$ cm or further), the proposed LGMD1 model remained quiet for all tested translating speeds. In this case, the translating object corresponds to a small target, which may be identified by other kinds of visual neurons like the small target movement detectors [43] but the LGMDs.

3.2.3 Further Discussion

In Section 3.1, we have demonstrated the effectiveness of ON and OFF visual pathways in a computational structure to meet the neural characteristics and functions of biological LGMD2 neurons. In this section, through systematic experiments ranging from off-line to on-line tests, we have shown that such a bio-plausible structure can also realise biological LGMD1 neurons. The modelled neural network with the proposed polarity pathways and spike frequency adaptation mechanism, demonstrate similar characteristics to the biological LGMD1 neurons and models (Fig. 3.24). Such a framework thus can be regarded as a general model to implement both the LGMD1 and the LGMD2 in locust visual systems.

Importantly, compared with a similar LGMD1 model from the literature that deals with visual processing in a single pathway [9, 6], the collision selectivity in the proposed model has been further enhanced to looming objects over other regular visual challenges, which have been exhibited by the above experiments. Unlike other animals such as the flies, the biological ON and OFF pathways have not yet been anatomically and physiologically identified in locusts, leaving little evidence to computational modellers. However, this research, via systematic experimenting, could evidence the existence of similar pathways or mechanisms in locust visual systems.

Despite the ON and OFF pathways, another important achievement of this research is to demonstrate the efficacy of an SFA mechanism in shaping the collision selectivity. However, there is valuable data on different protocols for shaping the collision selectivity in LGMD1 that has not been compared thoroughly in this work. For example, a seminal work of a non-linear LGMD1 neuron model has demonstrated a non-linear correlation between the feed-forward inhibitory and excitatory responses [18]. The F-FI mechanism could also contribute effectively in mediating the collision selectivity of an LGMD1 neuron, which cannot be disregarded. We would like to compare the different mechanisms and investigate the collaboration of them in shaping the LGMD1's collision selectivity in the near future work.

The arena tests have verified the effectiveness and robustness of the proposed neuron model for guiding collision avoidance in robot near range navigation (Table 3.4).

The comparative arena tests have also demonstrated the improved performance of collision detection of the proposed model over the comparative model (Table 3.5). Again, the efficacy of ON and OFF pathways for looming perception has been validated by the comparative experiments. We would like to further investigate the efficacy of this embedded collision-detecting vision system for collision detection in dynamic scenes mixed with multiple robots.

3.2.4 Concluding Remarks

Shaping the collision selectivity in vision-based artificial collision-detecting systems is still an open challenge. In this section, continuing with the modelling studies on biological LGMD2 neurons in Section 3.1, our research has demonstrated that the proposed ON and OFF pathways can realise biological LGMD1 neurons, as well. This polarity mechanism can separate both dark and light looming features for parallel spatiotemporal computations. This works effectively on perceiving a potential collision from dark or light objects that approach; such a bio-plausible structure can also separate the LGMD1's collision selectivity to its neighbouring looming detector – the LGMD2. The SFA mechanism can enhance the LGMD1's collision selectivity to approaching objects rather than receding and translating stimuli, which is a significant improvement compared with similar LGMD1 neuron models.

This computational modelling research provides effective solutions to enhance the collision selectivity of looming objects over other visual challenges. The proposed LGMD1 model has been tested using off-line tests of synthetic and real-world stimuli, as well as on-line bio-robotic tests. The enhanced collision selectivity of the framework has been validated in systematic experiments. The computational simplicity and robustness of this work have also been verified by the bio-robotic tests, which demonstrates potential in building neuromorphic sensors for collision detection in both a fast and reliable manner. Notably, this looming perception neural network could be treated as a general LGMDs model which can satisfy the biological functions of both LGMD1 and LGMD2 neurons in locusts.

3.3 Chapter Summary

Within this chapter, this thesis has demonstrated the computational modelling of locust looming perception neuronal models. Two looming sensitive visual neurons – LGMD1 and LGMD2, each with specific looming selectivity, have been satisfactorily constructed via low-level spatiotemporal computation with design and modelling of bio-plausible visual pathways and mechanisms. Crucially, compared with all previous modelling research in LGMDs, this has proposed a general model that can realise either the LGMD1 or the LGMD2 neuronal characteristics and functionality in collision detection. The systematic and comparative experiments have validated the proposed methodologies to implement the LGMDs. These computational models all represent speed and contrast sensitivity that behave like real LGMDs neurons in locusts. The bio-robotics tests including arena tests have also demonstrated the efficacy, efficiency and robustness of the proposed algorithms that work on the embedded system for real-time collision detection. Compared to traditional computer vision methodologies for recognising collision, we have demonstrated the potentials of proposed methods to build neuromorphic vision sensors for quick collision detection in navigation; this could provide alternative solutions for future intelligent machines, like automatic cars, for collision recognition and avoidance.

Furthermore, biologists have also explored similar looming sensitive visual neurons in other animals; these include fruit flies (drosophila) [141, 242, 174, 243] and arthropods like crabs [244] and etc. The lobula giant neurons (LGNs) in crabs have been identified as looming detectors that are located in the lobula layer and correspond to reactive collision avoidance behaviours [245, 246, 247]. The possible computational roles of such visual neurons have also been proposed in [142]. However, there are no systematic studies, models and applications of such fascinating looming detectors in crabs, which have represented great potential in building reactive collision avoidance systems for mobile machines. Though the LGNs have different neuromorphology compared with the LGMDs, the computational modelling of LGNs may learn from the practical experience of the existing LGMDs models.

Chapter 4

Modelling of Fly Translating Perception Visual Neural Networks

In this chapter, this dissertation introduces the computational modelling of translating motion perception visual neural networks inspired by direction selective neurons (DSNs) in the fly's preliminary motion vision pathways. As presented in Chapter 2, flies have been prominent models to study animals' motion detection strategies for decades. More precisely, the DSNs, with preference to certain orientation visual stimulus, have been found in both vertebrates and invertebrates for decades, for example flies [61], locusts [87], cats [92], monkeys [248], mice [58], rabbits [91] and etc. In this chapter, we focus on presenting the modelling of fly DSNs and mimic higher behavioural response of motion tracking and fixation.

More specifically, extracting useful motion cues from dynamic and visually cluttered scenes, in a both efficient and robust manner, is still a pronounced challenge for building artificial motion sensitive systems. The nature endows animals robust vision systems to take up this challenge that can recognise different motion cues indicating movements by predators, preys and mates and etc. Insects, in particular, have relatively smaller number of visual neurons, but can navigate smartly through unpredictable environments. Therefore, contrary to conventional computer vision methods, visual processing mechanisms in animals such as insects, may provide very simple and effective solutions for motion detection. With respect to cutting-edge biological findings underlying the fly physiology in the past decade, we present the systematic computa-

tional modelling of fly DSNs and corresponding neural pathways, with a feed-forward structure and entirely low-level visual processing. The DSNs are mainly sensitive to wide-field translational movements in four cardinal directions. Such specific functionality can be carried out in a neuropile layer of lobula plate by lobula plate tangential cells (LPTCs) [97]. In the modelling of fly DSNs, we also highlight the functionality of ON and OFF pathways, separating motion information for parallel computation corresponding to light-on and light-off selectivity.

In the remainder of this chapter, we firstly introduce the background including cutting-edge biological research in fly physiology that elicits the characteristics of preliminary visual processing pathways and neurons in Section 4.1. After that, the directionally selective neural network (DSNN) is presented in Section 4.2 with systematic and comparative experiments. Then this proposes methodologies to extend the DSNN to behavioural levels of visual tracking and fixation behaviours in Section 4.3. In addition, the proposed translational motion detection and tracking model is realised on the embedded system in our *Colias* micro-robot within Section 4.4. Finally, we have further discussion on remaining challenges of current translational motion sensitive neural systems in Section 4.5, and summarise this chapter in Section 4.6.

4.1 Background

In the insects' visual systems, it is believed that various groups of neurons possess specialised functionality for perceiving different motion cues, which can further act together to fuse various motion features. Different identified visual neurons, each with specifically physiological properties, have motivated the creation of unique computing efficient neural networks. For instance, the LGMDs (introduced in Chapter 3) in the locust's visual system have been implemented for quick and flexible looming (collision) detectors in ground-vehicle scenarios, e.g. [161, 151, 146, 17], and realised as neuromorphic vision sensors for robots, e.g. [7, 84, 85, 20, 21], and UAVs [12, 148]. The optic flow-based collision avoidance systems have been widely used in near-range navigation of flying robots, e.g. [59, 35, 176, 37], that are mainly implemented by the elementary motion detectors (EMDs), that is, a classic mathematical

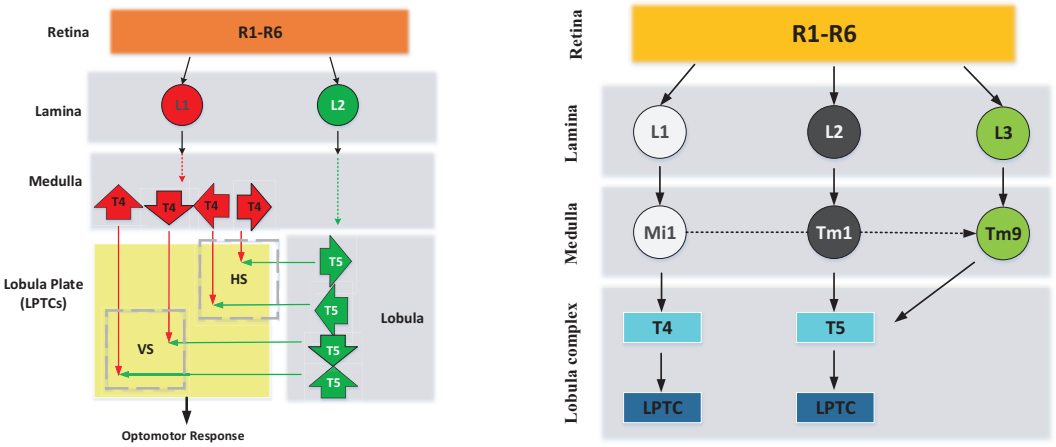

(a) ON and OFF visual pathways

(b) an extra position (L3-Tm9-T5) pathway

Figure 4.1: (a) A sketch map of fly (drosophila) preliminary visual pathways throughout five neuropile layers: the first retina layer with R1-R6 neurons denotes photoreceptors, which convey motion information to lamina mono-polar cells (L1 and L2). Visual signals are thereby split into parallel ON and OFF pathways, which are indicated by red and green arrows. The direction selectivity (DS) of motion information is generated in the medulla and lobula layers tuned by four groups of directionally specific T4 and T5 neurons. The lobula plate tangential cells (LPTCs) pool each group of directionally specific neural response to form the horizontal sensitive system (HSS) and vertical sensitive system (VSS). The outputs of these two systems guide higher level behavioural responses. (b) is similar to (a) and adapted from [52] (Fu and Yue, 2017). ON and OFF pathways form the motion-detecting pathway; in addition to it, another pathway starting from L3 to T5 forms the position pathway. Dashed lines denote the putative interactions between interneurons of both pathways.

model which originated from the fly visual system research and came out earlier than any other kinds of bio-inspired visual strategies [89]. In addition, another group of neurons, i.e. the small target motion detectors (STMDs), have also been explored in dragonflies and hover flies, which have specific sensitivity to movements caused by dark objects with a very small or limited size [249]; such bio-inspired strategies have been computationally modelled and implemented as artificial small motion detectors, e.g. [250, 43, 251, 44, 103].

In this chapter, we present a visual neural network for the purpose of studying a specific group of neurons, so-called the DSNs in the fly's preliminary motion-detecting pathways, which are mainly sensitive to wide-field translational motion in a visual field. In the recent decade, with latest developments of biological techniques, much progress has been made anatomically by biologists underlying the fly (drosophila) preliminary motion-detecting pathways. As reviewed in Chapter 2, numerous promi-

nent physiological studies have emerged to explain fly motion vision strategies, e.g. [61, 62, 28, 58, 93, 94, 39, 40, 99, 97, 32, 96, 98, 111, 100, 101]. However, the fundamental cellular implementation of fly visual systems still remains largely unknown. This chapter presents the computational modelling research in fly motion vision pathways with our understanding of the very complicated insect visual systems.

More precisely, as illustrated in Fig. 4.1, the motion detection starts with splitting the visual signals from the Retinal layer into parallel ON and OFF pathways in the Lamina neuropile layer by large mono-polar cells (LMCs), encoding brightness increments (ON) and decrements (OFF), separately [93]. After that, there are specific interneurons that synapse ON units in the Medulla neuropile layer to form the ON pathway, and OFF units in the Lobula neuropile layer for the OFF pathway, respectively [97]. The relayed visual signals are directionally selective with motion information calculated along each cardinal direction within the dual-pathways, and the direction selectivity (DS) is already formed in T4 and T5 neurons in the Medulla and Lobula layers [97]. Finally, the outputs of different directional motion detectors are sorted and pooled in the Lobula Plate, i.e. the neurons regarding to the same directional tuning converge in an unanimous sub-layer of the Lobula Plate, jointly providing the input downstream to following circuits like the motion-driven neural systems [97]. In Fig. 4.1, the Lobula Complex is composed of both the Lobula layer and the Lobula Plate. In general, there are four sub-groups of LPTCs covering all cardinal directions, generating selective signals. Very importantly, these biological findings demonstrate visual information in the LPTCs, which are delivered from the dendrites of second and third neuropile layers, are already directionally selective; this reveals the Medulla and Lobula layers convey polarity visual streams, separately, and both can be the well place where same polarity signals from neighbouring columns (ON-ON or OFF-OFF) interact with each other so as to generate the DS to four cardinal translational motion.

A famous theory pointed out that visual neurons compute the direction of motion corresponding to the well-known Hassenstein-Reichardt Correlation (HRC) model [89]. This explains how non-linear algorithm is mapped onto neuronal hardware and implemented by neural networks, also a milestone toward understanding how the brain

computes based on sensory inputs [125, 28, 53]. The fly EMDs represent similar computational roles of HR detectors; with respect to the cutting-edge biological findings on fly ON and OFF pathways and LPTCs, researchers have found the proper location for the EMDs to extract movement directions.

4.2 Directionally Selective Neural Network

In this section, we present the modelling of fly ON and OFF pathways and LPTCs in detail with systematic experiments. The proposed model is denominated a 'directionally selective neural network' (DSNN). Compared to the looming sensitive visual neural networks proposed in Chapter 3, the DSNN is only sensitive to translating movements in four prime directions. An important biological theory guiding the proposed DSNN modelling is that visual information is separated into ON and OFF pathways for parallel computation, as shown in Fig. 4.1. The onset and offset responses, evoked by luminance increments and decrements, are processed by interneurons in the dual-pathways, separately until converging in the final LPTCs. More importantly, the DS to ON-edge and OFF-edge movements is encoded and formed well before the LPTCs. Finally, in the Lobula Plate, the LPTCs pool directionally selective motion from four groups of direction selective T4 and T5 neurons in the Medulla and Lobula layers to form two directionally sensitive systems, that is, the horizontal and vertical sensitive systems (HSS and VSS). Interestingly, both systems respond to visual motion with fixed preferred and non-preferred (or null) directions regardless of colour or contrast of both the visual stimuli and the background [93]. More concretely, the fly DSNs, namely LPTCs, are rigorously activated by motion along the rightward and downward, i.e. preferred directions (PDs), while inhibited by motion along the leftward and upward, i.e. non-preferred directions (NDs) [93]. Despite that, how the DS forms by signal processing within the polarity ON and OFF pathways is still controversial [94, 99].

Biologically plausible motion detectors As introduced in Section 4.1, the fly preliminary motion-detecting pathways including ON and OFF pathways and LPTCs have been revealed the appropriate places to implement the HR detectors or EMDs (Fig.

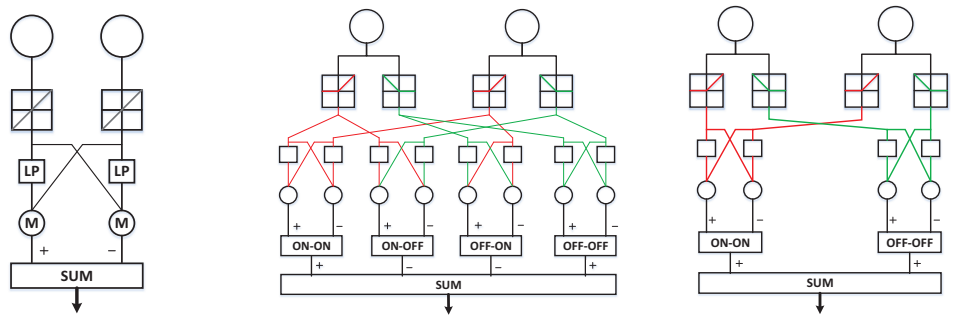

(a) (b) (c)

Figure 4.2: Different biological models for visual motion detection: (a) A symmetric HR detector or EMD as a standard model for motion detection: LP and M components indicate the low-pass filtering and multiplication. (b) A four-quadrant (4-Q) model processes input combinations of ON-ON, ON-OFF, OFF-ON, and OFF-OFF local detectors. Each combination replicates the structure of HR detector. This model is mathematically identical to the original EMD. (c) A two-quadrant (2-Q) model processes only input combinations of the same sign signals (ON-ON, OFF-OFF).

4.2a). Nevertheless, in former EMDs-based models, e.g. [54, 31, 177, 179, 181], visual signals are processed only in a single pathway, unlike the newly revealed structure of fly physiology, shown in Fig. 4.1. It appears that the separated ON and OFF pathways are playing crucial roles in the identified parts of preliminary motion-detecting circuits. However, there is no systematic modelling research on this promising field underlying translational motion perception. To fill this gap, the proposed DSNN may provide an useful paradigm to construct the cutting-edge biological findings on fly visual system, to demonstrate its characteristics and significance.

There are several biological models arguing for different motion detection strategies with different combinations of ON and OFF rectifying transient cells (RTCs) in the dual-pathways [39, 40, 94, 99]. The first assumption is the **4-Q** detectors with communications between both the same and opposite polarity cells (Fig. 4.2b). Technically speaking, it mathematically conforms to a symmetric combination of HR detectors processing visual signal in a single pathway (Fig. 4.2a). The second important speculation is the **2-Q** model that is in accordance with electro-physiological recordings from LPTCs [39]. Contrary to the four-quadrant model, it processes only input combinations of the same sign signal, i.e. ON-ON and OFF-OFF, as shown in Fig. 4.2c. In this study, the 2-Q instead of 4-Q association of motion detectors was recommended to exist in the fly motion-detecting circuitry, through physiological investigation.

Furthermore, there is another biological model based on behavioural experiments, which supports that both polarity pathways convey motion information about both positive and negative contrast change in the motion-detecting circuitry [40], as illustrated in Fig. 2.26 in Chapter 2. In this research, a framework of **6-Q** detectors was proposed with interactions between both polarity cells in either pathways. Compared with the structure of 4-Q model (Fig. 4.2b), it also processes light-off (OFF-OFF) response in the ON pathway and light-on (ON-ON) response in the OFF pathway. Moreover, this biological model emphasises the importance of edge selectivity in motion detection.

Given these biological motion detectors, the different combinations of ON and OFF RTCs all depict a picture of how the fly's neural circuits implement the HR detectors to shape the DS to translating movements. To decide among these alternatives, a subsequent research provided strong evidence of the existence of 2-Q versus 6-Q motion detectors for producing the directional signals, via genetically blocking either ON or OFF pathways [94].

In the proposed DSNN modelling, we are consistent with the combinations of only same-sign polarity cells, i.e., the 2-Q motion detectors, for guiding the neural computations within the separate ON and OFF pathways. We also highlight the significance of edge selectivity to movements of ON-edges and OFF-edges in translating perception, especially in a visually cluttered environment.

4.2.1 Network Architecture

Within this subsection, we introduce the proposed bio-inspired visual neural network inspired by fly visual systems, fully with algorithms and parameters selection. A key feature of the DSNN is that it is only sensitive to translational motion cues in four fundamental directions, unlike the proposed LGMDs models inspired by locusts in Chapter 3. And compared with a related partial modelling work in [53], we incorporate in this framework temporal dynamics of 'fast onset and slow decay' mechanism and the spike coding to realise the fly DSNs as spiking neurons similarly to 'integrate-and-fire' neurons.

In general, there are five computational neuropile layers constituting the motivated

motion-detecting pathways for mimicking DSNs in the fly visual systems. The core structure is the separated ON and OFF pathways splitting motion information for parallel computations, encoding specific selectivity to moving ON-edges and OFF-edges, respectively. This neural network is also featured by spatiotemporal filtering both prior to and within the dual-pathways, locationally, in order to achieve more robust motion detection performance in real world with dynamic and visually cluttered scenes. It is also worth clarifying that the whole motion-detecting pathways possess a completely feed-forward structure, and only uses low-level image processing methods; those computationally expensive algorithms for objects classification, scene or activity analysis and parameters learning are not considered, accordingly. This model perceives motion by reacting to translating ON-edges and OFF-edges. Within the ON and OFF pathways, we put forth ensembles of ON-ON and OFF-OFF cells, encoding brightness increments and decrements, collaboratively. Each pairwise connection is constituted by a symmetric HR motion detector. In addition, we apply spatial pre-filtering of motion information with polarity properties in order to achieve the edge selectivity. Dynamic temporal filters are used to further enhance the speed response to translating features. An illustration of the proposed DSNN is depicted in Fig. 4.3. More detailed novel structures and mechanisms are shown in Fig. 4.4 and 4.5.

4.2.1.1 The Computational Retina Layer

In the first computational neural layer of Retina, we model the fly compound eyes simply with photoreceptors arranged in a two-dimensional matrix form, which capture grey-scale and pixel-wise luminance from video clips or visually sensing modalities. The brightness obtained by photoreceptors goes through a first-order high-pass filtering in order to get moving features by the differential image between every two successive frames:

$$P(x, y, t) = L(x, y, t) - L(x, y, t-1) + \sum_{i}^{N_p} a_i \cdot P(x, y, t-i), \tag{4.1}$$

where $P(x, y, t)$ is the change of luminance according to each local pixel at frame t. x and y are the abscissa and ordinate in the visual field. $L(t)$ and $L(t-1)$ are

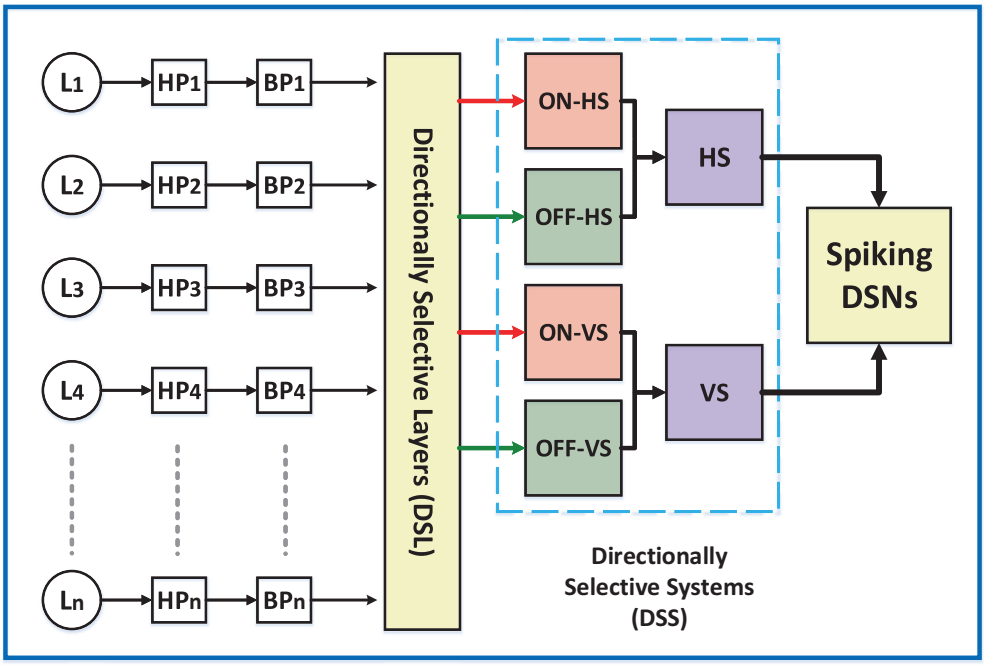

Figure 4.3: A general signal processing flowchart of the proposed DSNN: the motion information spatiotemporal filtering goes through a directionally selective layer(DSL) including ON and OFF pathways to form two flows of directionally selective systems(DSS), that map neural response to spikes toward further behavioural control neural systems.

the brightness of two continuous frames. The luminance change could last and decay for a short while: N_p indicates the total number of frames constituting the duration of residual visual information, and the coefficient a_i is defined by $a_i = (1 + e^{u \cdot i})^{-1}$ wherein $u = 1$. Increasing u leads to faster decay of remaining luminance change.

4.2.1.2 The Computational Lamina Layer

After that, as depicted in Fig. 4.3, we apply a spatial band-pass filtering for dynamic features, which is mathematically represented by a two-dimensional form of 'Difference of Gaussians' (DoGs) algorithm, so as to enhance the underlined edge selectivity in the motion-detecting circuitry, and maximise information transmission by spatially removing redundant environmental noise. Such a mechanism embodies the biological functions of LMCs in the Lamina neuropil layer, which was considered a suitable filter prior to the site of motion detection in insects' vision system [252, 18, 43]. With this mechanism, we can realise the centre-surrounding antagonism for each local lamina cell, with the centre-positive and surrounding-negative Gaussian representing the

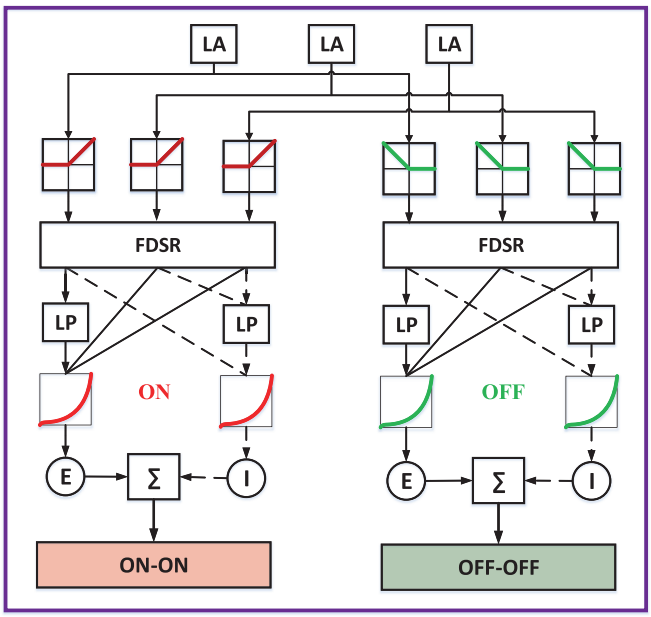

Figure 4.4: A schema of the DSL in DSNN taken three connected lamina neurons (LA) for illustration.

excitatory and inhibitory fields, respectively:

$$P_e(x,y,t) = P(x,y,t) \overset{x,y}{*} G_{\sigma_e}(x,y),\ P_i(x,y,t) = P(x,y,t) \overset{x,y}{*} G_{\sigma_i}(x,y), \tag{4.2}$$

where $\overset{x,y}{*}$ indicates the convolution at each local cell (x,y) in the visual field, σ_e and σ_i indicate the excitatory and inhibitory standard deviations. G is the convolution kernel, which satisfies with a two-dimensional Gaussian distribution:

$$G_\sigma(x,y) = \frac{1}{2\pi\sigma^2}\, exp(-\frac{x^2+y^2}{2\sigma^2}). \tag{4.3}$$

Therefore, this kernel is created by having each point to be the weighted average of the points surrounding it, and the weightings take a form of two Gaussian distributions, respectively. In the DoGs algorithm, the broader inhibitory Gaussian is subtracted from the narrower excitatory one, along with the polarity selectivity to fit the functionality of the following first-order ON and OFF RTCs:

$$LA(x,y,t) = \begin{cases} |P_e(x,y,t) - P_i(x,y,t)|, \text{ if } P_e(x,y,t) \geq 0 \ \& \ P_i(x,y,t) \geq 0 \\ -|P_e(x,y,t) - P_i(x,y,t)|, \text{ if } P_e(x,y,t) < 0 \ \& \ P_i(x,y,t) < 0 \end{cases}. \tag{4.4}$$

The RTCs split edge-motion information into parallel ON and OFF pathways, encoding light-on and light-off responses, separately. Technically speaking, such neural mechanisms fulfil the 'half-wave' rectifiers (Fig. 4.4) filtering out negative and positive input for ON and OFF channels, respectively, as well as inverting negative information to positive for OFF channels. Each LMC corresponds to a pairwise combination of ON and OFF polarity interneurons:

$$\begin{aligned} LA_{on}(x,y,t) &= (LA(x,y,t) + |LA(x,y,t)|)/2 + \sigma_l \cdot LA_{on}(x,y,t-1), \\ LA_{off}(x,y,t) &= |(LA(x,y,t) - |LA(x,y,t)|)|/2 + \sigma_l \cdot LA_{off}(x,y,t-1), \end{aligned} \tag{4.5}$$

where $LA_{on}(x,y,t)$ denotes the ON cell value, and similarly for the OFF cell value. In addition, we allow a small fraction (σ_l) of original information in parallel to pass through, mimicking the residual visual information in the motion-detecting circuitry of insects [39].

For each independent polarity neuron, an 'adaptation state' is formed by a biologically plausible mechanism, i.e., the temporal dynamics of 'fast depolarizing slow re-polarising' (FDSR in Fig. 4.4), which matches the neural characteristic of 'fast onset and slow decay' phenomenons. As depicted in Fig. 4.5b, we do the gradient check for relayed signals from RTCs before the processing of low-pass filtering:

$$\frac{dD(x,y,t)}{dt} = \begin{cases} \frac{1}{\tau_{fast}}(LA'(x,y,t) - D(x,y,t)), \text{ if } \frac{dLA'(x,y,t)}{dt} \geq 0 \\ \frac{1}{\tau_{slow}}(LA'(x,y,t) - D(x,y,t)), \text{ if } \frac{dLA'(x,y,t)}{dt} < 0 \end{cases}, \tag{4.6}$$

where LA' designates the input from either ON/OFF RTCs, and D denotes the delayed polarity signals. Intuitively, if the gradient is non-negative, we employ a very short delay – τ_{fast} (1 millisecond in our case) – realising the 'fast onset' response; otherwise, the delay is set to 100ms for the 'slow decay'. Because the digital signal does not have a continuous derivative, we do check the gradient through comparative analysis between discrete frames. After that, in the FDSR mechanism, the delayed signal is subtracted

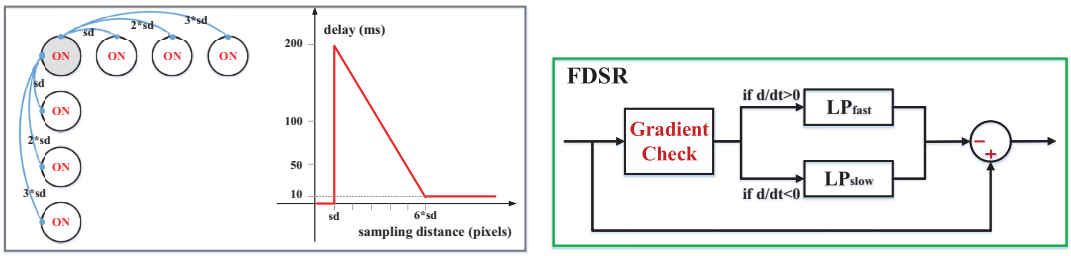

Figure 4.5: (a) Spatial multi-connections of ON cells for each local cell in two directions and the temporal delay function for combinations with different sampling distances (sd) in the DSL, similarity for connections of OFF cells, (b) biologically plausible temporal mechanism of FDSR in both ON and OFF channels in the DSL.

to the original passed one:

$$\begin{aligned} F_{on}(x,y,t) &= LA_{on}(x,y,t) - D_{on}(x,y,t), \\ F_{off}(x,y,t) &= LA_{off}(x,y,t) - D_{off}(x,y,t). \end{aligned} \tag{4.7}$$

Such a mechanism contributes to temporally filter out irrelevant motion from relevant motion in dynamic and complex environments.

4.2.1.3 The Computational Medulla and Lobula Layers

Next, the Medulla and Lobula neuropil layers, as shown in Fig. 4.1, have been proposed to be the most likely places where neighbouring interneurons interact with each other in a non-linear way producing directionally selective signal to the following lobula plate [97]. We computationally model these two layers as the DSL shown in Fig. 4.3. To be more specific, there are two kinds of flows – excitation and inhibition generated in ON/OFF channels of the Medulla/Lobula layers. Importantly, compared with the DSNs modelling works motivated by neurons in locusts' visual pathways [24, 25], wherein the inhibitory connections are modelled in four or eight directions to generate the directionally selective information, we shape the directional tuning in the proposed DSNN via design of connections of same-polarity (ON-ON/OFF-OFF) cells in only two orientations by similar non-linear computation to the HR detectors: the excitation and inhibitions form in the start and adjacent connected cells, respectively, as illustrated in Fig. 4.5a.

Contrary to a number of EMDs-based computational models, we not only imple-

ment the lateral multi-connections for each local cell in the computational medulla and lobula layers, but also adopt dynamically temporal filtering, wherein the delays vary in each directional combination of ON-ON/OFF-OFF motion detectors depending on different spacings or sampling distances (sd) and obey a linearly decaying function, as shown in Fig. 4.5a. In the experiments, we will demonstrate that such a structure has potential to improve speed response of translating sensitive neural systems. Firstly, calculations of the ON-pathway HSS are as follows:

$$\begin{aligned} E_{on}^{hs}(x,y,t) &= \sum_{i=d}^{d\cdot N_{con}} D_{on}(x,y,t)\cdot F_{on}(x+i,y,t), \\ I_{on}^{hs}(x,y,t) &= \sum_{i=d}^{d\cdot N_{con}} D_{on}(x+i,y,t)\cdot F_{on}(x,y,t), \\ ME^{hs}(x,y,t) &= E_{on}^{hs}(x,y,t) - w_i \cdot I_{on}^{hs}(x,y,t), \end{aligned} \tag{4.8}$$

where N_{con} and d designate the number of connected polarity cells and the increment in sd. w_i is a local bias to form a partially balanced model with stronger response to the preferred directional translations. The delay function in either ON/OFF pathways conforms to Eq. 4.6 – a low-pass filtering but with a dynamic time parameter τ_s, which can vary from tens to hundreds of milliseconds, as illustrated in Fig. 4.5a:

$$\begin{aligned} \frac{dD_{on}(x,y,t)}{dt} &= \frac{F_{on}(x,y,t) - D_{on}(x,y,t)}{\tau_s}, \\ \frac{dD_{off}(x,y,t)}{dt} &= \frac{F_{off}(x,y,t) - D_{off}(x,y,t)}{\tau_s}. \end{aligned} \tag{4.9}$$

And similarly for computations of the VSS for the ON pathway:

$$\begin{aligned} E_{on}^{vs}(x,y,t) &= \sum_{i=d}^{d\cdot N_{con}} D_{on}(x,y,t)\cdot F_{on}(x,y+i,t), \\ I_{on}^{vs}(x,y,t) &= \sum_{i=d}^{d\cdot N_{con}} D_{on}(x,y+i,t)\cdot F_{on}(x,y,t), \\ ME^{vs}(x,y,t) &= E_{on}^{vs}(x,y,t) - w_i \cdot I_{on}^{vs}(x,y,t). \end{aligned} \tag{4.10}$$

With similar ideas, in the Lobula layer, the HSS for the OFF pathway is computed as:

$$\begin{aligned} E^{hs}_{off}(x,y,t) &= \sum_{i=d}^{d\cdot N_{con}} D_{off}(x,y,t)\cdot F_{off}(x+i,y,t), \\ I^{hs}_{off}(x,y,t) &= \sum_{i=d}^{d\cdot N_{con}} D_{off}(x+i,y,t)\cdot F_{off}(x,y,t), \\ LO^{hs}(x,y,t) &= E^{hs}_{off}(x,y,t) - w_i \cdot I^{hs}_{off}(x,y,t), \end{aligned} \tag{4.11}$$

and calculations of the VS system for the OFF pathway are defined as:

$$\begin{aligned} E^{vs}_{off}(x,y,t) &= \sum_{i=d}^{d\cdot N_{con}} D_{off}(x,y,t)\cdot F_{off}(x,y+i,t), \\ I^{vs}_{off}(x,y,t) &= \sum_{i=d}^{d\cdot N_{con}} D_{off}(x,y+i,t)\cdot F_{off}(x,y,t), \\ LO^{vs}(x,y,t) &= E^{vs}_{off}(x,y,t) - w_i \cdot I^{vs}_{off}(x,y,t). \end{aligned} \tag{4.12}$$

4.2.1.4 The Computational Lobula Plate

In the final layer of Lobula Plate in the motion-detecting pathways, there are four groups of LPTCs. Each group has the specific DS to one prime direction, as illustrated in Fig. 4.1a. We computationally model these LPTCs as the DSS in Fig. 4.3, via linearly integrating relayed excitations from ON and OFF pathways forming the neural responses represented by membrane potentials of four cardinal directions:

$$\begin{aligned} LP^{hs}_{on}(t) &= \sum_{1}^{C}\sum_{1}^{R} ME^{hs}(x,y,t),\ LP^{vs}_{on}(t) = \sum_{1}^{C}\sum_{1}^{R} ME^{vs}(x,y,t), \\ LP^{hs}_{off}(t) &= \sum_{1}^{C}\sum_{1}^{R} LO^{hs}(x,y,t),\ LP^{vs}_{off}(t) = \sum_{1}^{C}\sum_{1}^{R} LO^{vs}(x,y,t), \end{aligned} \tag{4.13}$$

where C and R indicate the numbers of columns and rows in the two-dimensional visual field. The LPTCs response is tuned to be rigorously positive to PD stimuli, i.e., rightward and downward translations, and negative to ND stimuli – leftward and upward translations. To further reduce noise signals, we low-pass filter the LPTCs response along each direction, the equation of which is similar to Eq. 4.9 but with a fixed time parameter τ_{mp} in milliseconds.

Moreover, like other artificial neurons, e.g. the proposed LGMDs models in Chapter 3, we apply an activation function to realise spiking DSNs with an exponential mapping of the LPTCs neural response that can be explained in terms of a sigmoid transformation [253]. Let the LPTCs membrane potential be x, the activation function is expressed as:

$$f(x) = \text{sgn}(x) \cdot ((1 + e^{-|x| \cdot (C \cdot R \cdot K_{sig})^{-1}})^{-1} - \Delta_C), \tag{4.14}$$

where K_{sig} is a small coefficient. The output is normalised to $[0, 0.5)$ for the positive input, and $(-0.5, 0]$ for the negative input, by setting the coefficient Δ_C to 0.5: without such a coefficient, the output is within the range of $(-1, -0.5]$ for the negative input and $[0.5, 1)$ for the positive input, which are not successive. Therefore, as depicted in Fig. 4.3, the SMPs of four groups of LPTCs ($\hat{LP}$) congregate at the HSS and VSS, separately, each output of which is between $(-1, 1)$:

$$HS(t) = \hat{LP}^{hs}_{on}(t) + \hat{LP}^{hs}_{off}(t), \quad VS(t) = \hat{LP}^{vs}_{on}(t) + \hat{LP}^{vs}_{off}(t). \tag{4.15}$$

4.2.1.5 Spiking Fly DSNs

In the proposed DSNN, we for the first time implement the fly DSNs as spiking neurons by mapping the SMP of either HSS or VSS to firing rate, exponentially:

$$S^{spike}_{hs}(t) = \left\lfloor e^{[K_{sp} \cdot (|HS(t)| - |T_{sp}|)]} \right\rfloor, \quad S^{spike}_{vs}(t) = \left\lfloor e^{[K_{sp} \cdot (|VS(t)| - |T_{sp}|)]} \right\rfloor, \tag{4.16}$$

where $\lfloor x \rfloor$ indicates a mathematical'floor' function to obtain the largest integer less than or equal to the input number. K_{sp} denotes a coefficient, which can directly affect the firing rate, i.e., increasing it will lead to higher firing rate. T_{sp} designates the spiking threshold, which is positive to PD output yet negative to ND output. Through such a spiking mechanism, more than one spikes could be generated at each discrete frame.

Table 4.1: Predefined Parameters of the proposed DSNN

Name	Value	Name	Value	Name	Value
C, R	adaptable	K_{sp}	$1 \sim 3$	τ_s	$10 \sim 200$ms
w_i	0.9	N_{con}	$4 \sim 8$	d	$1 \sim 4$
σ_e, σ_i	d, $2 \cdot d$	N_p	$0 \sim 6$	σ_l	0.1
τ_{fast}	1ms	τ_{slow}	100ms	τ_{mp}	10ms
K_{sig}	0.01	Δ_C	0.5	T_{sp}	$\pm 0.16 \sim \pm 0.2$

4.2.1.6 Parameters Selection

All model parameters of the proposed DSNN are decided empirically with considerations of the functionality of fly DSNs for translational motion detection in dynamic and complex scenes, as well as the implementation on embedded system. There are currently no parameters training methods involved in this framework. Table 4.1 presents the predefined parameters of the DSNN. The adaptable parameters C and R are decided by the resolution of input images. In the DoGs algorithm, we shape the Gaussians by balancing the standard deviations on two dimensions, and make the outer negative-Gaussian twice the size of the inner positive-Gaussian for forming the specific selectivity to translating ON-edges and OFF-edges. It also appears that the widths of Gaussians depend on the spacing between the nearest neighbouring ON/OFF motion detectors, i.e., it is essentially determining the spatial frequency resolution in the band-pass filtering of the computational Lamina layer. In addition, as mentioned above, a critically important feature of this neural network is the building of ensembles of motion detectors in ON and OFF pathways. Increasing the number of connected cells (N_{con}) for each local unit in the dual-pathways could further improve the potential speed response of translating motion detectors to moving dark/light features, at the cost though of more computational consumption.

In next subsection, we will represent the systematic experiments and results along with analysis. These will clearly demonstrate how the outputs of proposed translating sensitive neural system, that is, the membrane potential and spiking frequency, reflect the foreground translation direction and intensity against a visually cluttered and dynamic background.

4.2.2 Experiments and Results

In this subsection, we present systematic and comparative experiments and results along with analysis and discussion. The main objectives are firstly to assess the fundamental functionality and effectiveness of the proposed DSNN on translational motion perception; second, we systematically investigate its internal properties, and compare to an EMDs-based model [31, 54], as well as a preliminary modelling work of fly DSNs [53]. Importantly, we also examine its feasibility and robustness as an embedded vision system in an autonomous ground micro-robot. All the experiments can be categorised into two types of tests: off-line and on-line tests. In the off-line tests, the visual stimuli comprise computer-simulated and real physical scenarios. In the on-line tests, the proposed DSNN is tested on embedded system.

4.2.2.1 Experimental Setting

We first introduce the software and hardware set-ups. In the off-line tests, the frameworks of DSNN and two comparative models were all set up in Visual Studio 2015 (Microsoft Corporation). Data analysis and representations were accomplished in Matlab 2015 (The MathWorks, Inc. Natick, USA). The resolutions of synthetic visual streams are 320×180 and 540×180 for translational movements embedded in clean and natural backgrounds, respectively. The resolution of real-world visual stimuli is 320×180. All the video images are converted to the grey-scale format at the sampling frequency of 30Hz for the processing of neural networks. In the on-line tests, the micro-robot used was the *Colias*-IV, the same as introduced in Chapter 3.1 and Fig. 3.5b. It is necessary to state here that in this research, the monocular camera was the only applied sensor, as well. We did not investigate the performance of DSNN in robot navigation, that is, the motion unit was disabled in this research. The robot with the proposed DSNN on embedded system was stimulated by various kinds of movements. An extension model to the DSNN will be tested in moving robots with behavioural response in the following Section 4.4.

4.2.2.2 Synthetic Stimuli Tests

First of all, the experiments started at testing the DSNN using computer-simulated visual stimuli consisting of the movements of darker and lighter objects embedded in clean and visually cluttered backgrounds, respectively. All the synthetic stimuli can be categorised into the following types: the depth-movements including approaching and receding of objects, translations in both horizontal and vertical directions.

Tested by visual stimuli embedded in a clean background As described above, the first and basic objective is to show the basic functions of the proposed DSNN. First, challenged by translational motion in four cardinal directions (Fig. 4.6a – 4.6d), the proposed DSNN represents successively positive sigmoid membrane potential (SMP) by motion in PDs (rightward and downward for the HSS and VSS), while negative responses against motion in NDs – leftward for the HSS and upward for the VSS. The motion direction is well tuned by the symmetric structure of HR detectors within the ensembles of ON-ON and OFF-OFF local polarity detectors in the computational Medulla and Lobula layers, namely the DSL. The results well match outcomes of a biological research [94].

Second, we tested the DSNN with approaching and receding movements of either dark (Fig. 4.6e) or light (Fig. 4.6f) objects embedded in light and dark backgrounds. The results illustrate that the proposed neural network is rigorously inhibited during each entire-course of movements in depth. Interestingly, compared to the looming detectors proposed in Chapter 3 that respond to approaching over translating visual stimuli, the proposed DSNN represents totally reverse response. We will further investigate these fundamental characteristics in the on-line experiments.

Moreover, motivated by the physiological experiments on blocking either ON or OFF pathways demonstrated in [94], we examined the specialised functionality of ON and OFF pathways in the proposed computational model. With similar ideas, we compared the neural response generated by intact ON and OFF pathways with either ON-blocked or OFF-blocked systems. Taken the dark object translating as an example, the results illustrated in Fig. 4.7 and 4.8 demonstrate that blocking either ON/OFF path-

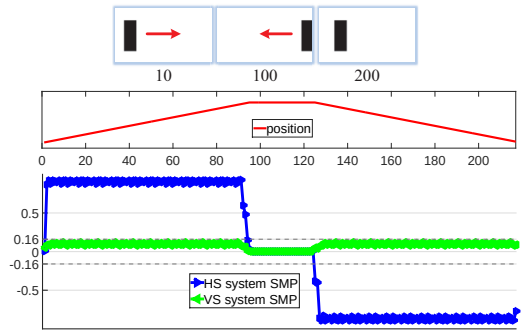

(a) a darker object translating horizontally

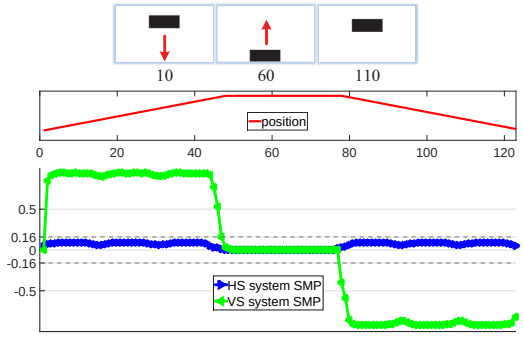

(b) a darker object translating vertically

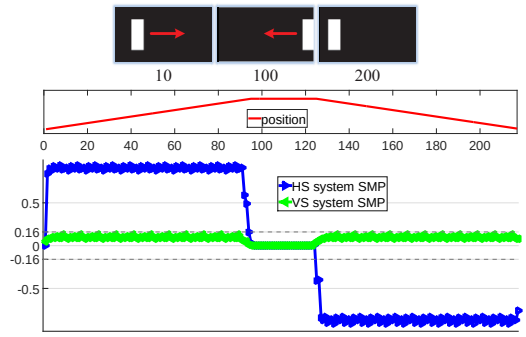

(c) a lighter object translating horizontally

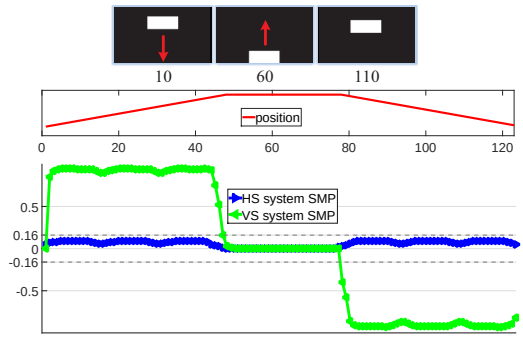

(d) a lighter object translating vertically

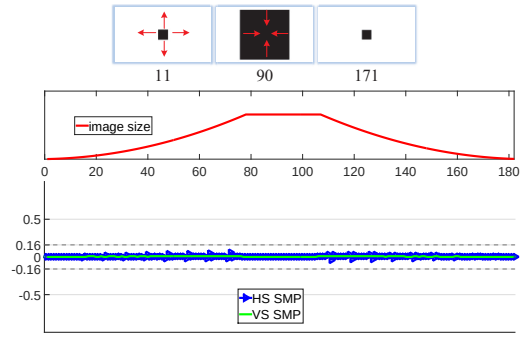

(e) a darker object looming – receding

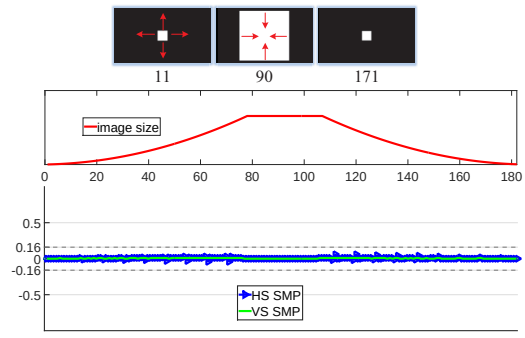

(f) a lighter object looming – receding

Figure 4.6: The proposed DSNN is challenged by synthetic visual stimuli of dark and light objects approaching, receding and translating against light and dark backgrounds, respectively. The example views of input frames are shown at top of each result. The changes of object position or size in the visual field are depicted below the snapshots. The sigmoid membrane potentials (SMP) of HSS and VSS of DSNN are represented, separately. The horizontal dashed lines indicate the predefined spiking thresholds (± 0.16). X and Y axes denote the time course in frames and the SMP.

ways abolishes the corresponded functions of ON/OFF RTCs, so that cutting down the output of either HSS or VSS to its half-level produced by the intact pathways. This turns out that ON-blocked or OFF-blocked model only possesses the ability of sensing light-off (offset) or light-on (onset) response. To be more concrete, for a dark translating object embedded in a light background, the moving leading edge generates an offset response by the light-to-dark luminance change so that rigorously activating the OFF RTCs in the computational Lamina layer, whilst the trailing edge leads to an onset

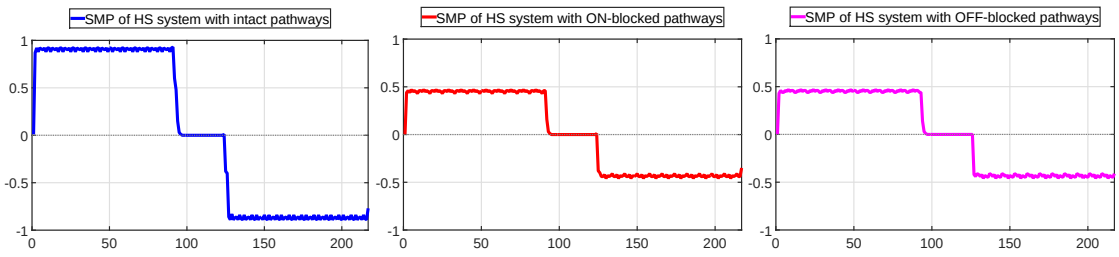

Figure 4.7: Neural response (SMP) of DSNN with intact ON and OFF pathways (a), ON-blocked pathways (b), and OFF-blocked pathways (c), challenged by a dark object translating horizontally against a light background corresponding to Fig. 4.6a.

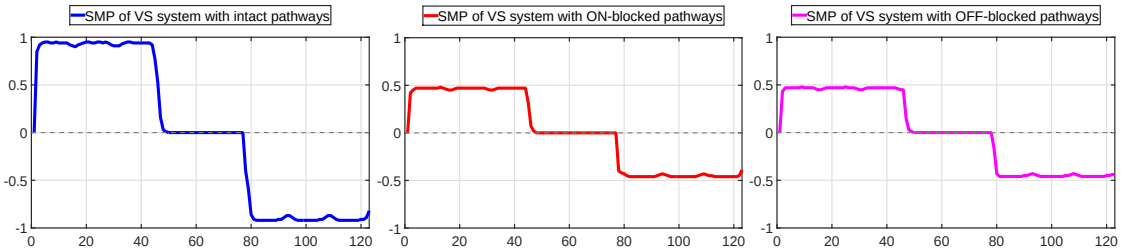

Figure 4.8: Neural response (SMP) of DSNN with intact ON and OFF pathways (a), ON-blocked pathways (b), and OFF-blocked pathways (c), challenged by a dark object translating vertically against a light background corresponding to Fig. 4.6b.

response by the dark-to-light luminance change activating the ON RTCs. The opposite happens for a light translating object embedded in a dark background, where the leading and trailing edges rigorously activate ON and OFF RTCs, respectively. The results verify that the functionality of the proposed DSNN well matches the underlying fly physiology revealed by [94]. Moreover, since we put forth a bias in all inhibitory flows within ON and OFF pathways to form a partially balanced structure, higher neural response is generated by motion in PDs.

Tested by visual stimuli embedded in a shifting natural background After demonstrating the basic functions of the proposed framework, we designed synthetic stimuli in a natural and cluttered background with global shifting, to further inspect its robustness in translational motion perception in dynamic and complex scenes. We compare the performance with two related translating sensitive models – an EMDs-based model [31, 54] and a preliminary fly DSNs model [53] from our previous research.

First, similarly to former tests in clean background, we challenged the proposed DSNN and two comparative models by the movements of dark and light objects ap-

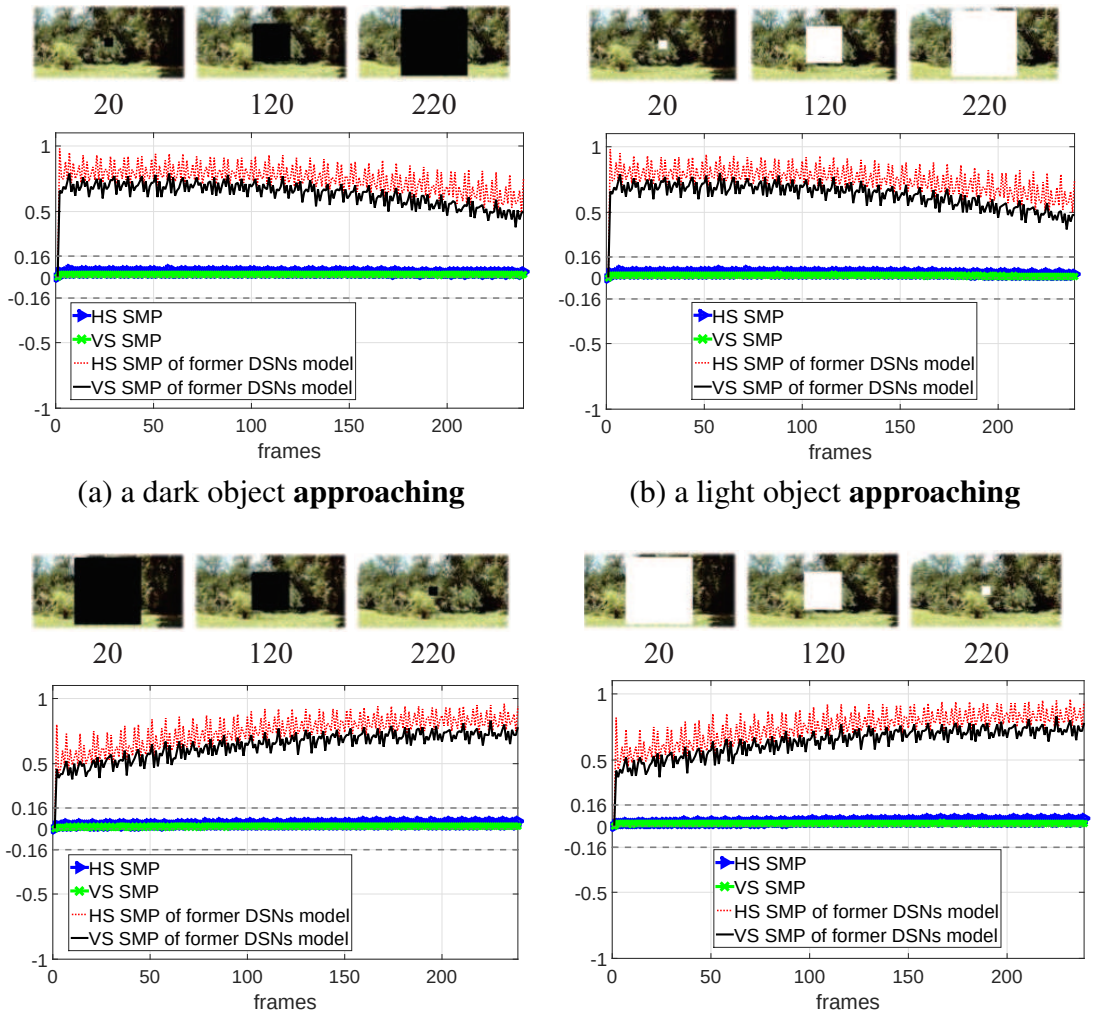

(a) a dark object **approaching**

(b) a light object **approaching**

(c) a dark object **receding**

(d) a light object **receding**

Figure 4.9: The proposed DSNN and comparative DSNs models [53] are challenged against dark and light objects approaching, receding embedded in a cluttered background shifting rightward at the speed $Vb = 8$ (pixels per frame). The HSS and VSS outputs of both models are depicted. The horizontal dashed lines indicate the spiking threshold (± 0.16).

proaching, receding and translating against a shifting natural background, as shown in Fig. 4.9. When tested by movements in depth, both the HSS and VSS of the proposed DSNN remain quiet. The results match tests in Fig. 4.6e and 4.6f, perfectly. On the other hand, both the HSS and VSS of the former fly DSNs model [53] are greatly activated. In that modelling study, the comparative DSNs model demonstrated robust performance in extracting useful translational motion cues from a cluttered but stationary background via the modelling of a spatial pre-filtering mechanism prior to the ON and OFF pathways. However, in this research, we found that it is easily affected by the natural background shifting. A fly may handle this situation well, like our results shown in Fig. 4.6, to discriminate objects that approaching from translating.

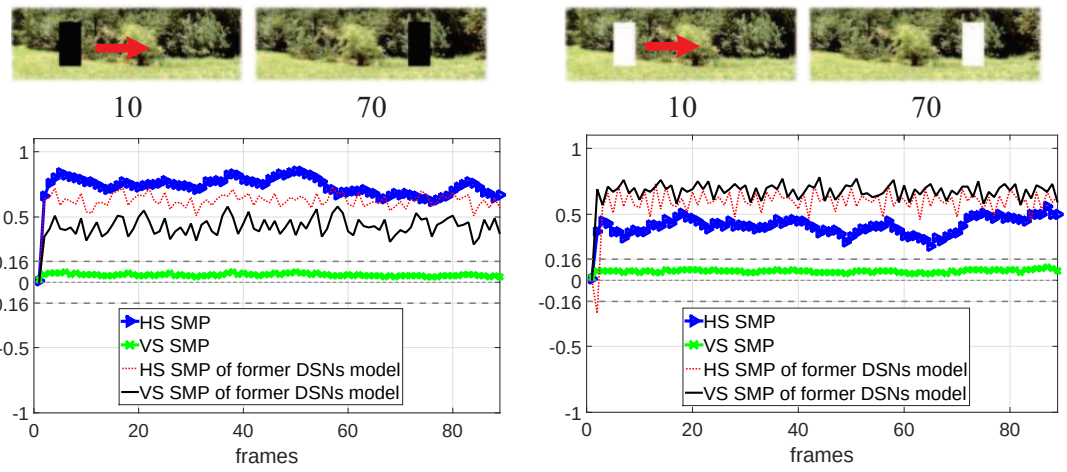

(a) a dark object translating rightward (b) a light object translating rightward

Figure 4.10: The proposed DSNN and comparative DSNs models [53] are challenged against dark and light objects translating rightward embedded in a shifting cluttered background moving in the opposite direction $Vb = -8$ (pixels per frame).

Therefore, very importantly, this research provides an important suggestion towards building a dynamic vision system: a robust artificial motion detector requires both spatial and temporal processes to deal with background noise filtering out irrelevant motion from relevant motion. In the proposed DSNN framework, we demonstrate the effectiveness of a bio-plausible solution, that is, an FDSR temporal mechanism in the motion-detecting pathways to enhance the antagonism to background noises in artificial motion perception systems.

Tested by rightward-translating movements accompanied by the background shifting in an opposite direction, as illustrated in Fig. 4.10, the HSS of both comparative neural networks produce successively positive membrane potential. The VSS of proposed DSNN remains inactive, whilst the VSS of the comparative model is highly activated by the moving background rather than the translating object. For deepening our understanding of the advantages of proposed DSNN, we designed systematic tests on both neural networks with visual stimuli of dark and light objects translating at three constant-speed levels. All stimuli are embedded in a shifting natural background to an opposite orientation, and at five constant velocities, respectively. The statistics illustrated in Fig. 4.11 allow the following conclusions to be drawn: both comparative models show speed response to translating stimuli at varied velocities; the HSS of proposed DSNN represents a more significant rising with larger gradient and smaller

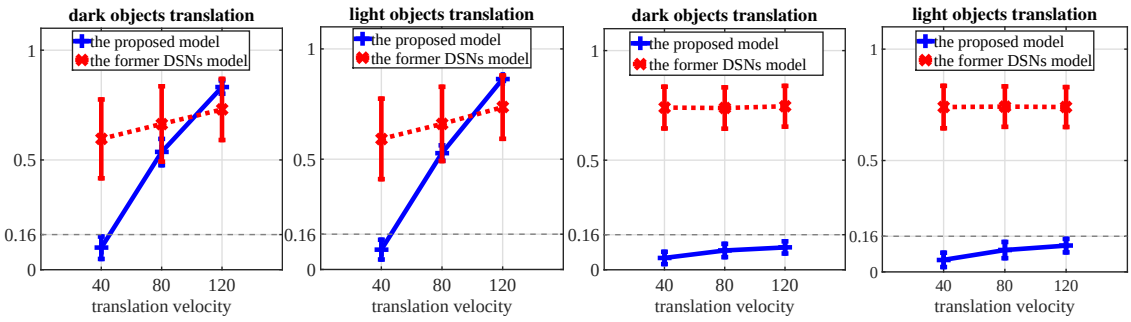

(a) **HSS** peak (b) **HSS** peak (c) **VSS** peak (d) **VSS** peak

Figure 4.11: Statistical results of peak response of two comparative models, tested by the dark and light objects translating rightward at three individual speeds: 40, 80, 120 pixels per frame (p/f), each against the leftward shifting background, at five velocities: -2, -4, -6, -8, -10 p/f, respectively. Horizontal dashed line indicates the predefined spiking threshold (0.16).

invariance on peak neural response; this implies more stable performance to translating against a shifting natural scene at all tested velocities (Fig. 4.11a, 4.11b). In addition, it can be clearly seen from Fig. 4.11c and 4.11d that the peak responses of the proposed VSS are all below the spiking threshold; whilst the VSS of comparative model is highly activated by horizontal translating stimuli. The results match Fig. 4.10. Informative results of comparative experiments have demonstrated that the proposed DSNN outperforms the former fly DSNs model from our previous research. The proposed model shows robust performance to detect directional translational motion in more complex and dynamic background, a situation which is reminiscent of animals' self-motion in navigation.

Furthermore, we also compared the proposed DSNN with a classic EMDs model [31, 54] for the purpose of inspecting the effects of translating speed and object contrast on peak neural response that is represented by the SMPs of the proposed DSNN and the logarithmic output of the comparative model. First, the results in Fig. 4.12 indicate satisfactory speed response and contrast sensitivity of the proposed DSNN, i.e., it produces stronger response to the faster translating stimuli; it is more sensitive to larger-contrast objects. Second, contrary to the comparative model, the statistical results in Fig. 4.13 reveal that the proposed DSNN performs more robustly against the shifting of visually cluttered background representing better speed response to the translating of all grey-scale objects. More precisely, the SMPs of the proposed D-SNN smoothly peak at higher level along with the increasing of translating speed (Fig.

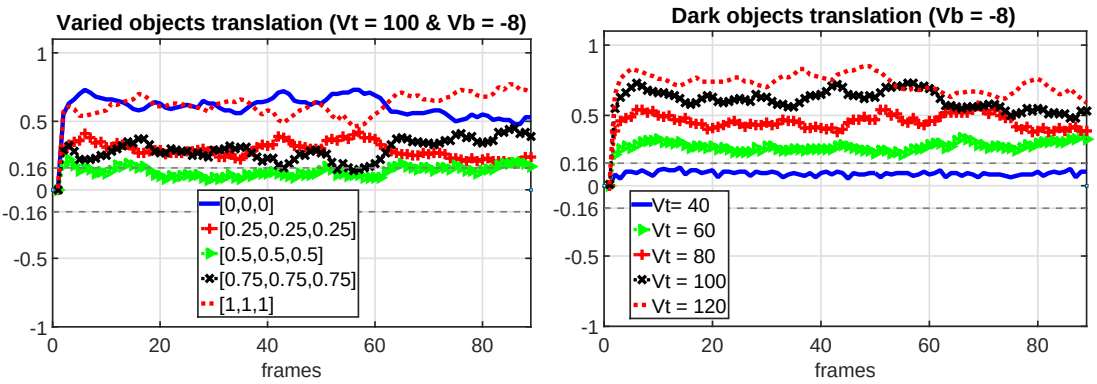

(a) (b)

Figure 4.12: Neural response of the HSS of DSNN, challenged by five grey-scaled objects translating rightward, respectively, at an identical speed (a), and by a fixed grey-scale object translating at five velocities (b): all movements are embedded in a cluttered background shifting leftward $Vb = -8$ p/f. Horizontal dashed lines indicate the predefined spiking thresholds (± 0.16).

4.13a); while the comparative model is not sensitive to all grey-scale objects that translate at varied speeds but the darkest and the lightest objects (Fig. 4.13c).

Moreover, Fig. 4.13b and 4.13d also indicate that the proposed DSNN performs robustly on all tested grey-scaled objects that translate at varied speeds. This can perceive translating stimuli even at the lowest velocity or with the smallest contrast in a shifting natural background. Intuitively, the peak neural responses reach the valley tested by the translating of moderate grey-scale objects with relatively smaller contrast to the background (Fig. 4.13b). On the contrary, the comparative model is not able to detect all grey-scale objects that translate at velocities lower than 60 p/f; the performance of the previous model is greatly affected by the shifting of cluttered background (Fig. 4.13d).

4.2.2.3 Real World Stimuli Tests

Next, we present the off-line experiments in real world scenarios. Compared with the synthetic stimuli tests, the degree of complexity of real physical scenes is relatively higher, including more environmental noise and/or irrelevant motion like windblown vegetation. We tested the proposed framework by horizontally translating movements embedded in two scenes using recorded video clips: a campus avenue and a street view, as shown in Fig. 4.14.

In general, the results in Fig. 4.14 demonstrate that the proposed DSNN is able to

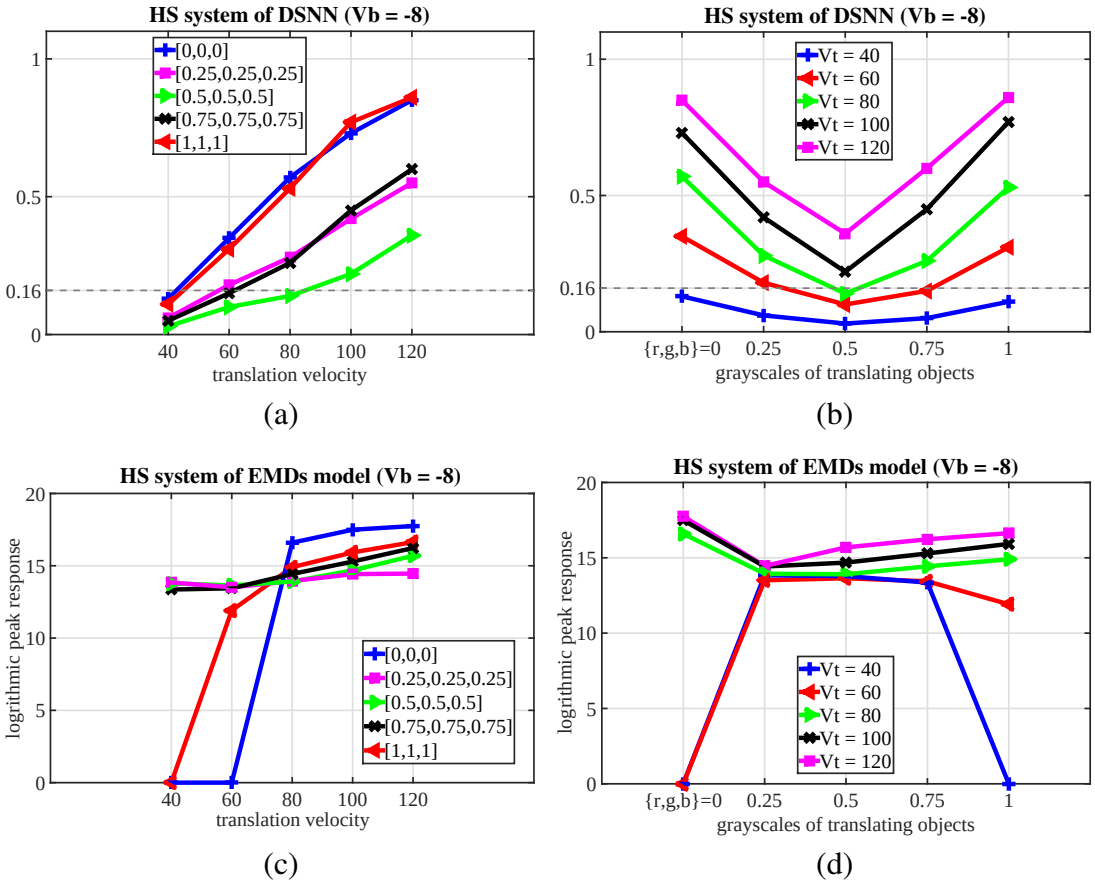

Figure 4.13: Statistical results of peak-response generated by the HSS of two comparative models – the proposed DSNN and an EMDs-based model [31, 54], challenged by five grey-scale objects translating rightward, at five velocities (Vt), respectively: all movements are embedded in a cluttered background shifting leftward $Vb = -8$. (a)(b) The peak-SMPs of the HSS of proposed DSNN, (c)(d) the logarithmic peak-response of the HSS of EMDs.

detect all the wide-field translational motion in real world scenes. This fulfils requirements of a robust motion detector for real-world visual tasks. To be more specific, the useful motion cues, including translating direction and magnitude, are extracted from the busy backgrounds by the HSS of the proposed DSNN. The translating information is mapped to positive and negative neural response for movements in PD and ND. On the contrary, the neural response of VSS remains mainly at much lower level, below the predefined spiking threshold. Fig. 4.14a, 4.14b, 4.14c and 4.14d illustrate that the proposed DSNN works robustly in extracting translating cues mixed with background noise like windblown vegetation. Fig. 4.14e and 4.14f indicate that it can also detect the same directional translation of a grouped objects. However, it is necessary to state that since the proposed framework only detects translational motion across a wide-field of the visual field, it is not able to provide translational motion information

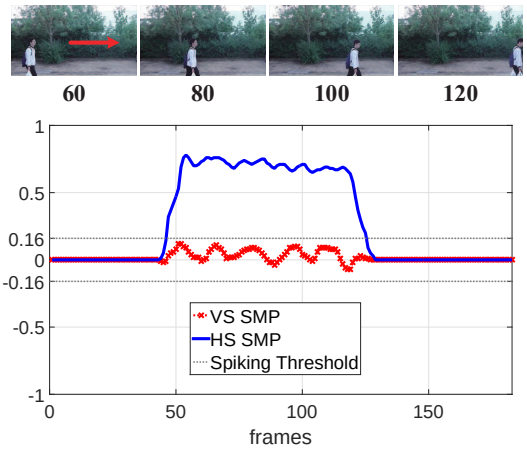

(a) a pedestrian translating rightward

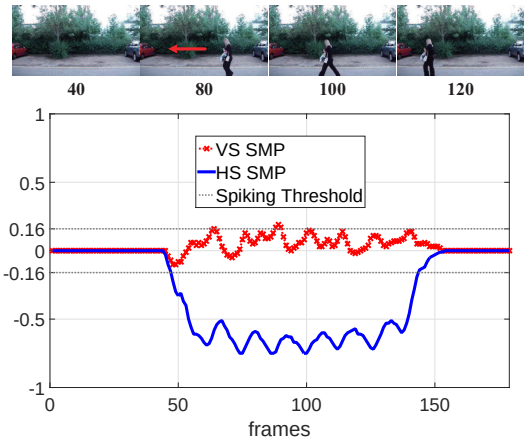

(b) a pedestrian translating leftward

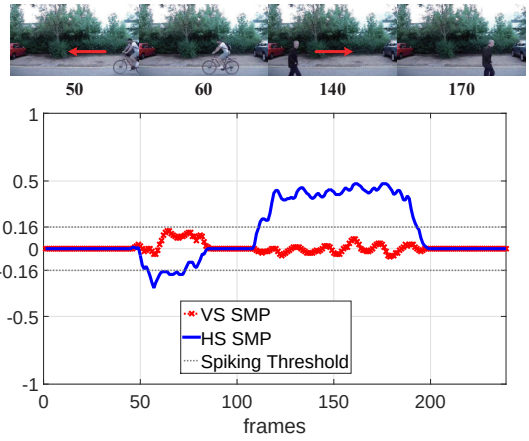

(c) translations in both horizontal directions

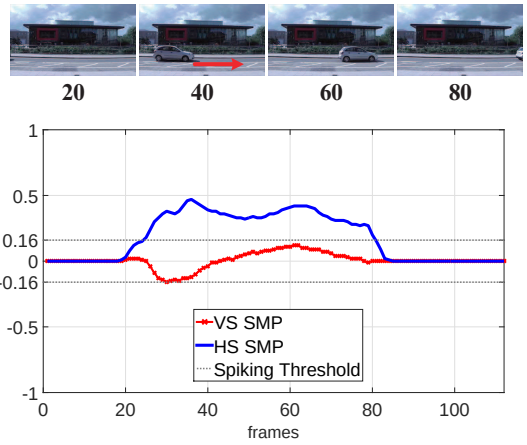

(d) a car translating rightward

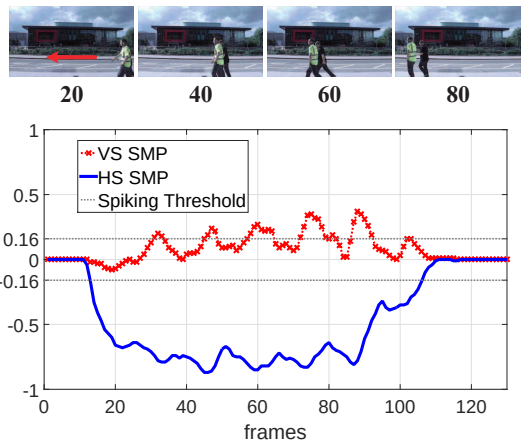

(e) a grouped people translating leftward

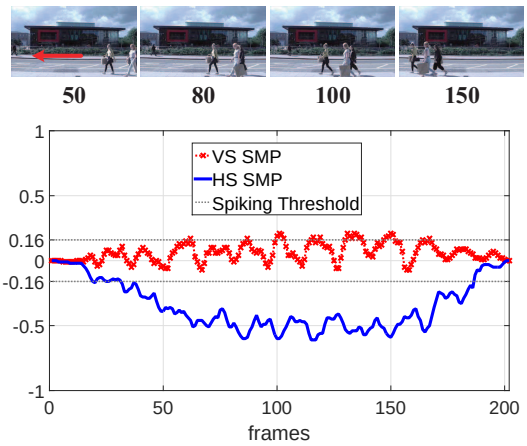

(f) a grouped people translating leftward

Figure 4.14: The proposed DSNN is challenged by translating stimuli in real physical scenes all mixed with a visually cluttered and dynamic environment including wind-blown vegetation. All the translations are in horizontal directions.

locally for each individual translating object without the segmentation and/or visual attention-based functions.

To summarise the off-line tests, first, using simple visual stimuli generated by computers, we have shown the proposed DSNN possesses similar characteristics and func-

tionality to the fly ON and OFF pathways and DSNs (LPTCs) in the preliminary visual system. Compared to the looming sensitive model inspired by locusts in Chapter 3, this neural network perceives translational motion cues rather than other kinds of stimuli. Importantly, through systematic and comparative tests to previous two related translating sensitive neural systems, we highlight: 1) the functions of modelled ON and OFF pathways correspond to relevant biological research findings; 2) the importance of spatiotemporal filtering of visual motion cues to deal with motion detection in high-level complexity required environments. The proposed DSNN outperforms the comparative models and may provide useful solutions for coping with the shortcomings of previous translational motion sensitive systems. The model represents both the speed response and contrast sensitivity to translating stimuli. We will further discuss on this in Section 4.5. The proposed neural network has also been verified a suitable dynamic vision system for real-world motion-detecting tasks. In the next part, we will present the on-line robot experiments to investigate its potential in robotic vision applications.

4.2.2.4 Preliminary Tests of DSNN on the Embedded System

In the last type of experiments, the proposed DSNN was for the first time implemented on embedded system in the *Colias* micro-robot (Fig. 3.5c) and tested in real time, for the purpose of evaluating its effectiveness and potential in robotic vision applications, along with deepening our understanding underlying characteristics of the proposed translating sensitive neural system. We call these experiments 'initial tests' since the motion unit was closed in this investigation, that is, the tested *Colias* robot was stationary and stimulated by translating movements. We will look into the performance of proposed DSNN in robot navigation with optical flow caused by ego-motion in Section 4.4. Back to this research, we designed two kinds of tests: the first was similar to the off-line tests to inspect the fundamental motion-detecting ability using general stimuli of objects that approach, recession and translations; the second sort involved systematic investigation on translation, angular-approach and angular-recession tests. The experimental settings are illustrated in Fig. 4.15: another mobile robot was used as stimuli to the tested robot where we collected model outputs including the SMP and

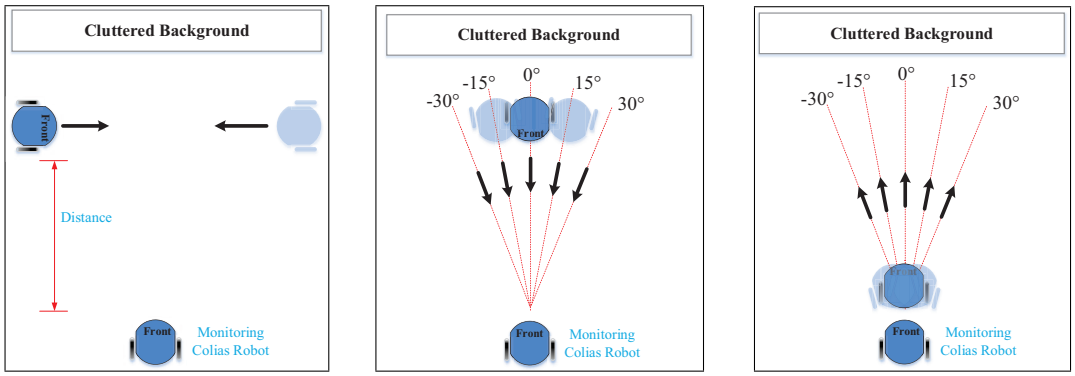

(a) translation tests (b) angular-approach tests (c) angular-recession tests

Figure 4.15: Real-time robot experiments set-ups – in all the tests, the readouts are from the monitoring *Colias*. Another *Colias* was used as the visually translating stimuli. Dark arrows indicate motion directions.

spikes from. As the robot is only able to run on a 2D surface, we investigated the HSS of embedded DSNN.

Tested by basic visual stimuli In the first round of on-line robot tests, the *Colias* robot was challenged by basic movements including approaching, receding and translating objects that are very frequent visual stimuli to mobile machines. Fig. 4.16 illustrates the example of first-views from the tested *Colias* robot and the neural response including the SMPs and spikes as outputs of the HSS. Similarly, the HSS remains quiet during the whole course of either proximity or recession stimuli, i.e. movements in depth. It is activated by translating movements and the membrane potential is tuned to be positive by PD translations, and negative by ND translations. It appears that the on-line robot tests results are consistent with the previous off-line tests, e.g. Fig. 4.6, 4.9, 4.10 and 4.14). Very importantly, the proposed model fulfils requirements of realisation on embedded system for in-chip real-time visual processing, that is, the frame rate can reach up to 30 fps with the proposed DSNN. This demonstrates that the computational simplicity and efficacy of the proposed framework on embedded system, which can be regarded as a neuromorphic solution for translational motion perception.

Systematic translation tests In the second round of real-time robot experiments, we looked deeper into the underlying properties of the proposed DSNN as an embedded vision system. The *Colias* robot was tested by systematic translating movements in visual clutter. In this case, as illustrated in Fig. 4.15a, the rightward translating move-

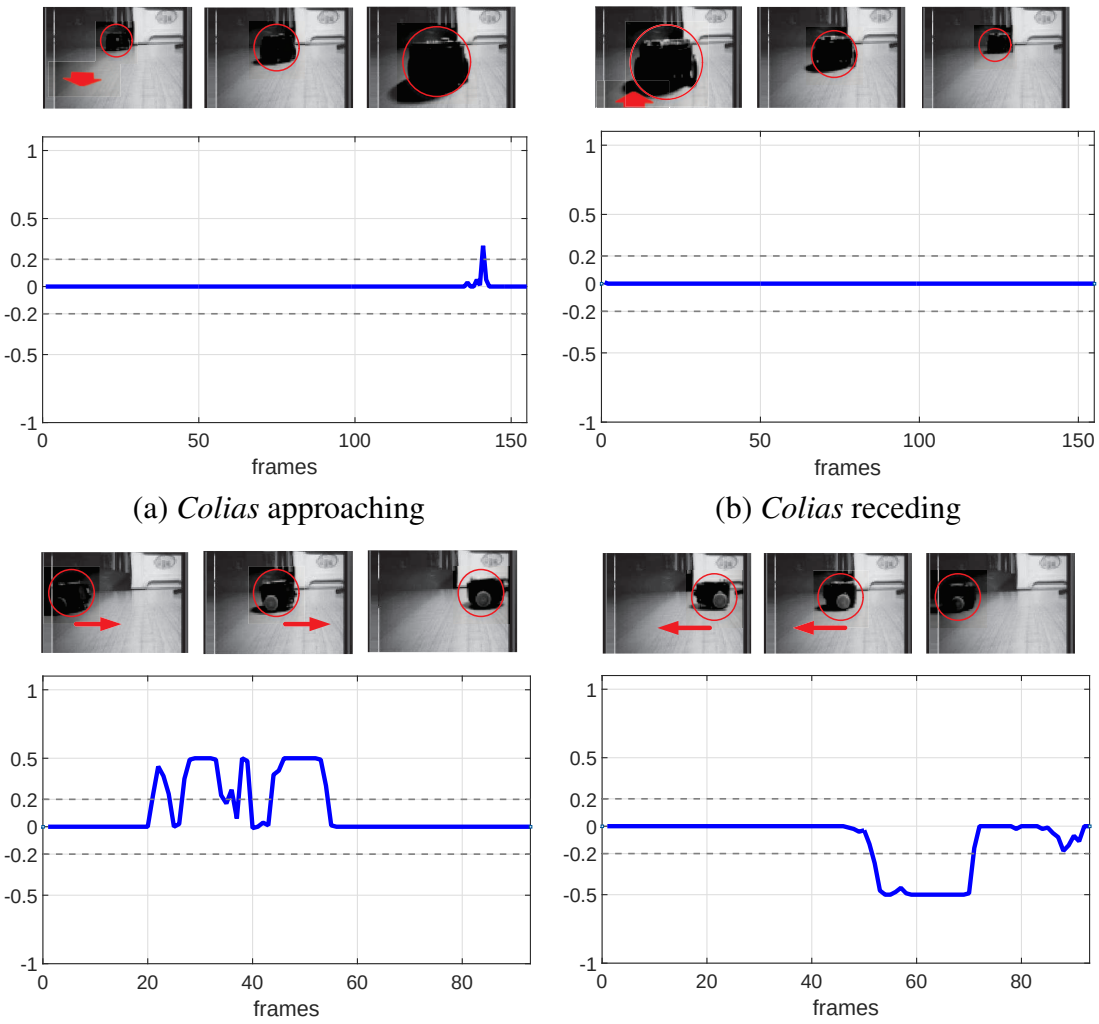

(a) *Colias* approaching

(b) *Colias* receding

(c) *Colias* translating rightward

(d) *Colias* translating leftward

Figure 4.16: The proposed DSNN on embedded system is challenged by an approaching, receding and translating moving robot, respectively. The example frontal-views captured by the stimulated *Colias* are shown at the top of each result. The spiking thresholds are set at ± 0.2.

ments happen from different distances or at distinct linear speeds.

First, we examined if the embedded DSNN shows good speed response to translational motion as explored in the off-line tests (Fig. 4.11 and 4.13). We represent the output as spike frequency by accumulating the elicited spikes of the HSS during each translation course with an approximately same length of time window, each throughout repeated tests. The statistical results shown in Fig. 4.17a demonstrate that tested by translations from a fixed distance of 8cm and at different speeds, the spike frequency increases along with the movement speeding up, and peaks around the translations at roughly 6cm/s. Interestingly, the spike rate is not always increasing by faster translating stimuli, i.e., it declines after the peak. The results are in accordance with the se-

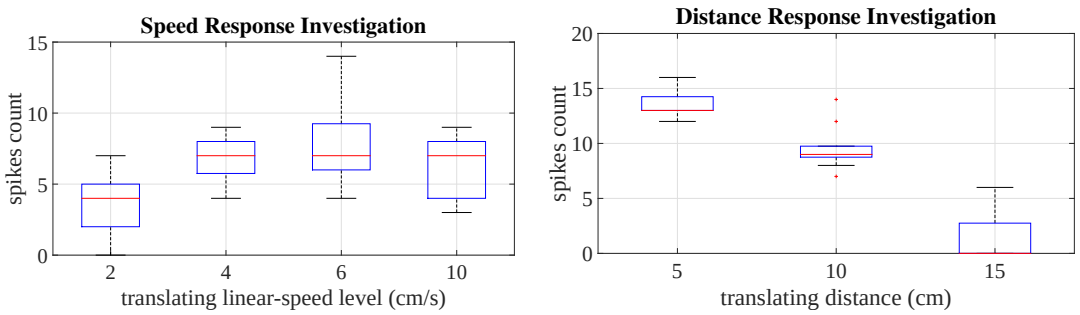

(a) (b)

Figure 4.17: Statistical results of systematic translation tests: (a) the distance between the stimulated *Colias* and the translating *Colias* was fixed at 8cm, whilst the translating linear-speed varied at 2, 4, 6 and 10cm/s, each throughout 10 repeated tests. (b) The linear-speed was fixed at 6 cm/s, whilst the distance changed at 5, 10 and 15 cm, each throughout 10 repeated tests.

lection of sampling distance between each combination of ON/OFF motion detectors and the number of directional connections for each local cell in the dual-pathways. As mentioned above, such a structure improves the speed tuning of the HR-based translating sensitive models. Its functionality nevertheless is restricted by the predefined parameters corresponding to the design of ensembles of motion detectors (Fig. 4.3). More precisely, based on the parameters setting in this kind of experiments, increasing either the sampling distance between each pairwise ON/OFF correlators or the number of connected local detectors could further improve the speed response, i.e. the DSNs spike at higher frequency tested by translations faster than the 6cm/s. However, this would be more computationally costly.

Second, we examined the influence of translating distance on the spiking rate. Intuitively, the results in Fig. 4.17b illustrate the spiking rate shrinks dramatically as the distance between the moving and the monitoring robots increases. The peak and valley of firing rate occurs at the smallest and largest distances. Since the fly DSNs are well-known to be wide-field motion detectors [193, 189], it is conceivable that the fly DSNs are not able to smoothly recognise the translating objects with a very small size, a situation of which is similar to our tests. As mentioned in Chapter 2, there is another group of visual neurons in the fly visual system that are specialised in the detection of small targets movements, e.g. [43, 95, 103].

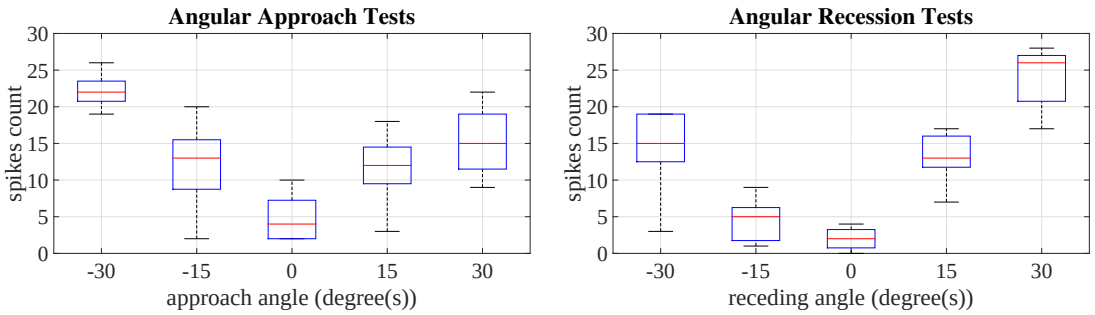

(a) (b)

Figure 4.18: Statistical results of systematic angular-approach (a) and angular-recession (b) tests: each kind of tests involved movements from five angles, respectively, each throughout 10 repeated tests.

Angular approach and recession tests In the third round of systematic robot experiments, the *Colias* equipped with the DSNN was tested by angular approaching and receding stimuli, as shown in Fig. 4.15b and 4.15c. We aim to compare its performance with similar experiments in Chapter 3 to the looming sensitive neuron models. Fig. 4.18 illustrates the statistical results of the spike frequency throughout repeated tests. To be more specific, the embedded DSNN spikes at the lowest rates tested by the direct approaching and receding stimuli from the angle of $0°$. On the other hand, it is rigorously activated by the angular approaching and receding movements from other angles - the spike frequency gets higher if the angle of proximity and recession increases. As a matter of fact, for the stimulated *Colias*, the angular approach from left-side (angles $-30°$ and $-15°$) and the right-side (angles $15°$ and $30°$) will give rise to rightward and leftward translating features, respectively. The opposite situations happen to the angular recession. Interestingly, since a partially balanced structure has been put forth in the dual-pathways, this makes the neural network to respond more strongly to motion along the PD versus ND. The statistical results indicate higher firing rate for the angular approach and recession from the left and right sides of visual field of the tested *Colias*, respectively. Such an investigation on *Colias* has verified that the proposed DSNN on embedded system also possesses similar characteristics and functionality to the fly DSNs; the sensitivity has been well tuned to translating motion cues over other kinds of movements.

Interestingly, we have shown similar experiments in Chapter 3 to test the looming sensitive neuronal models, e.g. Fig. 3.13 and 3.37. The results presented in Fig. 4.18

demonstrate an opposite but complementary performance of the proposed DSNN to the LGMDs models; the latter spikes at the highest rate by the direct approaching. Therefore, we concern the possible cooperation of looming and translating neuron models. This may benefit the creation of more competitive dynamic vision systems to deal with more abundant motion features.

4.2.3 Summary

Within this section, this dissertation has proposed a directionally selective neural network, for the purpose of demonstrating our understanding of computational roles of fly ON and OFF pathways and LPTCs sensing translating stimuli. The fly DSNs are with unique sensitivity and direction selectivity to wide-field translational motion. Compared with the former bio-inspired translational motion detectors, like an EMDs-based model, the proposed framework splits motion information into ON and OFF visual pathways for parallel computation, encoding light-on and light-off responses, separately. This neural network finally integrates local excitations from four groups of LPTCs, each possessing certain DS to form the two systems of the HSS and VSS. The proposed computational architecture matches well the underlying drosophila physiology on motion detection.

Through this modelling study, we have emphasised the effectiveness of low-level spatiotemporal computations for improving the speed response in translating sensitive neural systems, via the design of ensembles of same-sign (ON-ON and OFF-OFF) motion detectors within the dual-pathways. We have demonstrated also the importance of a temporal FDSR mechanism with biological plausibility, which contributes to filter out irrelevant motion from a visually cluttered and dynamic background, to a great extent. The characteristics and functionality of fly DSNs have been achieved by this computational model and validated by the systematic and comparative experiments, ranging from off-line tests with synthetic and real-world scenarios to on-line robot tests. Specifically, the preliminary robot tests have demonstrated its computational efficacy and simplicity on the embedded system costing few computational resources for real-time image processing via a regular monocular camera. This hits at great po-

tential of building neuromorphic sensors for artificial machines for directional motion perception in a both flexible and efficient mode.

This work opens several directions for future research. First, the above experiments evidence that the functionality of the proposed DSNN can provide a perfect complement to the former collision-detecting neural networks like the proposed LGMDs in Chapter 3, with a similar structure of the parallel ON and OFF pathways. Therefore, it is possible to construct a hybrid visual model integrating the functionality of direction and collision sensitive neural networks, both inspired by insects physiology, for the extraction of diverse motion features. Moreover, its computational simplicity and flexibility, as an embedded vision system validated by the real-time robot experiments, also allow us to extend the proposed DSNN to higher behavioural levels, e.g. simulating fly motion tracking and fixation behaviours that will probably be useful in some vision-based swarm robotic scenarios.

4.3 Mimicking Fly Fast Motion Tracking and Fixation

Within this section, this dissertation continues to propose a hybrid neural network that is an extension of the proposed DSNN in Section 4.2 for mimicking fly motion tracking and fixation behaviours.

Computer vision techniques for motion tracking From traditional computer vision techniques to computational biology, motion tracking strategies can vary from high-level learning based or prediction schemes to low-level image processing methods. There have been many high-level methodologies showing good performance on motion detection and tracking, e.g. [254, 255]. Very recently, an approach was proposed to learn real-time tracking, which could reach 100 fps, with deep regression networks [256]. A new object-detection based fast tracking algorithm was presented in [257]. Using the statistical methods of hidden Markov models, the object motion tracking could be achieved in extremely crowded scenes [258]. In addition, a monocular vision based solution was implemented to estimate multi-body motion and successfully tested from vehicle-mounted cameras [65]. Moreover, the development of visual sensors

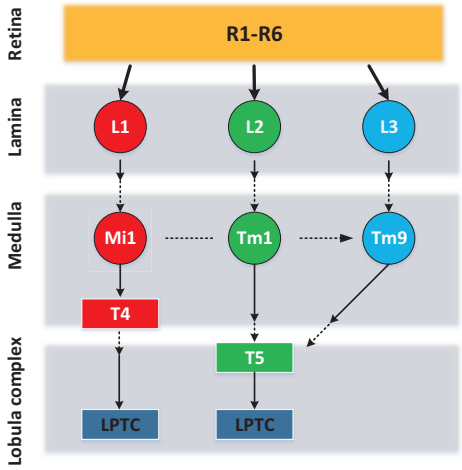

Figure 4.19: Schematic of fly preliminary visual circuit including motion and position pathways and neurons with signal processing throughout four neuropile layers, similarly to Fig. 4.1.

with more abundant features added in, e.g. the event-driven cameras [70, 69], RGB-D cameras [73] and etc. all can facilitate visual motion tracking.

However, balancing the performance and the efficiency still poses a big challenge towards building artificial motion tracking systems until today. An efficient and reliable dynamic vision system becomes more desirable for artificial machines, like autonomous robots and future robots. These state-of-the-art methods can achieve satisfactory performance on motion tracking. They nevertheless are either computationally costly, or heavily restricted to specialised hardware, like the DVS and etc. On the basis of existing challenges and problems on motion tracking, as introduced in Section 4.1, we can also take inspiration from the biological visual systems.

Fly motion tracking pathways Different visual features of a moving object, such as the position and the direction, are crucial to elicit two well-studied behaviours for animals, i.e., the optomotor and the fixation [32]. Motion tracking is vital for animals to possess the ability to extract useful motion cues from visual clutter timely, then evoke advisable behaviours, like the turning response, for maintaining moving targets within their receptive fields. The visual fixation response was first observed in flies which is one of the most important follow-up behaviours after the motion detection [32]. More precisely, when an object of interest appears in the view, a fly tends to keep it near the centre of frontal field of view, no matter the direction in which the object or

the background is moving.

A remarkable biological research has demonstrated recently that in the fly physiology, the tracking and fixation behaviours are mediated by parallel visual pathways, that is, the motion (or called motion-detecting) and the position (or position-locating) pathways [32, 189, 98]. In addition, these researches also signify that the fixation behaviour could be tuned by only the position pathway, whilst the motion pathway likely corresponds to the optomotor response. It nevertheless appears that both pathways give rise to collaborative effects on shaping the fixation behaviour to a translating object.

A diagram of signal tuning map in the fly preliminary visual system is represented in Fig. 4.19. This is as biological inspiration to the proposed motion tracking system based on the proposed DSNN in Section 4.2. In general, the motivated framework involves three visual pathways, which are computationally conducted as the motion and the position pathways. The ON (L1) and OFF (L2) pathways make up the motion-detecting pathway. A class of neurons (L3) with wide-field properties constitute the position pathway providing location instead of direction information, as shown in Fig. 4.19. This hybrid neural network possesses a simple feedback control towards fixation parameters (Fig. 4.20). Importantly, there are interactions of local motion information between the two pathways underlying the OFF-motion sensitivity across a wide visual field in the fly compound eyes [96, 98, 189].

In the following subsections, the neural network architecture with algorithms and parameters setting will be presented in Section 4.3.1. Followed by are the off-line experiments with results and analysis in Section 4.3.2. Finally a brief conclusion of this section is given in Section 4.3.3.

4.3.1 Modelling of Motion and Position Pathways

In this subsection, the dissertation will present the hybrid visual neural network with the motion and the position pathways as depicted in Fig. 4.20 and 4.21. It is necessary to clarify that the visual processing of the motion-detecting pathway for the most part conforms to the proposed DSNN in Section 4.2. Accordingly, we illustrate merely partial algorithms in the motion pathway with a brief presentation. In this neural

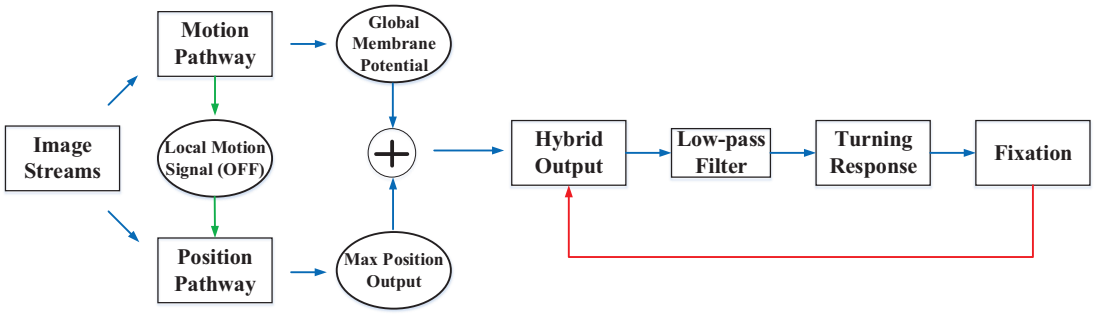

Figure 4.20: Signal processing pipelines in the proposed hybrid visual neural network: blue arrows specify the feed-forward processing flowchart toward the fixation response. Green arrows indicate the local interactions between the motion and the position pathways. A red arrow designates a linear feedback control. This is adapted from [52] (Fu and Yue, 2017).

network, we highlight the functionality of newly built position pathway and the hybrid neural network design for shaping the fixating response. In addition, it is also worth emphasising that contrary to the traditional tracking strategies like the regression based and search/segmentation based models, this biologically motivated neural network is guided by low-level visual processing reacting to wide-field translating objects with OFF-edges enhancement.

4.3.1.1 The Motion Pathway

The Retina layer In the modelling of motion pathway, the first Retina layer involves photoreceptors arranged in a 2D matrix form, the number of which corresponds to the resolution of input visual streams. Each photoreceptor captures grey-scale luminance then relays it to a simplified high-pass filter in order to get the luminance change between successive frames without visual residual compared with the DSNN in Section 4.2:

$$P(x, y, t) = L(x, y, t) - L(x, y, t - 1). \tag{4.17}$$

After that, for each local pixel, we also apply a band-pass filter in spatial for mimicking the centre-surrounding antagonism found in insects' visual system, which is consistent with the DoGs as introduced in the Eq. 4.2 in Section 4.2.1. This enhances the motion edge selectivity as suggested in a few modelling of fly motion detectors, e.g. [54, 40]; it also removes redundant environmental noise in spatial so that maximising relayed visual information transmission to the following layers [53].

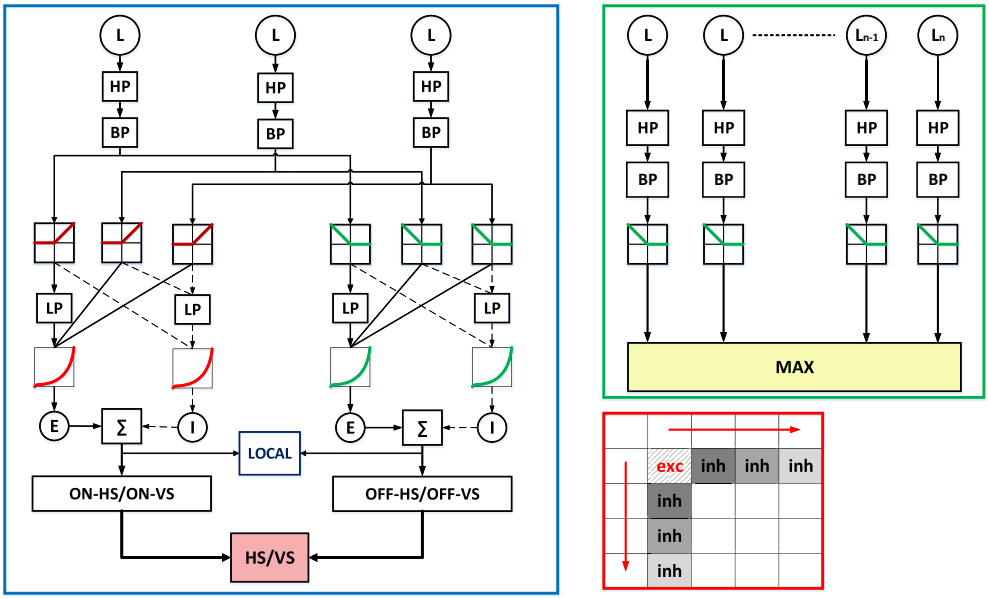

Figure 4.21: Illustration of the proposed motion (in the blue box) and the position (in the green box) pathways: a connection of three cells are shown for instance in the motion pathway with more details in Fig. 4.3 and Section 4.2. The red box depicts the lateral multi-connections of ON-ON and OFF-OFF motion detectors along two directions with distinct grey-scales indicate dynamic time delays, and generation of excitation and inhibition.

The Lamina layer In the second Lamina layer, the first-order inter-neurons of ON and OFF transient cells encode onset and offset responses by luminance increments and decrements, split visual information into separate ON and OFF pathways. Each photoreceptor corresponds to a pairwise ON and OFF cells. The computational roles of ON and OFF mechanisms conform to the Eq. 4.4 in Section 4.2.1. In addition, differently from the proposed DSNN in Section 4.2, a 'Lipetz' function with an exponent μ is applied to transform luminance analogue value of ON and OFF units to membrane potential in a roughly logarithmic manner:

$$LA(x, y, t) = \frac{X(t)^{\mu}}{X(t)^{\mu} + X'(t)^{\mu}}, \tag{4.18}$$

where we let the intensity of ON and OFF cells be expressed by X. And the X' satisfies a mid-level parameter set as a first-order low-pass filtered version of X with a time constant τ_1:

$$\frac{dX'(t)}{dt} = \frac{1}{\tau_1}(X(t) - X'(t)). \tag{4.19}$$

The Medulla and Lobula layers In the Medulla layer, the polarity signals in either ON or OFF pathways form two kinds of flows – the excitation and the inhibition. As depicted in Fig. 4.21, the computational role of each combination of same-sign (ON-ON and OFF-OFF) cells fits a pairwise and symmetric HR detectors. We build temporal dynamics within the dual-pathways, i.e., the delay represented by the first-order low-pass filtering depends on the sampling distance between each combination of local motion detectors. More specifically, we put forth the longest time span in the combination at the shortest sampling distance, and then gradually reduce it as the sd growing along both directional multi-connections. Taken one cell from the HSS in the ON pathway as an instance, the computation is as follows:

$$ME_{HS}(x,y,t) = \sum_{i=d}^{d\cdot N_{con}} (D(x,y,t)\cdot LA(x+i,y,t) - W_i \cdot D(x+i,y,t)\cdot LA(x,y,t))$$
$$\text{where, } d/dt\{D(x,y,t)\} = 1/\tau_s(LA(x,y,t) - D(x,y,t)), \tag{4.20}$$

where N_{con} denotes the number of connected polarity cells, d is the increasing step in sampling distance. τ_s indicates the dynamic time constant in milliseconds. W_i is a local bias to form a partially balanced model with stronger response to the PD over ND motion. The computations for the OFF pathway and the VSS of either ON/OFF channels obey the same rules which are not restated here.

There are also local motion detectors (LOCAL in Fig. 4.21) combining local excitations from ON and OFF channels in a supra-linear manner. That is,

$$LM(x,y,t) = \theta_1 \cdot ME(x,y,t) + \theta_2 \cdot LO(x,y,t) + \theta_3 \cdot ME(x,y,t) \cdot LO(x,y,t), \tag{4.21}$$

where $\{\theta_1, \theta_2, \theta_3\}$ is a combination of term coefficients and $\in [0, 10]$. ME and LO denote the local Medulla and Lobula cells in either the HSS or the VSS.

Very importantly, in the proposed hybrid neural network, they are additional inputs to the position pathway from the motion pathway, as shown in Fig. 4.19 and 4.20.

The Lobula Plate layer In the final layer of motion pathway, four groups of LPTCs linearly integrate all the directionally specific excitations of both ON and OFF path-

ways constituting the global membrane potential, then exponentially transfer them as the HSS and VSS outputs toward the hybrid pathway. The neural computation conforms to the Eq. 4.13 in Section 4.2.1. Positive outputs of the motion pathway will be generated by the PD (front-to-back and downward) translational motion, while negative outputs via the ND (back-to-front and upward) translational motion.

4.3.1.2 The Position Pathway

As illustrated in Fig 4.20 and 4.21, in parallel to the motion-detecting pathway, the first layer of the position pathway shares the same input of visual streams, encoded by a 2D array of photoreceptors as well. We also employ a high-pass filtering process expressed as:

$$\begin{aligned} &P^{'}(x,y,t) = \sigma_{hp} \cdot (P^{'}(x,y,t-1) + L(x,y,t) - L(x,y,t-1)), \\ &\text{where, } \sigma_{hp} = \tau_1/(\tau_1 + \tau_i), \end{aligned} \tag{4.22}$$

where τ_1 denotes a time constant in milliseconds and τ_i indicates the time interval between successive frames. After that, the filtered signals also go through spatial band-pass filtering represented by the DoGs algorithm, as well as the 'half-wave' rectifying, pertaining to the OFF-motion edges selectivity along with filtering out entire onset responses. Importantly, this provides the local offset response matrix to a following maximisation function (MAX in Fig. 4.21) indicating the location of maximum response in the motion pathway. Accordingly, the interaction between the two pathways is expressed as follows:

$$\begin{aligned} &LM(\hat{x},\hat{y},t) = max_{(x,y)\in\Omega(max_x,max_y)} \, ||\bar{LM}(x,y,t)||_2, \\ &\text{where, } \bar{LM}(x,y,t) = LM_{HS}(x,y,t)^2 + LM_{VS}(x,y,t)^2. \end{aligned} \tag{4.23}$$

Therefore, the output is the maximum local motion signal with position information $(\hat{x},\hat{y})$ in a neighbouring field $\Omega(max_x, max_y)$ centred by (max_x, max_y) of the maximum offset response elicited by the position pathway, and the radius of the field corresponds to the maximum sampling distance $(d \cdot N_{con})$ in the motion pathway. It is important to state that in the experiments, we only demonstrate the effect of motion

tracking along horizontal direction using $\hat{x}$ to activate the position pathway output via an exponential transformation as follows:

$$PP_{HS}(t) = \begin{cases} 1/e^{-((\hat{x}(t)-x_{vc}(t))/(C/4))^2} - 1, \text{ if } \hat{x}(t) - x_{vc}(t) \geq 0 \\ 1 - 1/e^{-((\hat{x}(t)-x_{vc}(t))/(C/4))^2}, \text{ otherwise} \end{cases}, \tag{4.24}$$

where x_{vc} is the horizontal location of image view centre (VC), and C is the number of columns in the visual field.

4.3.1.3 The Hybrid Pathway

In the hybrid pathway, as illustrated in Fig. 4.20, the outputs from both the motion (MP in this case) and the position (PP) pathways at a specific moment are integrated to form the hybrid turning response (TR) in a purely linear manner:

$$\begin{aligned} &TR(t) = \sigma_m \cdot MP_{HS}(t) + \sigma_p \cdot PP_{HS}(t), \\ &\text{and,} \quad \frac{d\{TR^{'}(t)\}}{dt} = \frac{1}{\tau_2}(TR(t) - TR^{'}(t)), \end{aligned} \tag{4.25}$$

where σ_m and σ_p are two gain factors. The output of hybrid pathway - the TR is also delayed by a low-pass filtering with a time constant τ_2 in milliseconds. Taken this response of behavioural level, we can simulate updating of the fly VC via:

$$x^{vc}(t) = x^{vc}(t) + TR^{'}(t). \tag{4.26}$$

Therefore, we demonstrate that a successful visual fixation behaviour should satisfy the following condition:

$$\lim_{t \to t_0} ||\hat{x}(t) - x^{vc}(t)|| \leq \gamma, \tag{4.27}$$

where γ is a predefined threshold which is normally set equally as the sampling distance in the motion-detecting pathway in this case. As shown in Fig. 4.20, we also design a simple feedback pathway for the purpose of adjusting the gain factor (σ_p) for the position pathway meeting the requirement of a successful fixation behaviour as

Table 4.2: Parameters Setting for the Proposed Motion Tracking System

Name	Value	Name	Value	Name	Value
N_{con}	8	d	2	W_i	0.89
σ_c	10	τ_s	$5 \sim 200$	C	adaptable
γ	N_{con}	σ_m	3	σ_p	10
τ_1	20	τ_2	10	τ_i	adaptable

required in the Eq. 4.27, more quickly. That is,

$$\sigma_p = \sigma_p + \sigma_c,\ if\ |\hat{x}(t) - x^{vc}(t)| > \gamma\ \&\ \frac{d\{|\hat{x}(t) - x^{vc}(t)|\}}{dt} \geq 0. \tag{4.28}$$

4.3.1.4 Parameters Setting

The chosen parameters in Table 4.2 were decided empirically based on consideration of the optimisation of functionality and implementation of the proposed framework for fast and precise motion tracking in off-line experiments with recorded videos as input visual stimuli. This has a feed-forward low-level visual processing structure without any complex parameters training methods. The adaptable parameters correspond to the resolution and the sampling frequency of input visual streams. More detailed parameters set-up of the motion pathway is suggested in Section 4.2.1 and a partial related modelling research [53]. Importantly, a shortcoming of the proposed visual tracking model is that the combination of gain factors in the hybrid pathway will influence its fixating performance: increasing the gain factors, especially in the position pathway, could accelerate the process to fit the requirement of a successful fixation. However, as the neural network is also sensitive to the velocity of translational motion, fluctuations of the relative position (RP) between the moving objects and the VC likely appear during fixating. Therefore, the learning methods are demanded in the near-future research for more robust parameters adjusting to adapt to more abundant visual challenges. We hope the follow-up experiments will provide useful conclusions or suggestions for designing artificial motion tracking system, and exploring the potential of biologically inspired neural networks in building dynamic vision systems.

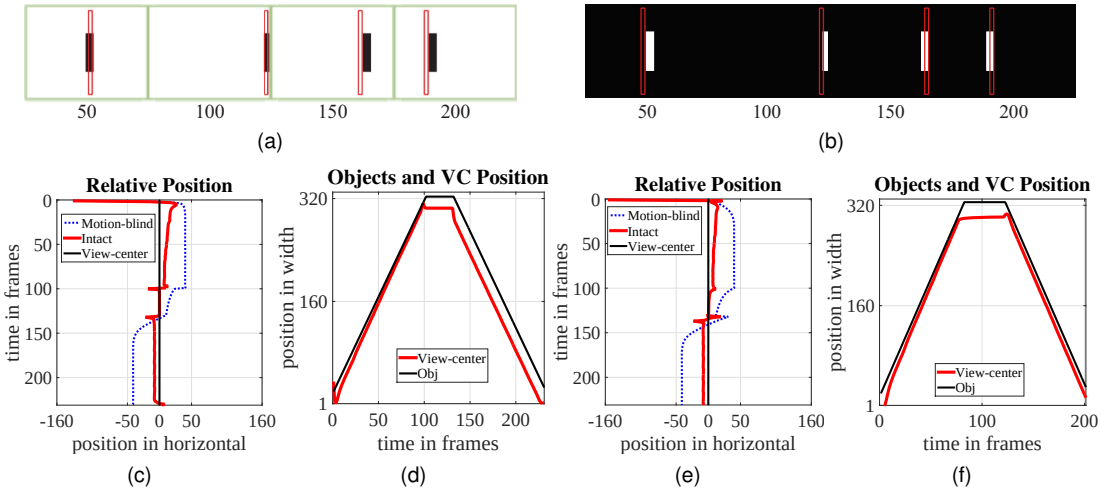

Figure 4.22: Fixation results represented by horizontal positions of the simulated VC and the translating object: (a)(c)(d) a darker object translating, (b)(e)(f) a lighter object translating: both the motion-blocked and the intact-pathways models are tested. Snapshots of input stimuli are shown at the top with frame numbers. These are adapted from [52] (Fu and Yue, 2017).

4.3.2 Experimental Evaluation

In this subsection, we will present the off-line experiments. These can be categorised into two kinds of tests, i.e. the synthetic stimuli tests and the real physical scene tests. All the input stimuli were converted to the grey-scale with resolution of 320×240 and 432×240 for synthetic and real-world visual streams, respectively. We show experiments results via the outputs of RP and simulated fly VC, during each tracking and fixating process. We also investigate and compare the different fixation responses between neural networks with the motion-blocked system and the intact-pathways system in the synthetic tests motivated by the investigation in a biological study [32], to inspect whether the proposed visual tracking model fulfils biological results.

4.3.2.1 Synthetic Visual Stimuli Tests

In the first kind of tests, we tested the proposed model against synthetic translational movements on both horizontal directions. The visual stimuli include a single darker or lighter object translating and elongating-shortening against a clean background. We also examine the fixating response by two different grey-scale objects translating, concurrently at the same or different constant speeds. There is not any background noise in these simulated scenarios.

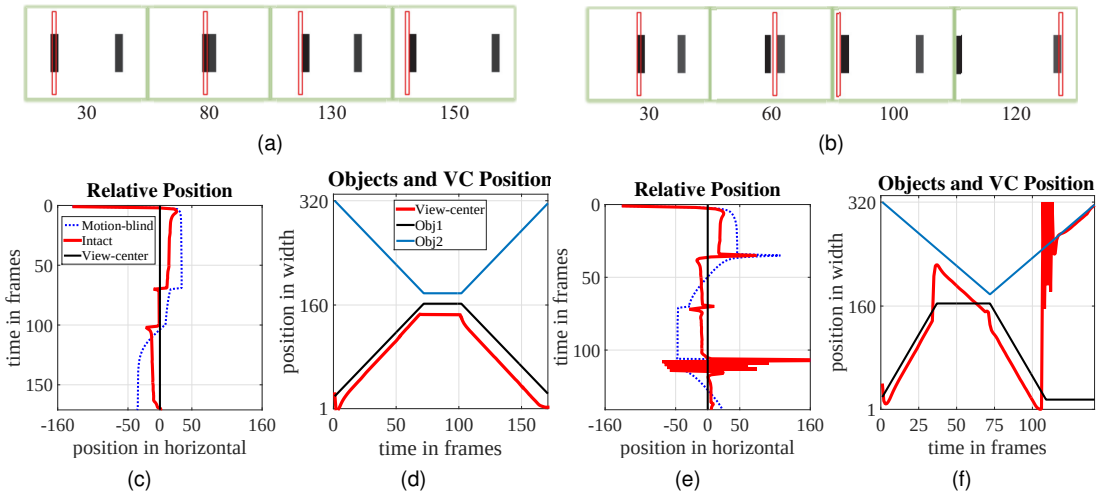

Figure 4.23: Fixation results represented by horizontal positions of the simulated VC and the translating objects: (a)(c)(d) two darker objects translating at a same speed, (b)(e)(f) two darker objects translating at distinct speeds, adapted from [52] (Fu and Yue, 2017).

The results illustrated in Fig. 4.22 and 4.23 allow the following conclusions to be drawn: first, when tested by either darker or lighter objects translating in both horizontal directions, the tracking and fixation behaviours elicited by both neural networks with the motion pathway blocked and the intact pathways are well achieved. During each tracking process, the RP quickly converges within a small range, that is, the simulated VC is dramatically conducted to reach around the exact position of translating object corresponding to a successful fixation behaviour. In addition, it appears that the visual model with complete pathways achieves more precise tracking performance with smaller RP.

Interestingly, when challenged by two dark objects translating simultaneously at an identical speed-level, the updated VC of fixation behaviour is always following the comparatively darker object movements. The results reveal the contrast sensitivity of the proposed framework with the preference to stronger offset response caused by OFF-edges translating. In addition, when the translating objects have different speeds in the visual field, the VC of fixation behaviour initially accompanies the darker object moving and then quickly jumps to another, once the darker object stops moving. Importantly, the results also provide a profound implication that the motion-detecting pathway is essential to the proposed hybrid visual neural network to elicit the fixation behaviour. This is only sensitive to motion features.

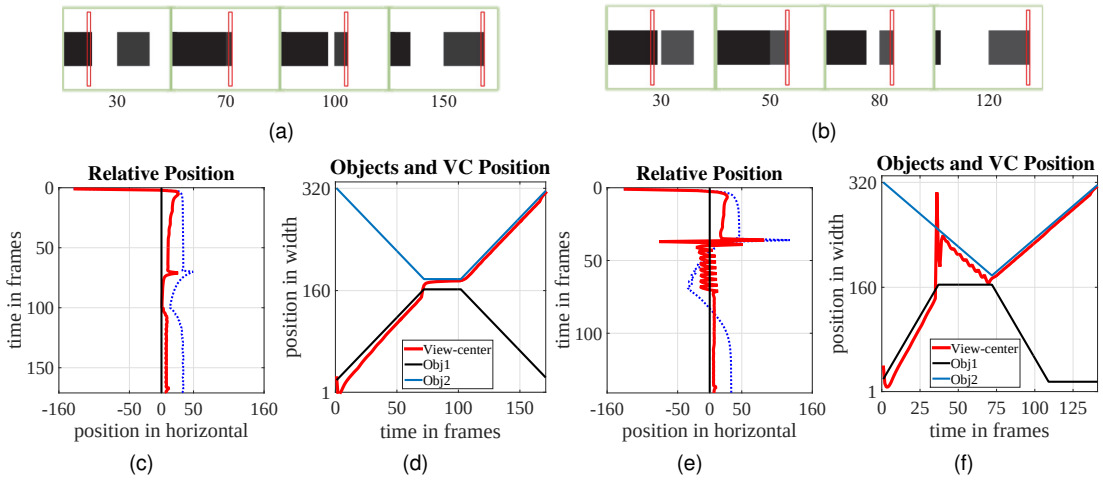

Figure 4.24: Fixation results represented by horizontal positions of the simulated VC and the elongating-shortening objects: (a)(c)(d) two darker objects elongating and shortening at a same speed, (b)(e)(f) two darker objects elongating and shortening at distinct speeds, adapted from [52] (Fu and Yue, 2017).

With similar ideas, we examined its performance against two dark objects elongating and shortening with only a single edge moving (Fig. 4.24). The visual fixating response is well realised as expected. However, the results point out the specific selectivity to the offset response. The simulated VC is always following the OFF-edge elongating (offset) rather than shortening (onset). Furthermore, the statistics shown in Fig. 4.25 demonstrates that the motion-blocked system represents similar turning response compared to that elicited by the intact-pathways system during motion tracking; blocking the motion pathway nevertheless leads to larger relative positions at all tested translating velocities, i.e, the tracking precision is much weakened.

4.3.2.2 Real-world Visual Stimuli Tests

In the second kind of off-line tests, we inspected the performance of proposed visual neural network using recorded real-world visual streams with visual clutter as input stimuli, as illustrated in Fig. 4.26. Compared to the synthetic tests, the visual stimuli are 'real' with environment noise. In this case, the proposed model will perform more practically. The translating stimuli involve a person crossing the visual field and the translations of five different grey-scale objects, all embedded in a busy background. Satisfactory results in Fig. 4.26 demonstrate the proposed visual model successfully mimics the fly motion tracking and fixation behaviours regardless of the

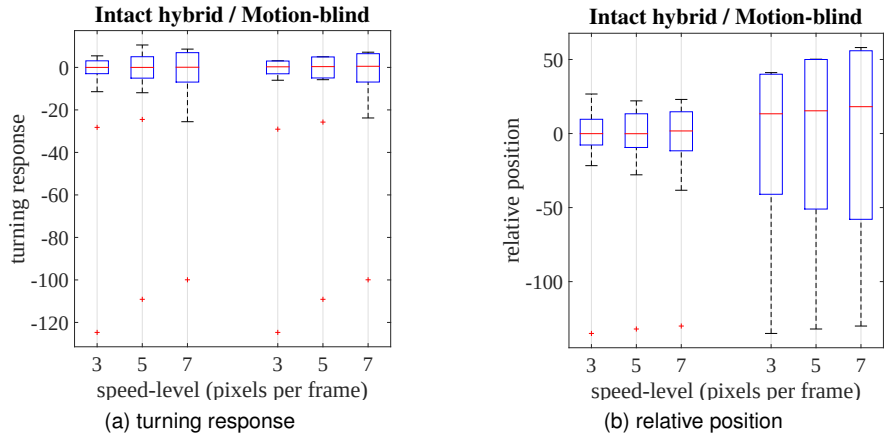

Figure 4.25: Statistical results of the (a) TR and the (b) RP during each entire tracking course for both the intact-pathways and motion-blocked neural networks, tested by a single darker object translating at three constant velocity levels, adapted from [52] (Fu and Yue, 2017).

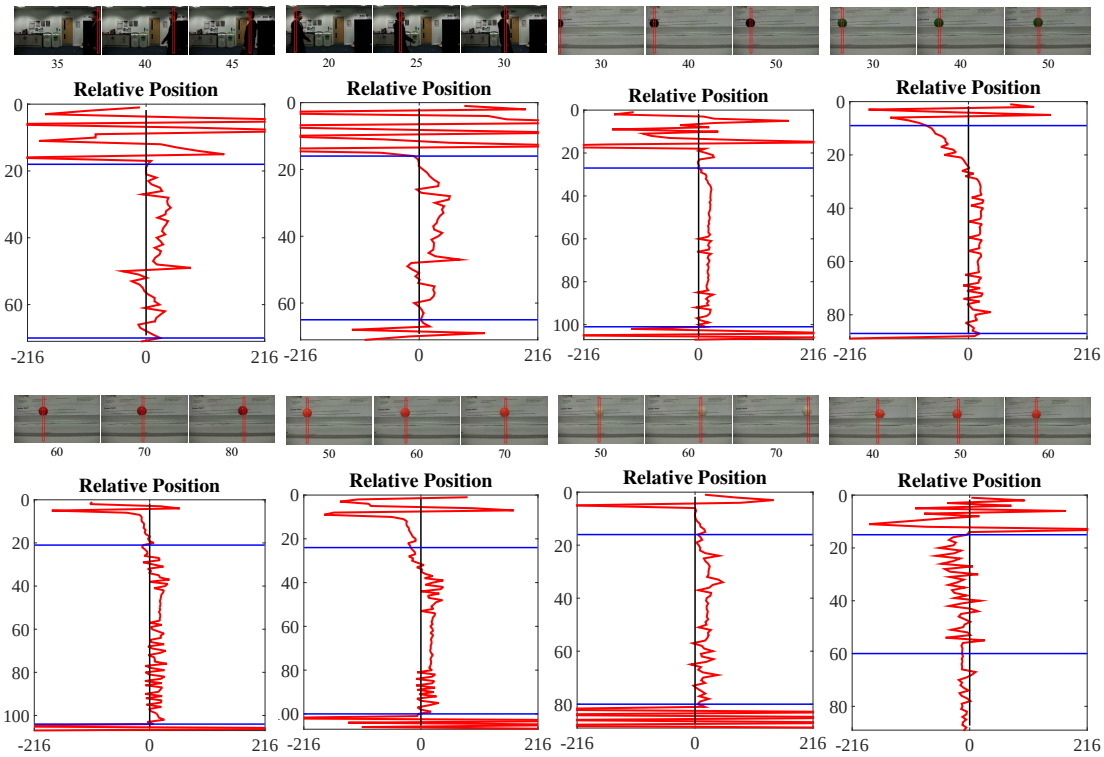

Figure 4.26: Fixation results of proposed hybrid neural network with intact pathways tested by real-world translating stimuli: eight sets of recorded videos are as inputs. Snapshots with labelled frames and calculated updating VC are shown at the top of each result. Two horizontal blue lines specify the time window between the target appearing and leaving the field of view. X-axis denotes the horizontal RP, and Y-axis designates the time sequence. These are adapted from [52] (Fu and Yue, 2017).

background complexity. It appears that without translational motion within the visual sensing field, the simulated VC is significantly affected by the background noise that wanders intensely within the visual field. However, if the translating objects ap-

pear, the motion-detecting pathway in the proposed model can well guide the motion tracking and fixation behaviours.

4.3.3 Summary

In this section, this dissertation has presented the computational modelling of a hybrid visual neural network for mimicking fly fast motion tracking and fixation behaviour, inspired by physiological and ethological research in fly preliminary visual system and corresponding fixating responses to translating bars. The motivated framework extends the DSNN in Section 4.2 to the higher level of behaviour. Two explored visual pathways are computationally modelled to cooperate in the mediation of fixating response. More precisely, the visual fixation behaviour is shaped by a hybrid pathway with turning response as the model output. Informative off-line tests results demonstrate that the proposed neural network is feasible to conduct fast motion tracking and fixation behaviours similarly to flies. Moreover, this hybrid visual neural network can cope with motion tracking in a fast and reliable manner against busy backgrounds. Importantly, the results match well a profound biological implication that the position pathway contributes more significantly in mediating the visual fixation whilst the motion pathway improves the precision and efficiency of tracking, effectively.

4.4 An Embedded Motion Tracking Vision System

In this section, this thesis goes on presenting realisation of the proposed fly motion tracking and fixation model on the embedded system in the *Colias* robot based on research presented in Section 4.2 and Section 4.3.

In the last section, the motion tracking system has been tested by off-line experiments involving synthetic and real-world visual stimuli. The ability to conduct fixation behaviour has been validated by these experiments. The potential of building low-energy neuromorphic sensor has also been demonstrated. Therefore in this section, we investigate the applications in the proposed *Colias* robot. Similarly to the hybrid neural network in Section 4.3, this dynamic vision system consists of two sub-systems that

cooperate effectively for robot motion control in a hybrid pathway. Compared with the presented neural networks in the former two sections, this embedded vision system has simplified structure with bio-inspired algorithms to fit the limited computational resources of the micro-robot for real-time on-board image processing.

In the following subsections, the model will be presented in Section 4.4.1. After that, the systematic bio-robotic experiments are exhibited in Section 4.4.2. Finally, conclusions and future work will be given in Section 4.4.3.

4.4.1 The Embedded Vision System

In this subsection, we present algorithms of the bio-inspired dynamic vision system motivated by the fly physiology, as shown in Fig. 4.19. Generally speaking, we highlight the collaboration of three separate visual pathways conducting motion tracking and fixation behaviours: the ON and OFF visual pathways constitute the motion-detecting system, which encode brightness increments and decrements in parallel channels and generate global motion direction with intensity; a third position pathway, with feedback OFF-edges motion information from the ON/OFF local motion detectors, is only sensitive to locational information of dark moving objects. A schematic diagram of the proposed embedded vision system is depicted in Fig. 4.27. The suggested parameters set-up is given in Table 4.3.

4.4.1.1 The Motion Sensing Subsystem

The proposed framework is a dynamic motion perception system. The main task for the motion-sensing system is the detection of translational movements embedded in either simple or visually cluttered backgrounds. As depicted in Fig. 4.27, the first computational layer consists of photoreceptors, arranged in a 2-D matrix, capturing grey-scale images and relaying pixel-wise luminance to a temporal high-pass filter. That is totally consistent with the Eq. 4.1 in Section 4.2.

After that, there is a spatial band-pass filter for each local pixel to achieve the edge selectivity and remove redundant environmental noise. Similarly to the Eq 4.2, it is represented by an algorithm of DoGs with two Gauss kernels. Importantly, in this bio-

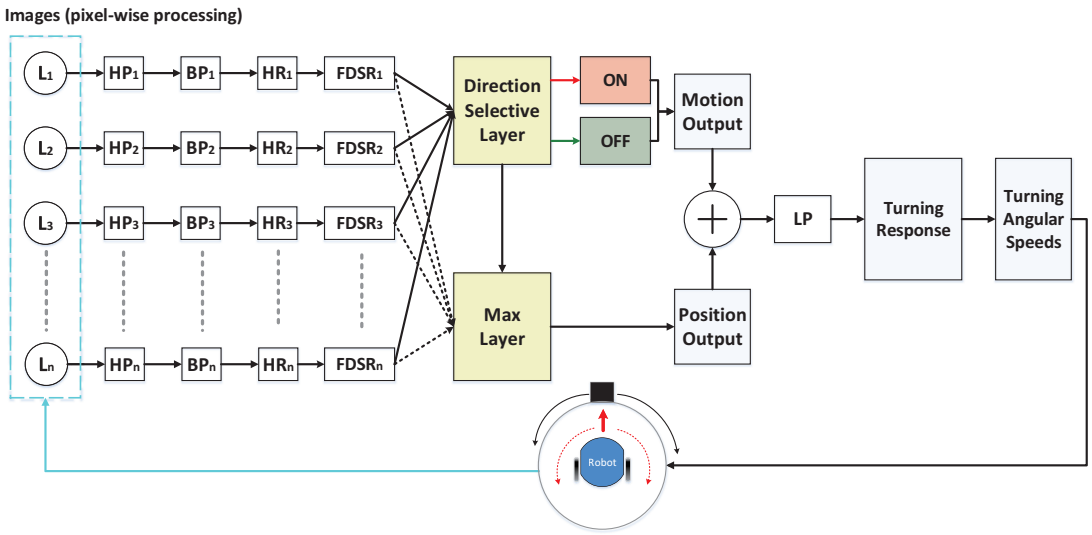

Figure 4.27: The proposed embedded vision system consists of the motion (ON/OFF) and the position pathways for fast motion tracking and fixation behaviours with micro-robots. The outputs of two partial vision systems are linearly combined to mediate the robot turning response for fixating a translating object in real time.

robotic study, we apply linearly distributed weightings in the two kernels so as to save computational power in case of limited resources. The excitatory kernel W_e is thus denoted by the following matrix:

$$W_e = \begin{bmatrix} 1/16 & 1/8 & 1/16 \\ 1/8 & 1/4 & 1/8 \\ 1/16 & 1/8 & 1/16 \end{bmatrix}. \tag{4.29}$$

The inhibitory kernel W_i is larger than W_e:

$$W_i = \begin{bmatrix} 1/128 & 1/64 & 1/32 & 1/64 & 1/128 \\ 1/64 & 1/32 & 1/16 & 1/32 & 1/64 \\ 1/32 & 1/16 & 1/8 & 1/16 & 1/32 \\ 1/64 & 1/32 & 1/16 & 1/32 & 1/64 \\ 1/128 & 1/64 & 1/32 & 1/64 & 1/128 \end{bmatrix}. \tag{4.30}$$

After that, the inhibition is subtracted from the excitation with the polarity selectivity like the Eq. 4.4. Followed by are the ON and OFF polarity cells encoding onset and offset responses, respectively, which can also be represented by the half-wave rectifier corresponding to the Eq. 4.5.

In line with the proposed DSNN in Section 4.2, this bio-robotic approach applies a bio-plausible mechanism – the FDSR achieving an 'adaptation state' with a fast onset and slow decay characteristic. Technically speaking, the previous step of band-pass filtering can remove environmental motion noise in space, and such a mechanism significantly reduces noise in time. The calculations conform to the Eq. 4.6 and the Eq. 4.7. After that, in either the ON or the OFF pathways within the motion-sensing subsystem, the filtered and neighbouring signals within the 'Direction Selective Layer' in Fig.4.27 correlate with each other generating the direction selectivity for each local cell. Generally speaking, we highlight a computational role that represents ensembles of HR detectors yet with dynamic temporal delays between each combination of ON or OFF local motion detectors compared to the EMDs. In this bio-robotic study, as the *Colias* robot can only move on a 2D surface, we calculate the horizontal motion information only. The computations of multiple ON or OFF correlators including temporal latencies comply with the Eq. 4.8 and Eq. 4.9. As a result, the output of the ON/OFF motion-sensing systems is a pooling from all local ON/OFF motion detectors:

$$\begin{aligned} MO_{on}(t) &= \sum_{1}^{C}\sum_{1}^{R} ON(x,y,t), \\ MO_{off}(t) &= \sum_{1}^{C}\sum_{1}^{R} OFF(x,y,t), \end{aligned} \tag{4.31}$$

where C and R are the numbers of columns and rows in the visual field. Both ON and OFF motion outputs are normalised via a sigmoid transformation:

$$f(x) = \mathrm{sgn}(x) \cdot ((1 + e^{-|x|\cdot(C\cdot R\cdot k)^{-1}})^{-1} - \Delta_C), \tag{4.32}$$

where k and Δ_C indicate two coefficients. The output is normalised to $[0, 0.5)$ for the positive input, and $(-0.5, 0]$ for the negative input, by setting Δ_C to 0.5. The global output of motion-sensing system (MO) is an integration of outputs from both ON and OFF motion-detecting pathways which is ranged within $(-1, 1)$:

$$MO(t) = MO_{on}(t) + MO_{off}(t). \tag{4.33}$$

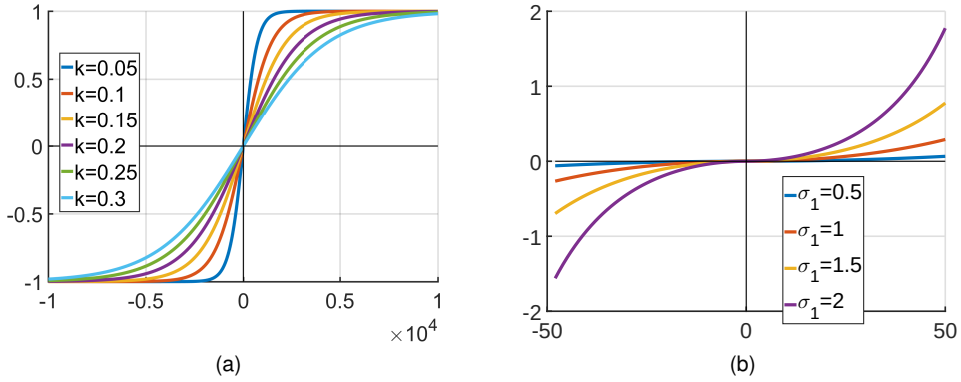

Figure 4.28: The outputs of two activation functions: (a) motion-sensing system outputs with a set of scale parameter k – X-axis denotes input motion potential. (b) Position-locating system outputs with a set of scale parameter σ_1 – X-axis denotes relative position of moving objects to the view centre.

4.4.1.2 The Position Locating Subsystem

Compared to a former modelling study [52], we present a simplified computational structure of the position-locating subsystem. As shown in Fig. 4.27, it shares the same spatiotemporal processes with the motion-sensing system until the filtered visual streams flow into a different 'Max Layer'. A maximisation operation is proposed here to retrieve the horizontal position of maximum offset response from the OFF pathway. Importantly, the DSL of the motion-sensing subsystem provides also the position-locating subsystem with local motion (LM) information to localise a sub-area in the visual field for the maximisation operation:

$$\begin{aligned} &\hat{LM}(\hat{x}, y, t) = MAX_{(x,y)\in\Omega(max_x,y)}\ LM(x, y, t), \\ &\text{where, } LM(x, y, t) = ON(x, y, t) + OFF(x, y, t). \end{aligned} \tag{4.34}$$

Here $\hat{x}$ indicates the abscissa of the location with maximum offset response by the position pathway, in a neighbouring field $\Omega(max_x, y)$ centred by (max_x, y), with the feedback of maximum local motion from the motion-sensing pathway. In addition, the radius of the neighbouring field Ω corresponds to the maximum sd in the motion sensing subsystem like the previous modelling studies. Therefore, the output of the position pathway (PO) is activated by an exponential transformation:

$$PO(t) = \text{sgn}(\hat{x}(t) - x_{vc}) \cdot (1/e^{-(\sigma_1 \cdot (\hat{x}(t) - x_{vc})/C)^2} - 1), \tag{4.35}$$

Table 4.3: Full Parameters Setting for the Embedded Motion Tracking System

Name	Value	Name	Value	Name	Value
N_c	$2 \sim 4$	d	$2 \sim 4$	γ	10
C	99	R	72	N_i	2
τ_1	1ms	τ_2	100ms	k	$0.05 \sim 0.3$
Δ_C	0.5	x^{vc}	$C/2$	σ_1	$0.5 \sim 2$
σ_2	20	σ_3	10	τ_3	10ms
τ_s	$10 \sim 100$ms	g_v	1	g_w	10

where x_{vc} is the horizontal location of VC in the visual field, and σ_1 is a scale parameter.

4.4.1.3 The Hybrid Motion Control System

Finally, we propose a simple motion control strategy for micro-robots in a hybrid system, which integrates the outputs of the two former visual systems in a linear manner, as shown in Fig. 4.27. A turning response (TR) is formed equalling to the Eq. 4.25. Finally in this bio-robotic study, we map the TR to an angular speed of the differentially driven mobile robot agent. Given an initial speed v_i, the motor powers of the right (P_R) and left (P_L) wheels can be described as follows:

$$\begin{aligned} P_R(t) &= g_v \cdot v_i(t) - g_w \cdot TR(t), \\ P_L(t) &= g_v \cdot v_i(t) + g_w \cdot TR(t), \end{aligned} \tag{4.36}$$

where g_v and g_w are gain values that control motion efficiency. According to previous research in Section 4.3.1, a satisfactory robotic fixation-behaviour should meet the following requirement:

$$\lim_{t \to t_0} ||\hat{x}(t) - x_{vc}|| \leq \gamma, \tag{4.37}$$

where γ is a predefined threshold. Importantly, this term sets a criterion for successful fixation responses.

4.4.1.4 Parameters Selection

The proposed model processes visual information with a feed-forward structure and low-level spatiotemporal computations. All the parameters were decided empirically,

with considerations of optimisation and realisation on micro-robots. Table 4.3 lists all the full parameters setting from [194] including the proposed ones in this subsection. The temporal parameters were chosen from related biological models for motion detection [39, 43]. Fig. 4.28 demonstrates the effects of scale parameters (k and σ_1) on the activation functions (Eq. 4.32 and 4.35) of the two sub visual systems, since both parameters contribute effectively to calculate the turning response for the robot. Concretely, the motion system represents positive and negative responses to PD (rightward) and ND (leftward) translational movements, whilst the position system is only sensitive to the relative location of dynamic dark features with respect to the robot view centre.

4.4.2 Experiments and Results

In the bio-robotic tests, we used the proposed *Colias* mini-robots, as illustrated in Fig. 3.5b, in order to demonstrate the model performance, and more important the robot fixation and follow behaviours. Similarly to the previous robot tests with *Colias*, the monocular camera is the only sensor applied in this research. We also used a Bluetooth device, which is connected with the upper vision-board, to retrieve real-time model data from the robot. The frame rate of the embedded vision system is between $25 \sim 45$Hz during the fixation tests, which can be regarded as real-time visual processing.

To clarify our goals and the significance of this bio-robotic approach, there are two kinds of tests to demonstrate. First, in the open-loop tests, we adopted three categories of movements, i.e. proximity, rightward and leftward translations, to stimulate a motion-blind *Colias* robot, aiming at demonstrating the specific response of the two visual systems and the hybrid system in Fig. 4.29. We also investigated both the speed and distance response of the proposed dynamic vision system in Fig. 4.30). Second, in the closed-loop tests, we examined the fixating response of a *Colias* robot to other translating robots in Fig. 4.32). In addition, an important biological finding has demonstrated that the flies' fixation behaviour could be achieved by the position system only, while the motion system can improve the fixating response [32]. For comparison with

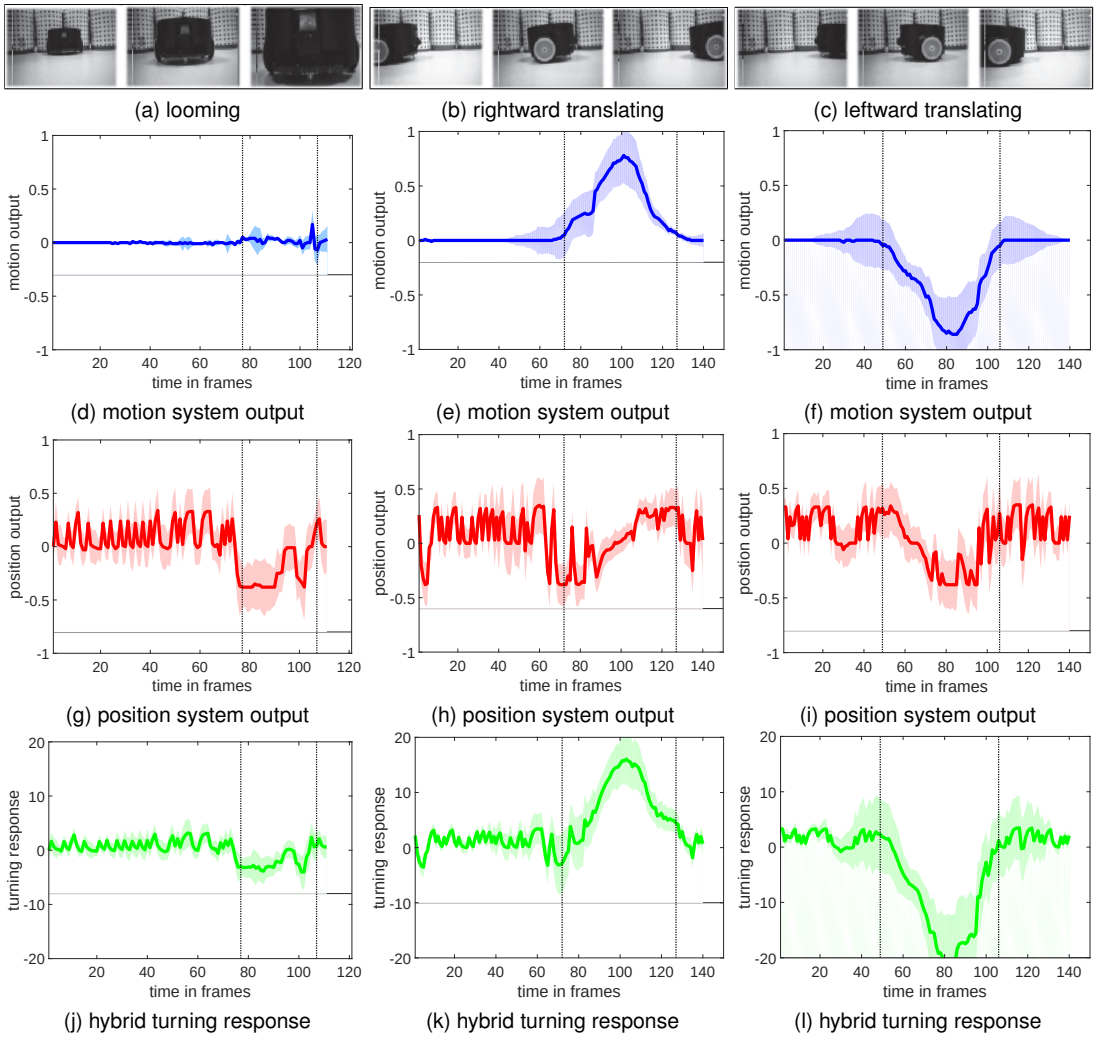

Figure 4.29: Neural response from the tested *Colias* robot under open-loop tests, including the outputs of the motion-sensing, the position-locating and the hybrid systems. The example views from the stimulated robot are shown at each top. Each kind of movements was repeated ten times, with colour-shadows indicating the continuous errors. Two vertical dashed lines designate the period that motion features are extracted by the dynamic vision system. (a)(d)(g)(j) the looming case, (b)(e)(h)(k) the rightward translation case, (c),(f),(i),(l) the leftward translation case.

the physiological results shown in Fig. 4.31, we also investigated that whether the robot shows similar behaviour to the fly in Fig. 4.33. Finally, we show examples of arena tests including robot tracking, fixation and follow behaviours in Fig. 4.34.

4.4.2.1 The Open-loop Tests

In the open-loop tests, as illustrated in Fig. 4.31a, we used another *Colias* robot as the visual stimuli and collected on-line outputs of the proposed embedded vision system from the stimulated and motion-blind *Colias*. All the stimuli can be categorised into

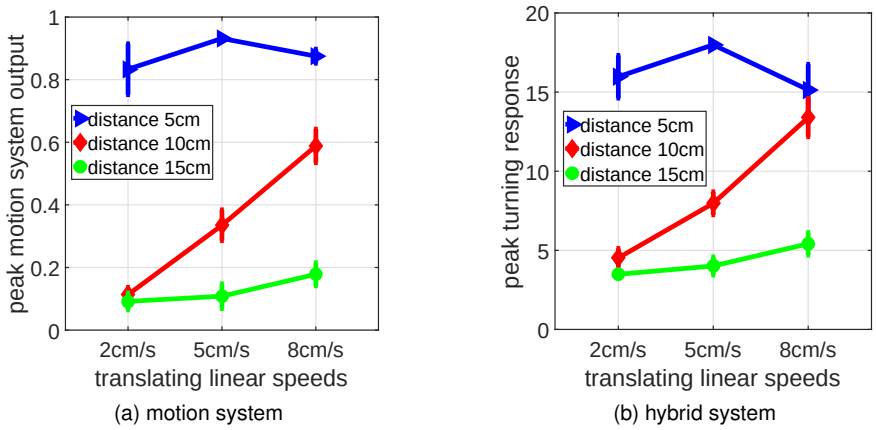

Figure 4.30: Statistical results of peak neural response of the motion and the hybrid neural systems: the proposed embedded vision system was repeatedly tested by translations at three constant linear speeds and three distances, respectively.

three kinds of movements: looming (i.e. approaching) in Fig. 4.29a, rightward translating (Fig. 4.29b) and leftward translating (Fig. 4.29c), which are basic and frequent visual challenges to both robots and insects.

Fig. 4.29 demonstrates the outputs of both the motion and the position visual systems, as well as the hybrid turning response. When challenged by an approaching object, both the motion-sensing system and the robot turning response remain quiet. However, when challenged by translating objects, the motion system is highly activated generating positive and negative response to rightward and leftward translations, respectively. Interestingly, the turning response represents a changing tendency similarly to the outputs of the motion system. Therefore, we can conclude that the motion-sensing system is only sensitive to translational motion features, with direction and intensity information. It also affects significantly the robot turning response, in fact.

On the other hand, the outputs of the position system reveal that it is only sensitive to the location instead of the direction of motion features. In practice, it generates a negative response when the object moves within the left-side of visual field, and a positive response to movements within the right-side of receptive field. The two half-fields are separated by the robot VC. Moreover, it appears that the position system is more easily influenced by noise, i.e., the response tends to fluctuate within the view field, if there are no apparent translating motion cues extracted. Therefore, in comparison with the position system, the motion system is more stable in extracting translational

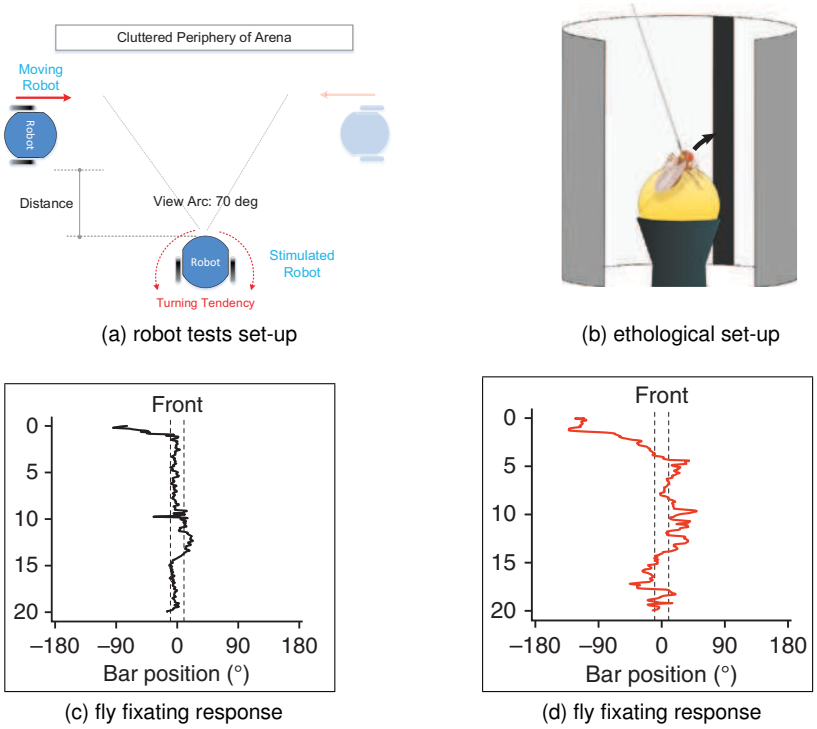

Figure 4.31: The proposed robot tests and previous biological study [32] set-ups: (a) the robot tests setting, (b) the tests on fixation behaviour of a motion-blind fly, (c) fly fixating response with intact visual pathways – Y-axis denotes the time sequence, and X-axis indicates the object relative position around the view centre in fixation behaviour. (d) Fly fixating response by blocking the motion pathway, (b)(c)(d) are adapted from [32] (Bahl et al., 2013).

motion features.

With respect to previous research in bio-inspired motion sensitive systems as proposed in Chapter 3 and 4, we investigated that whether the speed and/or distance of translations affect the proposed model, as this is a challenge to a practical dynamic vision system. The *Colias* robot was tested by rightward translations at three linear-speed levels from three different distances, respectively. Intuitively, Statistics in Fig. 4.30 demonstrates that the motion and the hybrid systems generate similar speed and distance sensitivity. More precisely, the maximum outputs of both systems are reached by translations from the shortest distance of 5cm. The speed response is much weakened by translations far from the view field (15cm in our case), i.e., the proposed model possesses selectivity to wide-field over small-target motion. Furthermore, the optimal speed response to translations, with linearly increased peak-response, occurs by translations at the medium distance of 10cm from the stimulated robot in this case. To conclude, the proposed visual tracking model on embedded system also shows speed

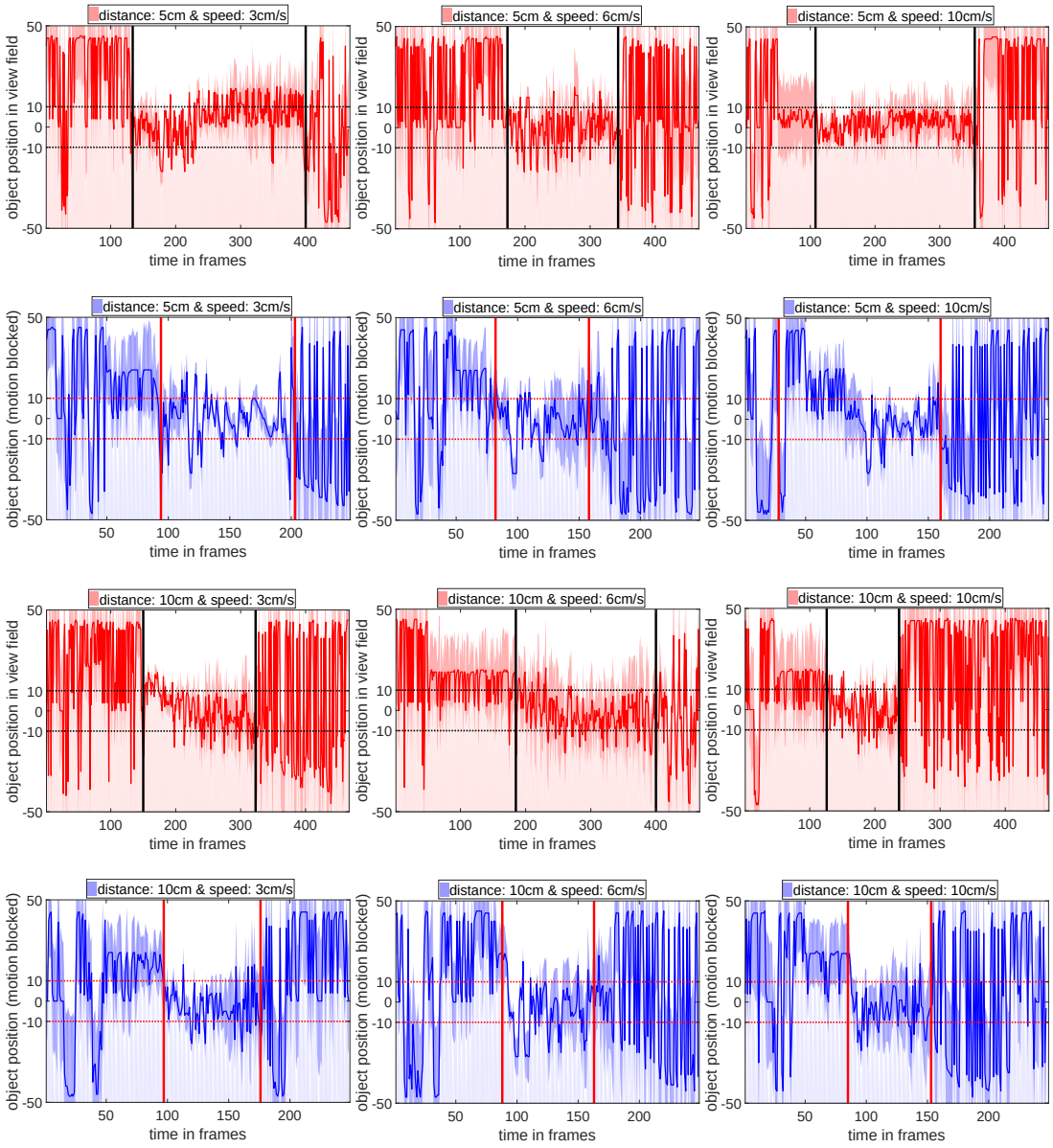

Figure 4.32: The *Colias* robot fixating response under closed-loop tests: both the whole system (red) and the motion-blocked system (blue) were tested by translations at three speeds and two distances, each throughout ten repeated tests. Two horizontal dashed lines specify the VC for successful fixation behaviour; and two vertical lines indicate the period that motion cues are extracted by the stimulated *Colias* robot.

and distance response as expected.

4.4.2.2 The Closed-loop Tests

In the closed-loop tests, we enabled the motion unit of the stimulated *Colias* robot to demonstrate its fixating response to translating robots by generated TR. The stimulated *Colias* robot was given different initialisations of v_i in Eq. 4.36: the robot could follow a translating robot by setting $v_i > 0$, as illustrated in Fig. 4.34c and 4.34d; whilst it

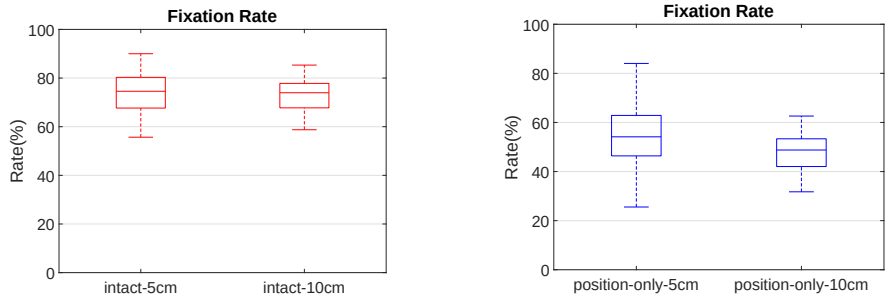

Figure 4.33: Integration of successful fixation rate throughout repeated tests by translations at three speeds and from two distances: both the intact and motion-blocked systems were tested.

only tracks a translating robot by setting $v_i = 0$, as illustrated in Fig. 4.34a and 4.34b.

The results in Fig. 4.32 demonstrate that the stimulated robot can smoothly fixate a translating robot at different speeds and from varied distances, which is similar to the fly fixation behaviour demonstrated in a biological research [32] and Fig. 4.31b. It also appears that the fixating response will wander within the whole view-field, if no apparent translational motion cues are extracted by the proposed dynamic vision system. This is like the results shown in the last section 4.3.2. In addition, Fig. 4.34a and 4.34b illustrate real-time captured snapshots of the robot fixating course.

Very importantly, similarly to the results in previous biological studies on motion-blind flies (Fig. 4.31c, 4.31d), the bio-robotic test results also show that the fixation behaviour could be mediated by the position-locating system only; while the motion-sensing system can improve the fixating response precision. In addition, the statistical results in Fig. 4.33 intuitively demonstrate higher fixation rate by the intact vision system compared to the motion-blocked system, for all tested speeds and distances. This also well matches our previous test results in the off-line tests in Section 4.3.2.

Finally, we also showed a potential application of the proposed embedded vision system for robot-to-robot following behaviour, by tracking and fixating a dynamic agent in navigation. The results in Fig. 4.34c and 4.34d reveal that this bio-inspired model could also enable further research in vision-based robot collective behaviours toward swarm intelligence.

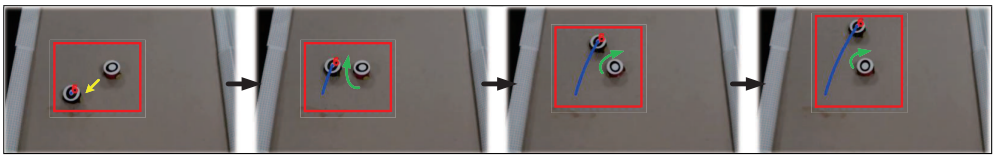

(a) motion tracking and fixation

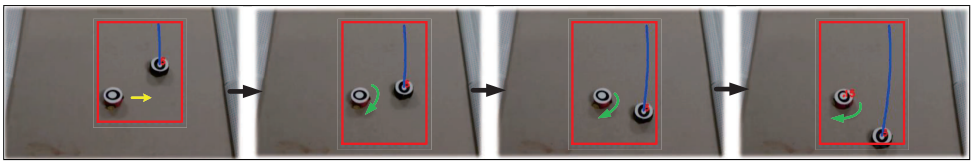

(b) motion tracking and fixation

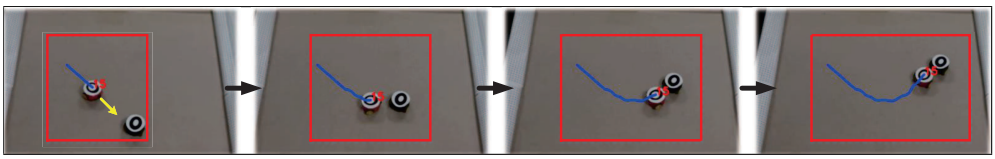

(c) motion tracking and follow

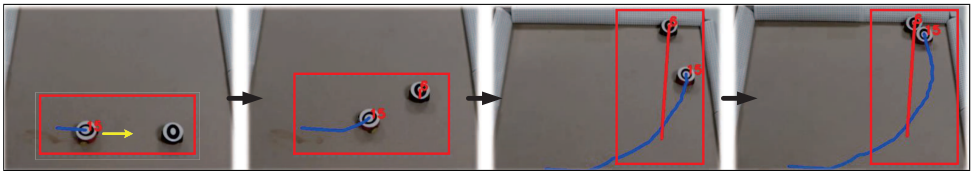

(d) motion tracking and follow

Figure 4.34: *Colias* performance in motion tracking, fixation and follow behaviours captured by a top-down fixed camera: (a)(b) *Colias* motion-unit was closed to form the fixation behaviour. (c)(d) *Colias* motion-unit was allowed to form the following behaviour. Yellow arrows indicate initial direction of the tested *Colias*; green arrows indicate turning direction; blue and red lines denote robot trajectories overtime.

4.4.3 Summary

In this subsection, this dissertation has presented a bio-robotic approach to mimic insect motion tracking strategy and fixation behaviour. The proposed visual motion tracking model has been successfully implemented on the embedded system in a monocular vision-based miniature robot, which has limited computational resources. Satisfactory experimental results have demonstrated both the effectiveness and the flexibility of this biorobotic approach for fast motion tracking and reaching to a behavioural level of fixation. Most importantly, we compared the on-line test results with biological research on fixation behaviours of motion-blind flies, and the micro-robots showed fixating response similarly to insects. This study could benefit the modelling of dynamic vision systems as neuromorphic sensors for mobile autonomous machines. Moreover, with experiments similar to ethological tests, this bio-robotic study could solidify the biological hypothesis that the motion-sensing neural pathway has significant influence

on generating turning response in motion vision tracking; while the position-locating neural pathway plays a crucial role in forming the closed-loop fixating response.

4.5 Further Discussion

In above sections, we have discussed the modelling of fly translating perception visual neural networks and demonstrated potential robotic applications. These computational models show similar visual processing strategies to the fly preliminary motion detection. However, there are currently a few unsolved problems in the modelling of translating sensitive neural systems. In this section, we will point out these.

To the best of our knowledge, a shortcoming of both former HR detector based models and the proposed models is the speed tuning in motion detection. In another word, a biological motion-detecting circuit may not tell the true velocity of visual stimuli [29]. The reason is that for each combination of 'delay and correlate' motion detectors, it is advisable to decide the spacing between each pairwise detectors, and the time span for the latency in follow-up non-linear computations. Each factor will greatly affect the model's performance in sensing translating objects [179]. For example, perceiving faster movements requires either a larger spatial span between detectors if fixing the delay, or a shorter time latency when the spacing is unchanged. In the modelling study of the proposed DSNN in Section 4.2, we found that building an ensemble of local motion detectors in the ON and OFF pathways has great potential of improving the speed response of motion sensitive neural networks, even though this method is more computationally expensive. More precisely, the same-sign (ON-ON and OFF-OFF) polarity cells are connected along both horizontal and vertical directions, and the number of connected cells for each local detector is manually defined rather than learned. With this idea, we can pre-define the sampling distance in each pairwise combination of same sign motion detectors in either ON/OFF pathways, as well as the number of connected cells for each local cell for speed tuning. Nevertheless, as demonstrated in the systematic experiments, this decides the speed sensitivity but costs great computational power with more connected cells. We also investigated the modelling of temporal dynamics within the directionally lateral interactions of

both ON-ON and OFF-OFF motion detectors. We found that a dynamically temporal filtering strategy for combinations of detectors with different spacings improves the velocity sensitivity to translational motion, as presented in the experiments. For the speed tuning, our proposed neural network outperforms other related models. Recently, the angular velocity sensitive models have been proposed, e.g. [33], inspired by the bees' visual systems and corresponding visually guided behaviours. This also hits at great potential of solving the current defect of translating sensitive neural systems.

Amongst various kinds of physical sensors, the visual sensing modality can gather a rich source of motion information. However, this includes much irrelevant background noise. As a result, another problem for the translating sensitive neural systems is the lack of flexible mechanisms for filtering out irrelevant motion from visual clutter. The current bio-inspired models are so easily influenced by environmental unrelated motion such as the windblown vegetation and the shifting of background, as shown in Section 4.2.2. At present, most biological and computational models are tested by only simple stimuli within a clean background rather than dynamic visual clutter, e.g. [39, 40, 31, 33]. Motivated by some physiological researches and models of insect motion detectors, e.g. [40, 95, 252, 125, 43]), our proposed neural networks have further demonstrated the effectiveness of a spatial pre-filtering (DoGs) of motion signals prior to the ON and OFF pathways in the computational Lamina layer, which can maximise the transmission of useful motion cues along with removing redundant environmental noise in a visually cluttered background. Moreover, we found that when challenged by a more dynamic background like the global shifting of a large area in the visual field, such a spatial pre-filtering dose not fully reach the desired performance for motion perception. In this research, we have continued to investigate a bio-plausible mechanism of the FDSR within the dual-pathways. This works effectively to further filter out irrelevant motions in a temporal way so that bettering the model performance in more dynamic scenes like the shifting of cluttered background. Generally speaking, combining both the spatial and temporal methods help largely filter out irrelevant motion, which has been demonstrated well by our experiments in Section 4.2.2.

At the current stage, learning methods are not involved in the models. The proposed

bio-plausible mechanisms are restricted by the spatiotemporal parameters which are not robust to deal with different complex natural scenarios. A 'real' intelligent dynamic vision system should be adaptive to motion detection in different environments.

4.6 Chapter Summary

In this chapter, this thesis has proposed the modelling of visual neural networks for sensing translational motion and mimicking visually guided behavioural responses of motion tracking and fixation. These computational models are rigorously based on biological research in fly (drosophila) preliminary visual systems including pathways, mechanisms, neurons and corresponding visually guided behaviours. Compared to physiological research in locust looming detectors, more studies have been carried out to explore the fly visual processing circuits, as introduced in Section 4.1. More precisely, the modelling of DSNN simulating the characteristics and functionality of fly motion-detecting ON and OFF visual pathways and LPTCs is presented in Section 4.2. Compared to the former related models, the proposed DSNN possesses ensembles of motion detectors in the dual-pathways improving the speed tuning, as well as spatiotemporal dynamics removing redundant irrelevant motion from a visually cluttered and dynamic background. After that, a bio-plausible position pathway is modelled to mimic fly fast motion tracking and a behavioural response to fixation in Section 4.3. At last, a visual fixation model is successfully realised on the embedded system in an autonomous vision-based miniature robot in Section 4.4. We have also further discussed about our achievements compared with previous translating sensitive neural systems, as well as unsolved problems in Section 4.5.

The proposed visual neural networks have been tested by systematic experiments including the off-line tests of synthetic and real-world scenarios and the on-line bio-robotic tests. The proposed bio-inspired algorithms or methodologies for directional translating perception have been validated by the experiments. The computational simplicity and flexibility have been also verified by the on-line robot tests. More specifically, the proposed translating sensitive neural networks can be implemented on the embedded system in real time; the in-chip image processing frequency can reach above

25Hz handling 99×72 pixels with only 192Kbyte internal SRAM. Taken biological inspiration, this chapter has provided effective solutions towards constructing a dynamic vision system for motion perception with low cost and energy consumption.

Chapter 5

Design of Hybrid Neural Vision Systems for Autonomous Mobile Robots

In this chapter, this dissertation will continue to present the modelling of hybrid motion sensitive vision systems that combine different modelled visual neurons in Chapter 3 and Chapter 4, each possessing specific DS to visual movements. Concretely, the proposed locust LGMDs neuron models respond most strongly to objects moving in depth that approach; whilst the proposed fly DSNs neural networks are only sensitive to translational motion in four cardinal directions. The complementary functionality makes possible cooperation of both kinds of bio-inspired dynamic vision systems.

The proposed hybrid models in this chapter have all been satisfactorily realised on the embedded system in our proposed micro-robot *Colias*, as illustrated in Section 3.1.3. This chapter will demonstrate the great potential in collaboration of different bio-inspird visual neurons to deal with more abundant motion features. These can direct more flexible visuomotor control including collision avoidance, motion tracking and following. These models featured by different DS are promising solutions to real-world visual challenges to mobile machines in navigation, which have been demonstrated through bio-robotic tests in arenas with dynamic scenarios mixed with multiple robot agents.

The remainder of this chapter is organised as follows: Section 5.1 discusses a hy-

brid LGMDs research in *Colias*. Section 5.2 presents a synthetic model integrating all the proposed computational neuron models in Chapter 3 and Chapter 4 for motion pattern recognition in dynamic robot scenes. We discuss about the feasibility of these bio-inspired visual models working with other image processing methods via an effort to a case study in Section 5.3. Finally, this chapter is summarised in Section 5.4.

5.1 A Hybrid LGMDs Embedded Vision System

In this section, we will study and compare the LGMD1 nad LGMD2 neuron models via design of a hybrid model in the robot visual sensing modality. In the locusts' visual brain, the LGMD1 and LGMD2 looming detectors have been identified to sense rapidly expanding objects, yet with different collision selectivity, as demonstrated in Chapter 3. Both neurons have been modelled and successfully applied in robotic vision system for perceiving potential collisions in an efficient and reliable manner. Chapter 3 presents the computational modelling of LGMD1 and LGMD2 neurons, separately. In this research, we conduct a hybrid LGMDs neuronal models, for the first time combining the functionality of LGMD1 and LGMD2 looming detectors, in the visual modalities of *Colias* robots. The results of systematic on-line experiments demonstrate three main contributions of this research:

- The arena tests involving multiple robots have validated the effectiveness and robustness of a reactive motion control strategy via integrating a bilateral pair of LGMD1 and LGMD2 models for collision detection in dynamic scenarios. *Colias* robots showed very high success rates of collision recognition.

- This research has pinpointed the different collision selectivity between LGMD1 and LGMD2 neurons in locusts have been fully demonstrated through the computational modelling of ON and OFF pathways and spike frequency adaptation mechanism.

- The utilised *Colias* robot is a feasible platform to introduce visual processing algorithms into robotics.

5.1.1 Motivations

For an autonomous robot, the ability of perceiving imminent collision, in a timely and robust manner, is essential. However, it is still a pronounced challenge for safe navigations of robots without human intervention, especially mixed with dynamic objects. There are now many collision-detecting sensors like the infra-red, laser, radar, ultrasound, vision, or combination of these sensors. However, those sensing modalities are restricted heavily to the applications of small robots, due to their size, reliability and/or energy consumption. For robotic applications, the neuromorphic vision sensors [57] in comparison with traditional sensing modalities using the segmentation and registration based computer vision techniques [72], can cope with the degree of complexity in real physical world for collision detection more efficiently. This can fulfil the utility in small mobile robots which have very limited computational resources and power.

Chapter 3 has demonstrated the similarities and differences of the LGMD1 and LGMD2 neuron models in looming detection. It leaves us an interest to investigate the possible cooperation of both looming detectors. Gathered in a robot agent, these modelled neurons should possess each specific collision selectivity as illustrated in Chapter 3. Therefore, in this study, we set up a hybrid visual system by integrating LGMD1 and LGMD2 neuron models on embedded system in *Colias* robots. Compared to previous presented arena tests in Chapter 2 and Chapter 3 that only a single robot was tested, we examine the collision-detecting performance of the proposed model in an arena mixed with multiple autonomous robots; each *Colias* robot applies the camera sensor as the only collision detector and implements the proposed model. In addition, a directional collision avoidance strategy with a bilateral pairwise LGMD1 and LGMD2 neuronal models is applied in the arena tests.

In the following subsections, the proposed hybrid model is presented in Section 5.1.2. Our systematic bio-robotic experiments including arena tests and neuron models investigation are illustrated in Section 5.1.3. A concise conclusion is given in Section 5.1.4.

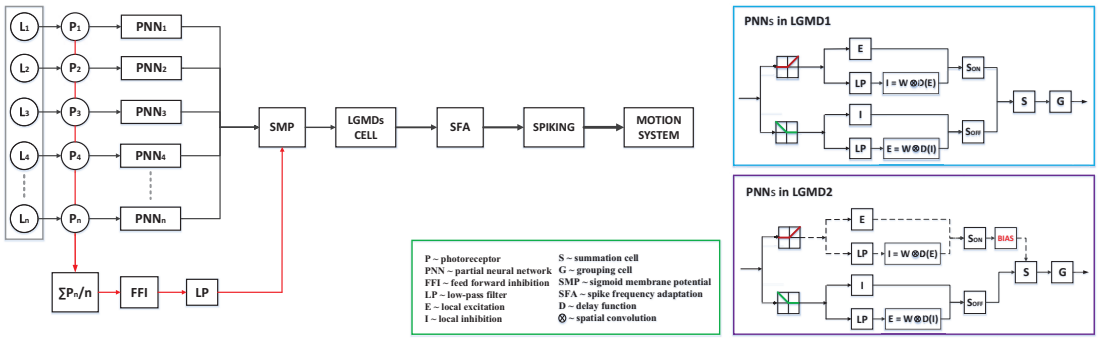

Figure 5.1: Schematic diagram of the proposed hybrid LGMD1 & LGMD2 model with ON and OFF visual pathways corresponding to the proposed general neural network in Section 2.2 and 3.2: this figure is adapted from [55] (Fu et al., 2017).

5.1.2 Model Description

In this subsection, we will present the embedded vision system and the motion control strategy adopted in the arena tests. Similarly to my proposed LGMD1 and LGMD2 models in Chapter 3, the core structure in the proposed hybrid model is the ON and OFF pathways that effectively separate the functionality between two modelled visual neurons. A spiking mechanism and competition between two activated neurons are also applied for angular collision recognition and reactive avoidance in *Colias* robots.

5.1.2.1 The LGMDs Neuronal Models

LGMD1 and LGMD2 neuron models share a general signal processing pipeline illustrated in Fig. 5.1. The algorithms are consistent with the proposed LGMD1 and LGMD2 models in Section 3.1 and Section 3.2, which are not restated here. However, we want to highlight the important role of ON and OFF pathways wherein the PNNs in the LGMD1 differ from the LGMD2. More precisely, a bias is put forth in all ON channels of the LGMD2 but LGMD1 models which rigorously sieves onset responses for achieving the different looming selectivity. With such a structure, the LGMD2 can respond to only darker objects that approach, as demonstrated in Chapter 3. We also emphasise the SFA mechanism in both LGMDs models that enhances the collision selectivity to approaching over receding and translating stimuli.

Compared with previous modelling works, here we only present a few updated mechanisms and design of visual and motion controls. As illustrated in Fig. 5.1, after ON and OFF mechanisms that separate visual information into parallel pathways, there

are different delayed information in spatiotemporal computation. In the ON pathway, ON cells elicit onset responses by brightness increments, i.e. the excitation is conveyed directly to its counterpart cell in the next layer, whilst the inhibition is delayed relative to the excitation, formed by convolving surrounding delayed-excitations:

$$\begin{aligned} E^{ON}(x,y,t) &= P^{ON}(x,y,t), \\ I^{ON}(x,y,t) &= \sum_{i=-r}^{r}\sum_{j=-r}^{r} D^{ON}(x+i,y+j,t)\cdot W(i,j), \end{aligned} \tag{5.1}$$

where r denotes the size of inhibited area. W indicates the convolution matrix. D^{ON} is the low-pass filtered excitation. Compared to previous modelling studies in Chapter 3 that the delayed information only spreads out to its neighbouring cells rather than to its direct counterpart, we allow a self-inhibition mechanism, which has been suggested recently in a biological research on both the LGMD1 and the LGMD2 [116]. This works effectively to mediate the collision selectivity to looming as well by strengthening the inhibiting effects for each local cell.

Similarity for the visual processing in the OFF pathway, OFF cells relay information to two flows for excitations and inhibitions. However, compared to signals processing in ON pathway, excitations are delayed relative to inhibitions, caused by offset responses of brightness decrements. Here is also a self-inhibition mechanism:

$$\begin{aligned} I^{OFF}(x,y,t) &= P^{OFF}(x,y,t), \\ E^{OFF}(x,y,t) &= \sum_{i=-r}^{r}\sum_{j=-r}^{r} D^{OFF}(x+i,y+j,t)\cdot W(i,j). \end{aligned} \tag{5.2}$$

After similar pre-synaptic visual processing to the proposed LGMDs general model in Section 3.2, both LGMDs cells pool all the local excitations from the dual-pathways to form the membrane potential that is transformed by a same sigmoid function. As illustrated in Fig. 5.1, there is the FFI mechanism in both LGMDs neuronal models to deal with a large area of photoreceptors activated simultaneously. This works effectively to inhibit the robot during turning response or nearby translations. After that, the neural computation of SFA and spiking mechanisms conform to the modelling of LGMD1 and LGMD2 neuron models in Section 3. The neural response is also expo-

Table 5.1: Robot Motion Behaviours in Arena Tests

F: go forward, R/L: turn right/left, S/SSS: stop/long stop
BR/BL: go backward then turn right/left

Condition	Motion	Condition	Motion
$DIR(t) = Right$	R	$DIR(t) = Left$	L
$S1(t) = S2(t)$	S	$Default$	F
$DIR = Right$ & $S2(t) \geq N_{sp}$	BR	$\bar{FFI}(t) \geq T_{ffi}$	SSS
$DIR = Left$ & $S1(t) \geq N_{sp}$	BL		

nentially mapped to the spike rate. Finally, a potential collision corresponds to a high spiking frequency above a predefine threshold.

The parameters setting of the hybrid LGMDs neuron model are consistent with the former modelling studies on LGMD1 and LGMD2 in Section 3.1.2 and Section 3.2.1. No parameter learning algorithms are currently involved in the embedded vision system. The hybrid model processes visual signals in a feed-forward structure, as well.

5.1.2.2 The Motion Control System

In this research, we integrated a bilateral pair of LGMD1 and LGMD2 neuron models that are in competition for reactive directional motion control. On the behaviour level, the LGMD1 neuron is revealed to arouse gliding response during locust flying or jumping from the ground; whilst the LGMD2 neuron likely elicit hiding behaviour of adolescent locusts [131, 19, 115, 114]. Although the biologists found that LGMD1 and LGMD2 elicit distinctive collision avoidance behaviours for locusts in different ages, in this study, we assume that they reproduce the escape directions in a comparable way, since the micro robot can only run on the 2D surface.

More specifically, as illustrated in Fig. 5.2, the robot visual field is split into two regions that handled by the LGMD1 (left) and the LGMD2 (right) neuron models, respectively. This corresponds to the control of robot right and left wheels for conducting turning response. The generated spikes are fed into a simple 'winner-take-all' strategy

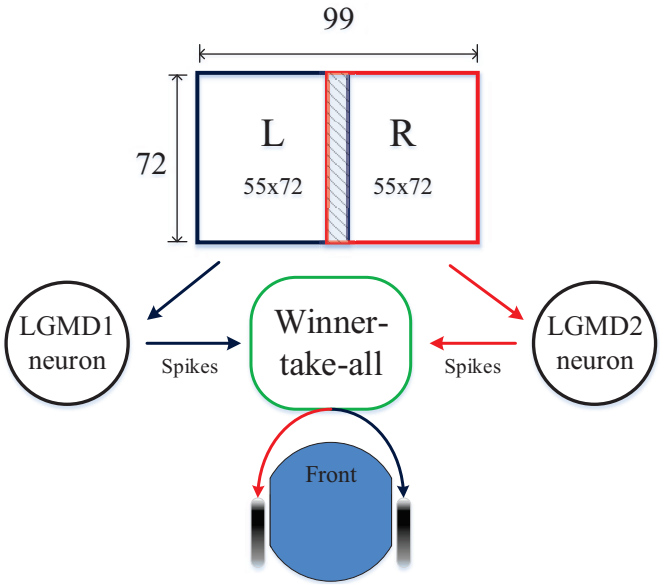

Figure 5.2: Illustration of image processing in the visual modality of *Colias* and the directional motion control strategy with a bilateral pair of LGMDs neuron models: each grey-scale frame (in full resolution of 99×72) is divided into two regions (55×72) with a small overlapping area. By default, the left and right half-regions is handled by LGMD1 and LGMD2 neurons, separately. Generated spikes go through a 'winner-take-all' competition towards activation of robot two-side wheels. This figure is adapted from [55].

similarly to [8, 85], for deciding the escape direction in avoidance behaviours:

$$DIR(t) = \begin{cases} Right,\ if\ S1(t) > S2(t)\ \&\ \sum_{i=t-N_{ts}}^{t} S1(i) \geq N_{sp} \\ Left,\ if\ S2(t) > S1(t)\ \&\ \sum_{i=t-N_{ts}}^{t} S2(i) \geq N_{sp} \end{cases}, \tag{5.3}$$

where $S1$ and $S2$ are the elicited spikes by the LGMD1 and the LGMD2 neuron models respectively. Occasionally, the left and right neuron models produce the same number of spikes. This would be rare for a locust, since its post-synaptic neuron to the LGMD spikes at very high frequency, much higher than our modelled neurons. However, when implemented in robots, either model works at approximately 30 Hz. Therefore, the left and right LGMD models may sometimes produce the same number of spikes at the time of escape. In addition, the FFI output also affects the performance of robot, thus we initiated extra escape behaviours in the arena tests as listed fully in Table 5.1.

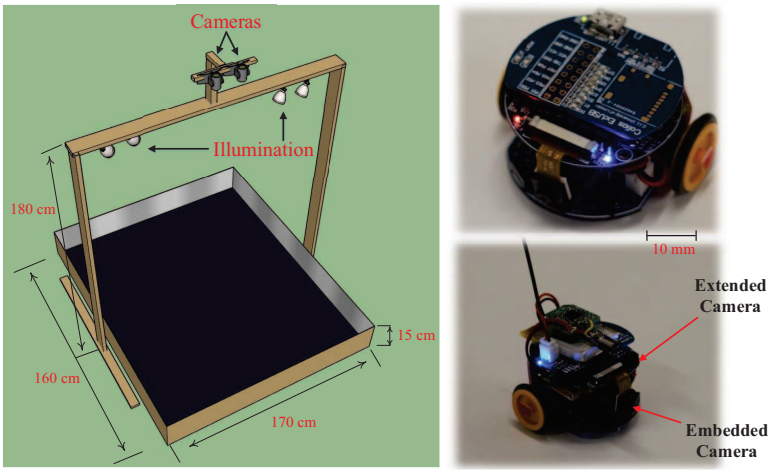

Figure 5.3: Schematic diagram of the arena and micro-robot used in on-line tests: compared with proposed robot tests in Chapter 3 and 4, the *Colias* was with an extension board of a wireless camera for recording frontal views in navigation. This figure is adapted from [55].

5.1.3 Experiments and Analysis

In this subsection, we will illustrate the systematic bio-robot experiments. All the trials can be sorted into two parts: the arena tests and the angular approach tests. It is important to note that in both kinds of experiments, we set up the dark and bright environments respectively, for inspecting the performance of integrating a bilateral pair of LGMD1 and LGMD2 models.

5.1.3.1 Multi-Robots Arena Tests

The first kind of experiments are the arena tests. The micro-robots used are our proposed *Colias* robots – *Colias*-IV, as illustrated in Fig. 3.5c. Each agent applies the monocular camera as the only sensor in experiments implementing the collision-detecting algorithms. Peripheries of the arena is decorated with dark patterns densely embedding in a white background, as shown in Fig. 5.4d. We set up a bright environment with full arena lights (Fig. 5.3) and the global illumination. Compared to former robot tests proposed in Chapter 3 and Chapter 4, we for the first time set up a dark environment with only a single arena light on for illumination. We have two main goals in designed arena tests: 1) to examine efficacy and robustness of the proposed algorithms for hybrid neuron models in collision detection mixed with multiple robots, that is, a more dynamic scenario, 2) to investigate the different looming selectivity be-

Table 5.2: Success Rates for Multiple *Colias* Robots in Collision Detection

Events: Avoiding (A), Waiting (W), Colliding (C) SR = (A + W) / (A + W + C) · 100%				
ID	Avoidance	Waiting	Colliding	SR
1	769	51	21	97.50%
6	867	36	37	96.06%
10	698	80	11	98.61%
11	715	43	33	95.83%
15	743	28	51	93.80%

tween modelled LGMD1 and LGMD2 neurons. For the purpose of just recording first views of robot navigation, we applied an extra wireless camera on the top of an agent, as illustrated in Fig. 5.3.

Firstly, in the bright environment, we examine its performance of collision detection in the arena tests involving multiple (5) *Colias* robots running simultaneously. With the help of top-down real-time tracking systems [56, 240, 241], we can get very precise trajectories of each agent with its specific pattern indicating an unique ID. Fig. 5.4 illustrates a few frontal first-views recorded from the extended wireless camera of an agent when running in the arena, representing some particular events, like quickly avoiding the looming dynamic agents (Fig. 5.4a, 5.4b), circumventing the surrounding walls (Fig. 5.4d), travelling towards the crossing robots (Fig. 5.4c). All the avoidance or waiting behaviours are invoked by the collaboration of the bilateral pair of LGMD1 and LGMD2 models, as introduced in Table 5.1. Interestingly, we can calculate the statistical success rates for all the tested *Colias* robots throughout repeated arena tests. we defined a successful collision detection comprises not only avoiding a potential approaching object (invoked by high frequency spikes), but also waiting for a near translating object (elicited by high level FFI output). Intuitively, Table 5.2 shows the statistics for these ID-specific *Colias* robots running together for approximately 2 hours in total. Satisfactory results demonstrate the effectiveness and robustness of the proposed algorithms for integrated and embedded LGMDs neuron models with reactive directional motion controls for the micro-robots in collision-detecting tasks with dynamic scenarios.

After that, we inspect the success rates of approaching a fixed lighter object in the

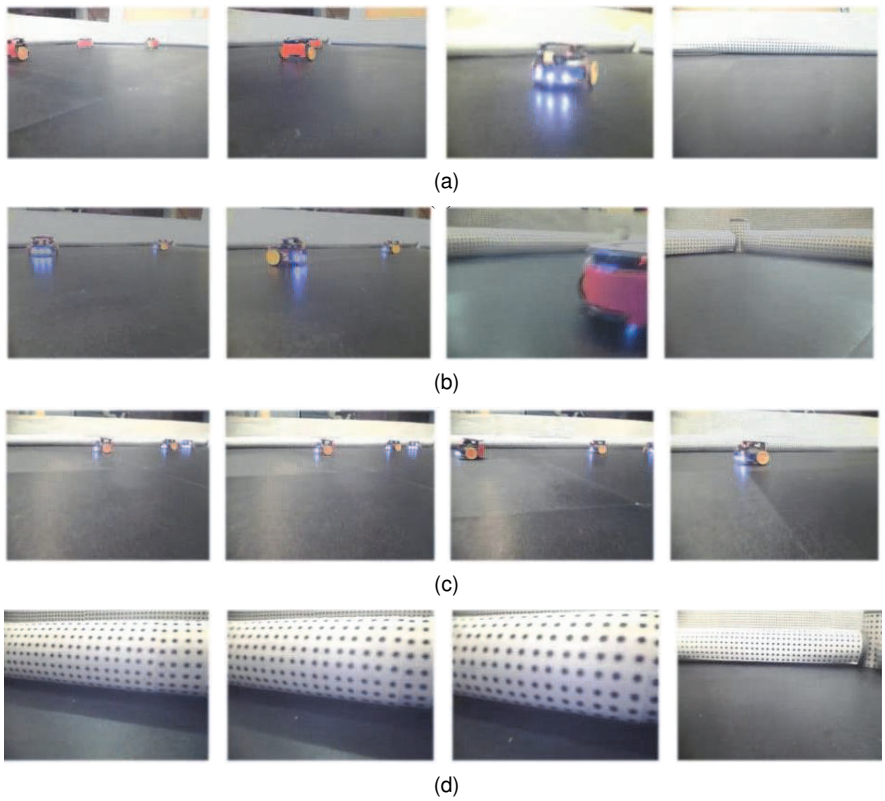

Figure 5.4: Four illustrative events of the arena tests in bright environment, represented by the first views from the wireless camera on a *Colias*: (a) a robot-to-robot collision avoidance, (b) successive collision avoidance, (c) challenged by translating robots, (d) a robot-to-obstacle collision avoidance, adapted from [55].

dark environment simulating the situation of 'night navigation'. In order to point out the different looming selectivity between LGMD1 and LGMD2, we let a *Colias* robot approach the lighter object from left and right sides, respectively (Fig. 5.5). By default, the LGMD1 and LGMD2 models handle the left and right region of receptive field, separately, as illustrated in Fig. 5.2. Fig. 5.5a and 5.5b demonstrate the *Colias* robot fails to recognise the collision to the lighter object approaching from the left side, yet succeeds in perceiving the collision approaching from the right side. Interestingly, after switching the processed regions by the LGMD1 and LGMD2 models, Fig. 5.5c and 5.5d illustrate totally reverse reactions of the *Colias* robot. More importantly, the informative statistics throughout repeated tests in Table 5.3 clearly demonstrates when challenged by lighter objects looming embedded in a dark background, the proposed hybrid neuron model is not as robust as the arena tests in fully bright scenes for collision recognition. Even though the LGMD1 model still works effectively on detecting light looming stimuli coming from its processed visual field, the LGMD2 model does

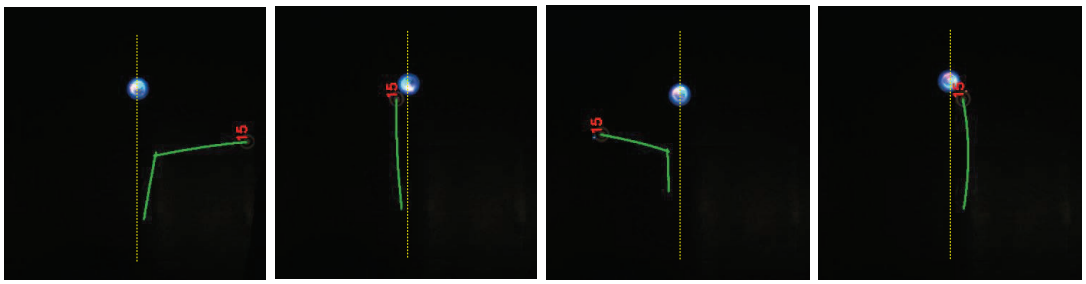

(a) (b) (c) (d)

Figure 5.5: Four illustrative results of the arena tests in a dark scene captured by a top-down camera – the *Colias* approached a stationary object from left and right sides, separately. (a)(b) The left and right regions of visual field are handled by LGMD1 and LGMD2, respectively. (c)(d) Conversely, the right and left regions of view are handled by LGMD1 and LGMD2, respectively. The yellow dashed line separates the two sides. The robot (ID-15) trajectory is depicted in green line. These are adapted from [55].

Table 5.3: Success Rates for Approaching a Lighter Object

Repeat: R, Avoidance: A, SR = A / R · 100%			
Left-LGMD1 & Right-LGMD2 Approaching Side	R	A	SR
Right Left	50 50	45 10	90% 20%
Right-LGMD1 & Left-LGMD2 Approaching Side	R	A	SR
Left Right	50 50	41 15	82% 30%

not – it has the defect of not responding to the dark-to-light luminance change well. The experimental results well match the related biological findings on biological LGMD1 and LGMD2 neurons [83, 79, 116, 19].

5.1.3.2 Angular Approach Tests

The second type of experiment includes the systematic angular approach tests, as illustrated in Fig. 5.6. Here we aim to deeply investigate the collision selectivity of hybrid looming detector via combining a bilateral pair of LGMD1 and LGMD2 neuron models. We collected the neural outputs from the monitoring *Colias* robot, containing the SMPs and spikes afterwards.

Comparative results in Fig. 5.7 and 5.8 allow the following analysis to be drawn: 1) when challenged by darker angular approaching stimuli (Fig. 5.7), both LGMD1

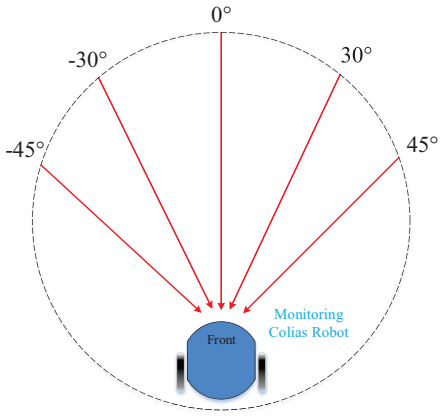

Figure 5.6: Experimental setting for the systematic angular approach tests: a motionless *Colias* (left-LGMD1 and right-LGMD2) was stimulated by an approaching *Colias* from different angles, repeatedly and in dark and light environments respectively. In the dark environment, the approaching robot is with the light source used in Fig. 5.5. This is adapted from [55].

and LGMD2 models represent high-level SMPs and high-frequency spikes, especially challenged by the direct approaching (Fig. 5.7c). More precisely, when the dark looming stimuli come from the left side, the LGMD1 model responds more vigorously and much earlier than the LGMD2 (Fig. 5.7a and 5.7b). Conversely, when stimulated by the right-side angular approaches, the LGMD2 contributes more significantly in collision detection, spiking at higher frequency (Fig. 5.7d and 5.7e).

Interestingly, when challenged against light angular approaching, Fig. 5.8 clearly demonstrates that the LGMD2 neuron is inhibited during light-looming from any angles; whilst the LGMD1 is rigorously activated – its spiking rate peaks at the direct approaching (Fig. 5.8c), and remains quiet by the looming from the right side with the largest approach angle (Fig. 5.8e) alike Fig. 5.7e. More intuitively, the statistics in Fig. 5.7f and 5.8f demonstrates the collision selectivity of the proposed hybrid neuron model fully: at least one LGMD neuron model can recognise the colliding of darker objects, yet only the LGMD1 model is robust in detecting lighter objects approaching. In addition, both LGMDs neurons spike at the highest frequency against the direct approaching, representing the most powerful strike from the predator to locusts.

5.1.4 Summary

In this research, we have introduced two locust looming sensitive neuron models into the visual modality of a ground mobile micro-robot. Although a few LGMD1 or

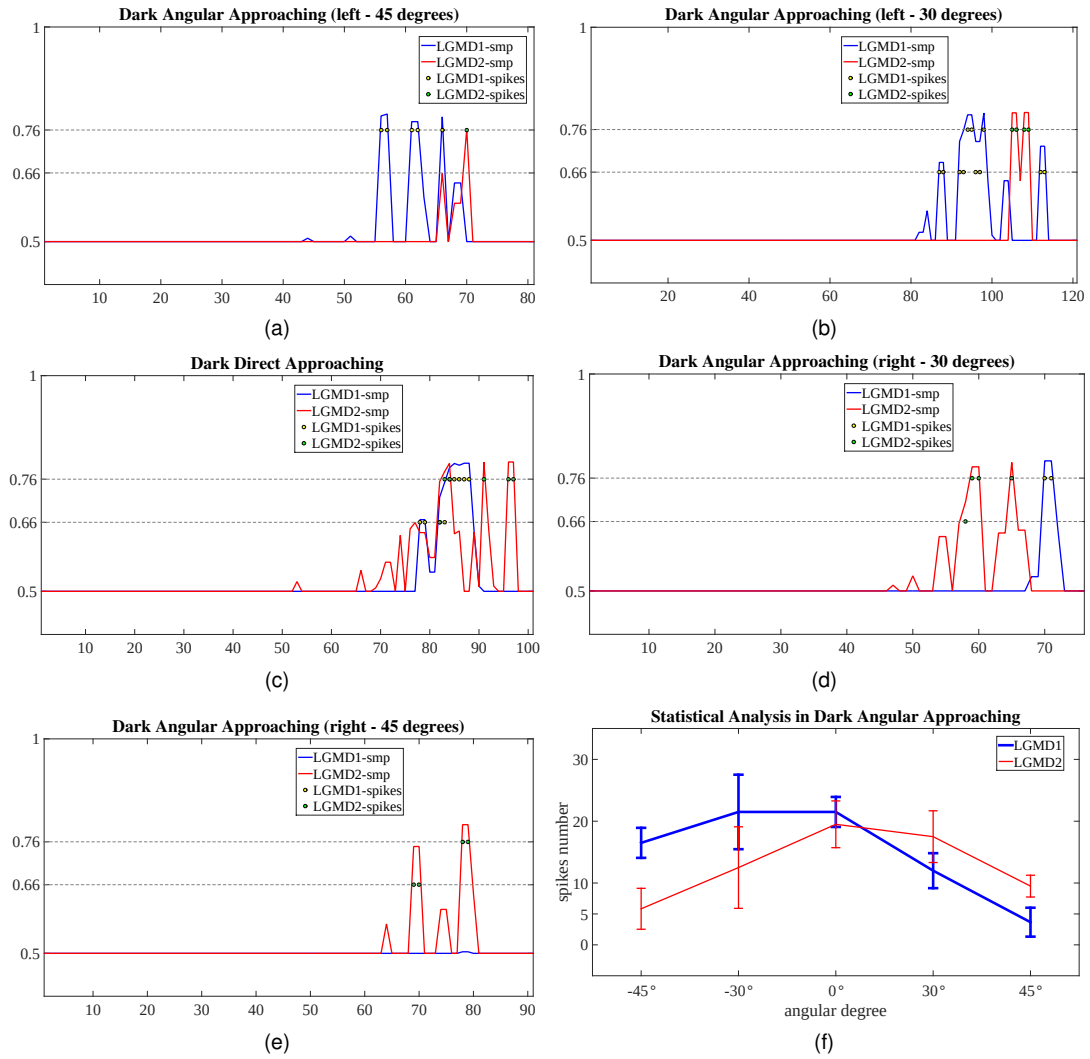

Figure 5.7: Neural responses of LGMD1 and LGMD2 neuron models challenged by angular approaching in the bright environment: (a)–(e) SMPs and generated spikes with two spiking thresholds: X and Y axes denote the time sequence in frames and the SMP level. (f) Statistical results with each angle throughout 10 repeated tests, adapted from [55].

LGMD2 based models have been successfully applied in robots, it is the first time to combine the functionality of both LGMDs neuron models to form a hybrid dynamic vision system for collision detection. The systematic experiments have verified its efficiency and flexibility with a bilateral pair of looming detectors for a reactive control strategy in the arena tests mixed with multiple robots. Moreover, the unique collision selectivity of both the modelled LGMD1 and LGMD2 has been pinpointed, which well match the revealed biological characteristics of two LGMDs neurons in locusts.

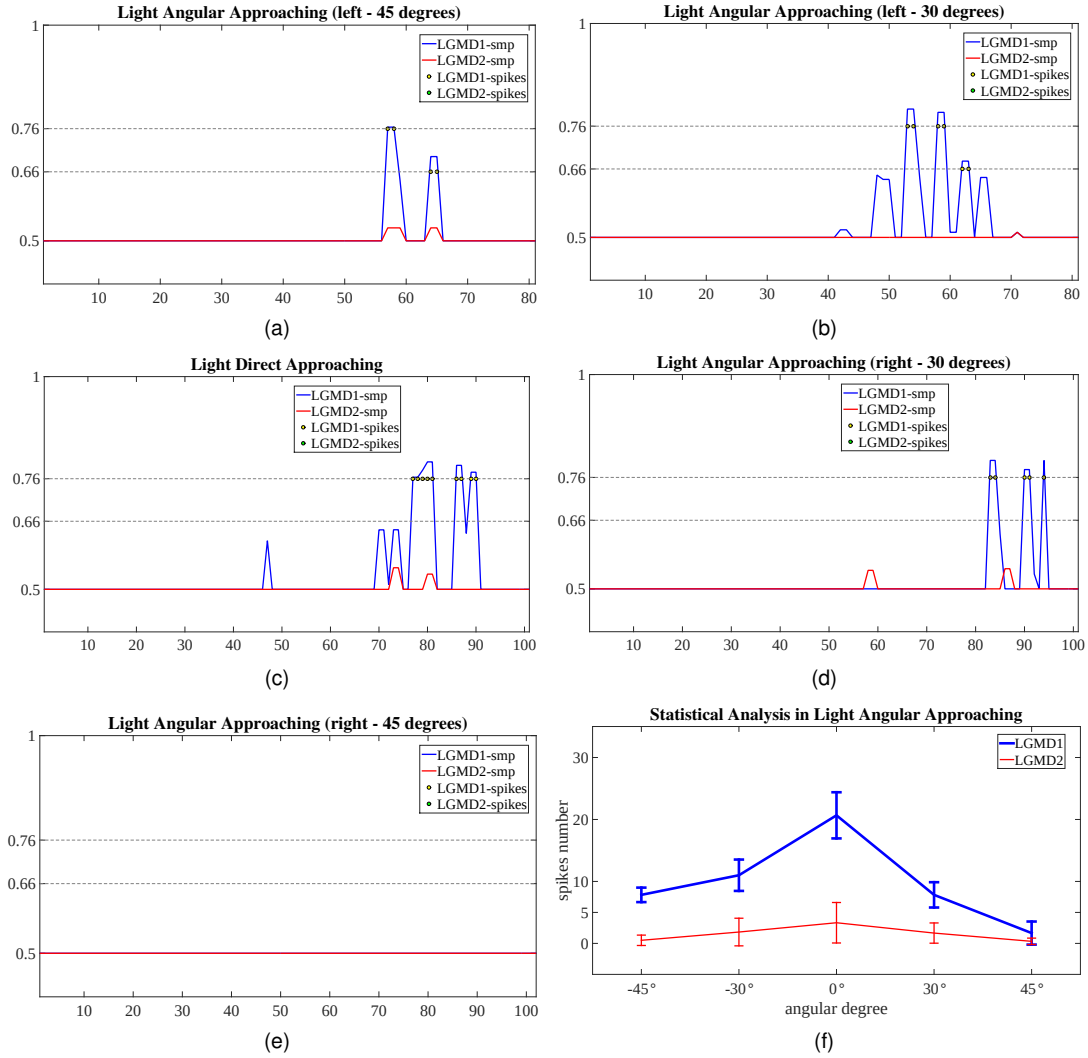

Figure 5.8: Similarly to Fig. 5.7 but in the dark environment, adapted from [55]

5.2 A Synthetic LGMDs and DSNs Neural System

Through the modelling studies on locust and fly visual systems for motion perception, we present a design of synthetic neural vision system in this section. As discussed in the future work of previous researches, this integrates the modelled LGMDs in Chapter 3 and DSNs in Chapter 4 which provides a possible neuromorphic solution to fast motion pattern recognition like insects. As a result, this synthetic hybrid neural model is realised on embedded system in the proposed autonomous micro-robots, to recognise motion patterns in dynamic robot scenes. Here the basic motion patterns are categorised into movements of looming (proximity), recession, translation, and other irrelevant ones. The presented system is a synthetic neural network, which comprises two complementary sub-systems with four spiking neurons – the LGMD1 and

LGMD2 in locusts for sensing looming and recession, and the DSN-R and DSN-L in flies for rightward and leftward translational motion extraction. Images are transformed to spikes via spatiotemporal computations towards a switch function and decision making mechanisms, in order to invoke proper robot behaviours amongst collision avoidance, tracking and wandering, in dynamic robot scenes. Our robot experiments demonstrate two main contributions of this hybrid model: 1) This neural vision system is effective to recognise the basic motion patterns corresponding to timely and proper robot behaviours in dynamic scenes. 2) The arena tests with multi-robots demonstrate the effectiveness in recognising more abundant motion features for collision detection, which is a great improvement compared with former studies in Chapter 3 and Section 5.1.

5.2.1 Motivations

Insects have tiny brains but complicated visual systems for motion perception. In this dissertation, a handful of insect visual neurons have been computationally modelled and successfully applied for robotics in Chapters 3, 4 and 5. Here it still remains a question about how different neurons can collaborate on motion perception.

Building a dynamic vision system in both a robust and efficient manner for motion-sensing in mobile machines, like robots, UAVs and etc, poses a big challenge to modellers. The state-of-the-art computer vision techniques, e.g. [69, 65, 257, 255], have achieved great improvements on motion/objects detection and tracking. However, these segmentation and/or learning based methods are either computationally costly, or heavily restricted to specific hardware, like event-driven cameras [69].

In nature, evolutionary development through more than millions of years endow animals with robust visual systems for motion perception. Insects, in particular, have relatively small number of visual neurons, but can navigate smartly through unpredictable and visually cluttered environments. The neural circuits processing visual information in insects are relatively simple compared to those in the human brain, and can be ideal models for optical sensors, as reviewed in [57, 37, 59]. Exploring and modelling of these amazing motion perception neural circuits will significantly

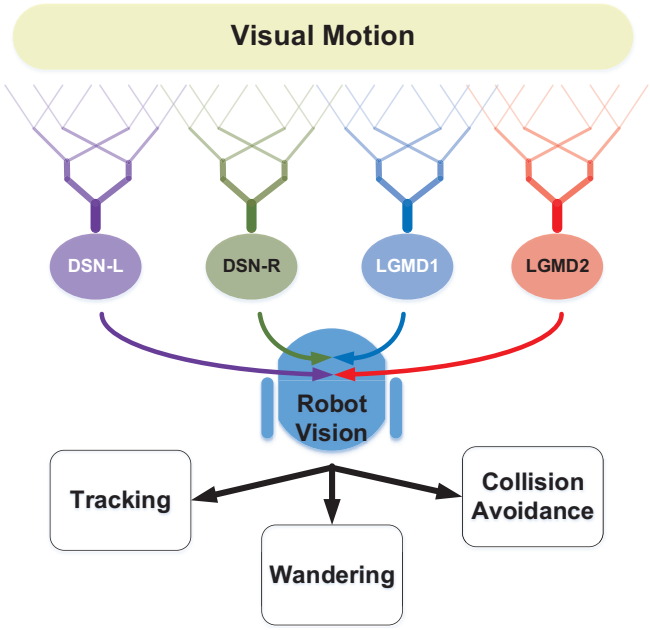

Figure 5.9: Framework of the proposed bio-robotic approach for visual motion features extraction and motion patterns recognition: the inputs to the neural vision system are images captured by a visual modality of the robot; four motion perception neurons (DSN-L, DSN-R, LGMD1, LGMD2) are integrated into the robot vision system to discriminate between different motion cues, in order to invoke distinct behaviours for robot motion control.

advance the applications in vision-based artificial machines [55, 59].

On the aspect of visually guided behaviours, insects, like flies, can make correct and timely decisions corresponding to different behaviours, like collision avoidance and target tracking with agile movements in dynamic scenes, while the current mobile robots possess much weaker ability to deal with both motion perception and decision making, especially in dynamic scenes [59]. In this study, we aim to develop new methods to robotic vision mimicking insects' visual processing strategies, as illustrated in Fig. 5.9.

The LGMDs are large interneurons in the optical lobe of the locust that responds most strongly to fast and direct looming (approaching) objects [116]. Two LGMDs, i.e. LGMD1 and LGMD2, have been identified by biologists, computationally modelled and successfully applied for collision detection in ground vehicles (e.g. [161, 17]), and mobile robots (e.g. [8, 147, 21, 20, 85, 55]). However, through my proposed bio-robotic studies in Chapter 3, we found that the LGMDs-based collision detection models also respond to nearby translating objects very frequently. The behaviour of collision avoidance is usually triggered by these translational motion patterns, espe-

cially in dynamic robot scenes, the situation of which may rarely happen in insects [163].

To solve this problem, we have explored a neuromorphic solution motivated by the DSNs in flies' visual circuits in Chapter 4. These visual neurons are only sensitive to wide-field translational motion rather than proximity and recession of objects that move in depth [28, 58], which can be ideal neural systems to sense translating over looming objects. The computational visual neural networks proposed in Chapter 4 have demonstrated also the complementary functionality of DSNs to both the LGMD1 and the LGMD2 for motion perception and tracking.

Most importantly, via the experience of computationally modelling the LGMDs and the DSNs visual neural networks, we found conspicuous commonality between the model structures of the collision and the translating sensitive neural systems. These bio-plausible models can share similar signal processing strategies in the pre-synaptic areas. Recent biological studies have also demonstrated the common circuit design of motion detectors in different animal species [28, 58]. However, as mentioned in above chapters, these visual neurons each have unique DS to different motion features. More specifically, in locusts, the LGMD1 can respond to the looming of either lighter or darker objects compared to the background, while the LGMD2 is only sensitive to the looming of darker objects [116]. Such different collision selectivity has been achieved by the modelling of ON and OFF mechanisms, as discussed in Chapter 3. With similar ideas, the functionality of the DSNs in flies, with the DS to four cardinal directional translations, has been realised by the modelling of ensembles of HR detectors in separated ON and OFF pathways, as discussed in Chapter 4.

How these different modelled visual neurons collaborate on motion detection is thus attractive to us to construct a dynamic vision system for recognising more abundant motion features. Only a handful of case studies have shown potentials in incorporating different neural systems. Yue and Rind developed a model that combines the LGMD1 and the DSNs neural systems, both of which were inspired by the locusts' visual system, to improve the collision detection ability in complex and dynamic driving scenes [163]. A follow-up study demonstrated the prominent collision-detecting abili-

ty of the LGMD1 amongst relevant neural systems [26]. Another study demonstrated also the great potential of integrating the locusts' LGMD1 [7] and DSNs [25] neural networks for collision detection in driving scenarios, by dividing the field of view into sub-regions processed by different neurons [164]. These works mostly were validated by off-line experiments with video clips as inputs to models. They nevertheless lacked investigation on real-time tests in more complex and dynamic 'real' scenes.

In this research, we apply a bio-robotic approach, for the first time integrating visual neuron models inspired by the visual circuits of two insect species, to handle visual motion pattern extraction and recognition. Compared to previous relevant works, we will demonstrate the following contributions:

- The proposed bio-robotic approach yields simple and effective solutions for fast motion pattern extraction and recognition, which only requires a monocular camera and fewer computational storage capabilities than conventional robotic systems.

- The LGMD2 neural system can discriminate darker objects recession from looming well. In the ground robotic scenes, most objects are darker than backgrounds, the recession pattern thus can be properly recognised, via combining the LGMD2 model with the LGMD1 model.

- The two DSNs neural systems largely enhance the collision selectivity by extracting translational movements in two horizontal directions. With more defined motion features, the arena tests demonstrate a great improvement to former two relevant studies for collision detection in dynamic robot scenes.

The rest of this section is organised as follows: the proposed methodologies will be presented in Section 5.2.2. The robot experiments and results will be illustrated in Section 5.2.3. Finally, we conclude this study and give future works in Section 5.2.4.

5.2.2 Model Description

In general, the proposed embedded vision system consists of two main parts for visual motion extraction and motion pattern recognition. The former comprises four neuron

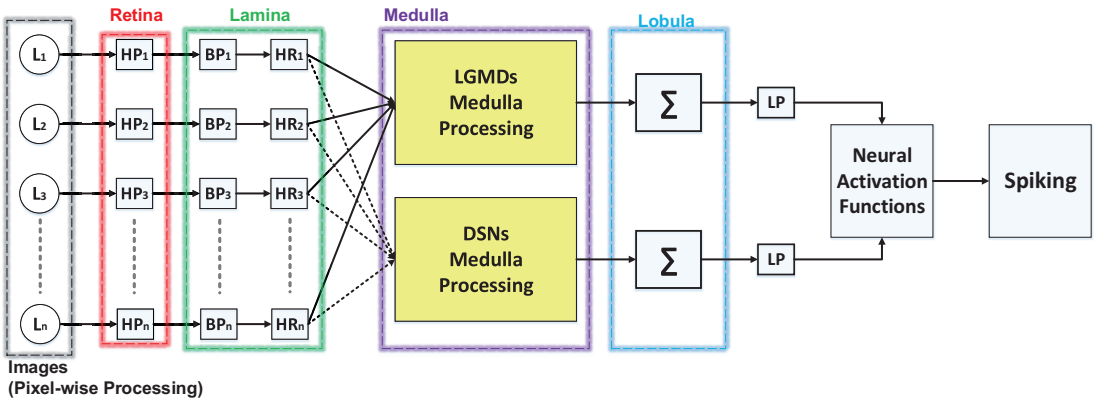

Figure 5.10: Schematic diagram of the synthetic motion sensitive system: the LGMDs and the DSNs models share the same visual processing in the Retina and Lamina layers; the different motion feature selectivity is generated in the Medulla layer by distinct spatiotemporal computations; the Lobula layer integrates local motion, spatially.

models with low-level spatiotemporal computations in a feed-forward structure. The latter is composed of a switch function and decision making mechanisms, for visually guided robot behaviours control.

With respect to my former studies on locusts' looming perception neurons in Chapter 3, and flies' translating perception neurons in Chapter 4, we highlight the functionality of separate ON and OFF visual pathways, encoding onset and offset response, respectively. Such ON/OFF mechanisms contribute significantly to separate the different looming selectivity between the LGMD1 and the LGMD2 neural systems in locusts, and match well the underlying signal processing circuits in the flies' preliminary visual system.

5.2.2.1 Motion Feature Extraction

The neural system for motion feature extraction is constituted by four computational neuropile layers. Very importantly, all four neurons possess mostly same spatiotemporal computation in the first two computational layers.

Computational Retina Layer In the first Retina layer, there are photoreceptors arranged in a 2D matrix form. As shown in Fig. 5.10, the photoreceptors retrieve grey-scale and pixel-wise luminance, then computes initially motion information by

first-order high-pass filters, temporally:

$$P(x,y,t) = L(x,y,t) - L(x,y,t-1) + \sum_{i}^{N_i} a_i \cdot P(x,y,t-i). \tag{5.4}$$

All notations are consistent with the former proposed algorithms in Chapter 3 and 4, which are not restated in this section and similarity for the following ones.

Computational Lamina Layer In the second Lamina layer, we apply band-pass filters to achieve the edge selectivity to motion features, as well as removing redundant environmental noise, spatially. Two linearly distributed Gauss kernels are used to convolve visual signals, so as to save computational power in case of limited computational resources:

$$P_{e/i}(x,y,t) = P(x,y,t) \overset{x,y}{*} W_{e/i}(x,y). \tag{5.5}$$

W_e, W_i are given in Table 5.4. In addition, the outer inhibitory kernel is with twice size of the inner excitatory kernel. The excitation is subtracted from the inhibition:

$$P^{'}(x,y,t) = P_e(x,y,t) - P_i(x,y,t). \tag{5.6}$$

After that, there are ON and OFF polarity interneurons splitting visual information into parallel ON and OFF channels, encoding onset and offset responses, respectively, by the mechanism of half-wave rectifier:

$$\begin{aligned} P_{on}(x,y,t) &= (P^{'}(x,y,t) + |P^{'}(x,y,t)|)/2, \\ P_{off}(x,y,t) &= |(P'(x,y,t) - |P^{'}(x,y,t)|)|/2. \end{aligned} \tag{5.7}$$

In this bio-robotic study, we also adopt a bio-plausible mechanism to realise an 'adaptation state', with a fast onset and slow decay characteristic, which significantly reduces noise in time. Let X, Y be short for $P_{on/off}(x,y)$ and delayed signal $D_{on/off}(x,y)$, the mathematical expression of the temporal mechanism is as follows:

$$dY(t)/dt = \begin{cases} (X(t) - Y(t))/\tau_1, \text{ if } dX(t)/dt \geq 0 \\ (X(t) - Y(t))/\tau_2, \text{ if } dX(t)/dt < 0 \end{cases}. \tag{5.8}$$

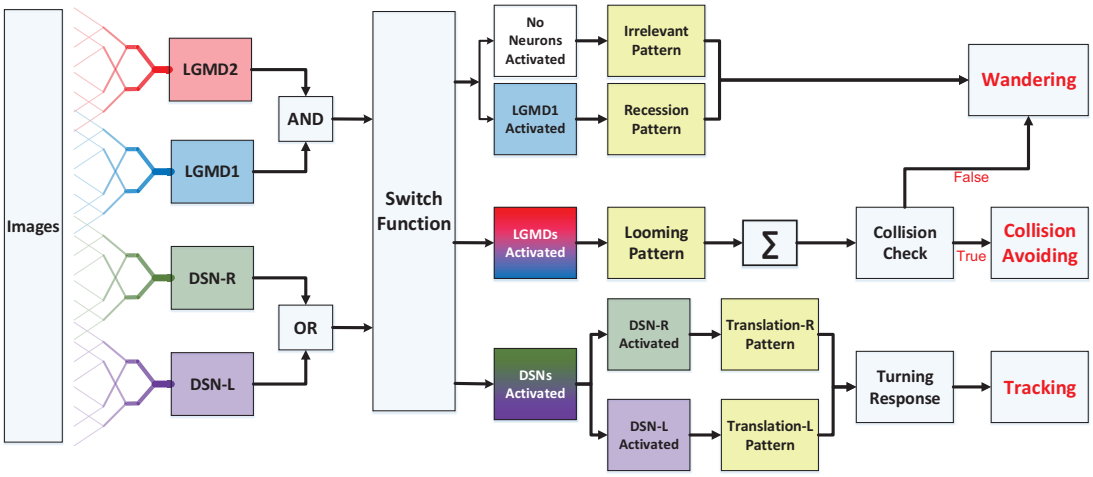

Figure 5.11: Diagram of the motion pattern recognition strategy, including motion feature extraction by four neurons, recognition and decision making mechanisms, as well as corresponding robot behaviours.

τ_1 and τ_2 are given in Table 5.4. Then, the filtered signal is subtracted to the original one:

$$\begin{aligned} F_{on}(x,y,t) &= P_{on}(x,y,t) - D_{on}(x,y,t), \\ F_{off}(x,y,t) &= P_{off}(x,y,t) - D_{off}(x,y,t). \end{aligned} \tag{5.9}$$

Computational Medulla Layer The third computational Medulla layer is of great importance in generating different motion feature selectivity or proposed DS. Concretely, the LGMD1 and the LGMD2 neurons are directionally selective to movements in depth, i.e. looming and recession, while the DSN-R and the DSN-L neurons are directionally selective to movements in two horizontal directions, i.e. rightward and leftward translations. Intuitively, the functionality of the DSNs provides perfect complement to the functionality of the LGMDs. Moreover, in comparison with former hybrid models [164, 26, 163], the specific looming selectivity of the LGMD2 neuron to darker objects only can advance the discrimination between looming and recession movements in ground robotics scenes.

First, for the modelling of LGMDs, both neurons detect potential collision by reacting to expanding edges of objects. In the ON pathway, the inhibition is formed by convolving surrounding delayed excitations, while in the OFF pathway, the excitation is formed by convolving surrounding delayed inhibitions. There are local summation

cells integrating the local excitations and inhibitions from the dual-pathways:

$$\begin{aligned} S_{on}(x,y,t) &= F_{on}(x,y,t) - w_1 \cdot D'_{on}(x,y,t) \overset{x,y}{*} W_l(x,y), \\ S_{off}(x,y,t) &= D'_{off}(x,y,t) \overset{x,y}{*} W_l(x,y) - w_2 \cdot F_{off}(x,y,t). \end{aligned} \tag{5.10}$$

W_l, w_1 and w_2 are given in Table 5.4. $D'_{on/off}$ is delayed by $F_{on/off}$ similarly to Eq. 5.8. Importantly, the following interactions between ON and OFF summation cells realise the different looming selectivity between LGMD1 and LGMD2 neurons:

$$S = \theta_1 \cdot S_{on} + \theta_2 \cdot S_{off} + \theta_3 \cdot S_{on} \cdot S_{off}. \tag{5.11}$$

In case of the modelled LGMD2 neuron, the excitations from the ON channels are rigorously suppressed, forming the looming selectivity to dark objects only.

Second, on the aspect of modelling the DSNs, we design ensembles of ON/OFF local motion detectors, each combination of which is composed of a pairwise HR detectors:

$$\begin{aligned} ON(x,y,t) &= \sum_{i=d}^{d \cdot N_c} (D'_{on}(x,y,t) \cdot F_{on}(x+i,y,t) - D'_{on}(x+i,y,t) \cdot F_{on}(x,y,t)), \\ OFF(x,y,t) &= \sum_{i=d}^{d \cdot N_c} (D'_{off}(x,y,t) \cdot F_{off}(x+i,y,t) - D'_{off}(x+i,y,t) \cdot F_{off}(x,y,t)). \end{aligned} \tag{5.12}$$

As the robot can only move on a 2D surface, we only calculate the directional motion in two horizontal directions. Compared to the LGMDs model, the spatiotemporal computations in Eq. 5.12 can realise the DS to translations versus looming and recession features.

Computational Lobula Layer In the Lobula layer, both the DSNs and the LGMDs neuron models integrate all local motion signals from the ON and OFF visual pathways, linearly and spatially. After that, the global excitations are transformed to the membrane potential via sigmoid functions $f(x) = (1 + e^{-|x|/(n \cdot K_{sig})})^{-1} - \Delta_C$, as the neural activation functions in Fig. 5.10. The outputs of the LGMD1 and the LGMD2 neurons are both normalised within $[0.5, 1)$, whilst the outputs of the DSN-R and the

DSN-L neurons are normalised within $[0, 1)$ for PD motion and $(-1, 0]$ for ND motion, respectively.

Spiking Mechanism In this bio-robotic approach, we implement these four visual neurons as spiking neurons. The SMPs are transformed to spikes at each frame, exponentially:

$$S^{spike}(t) = \left\lfloor e^{[K_{sp} \cdot (U(t) - T_{sp})]} \right\rfloor . \tag{5.13}$$

5.2.2.2 Motion Pattern Recognition

Generally speaking, we highlight a neural competition between the LGMDs and the DSNs in the motion pattern recognition mechanisms. The activation of either DSN-R or DSN-L neurons will rigorously inhibit both the LGMD1 and the LGMD2 neurons, and vice versa. As shown in Fig. 5.11, the generated spikes of these four neurons are conveyed to logical operations and a switch function, which generates three outcomes:

1. The situations of no neurons activated or LGMD1 neuron activated only, correspond to an **'irrelevant motion pattern'** or a potential **'recession pattern'**, respectively, followed by a **'wandering'** state for robot motion.

2. Once the LGMDs win the competition with higher spiking rate, a potential 'looming pattern' is recognised. However, a confirmation of collision detection should meet the following requirement:

$$Col(t) = \begin{cases} \text{true, if } \sum_{i=t-N_t}^{t} S^{spike}(i) \geq N_{sp} \\ \text{false, otherwise} \end{cases} . \tag{5.14}$$

   If the collision is verified, an **'avoidance'** behaviour will be triggered; otherwise, the robot will remain wandering.

3. If the DSNs represent higher spiking frequency, either a **'rightward translation'** or a **'leftward translation'** pattern is recognised, corresponding to a TR

Table 5.4: Predefined Parameters for the Proposed Synthetic Neural System

Name	Value	Name	Value	Name	Value
N_c, d	$2 \sim 4$	K_{sp}	$1 \sim 6$	$W_{e/i}$	$1/(4 \sim 128)$
W_l	$1/(4 \sim 8)$	w_1	0.3	N_i	2
τ_1	1	τ_2	100ms	K_{sig}	$0.1 \sim 0.6$
Δ_C	$0 \sim 1$	w_2	0.6	σ_1	15
θ_1, θ_2	$0 \sim 1$	θ_3	0	τ_3	10
τ_s	$10 \sim 200$	g_v	1	g_w	10
T_{sp}	$0.2, 0.7$	n	99×72	N_{sp}, N_t	$6, 4$

computed as follows:

$$\begin{aligned} &TR(t) = \sigma_1 \cdot U^{dsn}(t), \\ &\text{then, } d\{TR'(t)\}/dt = (TR(t) - TR'(t))/\tau_3. \end{aligned} \tag{5.15}$$

As a result, a **'tracking'** behaviour will be triggered, immediately.

5.2.2.3 Robot Motion Control

On the aspect of motion control strategies, a robot agent is given an initial speed v_i. If the current robot state is either the **'wandering'** or the **'tracking'**, the motor powers of the right (P_R) and left (P_L) wheels can be described as follows:

$$\begin{aligned} P_R(t) &= g_v \cdot v_i(t) - g_w \cdot TR'(t), \\ P_L(t) &= g_v \cdot v_i(t) + g_w \cdot TR'(t), \end{aligned} \tag{5.16}$$

where g_v and g_w are gain values that control motion efficiency. Otherwise, if the robot state is the **'collision avoiding'**, we implement a motion sequence in the robot agent to turn around with a radian over π, randomly to the left or right.

5.2.2.4 System Configuration

For the system configuration, this synthetic neural model has a relatively higher degree of computational complexity compared to the proposed embedded vision systems in Chapter 3 and 4, since this processes four modelled visual neurons. Therefore, to fulfil the requirements of real-time in-chip visual processing, all the model parameters were decided empirically according to the implementation and optimisation in *Colias*.

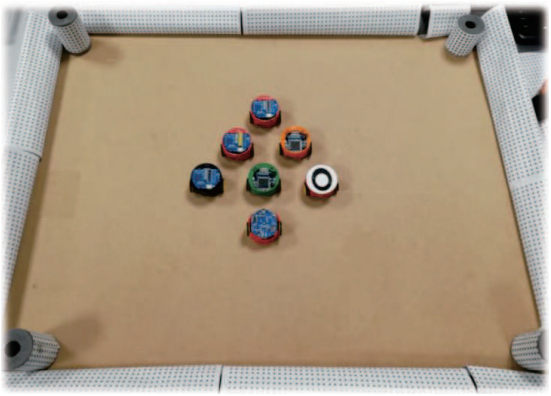

Figure 5.12: Illustration of the small arena and several micro-robots *Colias* used in the bio-robotic tests.

Table 5.4 lists the selection of parameters in this study. More specifically, the spiking thresholds for the LGMDs and the DSNs neural systems are 0.7 and 0.2, respectively. Importantly, these spiking thresholds and scale parameters K_{sig} in the neural activation functions, K_{sp} in the spiking mechanism greatly affect the spike frequency of these visual neuron. Some parameters could also vary within specific ranges. In this bio-robotic approach, we do not apply any learning methods or feedback control. Like the former proposed dynamic vision systems, this processes visual signals in a feed-forward structure.

The only sensor used in this research is the monocular camera in the vision board of *Colias* robots. We also used a Bluetooth device like the research proposed in Section 5.1, which is connected with the upper board, to retrieve real-time data from the robot. The frame rate of the embedded vision system can reach between $25 \sim 35$Hz, which well fits the requirement of most real-time visual tasks.

In designed arena tests with multi-robots, we also built a small arena for conducting dynamic robot scenes in arena tests and investigate the model performance in high-density robots scenarios. As illustrated in Fig. 5.12, the arena is with $70 \times 55cm^2$ in acreage. Peripheries of the arena were decorated with specific patterns, as textures for visual motion sensing.

5.2.3 Experiments and Results

In this subsection, this thesis presents the robot experiments and analyse the results. There are mainly two categories of tests: in the open-loop tests, we will firstly demon-

strate the neural response of different visual neurons to the four basic motion patterns, as illustrated in Fig. 5.13 and 5.14. To verify the effects of four neurons on different motion pattern extraction and recognition, we will demonstrate also the statistical investigation on activations (spiking rates) of these neurons, which are challenged by the four kinds of robot movements, at different constant speeds, repeatedly and separately in Fig. 5.15, 5.16, 5.17 and 5.18. Moreover, we will investigate the influence of angular approaching movements on motion pattern recognition, which are also frequent visual challenges to robots in dynamic scenes, in Fig. 5.19.

In the second type of tests, we will demonstrate the arena tests, with multiple *Colias* robots, forming the dynamic robot scenes in the small arena. To highlight the achievements of this bio-robotic approach, we will compare the success rate of collision detection with two former relevant studies [21, 55], with new motion patterns defined. More precisely, the translations are identified as non-collision events under identical robot densities. We also look deeper into the effect of robot density on the hybrid neuron model performance in collision detection. We recorded each test in order to calculate the statistics. Some video snapshots of the arena tests, captured by a top-down camera are shown in Fig. 5.20. The success rates of different events in arena tests are given in Table 5.5.

5.2.3.1 Open-loop Robot Tests

In the open-loop tests, we first demonstrate the neural responses of the LGMD1, LGMD2 and two DSNs sub-systems, challenged by the four basic motion patterns. We collected the neural outputs of each modelled neuron including spikes and SMPs, remotely through the Bluetooth device on the motionless stimulated robot, as shown in Fig. 5.12. Another *Colias* robot was used as the visual stimulus.

The results shown in Fig. 5.13 and 5.14 verify the complementary functionality of the LGMDs to the DSNs models. It is necessary to emphasise that the DSN-R and the DSN-L neurons are activated by positive and negative neural outputs of the DSNs sub-system, respectively. Compared to previous studies on integrating different insect visual neurons [26, 163], for the first time the LGMD2 model is incorporated in such

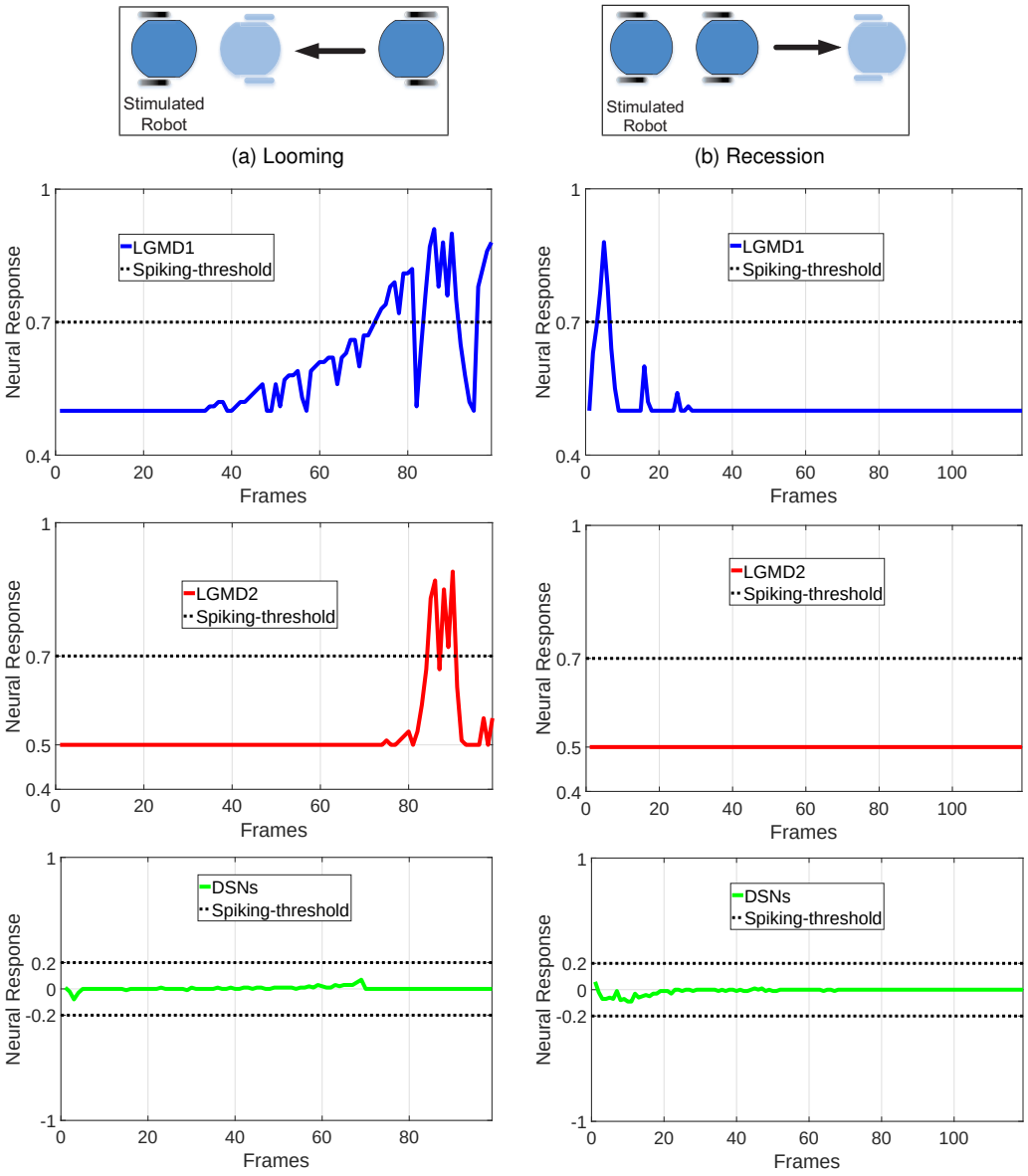

Figure 5.13: Neural responses of four visual neurons in the synthetic neural system challenged by a *Colias* robot (a) looming and (b) recession: X-axis indicates time window in frames, and Y-axis shows SMPs.

a synthetic neural system. The LGMD2 neuron has no response to the recession of darker objects compared to the background, which can be an ideal model for ground robotic vision system [21]. Interestingly, combining the functionality of the LGMD2 with the LGMD1 neural systems and a logical 'AND' operation can well recognise a recession pattern.

Moreover, we demonstrate the effects of each modelled spiking neuron on recognising different motion patterns. Intuitively, the statistical results in Fig. 5.15, 5.16, 5.17 and 5.18 demonstrate that the DSNs neurons spike at much higher rate than the LGMDs neurons, when challenged by translations from slow to fast speeds, respec-

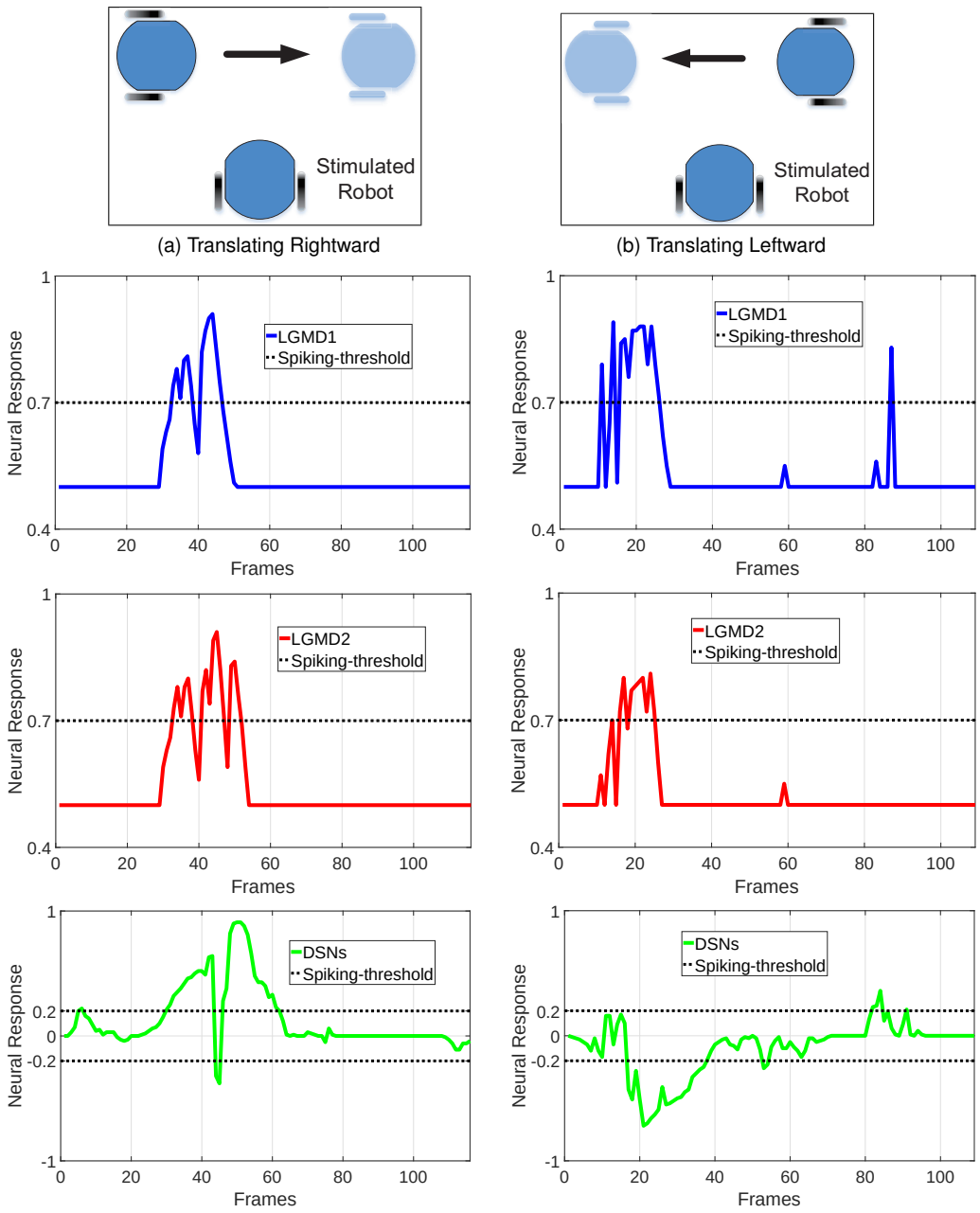

Figure 5.14: Neural responses of four visual neurons in the synthetic neural system challenged by a *Colias* robot (a) translating rightward and (b) leftward.

tively. More concretely, the DSN-R and the DSN-L rigorously spike at high rate by the rightward and leftward translations, respectively, even tested by very fast movements. On the other hand, the LGMDs are activated by fast approaching and also the nearby translations, while both are not activated by the looming at very slow speed ($3cm/s$ in my case). The LGMD1 normally spikes at higher rate than the LGMD2. However, the LGMD2 remains quiet during the robot recession, but the LGMD1 is not. In the switch function of the embedded vision system, the activation of DSNs will rigorously inhibit the LGMDs, and vice versa. Therefore, the results reveal great potential in enhancing

the collision selectivity and adding in new object tracking behaviour tested in dynamic robot scenes.

Furthermore, from my previous studies proposed in Section 5.1, we observed that the movements of angular approaching frequently happens to a vision-based agent in dynamic robot scenes. These visual stimuli usually activate the LGMDs neurons and trigger the collision avoidance behaviours. In this bio-robotic study, we also investigate the influence of angular looming on the motion pattern recognition. The experimental setting is shown in Fig. 5.19a. Each angular looming was repeated ten times. Similarly to the statistical tests in Fig. 5.15, the spikes count corresponds to the spike frequency during each motion course with an approximately identical speed. The statistics in Fig. 5.19b demonstrates that the two DSNs sub-system are more sensitive to the angular looming from large angles than the two LGMDs sub-system, corresponding to the results in Fig. 5.15. More precisely, the angular approaching from the left side of the view field gives rise to a rightward translation pattern, so that highly activated the DSN-R. The angular approaching from the right side of view thus corresponds to a leftward translation pattern, which is attractive to the DSN-L. As a result, the proposed synthetic neural vision system shapes the collision selectivity of the LGMDs to direct or small angular looming only.

In Chapter 3, we have proposed two intrinsic bio-plausible mechanisms, i.e. the ON/OFF and the SFA mechanisms, to shape the LGMDs' looming selectivity. In this bio-robotic study, it appears that the visual neurons that possess different DS can co-operate to enhance the selectivity to specific motion patterns, e.g. the collaboration between DSNs and LGMDs is an effective approach to enhance the looming selectivity of LGMDs to approaching objects. This may explain the generation of DS diversity in insects.

5.2.3.2 Arena Tests

In the second part of robot tests, we investigate the effectiveness of the proposed method in dynamic robot scenes. We designed arena tests and compared the proposed model performance with two former studies: a neural system with the LGMD2

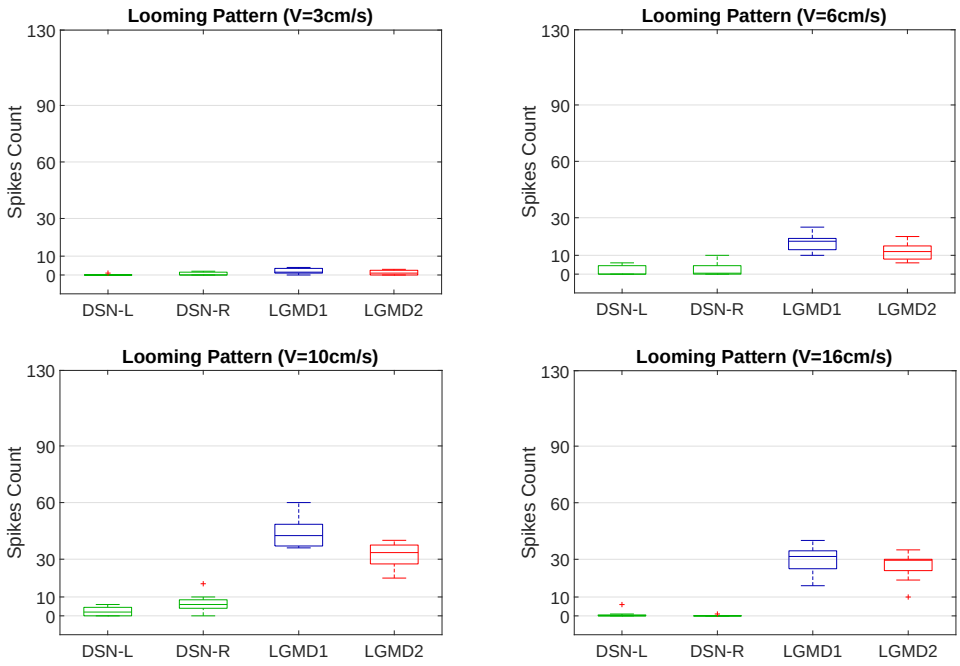

Figure 5.15: Statistics of the spike frequency in the open-loop tests on **looming pattern** at four constant speeds, respectively, each throughout ten repeated tests: the spikes during each course are accumulated.

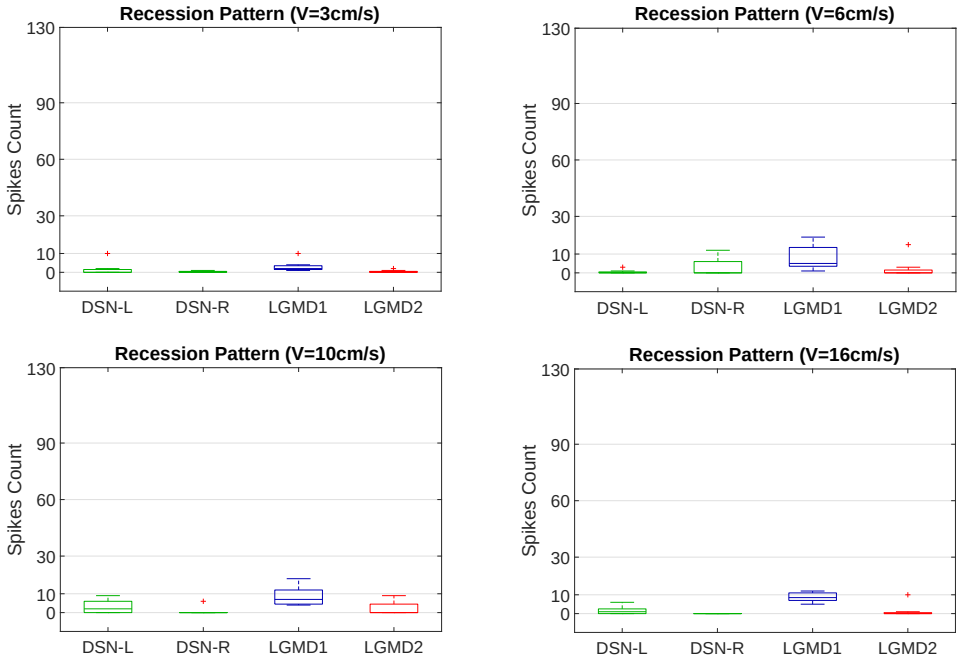

Figure 5.16: Statistics of the spike frequency in the open-loop tests on **receding pattern**.

neuron only [21], and a hybrid model with both LGMDs neurons [55], for the purpose of examining the enhanced looming selectivity with more motion features defined. In addition, two robot densities were investigated. The multiple *Colias* robots moved concurrently in the small arena at two tested speeds (6 and 10cm/s), respectively and

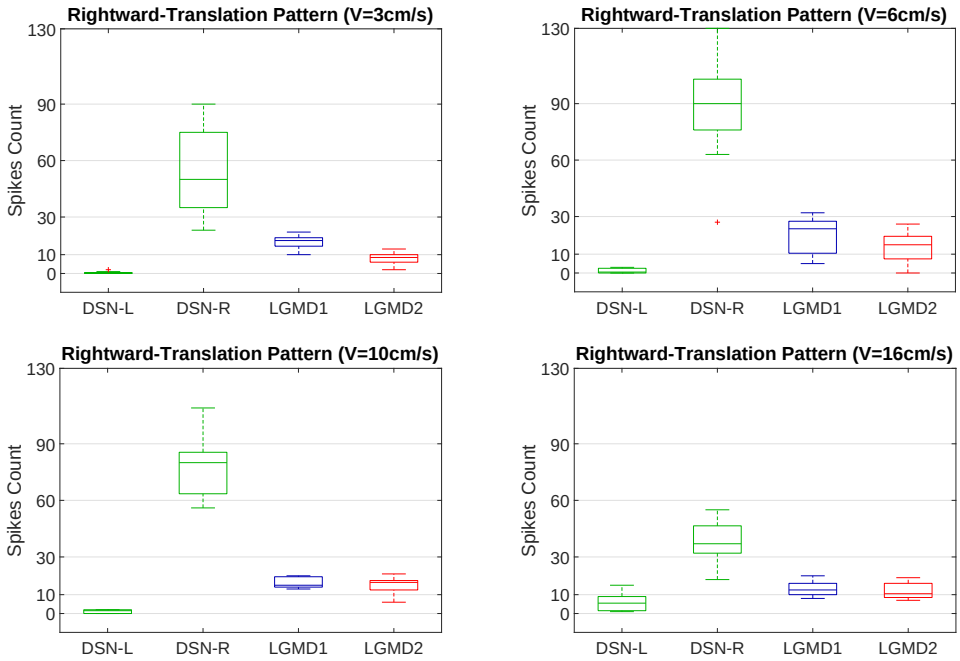

Figure 5.17: Statistics of the spike frequency in the open-loop tests on **rightward translating pattern**.

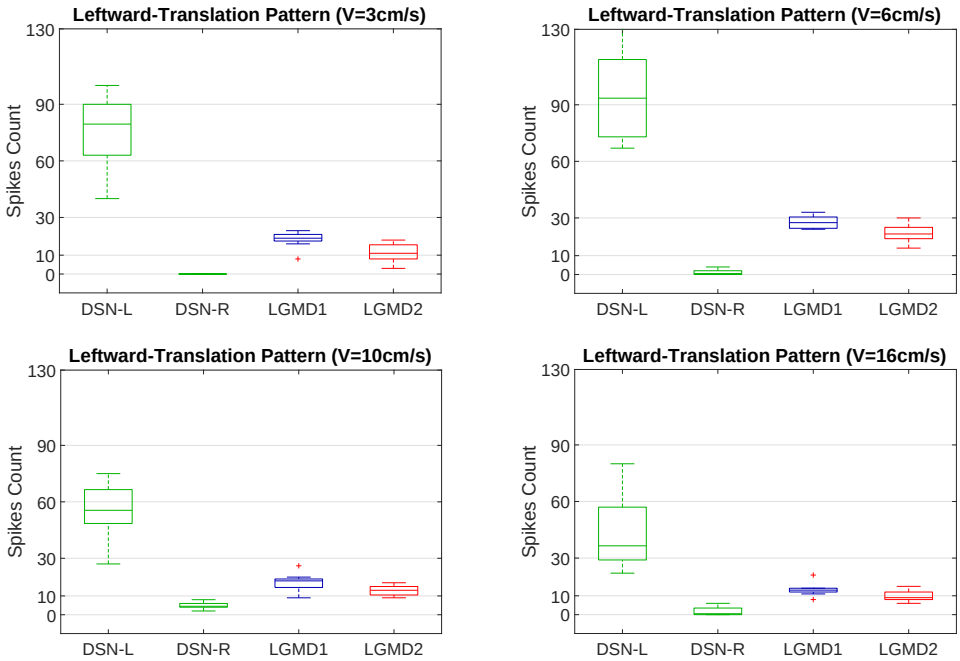

Figure 5.18: Statistics of the spike frequency in the open-loop tests on **leftward translating pattern**.

each lasting for one hour. We recorded the arena tests using a top-down camera and applied a robot localisation system [56].

The snapshots shown in Fig. 5.20 demonstrate some key events in the arena tests. Most importantly, since we added in new motion features in this research, we defined a new criterion to calculate the success rate, as shown in Table 5.5. Intuitively, in case of

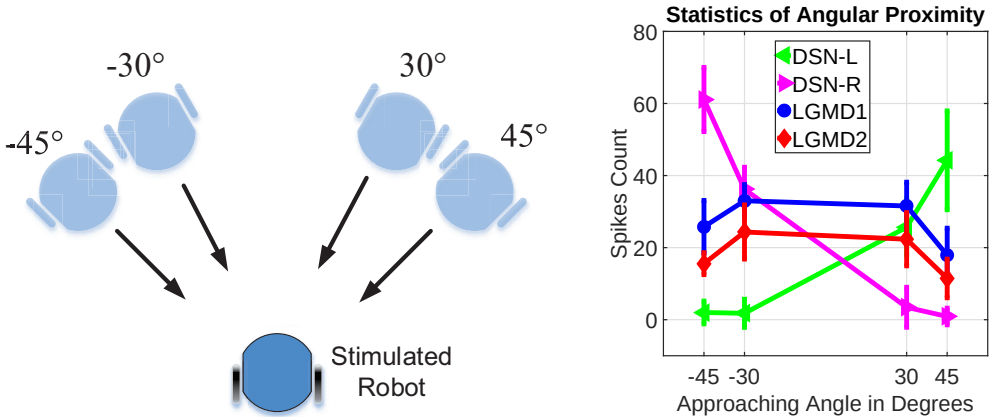

(a) experimental setting (b) spike rate

Figure 5.19: Statistics of the systematic robot angular-approaching tests: spikes are generated by the stimulated *Colias*.

Table 5.5: Success Rates of Looming Recognition in Arena Tests

Events: Colliding with Robots/Peripheries(CwR/CwP) Avoiding Looming/Translating Robots(ALR/ATR) or Peripheries(AP) SR1=AP/(AP+CwP)·100%, SR2=ALR/(ALR+ATR+CwR)·100%		
Neural Systems (4-Robots Scenes)	SR1	SR2
LGMD2	96.7%	80.0%
LGMD1 & LGMD2	88.1%	73.9%
LGMDs & DSNs	**90.3%**	**87.3%**
Neural Systems (7-Robots Scenes)	SR1	SR2
LGMD2	95.0%	75.2%
LGMD1 & LGMD2	81.7%	67.8%
LGMDs & DSNs	**83.4%**	**90.6%**

collision avoidance to moving robots, the proposed approach shows much higher success rates than the former comparative models tested at different speeds and densities of robots in dynamic robot scenes. It also appears that the proposed model is weaker in collision avoiding to the peripheries of the arena compared to the comparative LGMD2 model. The reason is that some angular approaching to the periphery patterns could highly activate the DSN-R or the DSN-L, so that inhibiting both the LGMDs neurons. Interestingly, another achievement of this bio-robotic approach is that we realise a tracking behaviour for micro-robots by the spiking DSNs and corresponding motion control in dynamic robot scenes.

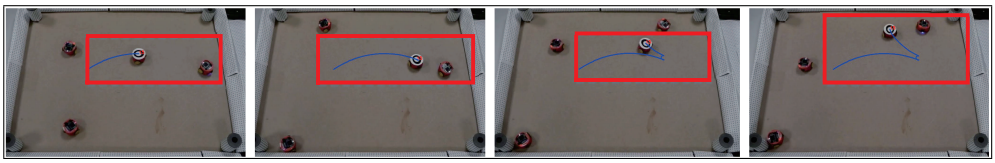

(a) collision avoidance

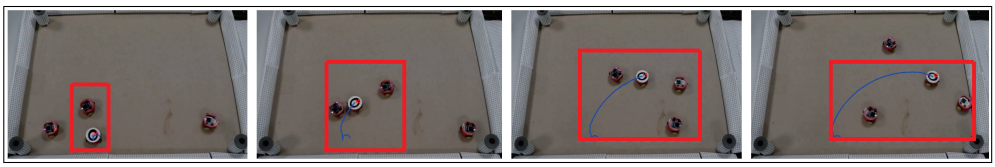

(b) tracking a translating robot

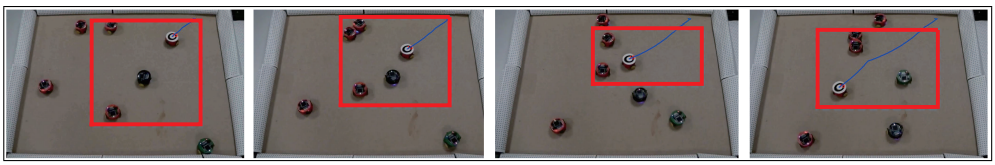

(c) non-collision with a translating robot

Figure 5.20: Snapshots of the arena tests captured by a top-down camera to demonstrate the robot-to-robot events: a multi-robots localisation algorithm [56] tracks the moving of ID-specific patterns on the top of each tested *Colias*. Red rectangles highlight the location where an event happens.

5.2.4 Summary

In this section, this dissertation has presented a synthetic neural network on the embedded system in autonomous mobile robots, for fast motion pattern recognition in dynamic robot scenes mixed with multiple agents. The novelty of the proposed bio-robotic approach is the design of collaboration of four modelled motion sensitive neurons motivated by insects' visual systems. The LGMDs neurons in locusts respond most strongly to looming objects, whilst the combination of LGMD1 and LGMD2 models can discriminate well between the looming and recession of darker objects. On the other hand, the DSNs in flies are only sensitive to translational motion. The perfectly complementary functionality of these modelled neurons significantly advance the modelling of motion perception system with the recognition of more abundant motion features for utility in artificial machines even with very limited computational resources, like our proposed *Colias* micro-robots.

We have demonstrated the specific characteristics of each neuron in the open-loop robot tests. The high spike frequency or activation of each neuron corresponds to a specific motion pattern. In addition, we control robot motion behaviours in a simply logical tree corresponding to the spiking frequency of four motion perception neurons.

This works effectively to indicate the recognition of specific motion patterns. Our arena tests with multi-robots have validated this approach. Moreover, compared with two former studies, we verified the enhanced collision selectivity of this neural system with higher collision-detecting SR by extracting new motion features.

In the future work, we will continue incorporating other bio-inspired modelled visual neurons in the synthetic neural system with more motion features extracted to enrich the 'library' of preliminary motion patterns. For example, as presented in Section 2.4, there are also specific neurons which are only sensitive to small target movements. Moreover, we will test the proposed approach with other mobile robot platforms or vehicles in more dynamic and complex real physical scenes. Our goal is to build low-cost, low-power and reliable neuromorphic sensors using these bio-inspired visual processing methodologies in the near future.

5.3 Further Discussion

In the above two Sections 5.1 and 5.2, we have discussed the integration of different bio-inspired motion sensitive models with specific DS, and demonstrated the efficacy in vision-based robotic applications. Since these computational models are flexible and low-energy consumptive, they can be also good candidates in the domains of computer vision and image processing for motion detection. Therefore, it is worth looking into the cooperation of bio-inspired motion detectors and traditional computer vision methodologies like the segmentation and registration based strategies for motion detection and applications to machine vision. To the best of our knowledge, there are very few computational modelling works and applications in the literature that have touched upon mixed categories in computer vision for visual motion sensing.

A recent case study of our relevant research has successfully combined two vision models from mixed categories: a bio-inspired collision avoidance LGMD1 model and a segmentation based target following model to form a hybrid visual based model for robot control [259]. This research has demonstrated the bio-inspired motion perception models can cooperate with other visual systems to achieve multi-tasks.

5.4 Chapter Summary

Within this chapter, this thesis has presented the computational modelling of hybrid neural vision systems through previous research on the looming perception LGMDs models in Chapter 3 and the translating sensing visual neural networks in Chapter 4. This has firstly proposed an unified looming sensitive model combining an LGMD1 and an LGMD2 neuron models with a bilateral visuomotor control for reactive collision avoidance in Section 5.1. Then, a synthetic hybrid motion sensitive neural model has been introduced which integrates the proposed LGMD1, LGMD2 and DSNs for fast motion pattern extraction and recognition in dynamic scenes in Section 5.2.

These bio-inspired hybrid visual models have all been satisfactorily realised on the embedded system for on-board real-time visual processing. The bio-robotic arena tests have verified both the efficiency and effectiveness in visual based tasks including collision avoidance and motion tracking. More specifically, in Section 5.1, the different neural characteristics of modelled LGMD1 and LGMD2 neurons have been illustrated, clearly. In Section 5.2, with more motion features extracted, the proposed hybrid model enables small mobile robots to run together in a small arena free of collision. The collision selectivity has been enhanced by the coordination between the LGMDs and the DSNs. In addition, the *Colias* robots can recognise different preliminary motion patterns corresponding to distinct behaviours, timely.

Animals are very smart to recognise diverse motion patterns in an unpredictable environment with agile movements; however, the performance of current state-of-the-art vision based artificial machines is far from acceptance. The modelling of biological visual systems may give us chances to move forward towards robust dynamic vision systems for future machine vision techniques. In the future work, these models need further test on plentiful mobile platforms and in intricate and more dynamic real-world scenarios. Learning methods are also necessary to be introduced into a flexible dynamic vision system handling multi-tasks.

Chapter 6

Conclusions and Future Work

Within this chapter, this dissertation is to be concluded. This first concludes main features of each proposed neuron model or neural network, and then points out possible future work on the modelling of insect visual systems with potential applications to hardware.

6.1 Conclusions

In nature, insects are prominent model systems to study visual motion perception strategies. Compared to vertebrates and humans, insects have tiny brains and compact visual systems for motion detection. Their robust motion vision systems enable them to survive more easily in every aspects of life from avoiding predators and chasing mates to foraging and etc. It is amazing that such motion perception abilities and corresponding behaviours can be accomplished by only hundreds or thousands of neurons in insects' visual brain. However, the underlying neural processing mechanisms remain largely unknown until today. While the biological substrates are elusive, the computational modelling and empirical studies are particularly useful to simulate unknown signal processing neurons or circuits. In addition, these computational models can be tested by bio-robotic approaches under similar conditions to ethological or physiological tests, which may provide meaningful implications to biologists via implementing visual processing algorithms in artificial machines and mimicking visually conducted behaviours in real world.

From the perspective of a neural system modeller, this thesis has provided effective approaches to construct underlying mechanisms, pathways and neurones in insect visual systems for motion perception. This has focused on the modelling of locust looming sensitive and fly translating sensitive neural networks. After that, this has preliminary investigation on integration of multiple neural systems for diverse motion patterns recognition. All these computational models of insect visual systems have been satisfactorily realised on the embedded system in a vision-based ground micro-robot. These models have provided possible solutions to mobile robots for motion perception in a both timely and reliable mode, which require only a monocular camera and low-energy consumption. Moreover, the neural computation in these motion perception models will significantly facilitate our understanding of the very complex biological visual systems. These models may give useful suggestions to build robust and energy-saving dynamic vision systems for future artificial machines like autonomous robots and vehicles. The computational modelling of animals' visual systems with bio-robotic approaches can also promote the collaborative research between the neuroscience and the robotics and relevant fields of study.

6.1.1 Summary of Chapter Contents

Within this subsection, the main contents in each chapter are summarised. Chapter 1 has introduced the research background including current-stage challenges and motivations to computationally model insect visual systems, as well as research contributions. Chapter 2 has reviewed computational models and applications of insect visual systems. Chapter 3 has proposed the computational modelling of two locust looming perception neurones – LGMD1 and LGMD2, with a novel bio-plausible structure of ON and OFF pathways. After that, in Chapter 4, the ON and OFF pathways have been constructed to realise translational motion perception visual neural networks inspired by fly visual systems; a behavioural response to fixation has also been accomplished. In Chapter 5, based on modelling studies on motion sensitive neural systems with different direction selectivity, the integration of fly and locust visual neural networks has been investigated for diverse motion patterns recognition in dynamic robot scenes.

Chapter 6 concludes this dissertation and discusses future work.

6.1.2 Summary of Model Features

In this subsection,the main features of each proposed computational model of insect motion sensitive neural systems are emphasised as follows:

- Chapter 3 has proposed the computational modelling of locust looming detectors, i.e. LGMD1 and LGMD2. Compared with previous related LGMD models, the core of both LGMDs model is the ON and OFF visual pathways that separate visual processing into parallel channels depending on light-on and light-off responses. Importantly, such a structure can well separate the looming selectivity between the LGMD1 and the LGMD2 neurones revealed by biologists. Therefore, a general LGMDs model has been proposed which can realise the characteristics of both LGMDs. In addition, an SFA mechanism has also been computationally modelled before the spike coding to further enhance the collision selectivity to objects that approach rather than other visual challenges. Compared to segmentation and/or registration based computer vision techniques for collision detection, the proposed bio-inspired models process visual information with low-level spatiotemporal computation in a feed-forward structure. These detect potential collision by reacting to the expanding edges of objects.

- The proposed DSNN in Chapter 4 is also featured by the ON and OFF pathways for translational motion perception. This neural network simulates thoroughly the visual processing within the fly preliminary motion vision pathways explored in latest biological researches. According to current challenges, in this modelling study, we have emphasised the importance of signal pre-filtering in a both spatial and temporal manner to improve the model performance especially in real-world scenarios with lots of background noise. The classic HR detectors are modelled in the ON and OFF parallel pathways. Compared with former related translating sensitive neural systems like the EMDs, the proposed DSNN is characterised by ensembles of ON-ON and OFF-OFF local motion detectors within the dual-pathways, which represent better speed response to translating

objects. In addition, this model has been extended to mimic an insect behavioural response from the open-loop motion tracking to the closed-loop fixation.

- The proposed hybrid neural vision systems in Chapter 5 have the specific DS to all proposed neuron models including the LGMD1, the LGMD2 and the DSNs. More precisely, the hybrid LGMDs model can realise the functionality of both LGMD1 and LGMD2 with a bilateral motion control strategy for reactive collision avoidance in ground mobile robots. And the hybrid LGMDs and DSNs agent is able to quickly recognise multiple motion patterns in dynamic robot scenes.

6.2 Future Work

This research opens several directions for future work:

- Originated from biological researches in insects visual systems, these computational models have demonstrated similar visual processing systems to insects. However, the biological neural responses of the looming and translating sensitive neurons to various kinds of movements have not been fully achieved by current proposed models. For example, the biological LGMD1 neuron can recognise looming embedded in dynamic visual clutter [5], yet the proposed models can not fully represent that which are restricted by the degree of complexity of background motion. A probable solution is to improve the lateral inhibition mechanism like enlarging the inhibiting area to shape the selectivity. In addition, the biological visual systems still remain largely unknown. In our opinion, the state-of-the-art bio-inspired models should be consistent with latest biological findings. Specifically for insects, there is no (or little) evidence showing how different kinds of visual neurons are coordinated in motion detection. The proposed synthetic hybrid neural systems (in Chapter 5) are constructed with our speculations and for the purpose of implementing fast motion pattern recognition and corresponding visually guided behaviours within dynamic scenes, like real insects.

- From a computational modeller's perspective, although this thesis has demonstrated the efficacy and efficiency of proposed neuron models or neural networks for motion perception; these models in fact need further testing or challenge on more abundant mobile platforms like UAVs, ground vehicles and other kinds of vision-based mobile robots, as well as in more complex scenes like driving scenarios. These computational models process visual information in a feed-forward structure; however, in insect visual systems, there are probably feedback signal processing to 'train' these spiking neurons. A 'real' intelligent dynamic vision system should be able to adaptive to different visual environments very quickly. Therefore, We will continue investigating learning methods to current proposed models. Furthermore, there are also similar motion sensitive neurons in invertebrates like the crabs, the computational modelling of which may learn from the proposed bio-inspired methods.

- From an engineering point of view, to achieve higher processing speed, larger scale or real-time visual processing solutions, the implementation of neuromorphic visual models on hardware could be extremely advantageous. Taking advantage from the compact design and low power consumption of bio-inspired visual models, the proposed dynamic vision systems could be built as neuromorphic visual sensors, either as single-chip solutions featured by the compact size and specialised functions (e.g. CMOS VLSI process), or high performance circuits such as the FPGA. These could be future trends of hardware realisation of visual processing.

Bibliography

[1] "Solved: the mystery of why locusts swarm." https://www.independent.co.uk/news/science/solved-the-mystery-of-why-locusts-swarm-1520409.html.

[2] F. C. Rind and P. J. Simmons, "Seeing what is coming: Building collision-sensitive neurones," *Trends in Neurosciences*, vol. 22, no. 5, pp. 215–220, 1999.

[3] F. Gabbiani, H. G. Krapp, C. Koch, and G. Laurent, "Multiplicative computation in a visual neuron sensitive to looming," *Nature*, vol. 420, no. 6913, pp. 320–324, 2002.

[4] S. Peron and F. Gabbiani, "Spike frequency adaptation mediates looming stimulus selectivity in a collision-detecting neuron," *Nat Neurosci*, vol. 12, no. 3, pp. 318–326, 2009.

[5] J. M. Yakubowski, G. A. Mcmillan, and J. R. Gray, "Background visual motion affects responses of an insect motion-sensitive neuron to objects deviating from a collision course," *Physiological Reports*, vol. 4, no. 10, p. e12801, 2016.

[6] S. Yue and F. C. Rind, "Collision detection in complex dynamic scenes using a LGMD based visual neural network with feature enhancement," *IEEE Trans. Neural Netw.*, vol. 17, no. 3, pp. 705–716, 2006.

[7] Y. Shigang and F. C. Rind, "A collision detection system for a mobile robot inspired by the locust visual system," in *IEEE International Conference on Robotics and Automation*, pp. 3832–3837, 2005.

[8] S. Yue, R. D. Santer, Y. Yamawaki, and F. C. Rind, "Reactive direction control for a mobile robot: A locust-like control of escape direction emerges when a bilateral pair of model locust visual neurons are integrated," *Autonomous Robots*, vol. 28, no. 2, pp. 151–167, 2010.

[9] C. Hu, F. Arvin, C. Xiong, and S. Yue, "Bio-Inspired Embedded Vision System for Autonomous Micro-Robots: The LGMD Case," *IEEE Transactions on Cognitive and Developmental Systems*, vol. 9, no. 3, pp. 241–254, 2017.

[10] M. S. Keil, E. Roca-Moreno, and A. Rodriguez-Vazquez, "A neural model of the locust visual system for detection of object approaches with real-world scenes," in *Proceedings of the Fourth IASTED International Conference Visualization, imaging, and image processing*, pp. 340–345, 2004.

[11] T. Yang, S. Wu, and D. Guo, "Dynamic range enhance of visual sensor circuits and application for multi-object motion detection," in *Proceedings - 2012 5th International Conference on Intelligent Computation Technology and Automation, ICICTA 2012*, pp. 151–154, 2012.

[12] L. Salt, G. Indiveri, and Y. Sandamirskaya, "Obstacle avoidance with lgmd neuron: Towards a neuromorphic uav implementation," in *Proceedings - IEEE International Symposium on Circuits and Systems*, 2017.

[13] H. Meng, S. Yue, A. Hunter, K. Appiah, M. Hobden, N. Priestley, P. Hobden, and C. Pettit, "A modified neural network model for Lobula Giant Movement Detector with additional depth movement feature," in *International Joint Conference on Neural Networks*, pp. 2078–2083, 2009.

[14] H. Meng, K. Appiah, S. Yue, A. Hunter, M. Hobden, N. Priestley, P. Hobden, and C. Pettit, "A modified model for the lobula giant movement detector and its fpga implementation," *Computer Vision and Image Understanding*, vol. 114, pp. 1238–1247, 2010.

[15] A. Silva and C. P. Santos, "Modeling disinhibition within a layered structure of the LGMD neuron," in *International Joint Conference on Neural Networks*, 2013.

[16] A. Silva and C. Santos, "Computational model of the LGMD neuron for automatic collision detection," pp. 1–4, 2013.

[17] M. Hartbauer, "Simplified bionic solutions: a simple bio-inspired vehicle collision detection system," *Bioinspiration and Biomimetics*, vol. 12, no. 2, 2017.

[18] S. B. I. Badia, U. Bernardet, and P. F. Verschure, "Non-linear neuronal responses as an emergent property of afferent networks: A case study of the locust Lobula Giant Movement Detector," *PLoS Computational Biology*, vol. 6, no. 3, p. e1000701, 2010.

[19] J. Sztarker and F. C. Rind, "A look into the cockpit of the developing locust: Looming detectors and predator avoidance," *Developmental Neurobiology*, vol. 74, no. 11, pp. 1078–1095, 2014.

[20] Q. Fu and S. Yue, "Modelling lgmd2 visual neuron system," in *IEEE International Workshop on Machine Learning for Signal Processing, MLSP*, 2015.

[21] Q. Fu, C. Hu, and S. Yue, "Bio-inspired Collision Detector with Enhanced Selectivity for Ground Robotic Vision System," in *British Machine Vision Conference*, pp. 1–13, 2016.

[22] Q. Fu, C. Hu, and S. Yue, "Collision selective visual neural network inspired by lgmd2 neurons in juvenile locusts," pp. 1–15, 2017.

[23] Q. Fu, C. Hu, J. Peng, and S. Yue, "Shaping the collision selectivity in a looming sensitive neuron model with parallel on and off pathways and spike frequency adaptation," *Neural Networks*, vol. 106, pp. 127–143, 2018.

[24] S. Yue and F. C. Rind, "A Synthetic Vision System Using Directionally Selective Motion Detectors to Recognize Collision," *Artificial Life*, vol. 13, no. 2, pp. 93–122, 2007.

[25] S. Yue and F. C. Rind, "Postsynaptic organizations of directional selective visual neural networks for collision detection," *Neurocomputing*, vol. 103, pp. 50–62, 2013.

[26] S. Yue and F. C. Rind, "Redundant neural vision systemscompeting for collision recognition roles," *IEEE Transactions on Autonomous Mental Development*, vol. 5, no. 2, pp. 173–186, 2013.

[27] N. Franceschini, A. Riehle, and A. Le Nestour, "Directionally selective motion detection by insect neurons," in *Facets of Vision*, pp. 360–390, 1989.

[28] A. Borst and T. Euler, "Seeing Things in Motion: Models, Circuits, and Mechanisms," *Neuron*, vol. 71, no. 6, pp. 974–994, 2011.

[29] M. Frye, "Elementary motion detectors," *Current Biology*, vol. 25, no. 6, pp. R215–R217, 2015.

[30] A. Arenz, M. S. Drews, F. G. Richter, G. Ammer, and A. Borst, "The temporal tuning of the drosophila motion detectors is determined by the dynamics of their input elements," *Current Biology*, vol. 27, no. 7, pp. 929–944, 2017.

[31] F. Iida and D. Lambrinos, "Navigation in an autonomous flying robot by using a biologically inspired visual odometer," *Sensor Fusion and Decentralized Control in RoboticSystem III Photonics East*, vol. 4196, pp. 86–97, 2000.

[32] A. Bahl, G. Ammer, T. Schilling, and A. Borst, "Object tracking in motion-blind flies," *Nature Neuroscience*, vol. 16, no. 6, pp. 730–738, 2013.

[33] A. J. Cope, C. Sabo, K. Gurney, E. Vasilaki, and J. A. Marshall, "A model for an angular velocity-tuned motion detector accounting for deviations in the corridor-centering response of the bee," *PLoS Computational Biology*, vol. 12, no. 5, pp. 1–22, 2016.

[34] H. G. Krapp, B. Hengstenberg, and R. Hengstenberg, "Dendritic structure and receptive-field organization of optic flow processing interneurons in the fly.," *Journal of neurophysiology*, vol. 79, no. 4, pp. 1902–17, 1998.

[35] W. E. Green and P. Y. Oh, "Optic-Flow-Based Collision Avoidance," *IEEE Robotics Automation Magazine*, vol. 15, no. 1, pp. 96–103, 2008.

[36] F. L. Roubieu, J. R. Serres, F. Colonnier, N. Franceschini, S. Viollet, and F. Ruffier, "A biomimetic vision-based hovercraft accounts for bees' complex behaviour in various corridors," *Bioinspiration and Biomimetics*, vol. 9, no. 3, 2014.

[37] N. Franceschini, "Small brains, smart machines: From fly vision to robot vision and back again," *Proceedings of the IEEE*, vol. 102, pp. 751–781, 2014.

[38] J. Haag, A. Arenz, E. Serbe, F. Gabbiani, and A. Borst, "Complementary mechanisms create direction selectivity in the fly," *eLife*, vol. 5, pp. 1–15, 2016.

[39] H. Eichner, M. Joesch, B. Schnell, D. F. Reiff, and A. Borst, "Internal Structure of the Fly Elementary Motion Detector," *Neuron*, vol. 70, no. 6, pp. 1155–1164, 2011.

[40] D. A. Clark, L. Bursztyn, M. A. Horowitz, M. J. Schnitzer, and T. R. Clandinin, "Defining the computational structure of the motion detector in Drosophila," *Neuron*, vol. 70, no. 6, pp. 1165–1177, 2011.

[41] K. Nordström, P. D. Barnett, and D. C. O'Carroll, "Insect detection of small targets moving in visual clutter," *PLoS biology*, vol. 4, no. 3, p. e54, 2006.

[42] K. Nordström, "Neural specializations for small target detection in insects," *Current opinion in neurobiology*, vol. 22, no. 2, pp. 272–278, 2012.

[43] S. D. Wiederman, P. A. Shoemaker, and D. C. O'Carroll, "A model for the detection of moving targets in visual clutter inspired by insect physiology," *PLoS ONE*, vol. 3, no. 7, pp. 1–11, 2008.

[44] H. Wang, J. Peng, and S. Yue, "A directionally selective small target motion detecting visual neural network in cluttered backgrounds," *IEEE Transactions on Cybernetics*, 2018.

[45] D. M. Bolzon, K. Nordström, and D. C. O'Carroll, "Local and large-range inhibition in feature detection," *Journal of Neuroscience*, vol. 29, no. 45, pp. 14143–14150, 2009.

[46] M. Egelhaaf, "On the neuronal basis of figure-ground discrimination by relative motion in the visual system of the fly. 3: Possible input circuitries and

behavioural significance of the fd-cells," *Biological Cybernetics*, vol. 52, no. 4, pp. 267–280, 1985.

[47] P. Hennig and M. Egelhaaf, "Neuronal encoding of object and distance information: a model simulation study on naturalistic optic flow processing," *Frontiers in neural circuits*, vol. 6, p. 14, 2012.

[48] C. M. Higgins and V. Pant, "An elaborated model of fly small-target tracking," *Biological cybernetics*, vol. 91, no. 6, pp. 417–428, 2004.

[49] P. Hennig, R. Möller, and M. Egelhaaf, "Distributed dendritic processing facilitates object detection: a computational analysis on the visual system of the fly," *PLoS One*, vol. 3, no. 8, p. e3092, 2008.

[50] C. Hu, Q. Fu, and S. Yue, "Colias iv: the affordable micro robot platform with bio-inspired vision," in *19th Towards Autonomous Robotic Systems Conference*, 2018.

[51] S. P. Peron and F. Gabbiani, "Role of spike-frequency adaptation in shaping neuronal response to dynamic stimuli," *Biol Cybern*, vol. 100, no. 6, pp. 505–520, 2009.

[52] Q. Fu and S. Yue, "Mimicking fly motion tracking and fixation behaviors with a hybrid visual neural network," in *IEEE Int. Conf. on Robotics and Biomimetics*, pp. 1636–1641, 2017.

[53] Q. Fu and S. Yue, "Modeling direction selective visual neural network with on and off pathways for extracting motion cues from cluttered background," in *International Joint Conference on Neural Networks*, pp. 831–838, 2017.

[54] A. Pallus and L. J. Fleishman, "A two-dimensional visual motion detector based on biological principles." https://muse.union.edu/visualmotion/main-article/. Accessed: 2014-07-01.

[55] Q. Fu, C. Hu, T. Liu, and S. Yue, "Collision selective lgmds neuron models research benefits from a vision-based autonomous micro robot," in *IEEE International Conference on Intelligent Robots and Systems*, pp. 3996–4002, 2017.

[56] T. Krajník, M. Nitsche, I. Faigl, P. Vaněk, M. Saska, L. Přeučil, T. Duckett, and M. Marta, "A practical multirobot localization system," *Journal of Intelligent and Robotic Systems*, vol. 76, no. 3-4, pp. 539–562, 2014.

[57] G. Indiveri and R. Douglas, "Neuromorphic vision sensors," *Science*, pp. 1189–1190, 2000.

[58] A. Borst and M. Helmstaedter, "Common circuit design in fly and mammalian motion vision," *Nature Neuroscience*, vol. 18, no. 8, pp. 1067–1076, 2015.

[59] J. R. Serres and F. Ruffier, "Optic flow-based collision-free strategies: From insects to robots," *Arthropod Structure and Development*, vol. 46, no. 5, pp. 703–717, 2017.

[60] R. M. MAY, "How many species are there on earth?," *Science*, vol. 241, no. 4872, pp. 1441–1449, 1988.

[61] A. Borst, J. Haag, and D. F. Reiff, "Fly Motion Vision," *The Annual Review of Neuroscience*, vol. 33, pp. 49–70, 2010.

[62] A. Borst, "Fly visual course control: behaviour, algorithms and circuits," *Nature Reviews Neuroscience*, vol. 15, pp. 590–599, 2014.

[63] F. C. Rind, "Motion detectors in the locust visual system: From biology to robot sensors," *Microscopy Research and Technique*, vol. 56, no. 4, pp. 256–269, 2002.

[64] R. Tron and R. Vidal, "A benchmark for the comparison of 3-d motion segmentation algorithms," in *2007 IEEE Conference on Computer Vision and Pattern Recognition*, pp. 1–8, June 2007.

[65] R. Sabzevari and D. Scaramuzza, "Multi-body motion estimation from monocular vehicle-mounted cameras," *IEEE Transactions on Robotics*, vol. 32, no. 3, pp. 638–651, 2016.

[66] M. Faessler, F. Fontana, C. Forster, and D. Scaramuzza, "Automatic reinitialization and failure recovery for aggressive flight with a monocular vision-based quadrotor," in *IEEE International Conference on Robotics and Automation*, 2015.

[67] M. Faessler, F. Fontana, C. Forster, E. Mueggler, M. Pizzoli, and D. Scaramuzza, "Autonomous, vision-based flight and live dense 3d mapping with a quadrotor micro aerial vehicle," *Journal of Field Robotics*, 2016.

[68] D. Falanga, E. Mueggler, M. Faessler, and D. Scaramuzza, "Aggressive quadrotor flight through narrow gaps with onboard sensing and computing using active vision," in *IEEE International Conference on Robotics and Automation*, 2017.

[69] H. Kim, S. Leutenegger, and A. J. Davison, "Real-time 3d reconstruction and 6-dof tracking with an event camera," in *European Conference on Computer Vision*, pp. 1–16, 2016.

[70] V. Vasco, A. Glover, E. Mueggler, D. Scaramuzza, L. Natale, and C. Bartolozzi, "Independent motion detection with event-driven cameras," in *International Conference on Advanced Robotics (ICAR)*, pp. 530–536, 2017.

[71] A. Mukhtar, L. Xia, and T. B. Tang, "Vehicle detection techniques for collision avoidance systems: A review," *IEEE Transactions on Intelligent Transportation Systems*, vol. 16, no. 5, pp. 2318–2338, 2015.

[72] G. N. DeSouza and A. C. Kak, "Vision for mobile robot navigation: A survey," *IEEE Transactions on Pattern Analysis and Machine Intelligence*, vol. 24, pp. 237–267, 2002.

[73] H. D., H. S., R. R.B., and B. S., "Real-time plane segmentation using rgb-d cameras," in *RoboCup 2011: Robot Soccer World Cup XV*, vol. 7416, Springer, 2012.

[74] B. Peasley and S. Birchfield, "Real-time obstacle detection and avoidance in the presence of specular surfaces using an active 3d sensor," in *Robot Vision (WORV), 2013 IEEE Workshop on*, 2013.

[75] B. Schmidt and L. Wang, "Depth camera based collision avoidance via active robot control," *Journal of Manufacturing Systems*, vol. 33, no. 4, pp. 711–718, 2014.

[76] M. O'Shea and J. L. Williams, "The anatomy and output connection of a locust visual interneurone; The lobular giant movement detector (LGMD) neurone," *Journal of Comparative Physiology*, vol. 91, no. 3, pp. 257–266, 1974.

[77] M. O'Shea and C. H. F. Rowell, "The Neuronal Basis of a Sensory Analyser, The Acridid Movement Detector System," *J. exp. Biol*, vol. 68, no. 2, pp. 289–308, 1976.

[78] F. C. Rind and P. J. Simmons, "Orthopteran dcmd neuron : a reevaluation of responses to moving objects . i . selective responses to approaching objects," *Journal of neurophysiology*, vol. 68, no. October 2015, pp. 1654–1666, 1992.

[79] F. C. Rind and D. I. Bramwell, "Neural network based on the input organization of an identified neuron signaling impending collision.," *Journal of neurophysiology*, vol. 75, no. 3, pp. 967–985, 1996.

[80] F. C. Rind, "Intracellular characterization of neurons in the locust brain signaling impending collision.," *Journal of neurophysiology*, vol. 75, no. 3, pp. 986–995, 1996.

[81] F. C. Rind and P. J. Simmons, "Local circuit for the computation of object approach by an identified visual neuron in the locust," *Journal of Comparative Neurology*, vol. 395, no. 3, pp. 405–415, 1998.

[82] S. P. Peron, P. W. Jones, and F. Gabbiani, "Precise Subcellular Input Retinotopy and Its Computational Consequences in an Identified Visual Interneuron," *Neuron*, vol. 63, no. 6, pp. 830–842, 2009.

[83] P. J. Simmons and F. C. Rind, "Responses to object approach by a wide field visual neurone, the LGMD2 of the locust: Characterization and image cues," *Journal of Comparative Physiology - A Sensory, Neural, and Behavioral Physiology*, vol. 180, no. 3, pp. 203–214, 1997.

[84] M. Blanchard, F. C. Rind, and P. F. Verschure, "How accurate need sensory coding be for behaviour? Experiments using a mobile robot," *Neurocomputing*, vol. 38-40, pp. 1113–1119, 2001.

[85] S. Yue and F. C. Rind, "Near range path navigation using lgmd visual neural networks," in *Computer Science and Information Technology, ICCSIT*, pp. 105–109, 2009.

[86] F. C. RIND, "A directionally selective motion-detecting neurone in the brain of the locust: Physiological and morphological characterization," *J. exp. Biol.*, vol. 149, pp. 1–19, 1990.

[87] F. Rind, "Identification of directionally selective motion-detecting neurones in the locust lobula and their synaptic connections with an identified descending neurone," *Journal of Experimental Biology*, vol. 149, pp. 21–43, 1990.

[88] E. Buchner, "Elementary movement detectors in an insect visual system," *Biol. Cybern*, vol. 24, pp. 85–101, 1976.

[89] B. Hassenstein and W. Reichardt, "Systemtheoretische analyse der zeit-, reihenfolgen- und vorzeichenauswertung bei der bewegungsperzeption des riisselkiifers chlorophanus," *Z Naturforsch*, pp. 513–524, 1956.

[90] A. Borst and J. Haag, "Neural networks in the cockpit of the fly," *Journal of Comparative Physiology*, vol. 188, no. 6, pp. 419–437, 2002.

[91] H. Barlow and W. Levick, "The mechanism of directionally selective units in rabbit's retina," *J. Physiol.*, vol. 178, pp. 477–504, 1965.

[92] T. W. Troyer, A. E. Krukowski, N. J. Priebe, and K. D. Miller, "Contrast-Invariant Orientation Tuning in Cat Visual Cortex: Thalamocortical Input Tuning and Correlation-Based Intracortical Connectivity," *The Journal of Neuroscience*, vol. 18, no. 15, pp. 5908–5927, 1998.

[93] M. Joesch, B. Schnell, S. V. Raghu, D. F. Reiff, and A. Borst, "ON and off pathways in Drosophila motion vision," *Nature*, vol. 468, no. 7321, pp. 300–304, 2010.

[94] M. Joesch, F. Weber, H. Eichner, and A. Borst, "Functional specialization of parallel motion detection circuits in the fly," *J Neurosci*, vol. 33, no. 3, pp. 902–905, 2013.

[95] S. D. Wiederman, P. A. Shoemaker, and D. C. O'Carroll, "Correlation between OFF and ON Channels Underlies Dark Target Selectivity in an Insect Visual System," *Journal of Neuroscience*, vol. 33, no. 32, pp. 13225–13232, 2013.

[96] N. Vogt and C. Desplan, "The First Steps in Drosophila Motion Detection," *Neuron*, vol. 56, no. 1, pp. 5–7, 2007.

[97] M. S. Maisak, J. Haag, G. Ammer, E. Serbe, M. Meier, A. Leonhardt, T. Schilling, A. Bahl, G. M. Rubin, A. Nern, B. J. Dickson, D. F. Reiff, E. Hopp, and A. Borst, "A directional tuning map of Drosophila elementary motion detectors," *Nature*, vol. 500, no. 7461, pp. 212–216, 2013.

[98] J. Rister, D. Pauls, B. Schnell, C.-Y. Ting, C.-H. Lee, I. Sinakevitch, J. Morante, N. J. Strausfeld, K. Ito, and M. Heisenberg, "Dissection of the Peripheral Motion Channel in the Visual System of Drosophila melanogaster," *Neuron*, vol. 56, no. 1, pp. 155–170, 2007.

[99] F. Gabbiani and P. W. Jones, "A genetic push to understand motion detection," *Neuron*, vol. 70, no. 6, pp. 1023–1025, 2011.

[100] A. Leonhardt, G. Ammer, M. Meier, E. Serbe, A. Bahl, and A. Borst, "Asymmetry of Drosophila ON and OFF motion detectors enhances real-world velocity estimation," *Nature Neuroscience*, vol. 19, pp. 706–715, 2016.

[101] K. Shinomiya, S.-y. Takemura, P. K. Rivlin, S. M. Plaza, L. Scheffer, and I. A. Meinertzhagen, "A common evolutionary origin for the ON- and OFF-edge motion detection pathways of the Drosophila visual system," *Frontiers in Neural Circuits*, vol. 9, no. 33, p. 33, 2015.

[102] H. Wang, J. Peng, and S. Yue, "An Improved LPTC Neural Model for Background Motion Direction Estimation," in *7th Joint IEEE International Conference on Development and Learning and on Epigenetic Robotics*, pp. 47–52, 2017.

[103] H. Wang, J. Peng, and S. Yue, "Bio-inspired small target motion detector with a new lateral inhibition mechanism," in *International Joint Conference on Neural Networks*, pp. 4751–4758, 2016.

[104] L. F. Tammero, "Spatial organization of visuomotor reflexes in Drosophila," *Journal of Experimental Biology*, vol. 207, no. 1, pp. 113–122, 2004.

[105] L. Zheng, G. G. de Polavieja, V. Wolfram, M. H. Asyali, R. C. Hardie, and M. Juusola, "Feedback network controls photoreceptor output at the layer of first visual synapses in drosophila," *The Journal of General Physiology*, vol. 127, no. 5, pp. 495–510, 2006.

[106] S.-y. Takemura, A. Bharioke, Z. Lu, A. Nern, S. Vitaladevuni, P. K. Rivlin, W. T. Katz, D. J. Olbris, S. M. Plaza, P. Winston, T. Zhao, J. A. Horne, R. D. Fetter, S. Takemura, K. Blazek, L.-A. Chang, O. Ogundeyi, M. a. Saunders, V. Shapiro, C. Sigmund, G. M. Rubin, L. K. Scheffer, I. a. Meinertzhagen, and D. B. Chklovskii, "A visual motion detection circuit suggested by Drosophila connectomics," *Nature*, vol. 500, no. 7461, pp. 175–181, 2013.

[107] A. K. Warzecha, R. Rosner, and J. Grewe, "Impact and sources of neuronal variability in the fly's motion vision pathway," *Journal of Physiology Paris*, vol. 107, no. 1-2, pp. 26–40, 2013.

[108] R. Behnia, D. A. Clark, A. G. Carter, T. R. Clandinin, and C. Desplan, "Processing properties of on and off pathways for Drosophila motion detection," *Nature*, vol. 512, no. 7515, pp. 427–430, 2014.

[109] Z. Zhang, S. Yue, and G. Zhang, "Fly visual system inspired artificial neural network for collision detection," *Neurocomputing*, vol. 153, pp. 221–234, 2015.

[110] J. C. S. Leong, J. J. Esch, B. Poole, S. Ganguli, and T. R. Clandinin, "Direction selectivity in drosophila emerges from preferred-direction enhancement and null-direction suppression," *Journal of Neuroscience*, vol. 36, no. 31, pp. 8078–8092, 2016.

[111] J. A. Strother, S. T. Wu, A. M. Wong, A. Nern, E. M. Rogers, J. Q. Le, G. M. Rubin, and M. B. Reiser, "The emergence of directional selectivity in the visual motion pathway of drosophila," *Neuron*, vol. 94, no. 1, pp. 168–182.e10, 2017.

[112] T. Biswas and C. H. Lee, "Visual motion: Cellular implementation of a hybrid motion detector," *Current Biology*, vol. 27, no. 7, pp. R274–R276, 2017.

[113] J. M. Missler and F. A. Kamangar, "A neural network for pursuit tracking inspired by the fly visual system," *Neural Networks*, vol. 8, no. 3, pp. 463–480, 1995.

[114] R. D. Santer, F. C. Rind, and P. J. Simmons, "Predator versus Prey: Locust Looming-Detector Neuron and Behavioural Responses to Stimuli Representing Attacking Bird Predators," *PLoS ONE*, vol. 7, no. 11, 2012.

[115] P. J. Simmons, F. C. Rind, and R. D. Santer, "Escapes with and without preparation: the neuroethology of visual startle in locusts," *J Insect Physiol*, vol. 56, no. 8, pp. 876–883, 2010.

[116] F. C. Rind, S. Wernitznig, P. Polt, A. Zankel, D. Gutl, J. Sztarker, and G. Leitinger, "Two identified looming detectors in the locust: ubiquitous lateral connections among their inputs contribute to selective responses to looming objects," *Scientific Reports*, no. 35525, 2016.

[117] S. Wernitznig, F. C. Rind, P. Polt, A. Zankel, E. Pritz, D. Kolb, E. Bock, and G. Leitinger, "Synaptic connections of first-stage visual neurons in the locust Schistocerca gregaria extend evolution of tetrad synapses back 200 million years," *J Comp Neurol*, vol. 523, no. 2, pp. 298–312, 2015.

[118] A. C. Paulk, A. M. Dacks, J. Phillips-Portillo, J.-M. Fellous, and W. Gronenberg, "Visual processing in the central bee brain," *Journal of Neuroscience*, vol. 29, no. 32, pp. 9987–9999, 2009.

[119] E. Baird, T. Kornfeldt, and M. Dacke, "Minimum viewing angle for visually guided ground speed control in bumblebees," *Journal of Experimental Biology*, vol. 213, no. 10, pp. 1625–1632, 2010.

[120] E. Baird, N. Boeddeker, M. R. Ibbotson, and M. V. Srinivasan, "A universal strategy for visually guided landing," *Proceedings of the National Academy of Sciences*, vol. 110, no. 46, pp. 18686–18691, 2013.

[121] J. Zeil, "Visual homing: An insect perspective," *Current Opinion in Neurobiology*, vol. 22, no. 2, pp. 285–293, 2012.

[122] R. C. Arkin, K. Ali, A. Weitzenfeld, and F. Cervantes-Pérez, "Behavioral models of the praying mantis as a basis for robotic behavior," *Robotics and Autonomous Systems*, vol. 32, no. 1, pp. 39–60, 2000.

[123] Y. Yamawaki, "Defence behaviours of the praying mantis Tenodera aridifolia in response to looming objects," *Journal of Insect Physiology*, vol. 57, no. 11, pp. 1510–1517, 2011.

[124] C. Clifford and M. Ibbotson, "Fundamental mechanisms of visual motion detection: models, cells and functions," *Progress in Neurobiology*, vol. 68, no. 6, pp. 409–437, 2002.

[125] A. Borst and M. Egelhaaf, "Principles of visual motion detection," *Trends Neurosci*, vol. 12, pp. 297–306, 1989.

[126] M. Egelhaaf and A. Borst, "A look into the cockpit of the fly: visual orientation, algorithms, and identified neurons," *J Neurosci*, vol. 13, no. 11, pp. 4563–4574, 1993.

[127] J. W. Aptekar and M. A. Frye, "Higher-order figure discrimination in fly and human vision," *Current Biology*, vol. 23, no. 16, pp. R694–R700, 2013.

[128] F. C. Rind and G. Leitinger, "Immunocytochemical evidence that collision sensing neurons in the locust visual system contain acetylcholine," *Journal of Comparative Neurology*, vol. 423, no. 3, pp. 389–401, 2000.

[129] F. C. Rind, R. D. Santer, and G. A. Wright, "Arousal Facilitates Collision Avoidance Mediated by a Looming Sensitive Visual Neuron in a Flying Locust," *J Neurophysiol.*, vol. 100, pp. 670–680, 2008.

[130] S. Judge and F. Rind, "The locust DCMD, a movement-detecting neurone tightly tuned to collision trajectories," *The Journal of experimental biology*, vol. 200, pp. 2209–16, 1997.

[131] P. J. Simmons, J. Sztarker, and F. C. Rind, "Looming detection by identified visual interneurons during larval development of the locust locusta migratoria," *J Exp Biol*, vol. 216, no. Pt 12, pp. 2266–2275, 2013.

[132] G. M. Card, "Escape behaviors in insects," *Current Opinion in Neurobiology*, vol. 22, no. 2, pp. 180–186, 2012.

[133] F. Iida, "Book review: flying insects and robots," *Artificial Life*, vol. 18, pp. 125–127, 2012.

[134] D. Floreano, J.-C. Zufferey, and J.-D. Nicoud, "From Wheels to Wings with Evolutionary Spiking Circuits," *Artificial Life*, vol. 11, no. 1-2, pp. 121–138, 2005.

[135] M. Srinivasan, J. Chahl, K. Weber, S. Venkatesh, M. Nagle, and S. Zhang, "Robot navigation inspired by principles of insect vision," *Robotics and Autonomous Systems*, vol. 26, no. 2-3, pp. 203–216, 1999.

[136] M. V. Srinivasan, "Visual control of navigation in insects and its relevance for robotics," *Current Opinion in Neurobiology*, vol. 21, no. 4, pp. 535–543, 2011.

[137] M. V. Srinivasan, "Honeybees as a model for the study of visually guided flight, navigation, and biologically inspired robotics," *Physiol Rev*, vol. 91, pp. 413–460, 2011.

[138] S. A. Huber and H. H. Bulthoff, *Visuomotor control in flies and behavior-based agents*. 2003.

[139] B. Webb, "What does robotics offer animal behaviour?," *Animal Behaviour*, vol. 60, no. 5, pp. 545–558, 2000.

[140] B. Webb, "Can robots make good models of biological behaviour?," *Behavioral and Brain Sciences*, vol. 24, no. 06, pp. 1033–1050, 2001.

[141] S. E. J. De Vries and T. R. Clandinin, "Loom-sensitive neurons link computation to action in the Drosophila visual system," *Current Biology*, vol. 22, no. 5, pp. 353–362, 2012.

[142] D. Oliva and D. Tomsic, "Computation of object approach by a system of visual motion-sensitive neurons in the crab neohelice," *Journal of Neurophysiology*, vol. 112, no. 6, pp. 1477–1490, 2014.

[143] F. Gabbiani, H. G. Krapp, N. Hatsopoulos, C. H. Mo, C. Koch, and G. Laurent, "Multiplication and stimulus invariance in a looming-sensitive neuron," *Journal of Physiology Paris*, vol. 98, no. 1-3 SPEC. ISS., pp. 19–34, 2004.

[144] J. R. Gray, J. K. Lee, and R. M. Robertson, "Activity of descending contralateral movement detector neurons and collision avoidance behaviour in response to head-on visual stimuli in locusts," *Journal of Comparative Physiology - A Sensory, Neural, and Behavioral Physiology*, vol. 187, no. 2, pp. 115–129, 2001.

[145] M. Blanchard, F. C. Rind, and P. F. Verschure, "Collision avoidance using a model of the locust LGMD neuron," *Robotics and Autonomous Systems*, vol. 30, no. 1, pp. 17–38, 2000.

[146] S. Yue, F. C. Rind, M. S. Keil, J. Cuadri, and R. Stafford, "A bio-inspired visual collision detection mechanism for cars: Optimisation of a model of a locust neuron to a novel environment," *Neurocomputing*, vol. 69, no. 13-15, pp. 1591–1598, 2006.

[147] C. Hu, F. Arvin, and S. Yue, "Development of a bio-inspired vision system for mobile micro-robots," in *IEEE ICDL-EPIROB*, pp. 81–86, 2014.

[148] J. Zhao, C. Hu, C. Zhang, Z. Wang, and S. Yue, "A bio-inspired collision detector for small quadcopter," in *IEEE International Joint Conference on Neural Networks*, 2018.

[149] D. Ianchis, V. Tiponut, S. O. Popescu, and Z. Haraszy, "Improved collision detection system inspired from the neural network of the locust," in *SISY 2011 - 9th International Symposium on Intelligent Systems and Informatics*, pp. 211–215, 2011.

[150] A. C. Silva and C. P. Santos, "Improving image reliability in very low light conditions : Application to a robotic vision system," 2014.

[151] A. Krejan and A. Trost, "LGMD-based bio-inspired algorithm for detecting risk of collision of a road vehicle," in *2011 7th International Symposium on Image and Signal Processing and Analysis (ISPA)*, pp. 319–324, 2011.

[152] M. Deng, A. Inoue, Y. Shibata, K. Sekiguchi, and N. Ueki, "An obstacle avoidance method for two wheeled mobile robot," in *Proceedings of the 2007 IEEE International Conference on Networking Sensing and Control*, pp. 689–692, 2007.

[153] F. Gabbiani, G. Laurent, N. Hatsopoulos, H. G. Krapp, F. C. Rind, and P. J. Simmons, "The many ways of building collision-sensitive neurons," *Trends in Neurosciences*, vol. 22, no. 10, pp. 437–438, 1999.

[154] F. Gabbiani, H. G. Krapp, C. Koch, and G. Laurent, "Multiplicative computation by a looming-sensitive neuron," in *Proceedings of the Second Joint EMBS/BMES Conference*, pp. 1968–1969, 2002.

[155] F. Gabbiani, H. G. Krapp, and G. Laurent, "Computation of object approach by a wide-field, motion-sensitive neuron.," *The Journal of neuroscience : the official journal of the Society for Neuroscience*, vol. 19, no. 3, pp. 1122–1141, 1999.

[156] F. Gabbiani, I. Cohen, and G. Laurent, "Time-dependent activation of feedforward inhibition in a looming-sensitive neuron.," *Journal of neurophysiology*, vol. 94, no. May 2005, pp. 2150–2161, 2005.

[157] F. Gabbiani, C. Mo, and G. Laurent, "Invariance of angular threshold computation in a wide-field looming-sensitive neuron.," *The Journal of neuroscience : the official journal of the Society for Neuroscience*, vol. 21, no. 1, pp. 314–329, 2001.

[158] M. S. Keil, "Emergence of multiplication in a biophysical model of a wide-field visual neuron for computing object approaches: Dynamics, peaks, & fits," in *Neural Information Processing Systems (NIPS)*, pp. 469–477, 2011.

[159] M. S. Keil, "Dendritic Pooling of Noisy Threshold Processes Can Explain Many Properties of a Collision-Sensitive Visual Neuron," *PLoS Computational Biology*, vol. 11, no. 10, pp. 1–17, 2015.

[160] S. Bermudez i Badia and P. F. Verschure, "A Collision Avoidance Model Based on the Lobula Giant Movement Detector (LGMD) Neuron of the Locust," in *2004 IEEE International Joint Conference on Neural Networks*, vol. 3, pp. 1757–1761, 2004.

[161] R. Stafford, R. D. Santer, and F. C. Rind, "A bio-inspired visual collision detection mechanism for cars: combining insect inspired neurons to create a robust system," *Biosystems*, vol. 87, no. 2-3, pp. 164–171, 2007.

[162] F. Gabbiani and H. G. Krapp, "Spike-Frequency Adaptation and Intrinsic Properties of an Identified, Looming-Sensitive Neuron," *Journal of Neurophysiology*, vol. 96, no. 6, pp. 2951–2962, 2006.

[163] S. Yue and F. Claire Rind, "Visual motion pattern extraction and fusion for collision detection in complex dynamic scenes," *Computer Vision and Image Understanding*, vol. 104, no. 1, pp. 48–60, 2006.

[164] G. Zhang, C. Zhang, and S. Yue, "LGMD and DSNs neural networks integration for collision predication," in *International Joint Conference on Neural Networks*, pp. 1174–1179, 2016.

[165] C. Gilbert, "Brain connectivity: Revealing the fly visual motion circuit," *Current Biology*, vol. 23, no. 18, pp. R851–R853, 2013.

[166] M. F. Kele and M. A. Frye, "Object-detecting neurons in drosophila," *Current Biology*, vol. 27, no. 5, pp. 680–687, 2017.

[167] W. Reichardt, "Evaluation of Optical Motion Information by Movement Detector," *International Journal of Computer Vision*, vol. 161, no. 2, pp. 533–547, 1987.

[168] R. A. Harris, D. C. O'Carroll, and S. B. Laughlin, "Adaptation and the temporal delay filter of fly motion detectors," *Vision Research*, vol. 39, no. 16, pp. 2603–2613, 1999.

[169] H. G. Krapp and R. Hengstenberg, "Estimation of self-motion by optic flow processing in single visual interneurons," *Nature*, vol. 384, pp. 463–466, 1996.

[170] K. Karmeier, "Encoding of Naturalistic Optic Flow by a Population of Blowfly Motion-Sensitive Neurons," *Journal of Neurophysiology*, vol. 96, no. 3, pp. 1602–1614, 2006.

[171] N. A. Browning, S. Grossberg, and E. Mingolla, "A neural model of how the brain computes heading from optic flow in realistic scenes," *Cognitive Psychology*, vol. 59, no. 4, pp. 320–356, 2009.

[172] N. Boeddeker, J. P. Lindemann, M. Egelhaaf, and J. Zeil, "Responses of blowfly motion-sensitive neurons to reconstructed optic flow along outdoor flight paths.," *Journal of comparative physiology. A, Neuroethology, sensory, neural, and behavioral physiology*, vol. 191, pp. 1143–1155, 2005.

[173] M. Egelhaaf, J. Grewe, R. Kern, and A. K. Warzecha, "Outdoor performance of a motion-sensitive neuron in the blowfly," *Vision Research*, vol. 41, no. 27, pp. 3627–3637, 2001.

[174] L. F. Tammero and M. H. Dickinson, "Collision-avoidance and landing responses are mediated by separate pathways in the fruit fly, Drosophila melanogaster," *The Journal of Experimental Biology*, vol. 205, pp. 2785–2798, 2002.

[175] A. A. ARGYROS, D. P. TSAKIRIS, and C. GROYER, "Biomimetic centering behavior," *IEEE Robotics and Automation Magazine*, pp. 21–31, 2004.

[176] O. J. N. Bertrand, J. P. Lindemann, and M. Egelhaaf, "A Bio-inspired Collision Avoidance Model Based on Spatial Information Derived from Motion Detectors Leads to Common Routes," *PLOS Computational Biology*, vol. 11, no. 11, pp. 1–28, 2015.

[177] F. Iida, "Biologically inspired visual odometer for navigation of a flying robot," *Robotics and Autonomous Systems*, vol. 44, no. 3-4, pp. 201–208, 2003.

[178] H. P. Snippe and J. J. Koenderink, "Extraction of optical velocity by use of multi-input Reichardt detectors," *J. Opt. Soc. Am. A*, vol. 11, no. 4, pp. 1222–1236, 1994.

[179] J. M. Zanker, M. V. Srinivasan, and M. Egelhaaf, "Speed tuning in elementary motion detectors of the correlation type," *Biological Cybernetics*, vol. 80, no. 2, pp. 109–116, 1999.

[180] J. M. Zanker and O. J. Braddick, "How does noise influence the estimation of speed?," *Vision Research*, vol. 39, no. 14, pp. 2411–2420, 1999.

[181] J. M. Zanker and J. Zeil, "Movement-induced motion signal distributions in outdoor scenes," *Network: Computation in Neural Systems*, vol. 16, no. 4, pp. 357–376, 2005.

[182] S. Rajesh, D. O'Carroll, and D. Abbott, "Man-made velocity estimators based on insect vision," *Smart Materials and Structures*, vol. 14, no. 2, pp. 413–424, 2005.

[183] H. Wang, J. Peng, P. Baxter, C. Zhang, Z. Wang, and S. Yue, "A model for detection of angular velocity of image motion based on the temporal tuning of the drosophila," in *27th International Conference on Artificial Neural Networks*, 2018.

[184] C. W. G. CLIFFORD and K. LANGLEY, "A model of temporal adaptation in fly motion vision," *Vision Research*, vol. 36, pp. 2595–2608, 1996.

[185] Z. Rivera-Alvidrez and C. M. Higgins, "Contrast saturation in a neuronally-based model of elementary motion detection," *Neurocomputing*, vol. 65-66, no. SPEC. ISS., pp. 173–179, 2005.

[186] E. Nakamura, M. Ichimura, and K. Sawada, "Fast global motion estimation algorithm based on elementary motion detectors," in *International Conference on Image Processing*, vol. 2, pp. 297–300, 2002.

[187] C. M. Higgins, "Nondirectional motion may underlie insect behavioral dependence on image speed," *Biological Cybernetics*, vol. 91, no. 5, pp. 326–332, 2004.

[188] F. L. Roubieu, J. Serres, N. Franceschini, F. Ruffier, and S. Viollet, "A fully-autonomous hovercraft inspired by bees: Wall following and speed control in straight and tapered corridors," in *2012 IEEE International Conference on Robotics and Biomimetics*, pp. 1311–1318, 2012.

[189] Y. E. Fisher, J. C. S. Leong, K. Sporar, M. D. Ketkar, D. M. Gohl, T. R. Clandinin, and M. Silies, "A Class of Visual Neurons with Wide-Field Properties Is Required for Local Motion Detection," *Current Biology*, vol. 25, no. 24, pp. 3178–3189, 2015.

[190] J. W. Aptekar, P. A.Shoemaker, and M. A. Frye, "Figure Tracking by Flies Is Supported by Parallel Visual Streams," *Current Biology*, vol. 22, no. 6, pp. 482–487, 2012.

[191] J. A. Strother, A. Nern, and M. B. Reiser, "Direct observation of on and off pathways in the drosophila visual system," *Current Biology*, vol. 24, no. 9, pp. 976–983, 2014.

[192] K. Shinomiya, T. Karuppudurai, T. Y. Lin, Z. Lu, C. H. Lee, and I. A. Meinertzhagen, "Candidate neural substrates for off-edge motion detection in drosophila," *Current Biology*, vol. 24, no. 10, pp. 1062–1070, 2014.

[193] B. Schnell, S. V. Raghu, A. Nern, and A. Borst, "Columnar cells necessary for motion responses of wide-field visual interneurons in Drosophila," *J Comp Physiol*, vol. 198, pp. 389–395, 2012.

[194] Q. Fu, N. Bellotto, C. Hu, and S. Yue, "Performance of a visual fixation model in an autonomous micro robot inspired by *drosophila* physiology," in *IEEE International Conference on Robotics and Biomimetics*, 2018.

[195] T. Collett, "Visual neurones for tracking moving targets," *Nature*, vol. 232, no. 5306, p. 127, 1971.

[196] T. Collett and M. Land, "Visual control of flight behaviour in the hoverflysyritta pipiens l.," *Journal of Comparative Physiology*, vol. 99, no. 1, pp. 1–66, 1975.

[197] R. M. Olberg, "Object-and self-movement detectors in the ventral nerve cord of the dragonfly," *Journal of Comparative Physiology*, vol. 141, no. 3, pp. 327–334, 1981.

[198] R. M. Olberg, "Identified target-selective visual interneurons descending from the dragonfly brain," *Journal of Comparative Physiology A: Neuroethology, Sensory, Neural, and Behavioral Physiology*, vol. 159, no. 6, pp. 827–840, 1986.

[199] D. O'Carroll, "Feature-detecting neurons in dragonflies," *Nature*, vol. 362, no. 6420, p. 541, 1993.

[200] K. Nordström and D. C. O'Carroll, "Small object detection neurons in female hoverflies," *Proceedings of the Royal Society of London B: Biological Sciences*, vol. 273, no. 1591, pp. 1211–1216, 2006.

[201] P. D. Barnett, K. Nordström, and D. C. O'Carroll, "Retinotopic organization of small-field-target-detecting neurons in the insect visual system," *Current Biology*, vol. 17, no. 7, pp. 569–578, 2007.

[202] K. Nordström, D. M. Bolzon, and D. C. O'Carroll, "Spatial facilitation by a high-performance dragonfly target-detecting neuron," *Biology letters*, vol. 7, no. 4, pp. 588–592, 2011.

[203] B. R. Geurten, K. Nordström, J. D. Sprayberry, D. M. Bolzon, and D. C. O'Carroll, "Neural mechanisms underlying target detection in a dragonfly centrifugal neuron," *Journal of Experimental Biology*, vol. 210, no. 18, pp. 3277–3284, 2007.

[204] S. D. Wiederman and D. C. OCarroll, "Biologically inspired feature detection using cascaded correlations of off and on channels," *Journal of Artificial Intelligence and Soft Computing Research*, vol. 3, pp. 5–14, Dec. 2013.

[205] Z. M. Bagheri, B. S. Cazzolato, S. Grainger, D. C. OCarroll, and S. D. Wiederman, "An autonomous robot inspired by insect neurophysiology pursues moving features in natural environments," *Journal of neural engineering*, vol. 14, p. 046030, Jul. 2017.

[206] Z. M. Bagheri, S. D. Wiederman, B. S. Cazzolato, S. Grainger, and D. C. O-Carroll, "Performance of an insect-inspired target tracker in natural conditions," *Bioinspiration & Biomimetics*, vol. 12, p. 025006, Feb. 2017.

[207] Z. M. Bagheri, S. D. Wiederman, B. S. Cazzolato, S. Grainger, and D. C. O'Carroll, "Properties of neuronal facilitation that improve target tracking in natural pursuit simulations," *Journal of The Royal Society Interface*, vol. 12, p. 20150083, Jun. 2015.

[208] M. Egelhaaf, "On the neuronal basis of figure-ground discrimination by relative motion in the visual system of the fly. 2: Figure-detection cells a new class of visual interneurons," *Biological Cybernetics*, vol. 52, no. 2, pp. 123–140, 1985.

[209] V. Gauck and A. Borst, "Spatial response properties of contralateral inhibited lobula plate tangential cells in the fly visual system," *Journal of Comparative Neurology*, vol. 406, no. 1, pp. 51–71, 1999.

[210] B. Kimmerle and M. Egelhaaf, "Detection of object motion by a fly neuron during simulated flight," *Journal of Comparative Physiology A*, vol. 186, no. 1, pp. 21–31, 2000.

[211] B. Kimmerle, A.-K. Warzecha, and M. Egelhaaf, "Object detection in the fly during simulated translatory flight," *Journal of Comparative Physiology A*, vol. 181, no. 3, pp. 247–255, 1997.

[212] A.-K. Warzecha, M. Egelhaaf, and A. Borst, "Neural circuit tuning fly visual interneurons to motion of small objects. i. dissection of the circuit by pharmacological and photoinactivation techniques," *Journal of Neurophysiology*, vol. 69, no. 2, pp. 329–339, 1993.

[213] H. G. Krapp, R. Hengstenberg, and M. Egelhaaf, "Binocular contributions to optic flow processing in the fly visual system," *Journal of Neurophysiology*, vol. 85, no. 2, pp. 724–734, 2001.

[214] C. Spalthoff, M. Egelhaaf, P. Tinnefeld, and R. Kurtz, "Localized direction selective responses in the dendrites of visual interneurons of the fly," *BMC biology*, vol. 8, no. 1, p. 36, 2010.

[215] H. Eckert and D. R. Dvorak, "The centrifugal horizontal cells in the lobula plate of the blowfly, phaenicia sericata," *Journal of Insect Physiology*, vol. 29, no. 7, pp. 547–560, 1983.

[216] W. Reichardt, T. Poggio, and K. Hausen, "Figure-ground discrimination by relative movement in the visual system of the fly. part ii: Towards the neural circuitry," *Biological Cybernetics*, vol. 46, no. 1, pp. 1–30, 1983.

[217] W. Reichardt, M. Egelhaaf, and A.-k. Guo, "Processing of figure and background motion in the visual system of the fly," *Biological cybernetics*, vol. 61, no. 5, pp. 327–345, 1989.

[218] J. Haag and A. Borst, "Dendro-dendritic interactions between motion-sensitive large-field neurons in the fly," *Journal of Neuroscience*, vol. 22, no. 8, pp. 3227–3233, 2002.

[219] M. Egelhaaf, A. Borst, A.-K. Warzecha, S. Flecks, and A. Wildemann, "Neural circuit tuning fly visual neurons to motion of small objects. ii. input organization of inhibitory circuit elements revealed by electrophysiological and optical recording techniques," *Journal of Neurophysiology*, vol. 69, no. 2, pp. 340–351, 1993.

[220] P. Hennig, R. Kern, and M. Egelhaaf, "Binocular integration of visual information: a model study on naturalistic optic flow processing," *Frontiers in neural circuits*, vol. 5, p. 4, 2011.

[221] H. Wang, J. Peng, and S. Yue, "A feedback neural network for small target motion detection in cluttered backgrounds," in *27th International Conference on Artificial Neural Networks*, 2018.

[222] B. Hu, S. Yue, and Z. Zhang, "A rotational motion perception neural network based on asymmetric spatiotemporal visual information processing," *TNNLS*, pp. 2803–2821, 2016.

[223] D. Abbott, A. Moini, A. Yakovleff, X. T. Nguyen, A. Blanksby, G. Kim, A. Bouzerdoum, R. E. Bogner, and K. Eshraghian, "New vlsi smart sensor for collision avoidance inspired by insect vision," in *Intelligent vehicle highway systems*, vol. 2344, pp. 105–116, International Society for Optics and Photonics, 1995.

[224] G. Indiveri, "Analog VLSI Model of Locust DCMD Neuron for Computation of Object Approach," *Neuromorphic Systems. Engineering Silicon from Neurobiology*, vol. 10, pp. 47–60, 1998.

[225] R. R. Harrison, "A biologically inspired analog ic for visual collision detection," *IEEE Transactions on Circuits and Systems I: Regular Papers*, vol. 52, no. 11, pp. 2308–2318, 2005.

[226] M. Sarkar, D. S. S. Bello, C. van Hoof, and A. J. Theuwissen, "Biologically inspired cmos image sensor for fast motion and polarization detection," *IEEE Sensors Journal*, vol. 13, no. 3, pp. 1065–1073, 2013.

[227] M. B. Milde, H. Blum, A. Dietmüller, D. Sumislawska, J. Conradt, G. Indiveri, and Y. Sandamirskaya, "Obstacle avoidance and target acquisition for robot navigation using a mixed signal analog/digital neuromorphic processing system," *Frontiers in Neurorobotics*, vol. 11, pp. 1–17, 2017.

[228] C. Posch, D. Matolin, and R. Wohlgenannt, "A qvga 143 db dynamic range frame-free pwm image sensor with lossless pixel-level video compression and time-domain cds," *IEEE Journal of Solid-State Circuits*, vol. 46, no. 1, pp. 259–275, 2011.

[229] M. B. Milde, O. J. Bertrand, R. Benosmanz, M. Egelhaaf, and E. Chicca, "Bioinspired event-driven collision avoidance algorithm based on optic flow," in *Event-based Control, Communication, and Signal Processing (EBCCSP), 2015 International Conference on*, pp. 1–7, IEEE, 2015.

[230] T. Zhang, H. Wu, A. Borst, K. Kuhnlenz, and M. Buss, "An fpga implementation of insect-inspired motion detector for high-speed vision systems," in *Robotics and Automation, 2008. ICRA 2008. IEEE International Conference on*, pp. 335–340, IEEE, 2008.

[231] T. Köhler, "Bioinspired motion detection based on an fpga platform," *Biologically Inspired Computer Vision: Fundamentals and Applications*, 2015.

[232] F. Aubépart and N. Franceschini, "Bio-inspired optic flow sensors based on fpga: Application to micro-air-vehicles," *Microprocessors and Microsystems*, vol. 31, no. 6, pp. 408–419, 2007.

[233] M. O'Shea, C. H. F. Rowell, and J. L. D. Williams, "The anatomy of a locust visual interneurone: The descending contralateral movement detector," *J. Exp. Biol.*, vol. 60, pp. 1–12, 1974.

[234] P. J. Simmons and F. C. Rind, "Orthopteran dcmd neuron: A reevaluation of responses to moving objects ii critical cues for detecting approaching objects," *J. Neurophysiol.*, vol. 68, pp. 1667–1682, 1992.

[235] L. Caponetti and G. Castellano, *Fuzzy Logic for Image Processing*. 2017.

[236] F. Arvin, J. Murray, C. Zhang, and S. Yue, "Colias: An autonomous micro robot for swarm robotic applications," *International Journal of Advanced Robotic Systems*, pp. 1–10, 2014.

[237] F. Arvin, A. E. Turgut, T. Krajník, and S. Yue, "Investigation of cue-based aggregation in static and dynamic environments with a mobile robot swarm.," *Adaptive Bebavior*, vol. 24, no. 2, pp. 102–118, 2016.

[238] F. Arvin and M. Bekravi, "Encoderless position estimation and error correction techniques for miniature mobile robots," *Turkish Journal of Electrical Engineering and Computer Sciences*, vol. 21, no. 6, pp. 1631–1645, 2013.

[239] J. Benda and J. Tabak, "Spike-frequency adaptation," *Encyclopedia of Computational Neuroscience*, pp. 1–12, 2014.

[240] P. Lightbody, M. Hanheide, and T. Krajník, "An efficient visual fiducial localisation system," *Applied Computing Review*, vol. 17, no. 3, pp. 28–37, 2017.

[241] P. Lightbody, M. Hanheide, and T. Krajník, "A versatile high-performance visual fiducial marker detection system with scalable identity encoding," in *32nd ACM Symposium on Applied Computing*, 2017.

[242] R. B. Dewell and F. Gabbiani, "Escape behavior: Linking neural computation to action," *Current Biology*, vol. 22, no. 5, pp. R152–R153, 2012.

[243] F. T. Muijres, M. J. Elzinga, J. M. Melis, and M. H. Dickinson, "Flies evade looming targets by executing rapid visually directed banked turns," *Science*, vol. 344, no. 6180, pp. 172–177, 2014.

[244] V. Medan, D. Oliva, and D. Tomsic, "Characterization of lobula giant neurons responsive to visual stimuli that elicit escape behaviors in the crab Chasmagnathus.," *Journal of neurophysiology*, vol. 98, no. 4, pp. 2414–28, 2007.

[245] D. Oliva, V. Medan, and D. Tomsic, "Escape behavior and neuronal responses to looming stimuli in the crab Chasmagnathus granulatus (Decapoda: Grapsidae)," *Journal of Experimental Biology*, vol. 210, no. 5, pp. 865–880, 2007.

[246] J. Sztarker and D. Tomsic, "Neuronal correlates of the visually elicited escape response of the crab chasmagnathus upon seasonal variations, stimuli changes and perceptual alterations," *Journal of Comparative Physiology A: Neuroethology, Sensory, Neural, and Behavioral Physiology*, vol. 194, no. 6, pp. 587–596, 2008.

[247] M. Bengochea and M. Berón de Astrada, "Organization of columnar inputs in the third optic ganglion of a highly visual crab," *Journal of Physiology Paris*, vol. 108, no. 2-3, pp. 61–70, 2014.

[248] L. Chariker, R. Shapley, and L.-S. Young, "Orientation selectivity from very sparse lgn inputs in a comprehensive model of macaque v1 cortex," *The Journal of Neuroscience*, vol. 36, no. 49, pp. 12368–12384, 2016.

[249] C. M. Higgins and V. Pant, "An elaborated model of fly small-target tracking," *Biological Cybernetics*, vol. 91, no. 6, pp. 417–428, 2004.

[250] S. D. Wiederman, R. S. A. Brinkworth, and D. C. O'Carroll, "Performance of a Bio-Inspired Model for the Robust Detection of Moving Targets in High Dynamic Range Natural Scenes," *Journal of Computational and Theoretical Nanoscience*, vol. 7, no. 5, pp. 911–920, 2010.

[251] K. J. Halupka, S. D. Wiederman, B. S. Cazzolato, and D. C. O'Carroll, "Discrete implementation of biologically inspired image processing for target detection," in *2011 Seventh International Conference on Intelligent Sensors, Sensor Networks and Information Processing*, pp. 143–148, 2011.

[252] B. V, "Patterns of projection in the visual system of the fly. i. retina-lamina projections.," *Exp Brain Res 3:*, pp. 271–298, 1967.

[253] C. Koch, "Biophysics of computation: Information processing in single neurons (computational neuroscience)," in *Single Neurons*, pp. 1213–1214, 1998.

[254] T. B. Moeslund, A. Hilton, and V. Kruger, "A survey of advances in vision-based human motion capture and analysis," *Computer Vision and Image Understanding*, vol. 104, pp. 90–126, 2006.

[255] A. Dosovitskiy, P. Fischer, E. Ilg, P. Häusser, C. Hazirbas, V. Golkov, P. van der Smagt, D. Cremers, and T. Brox, "Flownet: Learning optical flow with convolutional networks," in *IEEE International Conference on Computer Vision*, pp. 2758–2766, 2015.

[256] D. Held, S. Thrun, and S. Savarese, "Learning to track at 100 fps with deep regression networks," in *European Conference on Computer Vision*, 2016.

[257] J. Redmon and S. Divvala, "You only look once: Unified, real-time object detection," in *Conference on Computer Vision and Pattern Recognition*, pp. 1–10, 2016.

[258] L. Kratz and K. Nishino, "Tracking with local spatio-temporal motion patterns in extremely crowded scenes," in *IEEE Computer Society Conference on Computer Vision & Pattern Recognition*, pp. 693–700, 2010.

[259] C. Hu, Q. Fu, T. Liu, and S. Yue, "A hybrid visual-model based robot control strategy for micro ground robots," in *The 15th International Conference on the Simulation of Adaptive Behavior*, 2018.